

***Developing strategies and equipment for continuous
isolation of active pharmaceutical ingredients (APIs)
by filtration, washing and drying***

Sara Ottoboni

Thesis submitted to the Chemical and Process Engineering Department at
the University of Strathclyde in accordance with the requirements for the
degree of Doctor of Philosophy

2018

Declaration of Author's Rights

This thesis is the result of the author's original research. It has been composed by the author and has not been previously submitted for examination which has led to the award of a degree. The copyright of this thesis belongs to the author under the terms of the United Kingdom Copyright Acts as qualified by University of Strathclyde Regulation 3.50. Due acknowledgement must always be made of the use of any material contained in, or derived from, this thesis.

Signed:

Date: 10-12-2018

Acknowledgements

I would like to thank the following:

Dr. Chris Price, the person that four years ago decided to take the responsibility of my scientific and personal growth and that every day is supporting, supervising and co-existing with my enthusiasm (sometimes too energetic). I need to thank him also because he gave me the chance to meet amazing people and colleagues: Hien Nguyen, Layla Mir Bruce, Christopher Steven, Clarissa Forbes, Georgia Sanxaridou, Simon Coleman and Muhid Shahid.

People of CMAC and the Chemical Engineering Department that each day help me in my work and personal life.

Dr John Parkinson and Craig Irving who helped me with NMR experiments.

The people who collaborated with me to publish one of my first papers: the co-authors, Michael Chrubasik, Layla Mir Bruce, Hien Nguyen, Blair Johnston, Alastair Florence, Chris Price and the other people that contributed. I would like to thank Lauren O'Connor for her help with Raman Microscopy, Davide Erbogasto for his support with SEM analysis, Eleonora Paladino who made helpful suggestions about the TOF-SIMS methodology, Monika Warzecha who trained me in AFM and Laura Harvey who provided guidance in HPLC analysis.

All the people involved in Remedies project App B: Alistair Barton, Dr. Elizabeth Mehaan, Dr. Claire MacLeod, Sadie Finn, Paul Firth, Christopher Steven, Richard Sutherland, Andy Mitchell and Furqan Tahir who provided me with the opportunity to

contribute to the development of a new piece of equipment I would like to thank them also for the permission they gave me to publish this work.

The people who collaborated with me to publish the latest paper: Martin Simurda, Samantha Wilson, Andrew Irvine, Fraser Ramsay and Chris Price. I would like to thank also Marine Fraissinet, Marion Joannes and Lucie Pedussaut.

Dr. Elizabeth Mehaan, Dr. Claire MacLeod and Sadie Finn for their help and the opportunity they gave me to conduct research at Astra Zeneca for few months in an industrial placement.

People I met in Roche who hosted me and helped me during my industrial placement. I want to thank in particular Dr. Pirmin Hidberg, Dr. Marcello Bosco, Dr. Manuel Konrath and Dr. Francesca Perciballi.

Dr Georgina Zimbitas and Dr Michele Sevegnani for their kind offer to proof read my thesis.

I would like all the friends that constantly supported me.

My family and my partner for their constant support and encouragement throughout my studies, without them this study would not have been achievable.

Really thanks

Abstract

In pharmaceutical sector, compounds forming the drug and especially the active pharmaceutical ingredients (API's) are required to be pure, in accordance with the regulatory authorities' rules. The isolation stage is used to remove the impure liquid phase and to remove surface impurities from the crystalline product. Physico-chemical properties of crystals formed during the crystallization process and the solvents selected for the crystallization process influence the performance and the efficacy of isolation. Lots of effort was made in the last few decades to understand how to improve the crystallization stage. Relatively less effort has been made to understand the chemo-physical and process characteristics affecting the properties of the final isolated product. As consequence, the isolation stage can be responsible for extended API manufacturing time, the consumption of high quantities of materials and solvents and sometimes the requirement for isolated product post-processing to overcome variation of crystallized material properties caused by isolation.

The aim of this thesis is to understand from a microscopic to a macroscopic point of view how the physic-chemical properties of the crystallized material and the washing solvents used in combination with the filtration, washing and drying approaches used can influence the final isolated product characteristics. To broaden the field, an alternative analytical technique for pharmaceutical field, TOF-SIMS, allows investigating the surface/sub-surface of crystal to localize adsorption of related impurities to help to design isolation strategy and solvent selection.

A major objective of this work is to reduce API manufacturing time in the R&D stage, to minimize chemical, especially solvent consumption, and to maximize the isolation knowledge gathered to design an optimal isolation process. The work also addresses the development of an analytical workflows/procedures to characterize materials during each step of the isolation. The final component was the development of a lab/small scale isolation prototype unit for API's development, which was developed during this work.

Contents

Declaration of Author's Rights.....	ii
Acknowledgements.....	iii
Abstract.....	v
Table of figures.....	xii
Table of tables.....	xxi
Papers published and conference attended.....	1
1 Introduction.....	5
2.1 Abbreviations.....	9
References.....	9
2 Literature review.....	11
2.1 Introduction.....	12
2.2 Classic filtration theory.....	14
2.2.1 Dead end conventional cake filtration.....	18
2.2.2 Cross flow conventional cake filtration.....	24
2.3 Sedimentation theory.....	31
2.4 Washing theory.....	36
2.4.1 Continuous filter cake washing by using rotary filtration.....	45
2.5 Drying.....	48
2.5.1 Parameters affecting dried material size.....	53
2.6 How isoaltion parameters were calculated.....	60
2.7 Isolation solvents.....	65
2.8 Correlation between chemical-physical slurry properties and filtration process.....	67
2.8.1 Porosity and particle density.....	68
2.8.2 Particles size, particles size distribution and particles shape.....	70
2.8.3 Particles morphology.....	76

2.8.4	Wettability	82
2.8.5	Liquid transport in porous media	87
2.8.6	Solvent properties	102
2.9	Abbreviations	103
References	104
3	Aims and thesis structure.....	112
4	Materials and methods.....	117
4.1	Material: paracetamol	118
4.2	Materials: paracetamol related impurities.....	128
4.3	Materials: solvents	133
4.4	Methods.....	136
4.4.1	Physical characterization techniques	136
4.4.2	Surface characterization techniques	138
4.4.3	Solid state	142
4.4.4	Chemical analysis.....	143
4.4.5	Mechanical characterization techniques.....	145
4.4.6	Isolation units	148
4.4.7	Design of experiment approach.....	156
4.5	Abbreviations	162
References	163
5	The impact of paracetamol impurities on face properties: investigating the surface of single crystals using TOF-SIMS.	166
5.1	Introduction.....	167
5.2	Background	168
5.3	Materials and method.....	172
5.3.1	Materials	172
5.3.2	Methods	172
5.4	Results and discussions.....	177
5.4.1	Chemical character and surface texture evaluation.....	179
5.4.2	Raman and TOF-SIMS analysis.....	189
5.5	Conclusions	197
5.6	Abbreviations	201

References	202
6 Effect of filtration, washing and drying on the isolated product: Paracetamol case study.....	206
6.1 Introduction.....	207
6.2 Background	208
6.3 Materials.....	220
6.4 Method	221
6.4.1 Preliminary characterization.....	227
6.4.2 Filtration and washing procedure	231
6.4.3 Drying methodologies	232
6.4.4 Offline characterization.....	234
6.5 Results and discussions.....	234
6.5.1 Parameters affecting filtration.....	234
6.5.2 Parameters affecting washing.....	247
6.5.3 Parameters affecting drying.....	248
6.5.4 Agglomeration, mechanical properties and particle size of dried products.....	259
6.5.5 Model optimization and wash solvent screening.....	274
6.6 Analytical workflow procedure for isolation strategy development for continuous isolation.....	278
6.7 Conclusions.....	285
6.8 Abbreviations.....	289
References	290
7 Prototyping of a continuous isolation unit: development and tests	295
7.1 Introduction.....	296
7.2 Background	306
7.3 Materials and methods	315
7.3.1 Materials.....	315
7.3.2 Raw material characterisation	317
7.3.3 Slurry preparation: comparison AWL CFD20 with Biotage unit	318
7.3.4 Slurry preparation: Test AWL CFD25 with structurally related paracetamol compounds	318
7.3.5 Biotage manual filtration system overview	319
7.3.6 CFD20 and 25 continuous filtration, washing and drying system overview	319

7.3.7	Experimental design: comparison AWL CFD20 with Biotage unit.....	319
7.3.8	Experimental design: test AWL CFD25 with structurally related paracetamol compounds.....	321
7.3.9	Off-line filtrate and cake characterization techniques.....	323
7.4	Results and discussions.....	324
7.4.1	Comparison AWL CFD20 with Biotage unit.....	324
7.4.2	Test AWL CFD25 with structurally related paracetamol compounds ...	331
7.5	Conclusions.....	344
7.6	Abbreviations.....	346
	References	348
8	Conclusions and future works	352
8.1	Further work.....	360
8.1.1	Use of other crystallization solvents to evaluate variation in impurity interaction with paracetamol single crystal facets	360
8.1.2	Fundamental understanding of solid bridge formation during drying in presence of residual mother liquor and /or wash solvent.....	361
8.1.3	Investigation of alternative drying procedures to minimize particles agglomeration.....	361
8.1.4	Test the CFD25 with a series of different APIs and evaluate the unit in continuous (production) mode for an extended period.	362
9	Appendix	363
9.1	Materials and methods	364
9.2	Isolation parameters	368
9.3	Solubility by equilibration	368
9.4	The impact of paracetamol impurities on crystal face properties: investigating the surface of single crystals using TOF-SIMS.	369
9.4.1	4-aminophenol mass spectra.....	369
9.4.2	Single crystals crystallized in presence of other paracetamol related impurities	370
9.4.3	Mass spectra of other paracetamol related impurities	387
9.5	Effect of filtration, washing and drying on the isolated product: Paracetamol case study.....	395
9.6	Prototyping of a continuous isolation unit: development and tests	399
	References.....	405

Table of figures

Figure 1 Pharmaceuticals manufacturing stages.	12
Figure 2 Crossflow filtration vs dead end filtration. ¹¹	15
Figure 3 Different operations involved in cake filtration process: filtration, washing and deliquoring. ¹¹	16
Figure 4 Crossflow filtration equipment schemes Figure on the left represent the evolution of cake formation during the different stages of filtration (cake formation zone, washing zone and cake discharge). Figure on the right represents the different stages of a crossflow filtration and cake thickness evolution . ²¹	17
Figure 5 Scheme of cake filtration process. ²⁰	19
Figure 6 Forces and transport effects onto a particle in cross-flow filtration. ⁴⁸	25
Figure 7 Relative settling velocities and relative flux as function of the solid concentration. ⁵³	32
Figure 8 Scheme and quantities involved in filtration with sedimentation. ⁵³	32
Figure 9 Filtration height versus filtration time of kaolin slurry measured with X-ray tomography. ⁵³	34
Figure 10 Schematic representation of cake washing. ¹¹	36
Figure 11 Wash curve of effluent concentration vs wash ratio. ¹¹	39
Figure 12 Drying curve. ⁷⁴	50
Figure 13 Effect of temperature on (a) final average diameter and (b) aspect ratio. ⁷²	54
Figure 14 Effect of pressure on final average diameter at different temperatures: (rhomb), 200Torr (square) and 80Torr (triangle). ⁷²	55
Figure 15 Effect of agitation on (a) final average diameter, small graph is the final average diameter respect the number of revolution and, (b) aspect ratio. ⁷⁷	56
Figure 16 How different secondary effects prior/during filtration can influence Darcy's plot. ⁴⁸	61
Figure 17 Example of filtration flow rate of a filtration experiment at constant pressure filtration in case of cake formation during filtration. Experiment 2d of chapter 8. P-value calculated with ANOVA statistic are (confidence level 95%); exp 2D1, intercept, 0.0129, x variable, 0.0012; exp 2D2, intercept, 0.0045, x variable, 8.9E-05; exp 2D3, intercept, 0.0031, x variable, 9.5E-05.	62
Figure 18 Example of Darcy's plot (time/volume of filtrate collected versus volume of filtrate collected during a constant pressure filtration experiment where the cake is forming during the filtration experiment. Experiment 2d of chapter 8. Average value of slope 5.4969E+10 and standard deviation 5.9178E+09. Average value of intercept 1.9802E+05 and standard deviation 1.0863E+05.	63
Figure 19 Equivalent sphere for arbitrary particles. ¹⁰⁰	71
Figure 20 Solubility and supersolubility curves. ¹⁰⁷	77
Figure 21 Free energy as function of the cluster size. ⁵	79
Figure 22 Kinked, stepped and flat facets during crystal growth. ¹¹²	81
Figure 23 Schematic representation of isolated liquid surface for equilibrium analysis. ⁹⁵⁻¹¹⁵	83

Figure 24 Liquid drop equilibrium on a flat and horizontal surface. ^{99, 116}	85
Figure 25 Illustration of physical meaning of tortuosity. ⁹⁵	91
Figure 26 Representation of possible co-current steady two phase flow in porous media. ⁹⁹	92
Figure 27 Contact angle that taking place during liquid and surface contact. ¹⁴⁰	99
Figure 28 Hydrodynamic dispersion in porous media. ⁹⁹	101
Figure 29 Micro-fingers displacement. ⁹⁹	101
Figure 30 Mixing of two streams by molecular diffusion. ⁹⁹	102
Figure 31 Reduced continuous isolation program mind map.	115
Figure 32 Molecular structure of paracetamol.	118
Figure 33 Main faces of paracetamol form I. Paracetamol predicted morphology using the Bravais-Friedel-Donnay-Harker (BFDH) method assuming that the relative growth rates R_{hkl} of the crystal faces is inversely proportional to the inter-planar spacing d_{hkl} , without taking account of the chemical nature of the crystal, molecular packing arrangement or crystallising environment.	120
Figure 34 Space distribution and orientation in crystal lattice of paracetamol form I molecules.	122
Figure 35 Space distribution and orientation in crystal lattice of paracetamol form I molecules. 3*3 packing structure.	123
Figure 36 Schematic representation of the Washburn method. ³⁹	140
Figure 37 Washburn method setup with the Sartorius balance and density kit.	142
Figure 38 Example of three ABI indexes of a soft, middle hard and hard dried cakes.	147
Figure 39 Visual fragmentation of agglomerates within each shaking cycle.	147
Figure 40 Biotage filtration unit setup.	148
Figure 41 Biotage experimental procedure.	149
Figure 42 CFD20 Carousel filtration unit on the left and CFD25 on the right (detail of the modified carousel and camera).	153
Figure 43 AWL CFD20 schematic operative procedure.	155
Figure 44 Schematic of the camera arrangement for the vision system. a. The camera looks through the side of the glass tube (filtration vessel) b. The liquid and solid interfaces are visible to the camera.	155
Figure 45 Summary of fit of some of the responses selected for the DoE approach presented in chapter 7.	161
Figure 46 Solubility curve of paracetamol in ethanol (left hand side) and hexane (right hand side) in mg/g of solvent predicted by using COSMOTherm, evaluated from literature and measured by equilibration method. ^{26, 31} Solubility measurements were replicated three times. Standard deviation values are reported in chapter 9.	178
Figure 47 SC-XRD images of PP crystal (on the left) and P4%N crystal (on the right).	181
Figure 48 OM image in DIC mode, 10X, and SEM image of paracetamol crystal (PP). SEM operating conditions: distance 7210um, emission current 58.9mA, WD 7.21mm. Paracetamol surface texture is observed in OM and SEM image, with the characteristic edge steps.	183
Figure 49 AFM map of PP crystal collected in air using Scan Asyst mode, the area of detection is 10x10µm. Topography shows roughness of PP crystal and the typical crystal	

step growth of PP crystal with step ranging in the height from 10 to 30 nm (see white arrows).....	184
Figure 50 OM image in DIC mode, 10X, and SEM image of 4-nitrophenol crystal (PN). SEM operating conditions: distance 6220um, emission current 57.9mA, WD 6.22mm. 4-nitrophenol characteristics rounded steps are observed in OM and SEM image.....	184
Figure 51 OM image in DIC mode, 10X, and SEM image of cooling crystallization crystal (P4%N). SEM operating conditions: working distance 6700um, emission current 57.4mA, WD 6.7mm. Increase frequency of surface defects are apparent in OM and SEM images and are associated with the presence of the impurity 4-nitrophenol (see the arrow).....	185
Figure 52 Two different AFM maps of P4%N crystal obtained in air with Scan Asyst mode, scan area respectively 50 and 15um. From these two AFM topographic maps rough surface with nanometric steps can be evaluated (white arrow).....	186
Figure 53 OM image in DIC mode, 10X, and SEM image of drop crystal (PDN). Red arrow highlight the drop perimeter. SEM operating conditions: working distance 6360um, emission current 58.7mA, WD 6.36mm. Needle shape 4-nitrophenol crystals are observed in the drop area both in OM and SEM images (see the arrow).....	187
Figure 54 AFM maps of PDN crystal obtained in air with Scan Asyst mode, scan area 50µm. The perimeter drop can be observed. On the left side of the image the surface is smooth with macro roughness characteristic of paracetamol, while on the right side the increase of micro roughness is due to the needle like 4-nitrophenol crystal randomly orientated is observe.....	188
Figure 55 OM image in DIC mode, 10X, and SEM image of epitaxial crystal (PEN). Needle shape epitaxially growth 4-nitrophenol crystals are observed (arrow). SEM operating conditions: working distance 5820um, emission current 57.7mA, WD 5.82mm. Paracetamol steps substrate texture is seen from SEM image.	188
Figure 56 AFM maps of PEN crystal obtained in air with Scan Asyst mode, scan area respectively 50um. Nano and micro roughness can be observed.....	189
Figure 57 Raman spectra of paracetamol (PP) (top) and 4-nitrophenol (PN) bottom spectrum.....	191
Figure 58 Raman map of P4%N crystal. Crystal was analysed in a step area. Area of detection 20x20µm. Black dots on the map correspond to the position of the laser detection. Scale is related to the intensity of 4-nitrophenol peak within respect to the baseline.....	193
Figure 59 Raman map of PEN crystal. The area of the crystal analysed was in an area where 4-nitrophenol needle like crystals were concentrated. Area of detection 10x10µm. The black dots on the map correspond to the centres of the spectrum collections. Scale is related to the intensity of 4-nitrophenol peak within respect to the baseline.....	193
Figure 60 Paracetamol with 4% (mol/mol) of 4-nitrophenol. From left to right, 4-nitrophenol molecular ion image at 138 m/z (maximum counts = 16), paracetamol molecular ion image at 150 m/z (maximum counts = 83) and RGB overlay of paracetamol (red) with 4-nitrophenol (green).....	195
Figure 61 Paracetamol crystal with drop of 4-nitrophenol applied. From left to right, 4-nitrophenol molecular ion image at 138 m/z (maximum counts = 19), paracetamol molecular ion image at 150 m/z (maximum counts = 30) and RGB overlay of paracetamol (red) with 4-nitrophenol (green).....	196

Figure 62 Suggested paracetamol with 4-nitrophenol Epitaxy. From left to right, 4-nitrophenol molecular ion image at 138 m/z (maximum counts = 52), paracetamol molecular ion image at 150 m/z (maximum counts = 32) and RGB overlay of paracetamol (red) with 4-nitrophenol (green).....	197
Figure 63 Experimental workflow. Three different paracetamol grades were selected, micronised, powder and granular. Slurries were prepared by creating a saturated solution and then pouring the solid load required to build the cake with the selected paracetamol grade. Filtration was then performed to form the cake for the washing step. The selection of wash strategy for each experiment was set using DoE approach. After the drying process, the final material was analysed to evaluate loss on drying, residual solvent composition and quantity, extent of agglomeration and agglomerate strength using a friability analysis.....	219
Figure 64 Scheme of static drying with flowing nitrogen apparatus at room temperature.....	233
Figure 65 Scheme of flowing N ₂ drying apparatus at 60°C temperature.....	234
Figure 66 DoE variables affecting cake resistance during filtration.....	235
Figure 67 4D contour plot of the effect of solid load and driving force on cake resistance for slurry prepared with ethanol as crystallization solvent.....	237
Figure 68 DoE variables affecting media resistance during filtration.....	238
Figure 69 Filtration and reload experiment performed using a slurry made with 30% V/V of micronised paracetamol in isopropanol and filtered at 900mbar driving force.....	239
Figure 70 4D Response contour plot of cake resistance in step 1 (settled and then filtered) in the DoE addressing solids loading, driving force, filter medium pore size and paracetamol particle size range (powder and micronised) where the crystallization solvent was ethanol.....	241
Figure 71 4D response contour plot of cake resistance in step 2 (reload and filtered) in the DoE range of solid load and driving force, crystallization solvent ethanol, comparison of different filter medium pore size and powder and micronised paracetamol.....	242
Figure 72 4D response contour plot of cake resistance in step 1 (filtered) in the DoE range of solid load and driving force, crystallization solvent ethanol, comparison of different filter medium pore size and powder and micronised paracetamol.....	243
Figure 73 4D response contour plot of cake resistance in step 2 (reload and filtered) in the DoE range of solid load and driving force, crystallization solvent ethanol, comparison of different filter medium pore size and powder and micronised paracetamol.....	244
Figure 74 4D response contour plot of cake resistance in step 1 (settled and then filtered) in the DoE range of solid load and driving force, crystallization solvent isoamyl alcohol, comparison of different filter medium pore size and powder and micronised paracetamol.....	245
Figure 75 4D response contour plot of cake resistance in step 1 (reload and filtered) in the DoE range of solid load and driving force, crystallization solvent isoamyl alcohol, comparison of different filter medium pore size and powder and micronised paracetamol.....	246
Figure 76 Parameters affecting residual solvent content.....	250
Figure 77 Drying profile of wet cake samples where drying was achieved by flowing nitrogen at ambient temperature through the filter cake with a flow rate of 0.3l/min. ...	253

Figure 78 Drying profile of wet cake samples where drying was achieved by flowing nitrogen at 60°C through the filter cake with a flow rate of 0.3l/min.	253
Figure 79 4D response contour plot of residual solvent content in case of filtration halted at breakthrough showing dependence on solids loading of the slurry, pressure driving force and paracetamol grade for an input suspension in ethanol washed once with n-heptane and then dried using the static drying methodology.	256
Figure 80 4D response contour plot of residual solvent content in case of filtration halted at dryland showing dependence on solids loading of the slurry, pressure driving force and paracetamol grade for an input suspension in ethanol washed once with n-heptane and then dried using the static drying methodology.	257
Figure 81 4D response contour plot of residual solvent content in case of filtration halted at breakthrough showing dependence on solids loading of the slurry, pressure driving force and paracetamol grade for an input suspension in ethanol washed twice with n-heptane and then dried using the static drying methodology.	258
Figure 82 4D response contour plot of residual solvent content in case of filtration halted at dryland showing dependence on solids loading of the slurry, pressure driving force and paracetamol grade for an input suspension in ethanol washed twice with n-heptane and then dried using the static drying methodology.	259
Figure 83 Appearance of isolated and dried paracetamol (left) micronized (exp 21), (centre) powder (exp 40) and (right) special granular (exp 15) input material (experiments information reported in the appendix).	260
Figure 84 Examples of lump formation (left, exp 53, centre exp 52, right exp 24; experiments information reported in the supplementary information).	260
Figure 85 Isolated and dried filter cake from the three centre point replicate experiments in the DoE.	261
Figure 86 Parameters affecting the extent of agglomeration grouped by; filtration conditions, material particle size, washing and drying procedure and wash solvent identity	265
Figure 87 Investigating the effect of crystallization solvent. A 4D response contour plot of Sauter mean diameter (SMD) of the isolated product particles passing through the 1mm screen. In the case of filtration halted at dryland or breakthrough in the range of solid load of the slurry, driving force, paracetamol grade for an ethanol slurry washed 2 times with n-heptane and static drying methodology. SMD of raw powder and micronised paracetamol are respectively 46.35 and 18.66µm.	268
Figure 88 Investigating the effect of crystallization solvent. A 4D response Contour plot of Sauter mean diameter of particles smaller than 1mm in case of filtration halting at dryland or breakthrough in the range of solid load of the slurry, driving force, paracetamol grade for an isoamyl alcohol slurry washed 2 times with n- heptane and static drying methodology. SMD of raw powder and micronized paracetamol are respectively 46.35 and 18.66µm.	269
Figure 89 Investigating the effect of wash solvent volume (and number of washes). A 4D response Contour plot of Sauter mean diameter of particles smaller than 1mm in case of filtration halted at dryland or breakthrough in the range of solid load of the slurry, driving force, paracetamol grade for a isoamyl alcohol slurry washed 1 time with n- heptane and	

static drying methodology. SMD of raw powder and micronised paracetamol are respectively 46.35 and 18.66 μ m.	270
Figure 90 Investigating the effect of drying conditions. A 4D response Contour plot of Sauter mean diameter of particles smaller than 1mm in case of filtration halting at dryland or breakthrough in the range of solid load of the slurry, driving force, paracetamol grade for an isoamyl alcohol slurry washed 2 times with n- heptane and 60°C flowing nitrogen drying methodology. SMD of raw powder and micronised paracetamol are respectively 46.35 and 18.66 μ m.	271
Figure 91 Investigating the effect of solubility in the wash solvent on isolated particle properties. A 4D response Contour plot of Sauter mean diameter of particles smaller than 1mm in case of filtration halting at dryland or breakthrough in the range of solid load of the slurry, driving force, and paracetamol grade for an isoamyl alcohol slurry washed 2 times with acetonitrile with static drying methodology. SMD of raw powder and micronised paracetamol are respectively 46.35 and 18.66 μ m.	272
Figure 92 Visual appearance of samples generated during the validation DoE after drying. The best solvent selection to reduce agglomeration and obtain soft agglomerates is cyclohexane.	277
Figure 93 PSD profile of sample of the material isolated in the validation DoE.	278
Figure 94 Workflow for the development of an isolation strategy.	279
Figure 95 New product development process stages to develop a new prototype. ¹	297
Figure 96 AWL CFD20 prototype.	300
Figure 97 Filtration component of the Steadfast rotary drum filter. ¹⁹	307
Figure 98 D&M filter dryer unit. ⁸	308
Figure 99 Schematic representation of the BHS belt filter. ²⁰	309
Figure 100 (a) Uneven solids distribution after filtering successive batches of the same slurry (b) Particles and liquid left in a measuring cylinder after dispensing slurry and followed by repeated back transfers.	325
Figure 101 (a) the stirred slurry vessel, (b) the filtration unit with dosing vessel above and (c) the slurry dosing vessel.	326
Figure 102 Series of processed camera images as filtration progresses. The green crosses indicate the levels of the liquid and solid that the camera has determined.	327
Figure 103 (a) Patent blue mass removal at each stage in the filtration and washing of special granular paracetamol (D = 2 x 5mL wash, E = 2 x 10 mL wash) f = filtrate, w1 = wash 1, w2 = wash 2, c = cake) (b) Patent blue mass removal at each stage in the filtration and washing of micronised paracetamol.	329
Figure 104 (a) Residual patent blue mass in filter cakes comparing the AWL CFD and Biotage. (1= granular 2 = micronized, d = 2 x 5mL e = 2 x 10 mL) (b) Residual patent blue mass in filter cakes comparing filtration to dry-land (exp 2) and breakthrough (exp 4) for micronised paracetamol, b = 1 x 5mL, c = 1 x 10 mL, d = 2 x 5mL e = 2 x 10 mL).	329
Figure 105(a granular paracetamol) AWL CFD20 (first five columns) and Biotage (last two columns) fractions collected from sieving analysis. (b micronized paracetamol) AWL CFD20 (first five columns) and Biotage (last two columns).	330
Figure 106 DoE variables that affect cake volume during filtration.	332
Figure 107 DoE variables that affect filtrate flow rate during filtration.	333

Figure 108 Fitting summary of variable affecting the relative percentage of wash solvent in the dried cake moisture content.	335
Figure 109 Fitting summary of variable affecting the relative percentage of crystallization solvent in the dried cake moisture content.	335
Figure 110 Second filtrate orthocetamol concentration fittings with DoE variables.	336
Figure 111 The dependence of the concentration of the impurity orthocetamol in the different wash solvents on the DoE variables.	338
Figure 112 DoE variables that affect LOD of the dried samples.	340
Figure 113 DoE variables that affect extent of agglomeration of the dried samples.	340
Figure 114 DoE variables that affect ABI index of the dried samples.	341
Figure 115 Isopropanol - paracetamol saturated solution viscosity at different temperatures. ^{71, I}	366
Figure 116 Ethanol - paracetamol saturated solution viscosity at different temperatures. ^{72, II}	367
Figure 117 Isoamyl Alcohol - paracetamol saturated solution viscosity at different temperatures. ^{73, III}	367
Figure 118 Positive mass spectra of pure 4-aminophenol with TOF-SIMS in spectroscopy mode.	369
Figure 119 Negative mass spectra of pure 4-aminophenol with TOF-SIMS in spectroscopy mode.	370
Figure 120 Stereomicroscopy of crystal produced with cooling crystallization of paracetamol with 4% mol of 4'-chloroacetanilide, S=1.5 in ethanol, 1x. 4'-chloroacetanilide crystallized separately to paracetamol forming needle-shape (pure 4'-chloroacetanilide crystals) and hexagonal-like shape of pure paracetamol crystals.	372
Figure 121 Stereomicroscopy of crystal produced with cooling crystallization of paracetamol with 4% mol of acetaminophen acetate, S=1.5 in ethanol, 1.5x. Acetaminophen acetate crystallized separately to paracetamol forming needle-shape (pure acetaminophen acetate crystals) and hexagonal-like shape of pure paracetamol crystals.	373
Figure 122 Top: single crystal of paracetamol with 4% mol of acetamido benzoic acid, S=1.5 in ethanol, stereomicroscope 1x; Bottom left and right: two details of the surface of the single crystal of paracetamol with 4% mol of acetamido benzoic acid, S=1.5 in ethanol, stereomicroscope 1x. Different faces.	374
Figure 123 Stereomicroscopy of single crystal of paracetamol with 4% mol of 4-aminophenol, S=1.5 in ethanol, 1x. Different faces.	375
Figure 124 Stereomicroscopy of single crystal of paracetamol with 4% mol of 4-hydroxyacetophenone, S=1.5 in ethanol, 1.3x. Different faces.	376
Figure 125 Stereomicroscopy of single crystal of paracetamol with 4% mol of acetanilide, S=1.5 in ethanol, 1x. Different faces.	376
Figure 126 Stereomicroscopy of single crystal of paracetamol with 4% mol of 4-methylhydroxy benzoate, S=1.5 in ethanol, 1x. Different faces.	377
Figure 127 Example of craters formed by the 3D depth TOF-SIMS analysis evaluated with optical microscopy in DIC modes (5x).	379
Figure 128 Example of AFM topographic map (left) of the cooling crystallization crystal produced with paracetamol with 4% mol of 4-acetamido benzoic acid on the right side of	

the TOF-SIMS crater. On the right the image of the area where the analysis was done (no scale-bar is reported by the instrument).....	379
Figure 129 Example of AFM topographic map (left) of the cooling crystallization crystal produced with paracetamol with 4% mol of 4-acetamido benzoic acid of an internal area of the TOF-SIMS crater. On the right the image of the area where the analysis was done (no scale-bar is reported by the instrument).....	380
Figure 130 Positive mass spectra of pure 4-acetamido benzoic acid with TOF-SIMS in spectroscopy mode.....	381
Figure 131 Negative mass spectra of pure 4-acetamido benzoic acid with TOF-SIMS in spectroscopy mode.....	382
Figure 132 TOF-SIMS surface imaging of the sample secondary ion molecular images at 151m/z (maximum count = 15), left, corresponding to paracetamol, 178m/z (maximum count = 20) right, corresponding to 4-acetamido benzoic acid. Measurements taken on the bottom of the crystal face 1.....	383
Figure 133 Intensity count of paracetamol ion fragment red, green and light blue, corresponding to 150 and 151 and 153 m/z) and 4-acetamido benzoic acid ion fragment (light blue, 178 m/z). Crystal face 1. 3D depth profile shows constant paracetamol content along the sputtered depth, while 4 acetamido benzoic acid curve is increasing during the first 200s of sputtering and then it stabilizes.....	384
Figure 134 3D render overlay of paracetamol ion fragment (151m/z, grey) and 4-acetamido benzoic acid (178m/z, red). Different section of the 3D depth render of the crystal face 1.	385
Figure 135 intensity count of paracetamol ion fragment (blue, red and violet, corresponding to 152, 153 and 151m/z) and 4-acetamido benzoic acid ion fragment (pink, 178m/z). Crystal face 2. 3D depth profile shows constant paracetamol content along the sputtered depth, while 4 acetamido benzoic acid curve is increasing during the first 200s of sputtering and then it stabilizes.....	386
Figure 136 3D render overlay of paracetamol ion fragment (151m/z, grey) and 4-acetamido benzoic acid (178m/z, red). Different section of the 3D depth render of the crystal face 2.	387
Figure 137 Positive mass spectra of pure 4-hydroxy acetophenone with TOF-SIMS in spectroscopy mode.....	387
Figure 138 Negative mass spectra of pure 4-hydroxy acetophenone with TOF-SIMS in spectroscopy mode.....	388
Figure 139 Positive mass spectra of pure 4'-chloro acetanilide with TOF-SIMS in spectroscopy mode.....	389
Figure 140 Negative mass spectra of pure 4'-chloro acetanilide with TOF-SIMS in spectroscopy mode.....	390
Figure 141 Positive mass spectra of pure acetanilide with TOF-SIMS in spectroscopy mode.....	391
Figure 142 Negative mass spectra of pure acetanilide with TOF-SIMS in spectroscopy mode.....	392
Figure 143 Positive mass spectra of pure 4-methyl hydroxyl benzoate with TOF-SIMS in spectroscopy mode.....	393

Figure 144 Negative mass spectra of pure 4-methyl hydroxyl benzoate with TOF-SIMS in spectroscopy mode.....	394
Figure 145 Cumulative distribution and distribution density of raw granular paracetamol.	395
Figure 146 Cumulative distribution and distribution density of raw micronised paracetamol.	395
Figure 147 Cumulative distribution and distribution density of raw powder paracetamol.	396
Figure 148 Factors selected for the screening DoE (first DoE).	397
Figure 149 Responses of the screening DoE (first DoE).	398
Figure 150 Factors selected for the pre-settling DoE (second DoE).	398
Figure 151 Responses of the pre-settling DoE (second DoE).	399
Figure 152 Factors of the DOE.	400
Figure 153 Responses of the DoE.	403
Figure 154 HPLC calibration curve of paracetamol.	403
Figure 155 HPLC calibration curve of metacetamol and acetanilide.	404
Figure 156 HPLC calibration curve of acetaminophen acetate and orthocetamol.....	404

Table of tables

Table 1 Different models proposed in literature to improve filtration theory.....	23
Table 2 Dead end filtration theory parameters.....	28
Table 3 Cross flow filtration theory parameters.	30
Table 4 Filtration theory parameters: particles parameters affecting filtration.....	30
Table 5 Sedimentation theory parameters.....	35
Table 6 Dead end washing theory parameters.	46
Table 7 Washing theory parameters in case of cake desaturation.	47
Table 8 Cross flow washing theory parameters.	47
Table 9 Operating parameters and material properties that affect final particle size and morphology of the dried material.....	53
Table 10 Drying theory parameters.....	59
Table 11 Solubility theory parameters.....	75
Table 12 Parameters related to crystal nucleation and growth theory.	82
Table 13 Crystallographic and thermal properties of different paracetamol polymorphisms.....	119
Table 14 Molecular packing diagrams based upon the crystallographic structures: the (001) face showing more polar surface with exposed–OH and -NHCOCH ₃ groups in various directions; the (20-1) face showing mainly the–OH and -C=O groups exposed from the surface; the (011) face shows -NHCOCH ₃ group exposed; the (-110) face showing less polar with less functional groups –OH and -NHCOCH ₃ exposed. The molecules can be seen to be arranged alternatively nearly parallel and perpendicular to the surface. Face (11-1) shows -NHCOCH ₃ group exposed; the (200) face showing –OH and -NHCOCH ₃ exposed. The red shadow represents a crystal plane. Depth of the slice 10Å, Area of the slice 20Å.....	120
Table 15 IR frequency of paracetamol functional groups for three polymorphic forms of paracetamol. ¹⁴	124
Table 16 Values of advancing (θ_a), receding (θ_r) and contact angle hysteresis ($\Delta\theta$) of different paracetamol facets with different test liquids. ^{17, 18}	125
Table 17 Surface energy values of paracetamol facets determined by Owens-Wendt analysis. ^{17, 18}	125
Table 18 Material characteristics of the three paracetamol grades. True density values were determined with Helium pycnometer, x_{10} , x_{50} and x_{90} , SMD and VDM were determined using a QICPIC particle size analyser.....	127
Table 19 Major paracetamol impurities and their main properties. ^{2, 4}	129
Table 20 Solvent used during this work. ^{25, 26, 27, 28}	133
Table 21 Main properties of the solvent used during this ^{work29-33}	135
Table 22 Cooling crystallization of single crystals with the different impurities: supersaturation, mass of paracetamol, solvent and impurities used relative to 1mg of paracetamol.	173
Table 23 Crystallization procedure for single crystals prepared in this work.....	175
Table 24 Solubility of paracetamol related impurities used in this work in ethanol at 25, 40 and, 55°C.....	179

Table 25 Crystal lattice parameters, volume and lattice systems for PP, PN and P4%N.	180
Table 26 Stereomicroscopic images of the different crystal examined in this work: paracetamol crystal (PP), 4-nitrophenol crystal (PN), cooling crystallization crystal of paracetamol in presence of 4-nitrophenol (P4%N), pure paracetamol crystal with drops of 4-nitrophenol solution (PDN) and pure paracetamol crystal with 4-nitrophenol crystal epitaxial growth (PEN). Scale bar corresponds to 10mm	182
Table 27 Characteristic neutral fragment mass spectra peaks of paracetamol and 4-nitrophenol taking from NIST 08 MS Demo and AMDIS 2.6.	194
Table 28 Table of factors, responses and analytical techniques used to quantify the responses in the first DoE.	223
Table 29 Table of factor for pre-settling DoE (second DoE).	225
Table 30 Fixed parameters and variables of the third DoE.	226
Table 31 Paracetamol solubility in the three different crystallization solvent used for this work.	228
Table 32 Paracetamol solubility in the different wash solvent used for this work.	228
Table 33 Geometric coefficient K and contact angle for the three saturated solutions of crystallization solvent. The contact angles for ethanol and 2 propanol where calculated using the K value determined for isoamyl alcohol solution.	229
Table 34 True density value of micronised, powder and granular paracetamol.	230
Table 35 Pure solvent density and viscosity (*Detherm database ⁶⁰) and mother liquor viscosity calculated with the GV500 viscometer.	230
Table 36 Cake resistance and medium resistance for experiments where filtration followed by reloading the filtrate and filtering using a slurry made with 30% V/V of micronized paracetamol in isopropanol and filtered at 900mbar driving force (the data correspond to the Darcy plot shown in Figure 9).	240
Table 37 Literature values of boiling point, enthalpy of vaporization, viscosity, density and surface tension of the solvent used as wash and crystallization solvents. ⁶⁷⁻⁶⁹	250
Table 38 Residual moisture content consistency between experiments replicas determined at the end of filtration and deliquoring but prior to drying.	251
Table 39 Variables and set points for the centre point experiments of the DoE.	261
Table 40 ABI index and extent of agglomeration values of some of the experiments of the DoE.	266
Table 41 x10, x50, x90, SMD and VDM values of few samples determined at 0.5bar and 4bar to determine particles stability under different feeding pressure of the QICPIC.	273
Table 42 Ideal isolation parameters to minimize increase of agglomerates and PSD of single particles and formation of soft agglomerates.	274
Table 43 Residual wash and crystallization solvent remained in cake after drying and drying time related to the nature of wash solvent.	275
Table 44 Mechanical properties of agglomerates produced from second DoE.	276
Table 45 Experimental conditions.	320
Table 46 Design of experiment factors and responses selected to investigate a multivariable problem.	322

Table 47 Cake and filter medium resistance values calculated using Darcy's equation to analyse the data collected in experiments 2 and 4, conducted using the Biotage and CFD20 systems.	328
Table 48 “Antisolvent screening” to determine suitable wash solvent mixture for washing 1 to prevent nucleation of particles from mother liquor and reduce paracetamol dissolution. In bold the ratio of crystallization solvent, while not in bold the ratio of wash solvent used.	331
Table 49 Solubility by equilibration of paracetamol in ethanol and hexane and 4-nitrophenol in ethanol and hexane.	368
Table 50 Experiments parameters of the cake shown in Figure 80 and Figure 81 of the main manuscript.	399

Papers published and conference attended

Conference Proceedings:

- Investigating the isolation performance of a novel continuous filtration unit for pharmaceutical process development and manufacturing: A case study using paracetamol and related impurities. Sara Ottoboni, Muhid Shahid, Christopher Steven, Elizabeth Meehan, Alastair Barton, Paul Firth, Richard Sutherland, Andy Mitchell, Furqan Tahir, Chris Price; FiltCon 2018, 24th – 25th April, 2018, Prior Lake, MN, USA

Conference presentation:

- The impact of paracetamol impurities on face-specific properties: investigating the surface of single crystals using TOF-SIMS. Sara Ottoboni, Michael Chrubasik, Layla Mir Bruce, Hien Nguyen, Blair Johnston, Alastair Florence, Chris Price; 12th International Workshop of the Crystal Growth of Organic Material & 47th Annual British Association of Crystal Growth Conference Joint Conference, 26th-30th June, 2016, University of Leeds, UK
- Development of a novel continuous filtration unit for pharmaceutical process development and manufacturing: A case study using paracetamol. Sara Ottoboni, Chris John Price, Christopher Steven, Elizabeth Meehan, Alastair Barton, Andy Mitchell et al.; FILTECH 2016, 11th-13th October, 2016, Cologne, Germany
- Investigating the isolation performance of a novel continuous filtration unit for pharmaceutical process development and manufacturing: A case study using paracetamol and related impurities. Sara Ottoboni, Muhid Shahid, Christopher

Steven, Elizabeth Meehan, Alastair Barton, Paul Firth, Richard Sutherland, Andy Mitchell, Furqan Tahir, Chris Price; FiltCon 2018, 24th – 25th April, 2018, Prior Lake, MN, USA

Contribution to conference presentation:

- Addressing the Challenges of Continuous Filtration, Washing and Drying. Chris Price, Sara Ottoboni; CM2017 Adoption of Continuous Manufacturing in the Pharmaceutical Industry - International Industrial, Regulatory and Academic Workshop Dublin Feb 2017
- Continuous Filtration Washing & Drying: Addressing a Critical Gap in Developing Continuous Pharmaceutical Manufacturing Processes. Chris Price, Sara Ottoboni, Christopher Steven, Paul Firth, Alastair Barton; RSC Conference, Chem Spec Munich May 2017
- Developing a Strategy to Optimise Active Pharmaceutical Ingredient Filtration and Washing. Chris Price, Sara Ottoboni, Muhid Shahid. FiltCon 2018, 24th – 25th April, 2018, Prior Lake, MN, USA
- Developing a Platform for Continuous Filtration. Chris Price, Sara Ottoboni, Paul Firth and Alastair Barton; Continuous Manufacturing Today: Taking the Pulse of Emerging Technology International Society for Pharmaceutical Engineering, Continuous Manufacturing Workshop 6th – 7th June 2018, Arlington, VA, USA.

Conference poster:

- Development of a novel continuous filtration unit for pharmaceutical process

development and manufacturing: modelling and experimental approach to estimate cake properties. Sara Ottoboni, Chris Price, Christopher Steven, Elizabeth Meehan, Alastair Barton, Paul Firth, Andy Mitchell, Furqan Tahir; APM Forum 2017, 25th -26th April, 2017, London, UK

- Investigating the isolation performance of a novel continuous filtration unit for pharmaceutical process development and manufacturing: A case study using paracetamol and related impurities. Sara Ottoboni, Muhid Shahid, Christopher Steven, Elizabeth Meehan, Alastair Barton, Paul Firth, Richard Sutherland, Andy Mitchell, Furqan Tahir, Chris Price; FiltCon 2018, 24th – 25th April, 2018, Prior Lake, MN, USA (Conference poster presentation first prize).

Peer reviewed journal papers:

- The impact of paracetamol impurities on face-specific properties: investigating the surface of single crystals using TOF-SIMS. Sara Ottoboni, Michael Chrubasik, Layla Mir Bruce, Hien Nguyen, Blair Johnston, Alastair Florence, Chris Price; Crystal Growth and Design 2018, 18, 2750-2758
- Development of a novel continuous filtration unit for pharmaceutical process development and manufacturing. Sara Ottoboni, Chris Price, Christopher Steven, Elizabeth Meehan, Alastair Barton, Paul Firth, Andy Mitchell, Furqan Tahir; Accepted 07/2018 and selected for inclusion in the Special Topic Issue of the Journal of Pharmaceutical Sciences which will be published as the January 2019 issue
- Understanding effect of filtration and washing on dried product. Paracetamol case study. Sara Ottoboni, Martin Simurda, Samantha Wilson, Andrew Irvine, Fraser Ramsay,

Chris Price. (Submitted 08/2018 to OPR&D)

1 Introduction

Purification by isolation is a key step in chemical production because it achieves removal of impurities generated during synthesis. Various components, including residual solvents, trace amounts of inorganic, and organic components can be incorporated into the process during the synthesis. Those components remaining in the final Active Pharmaceutical Ingredient (API) are considered as impurities. According to the International Conference on Harmonisation (ICH) Guidelines¹; impurities are defined as any components present in the drug substance that are not the chemical entity defined as the drug substance. Possible API impurities are starting materials, by-products and residual solvents from the API synthesis, degradants formed during processing and on long-term storage, contaminants from packaging components and other drug products manufactured in the same facility. Therefore, after synthesis, purification processes are required to remove as far as practicable all the impurities formed during synthesis. Sometimes impurities must be removed due to their hazardous nature (carcinogenic, teratogenic, etc.). In case of impossibility of removal alternative synthesis approach must be considered. Purification is mainly divided into two different steps: crystallization; and filtration followed by washing and drying, named as isolation. Crystallization is the first purification step, which produces API crystals with high purity and with defined crystal properties, such as particle size distribution (PSD), shape, etc. Crystallization, however, can only provide impurity segregation by collecting mainly the desired molecules into the crystal and leaving most of the impurities in the mother liquor. So a second step of purification after crystallization, filtration, is required to remove mother liquor and to wash the crystal surfaces prior to drying. Drying step is used to remove/reduce residual solvent trapped between particles to get a dried/semi-dried product. Dried material is

required to guarantee the stability of material during storage, to avoid degradation, change in particles size, polymorph due to residual solvent trapped in the material.

During filtration, a suspension of solid and liquid is separated using a mesh or cloth to collect the solid part, while the liquid is removed by passing through the mesh medium.² Filtration theory is expressed in Darcy's law that describes the flow of a fluid through a porous media. Equation 1 shows Darcy's law for constant pressure³

$$\frac{dV}{dt} = \frac{A^2 \Delta P}{\mu (\alpha_{av} cV + AR_m)} \quad (1)$$

Where ΔP ($\text{kg m}^{-1} \text{s}^{-2}$) is the pressure drop along the filter axis, A (m^2) is the filter area, μ ($\text{kg m}^{-1} \text{s}^{-1}$) is the filtrate viscosity, α_{av} (m kg^{-1}) the specific cake resistance is related to the cake filterability, R_m (m^{-1}) is the filter medium resistance and c (kg m^{-3}) is the dry cake mass per unit volume of filtrate. This equation evaluates the physical properties of slurry, but excludes all the possible chemical interactions that can occur between API, impurities and solvents during filtration process. This exclusion of chemical aspects and lack of consideration of the role of washing in impurity removal will be investigated in the purification and isolation aspects of this thesis.

These two lines of investigation, chemical interactions and wash solvent selection are studied to link together slurry physical and chemical properties in order to optimize the filtration process to obtain consistent pure particles. This project is focused on improving isolation knowledge to reduce risks of crystal modification occurring during and after filtration (agglomerations, breakages, reduction of crystal purity, polymorphic changes,

etc.) and to maintain the crystal properties generated during crystallization. This research forms part of a wider continuous isolation research program, the research reported in this thesis focuses on evaluating crystal, solvent and impurity properties at a molecular and microscopic scale and linking them with equipment parameters to create a “robust” and “efficient” method to determine impurity removal performance during a filtration process.

During isolation process, a variety of parameters influences process performance and product crystal purity. Evaluating the surface properties of crystals allows the role of their chemical characteristics to be considered in the adsorption and desorption of impurities or solvents on the crystal faces.

Today, in the chemical industry, solvents are used in large quantities. In particular, in fine-chemical and pharmaceutical production, large amounts are used per unit mass of final products produced.⁴ Organic solvents are commonly used in the pharmaceutical industry as reaction media, in separation and purification of synthesis products, during the secondary processes and formulation, during packaging and also for cleaning of equipment.⁵ Therefore, solvents constitute a major part of the environmental impact of a process, they also affect cost, safety and health^a. Traditional solvents are mostly toxic and once contaminated with impurities are not readily recyclable (less than 50% of solvent used in pharmaceutical manufacturing is recycled and reused).⁶ According to the USA

^a Residual solvent in the final drug product must be considered as impurity. For toxicological reasons and the possibility that residual solvent can accelerate the compound degradation, manufacturer try to minimize the number and amount of solvents used during the drug manufacturing.⁴

Environmental Protection Agency (EPA), pharmaceutical companies produced 530 million tons of toxic waste in 2005 and 90% of that waste was made of 20 solvents (methanol, dichloromethane, formaldehyde, toluene, acetonitrile, hexane, isopropanol, n-butyl alcohol, tert-butyl methyl ether, xylene, trichloroethane, ethanol and tetrahydrofuran).⁶ Solvent use accounts for the 80-90% of mass waste produced in a pharmaceutical process.⁶ This means that pharmaceutical companies incur significant costs to buy, use and dispose of used solvents. The estimation of the impact of solvents have on different operation is around 75-80% of plant energy usage and 75-80% of the overall environmental impact.

Reducing the amount of solvent used during the isolation step and possibly moving to a green solvent would reduce this industrial sector's environmental footprint.

The ultimate objective of this study is to understand and to support the selection of optimal isolation conditions and designing equipment to achieve this continuously.

2.1 Abbreviations

API, Active Pharmaceutical Ingredient, ICH, International Conference on Harmonisation, PSD, particle size distribution, EPA, Environmental Protection Agency.

References

1. U. S. Department of Health and Human Services, Food and Drug Administration, Center for Drug Evaluation and Research (CDER), Center for Biologics Evaluation and Research (CBER). Q3D Elemental Impurities, Guidance for Industry. ICH, 2015.
2. Tien, C. Principle of Filtration. Elsevier, 2012.
3. Wakeman R., 2007. The influence of particle properties on filtration. Sep. Purif. Technol., 234. Cue, B.W., Zhang, J., 2009. Green process chemistry in the pharmaceutical industry. Green Chemistry Letters and Reviews 2, 193.

4. Kolář, P., Shen, J.-W., Tsuboi, A., Ishikawa, T., 2002. Solvent selection for pharmaceuticals. Fluid Phase Equilibria, Proceedings of the Ninth International Conference on Properties and Phase Equilibria for Product and Process Design 194.
5. Wdfile website http://igss.wdfiles.com/local--files/kundai-marimira/KM_Solvents-web.pdf [cited 2018-08-05].

2 Literature review

2.1 Introduction

Pharmaceutical production can be divided in five main steps:

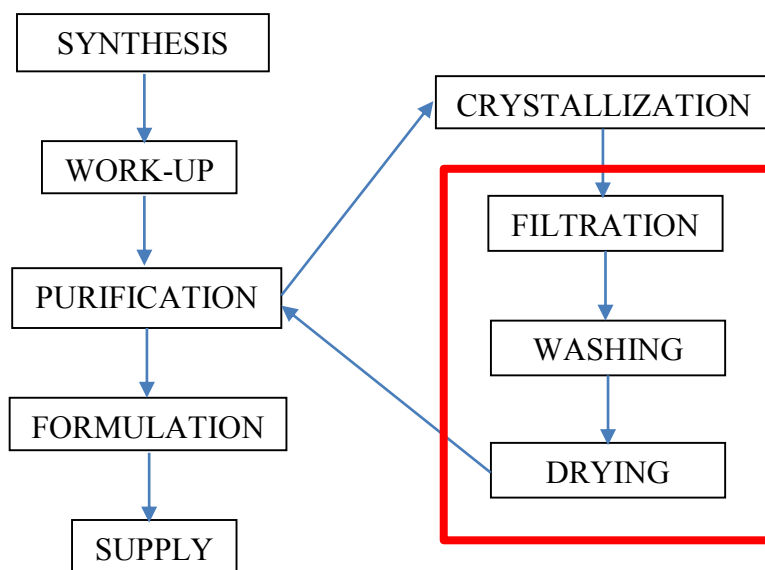


Figure 1 Pharmaceuticals manufacturing stages.

As seen in Figure 1, pharmaceutical manufacturing starts with API molecule synthesis, follows by the work-up step that refers to the series of manipulations required to isolate and purify the product(s) of a chemical reaction. Typically, these manipulations may include: quenching, cooling, precipitation, filtration, decantation, or centrifugation, solvent removal, extraction and purification. These procedures may not deliver an API which is suitable pure for formulation, so a further purification step may be required. The most widely used purification step is crystallization. Purification comprise crystallization, filtration, washing and drying. The focus of this thesis is the study of the filtration, washing and drying components.

Crystallization¹ is a purification technique and a separation process where an ensemble of randomly organized molecules, ions, or atoms in a fluid come together to form an ordered 3D molecular crystal. This purification method is one of the most reproducible isolation techniques inasmuch that similar crystals with consistent shape and size may be obtained by fixing appropriate operating conditions.

The process for creating a new solid phase from a solution is called nucleation.

Nucleation may occur spontaneously or it may be induced artificially. However, sometimes it is not possible to decide whether a system has nucleated spontaneously or if it has done so under the influence of some external stimulus.

Possible stimuli that may induce nucleation include agitation, cooling, evaporation,² adding an antisolvent,^{3,4} by chemical reaction,⁵ mechanical shock, friction, extreme pressure, electric or magnetic field, spark discharges, ultra violet light, X-ray, γ -ray, sonic, ultrasonic irradiation⁶⁻⁸ or cavitation applied to a solution.

Nucleation can be classified as primary nucleation if the system contained no crystalline matter (homogeneous) or particulate contamination (heterogeneous) prior to nucleation. The term of secondary nucleation describes the phenomenon of nucleation that occurs when the solution already has crystals present for example if seed crystals were added.^{2,9}

Industrially secondary nucleation is preferred to primary because it can be controlled to obtain the required product crystal properties by changing different parameters, such as temperature, concentration of solute into the solution, solvent composition, mixing, cooling rate and impurity loading and solution history.

Two different approaches and equipment types are used to crystallize pharmaceutical compounds: batch crystallization and continuous crystallization.

Continuous crystallization has been identified as a key element in improving manufacturing in the chemical and pharmaceutical industries, through more efficient use of reagents, solvents, energy and space whilst minimizing the production of waste materials and reactor downtime for reactor maintenance and cleaning. The drawback of this technology is that to obtain the product required, a large body of experimental data is needed to design and optimize the process in order to correctly set all the process parameters.¹⁰

Batch crystallizers are very widely used. They are simple, flexible, and require less capital investment than continuous units. Continuous crystallizers are usually purpose-built for a specific application, batch crystallizations tend to be carried out in a multipurpose plant, where the same vessel can be used for different processes.¹

2.2 Classic filtration theory

Filtration is a solid-liquid mixture (slurry) separation method that forces the slurry to flow through a filter media¹¹ in order to obtain at the end of the process a liquid filtrate free or nearly free of particles and a solid phase with a significantly reduced liquid content.

Over the years different research groups have investigated dynamics of filtration.¹²⁻¹⁷ The first was Ruth (Ruth, 1946)¹⁸; subsequently other researchers tried to model the filtration process.¹⁹

By applying pressure or vacuum, a solid/fluid suspension is forced to pass through a porous medium, which collects the solid part of the suspension on the upstream side of the medium and removes the liquid part. During filtration, particles of solid are deposited on the filter medium forming a filter cake. As time passes the cake thickness increases and the cake becomes more compacted increasing the resistance to fluid flow through it.

Different models to interpret the dynamic behavior of cake, the evolution of the cake structure and the history of the total filtrate in relation to set parameters are examined below.

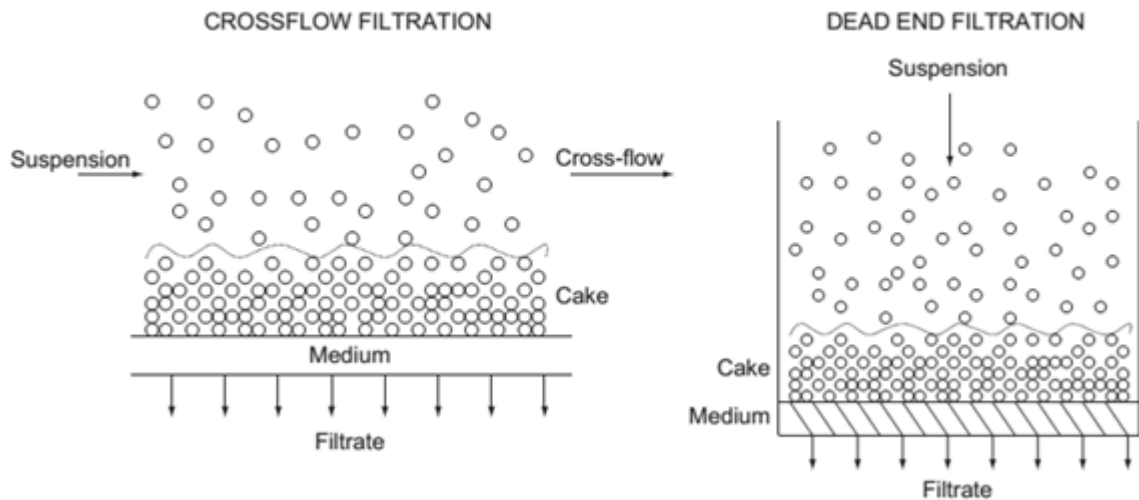


Figure 2 Crossflow filtration vs dead end filtration.¹¹

Cake filtration is classified in accordance with the slurry flow configuration as either dead end filtration or cross flow filtration (Figure 2).

Dead end filtration is the most common method of filtration. The slurry, with known composition (ϵ_{s0} is known as the solid fraction of the slurry), is placed in a pressurized chamber, where P_0 is the initial pressure applied to the system; a pressure drop is applied across the filter medium and the suspension s forced to move toward the medium, which allows the flow of the liquid but retains the solids. Consequently, a cake of solid particles is formed on the top of the medium as the filtrate passes through and its thickness $L(t)$ increases with time. During this process the cake continuously changes its structure due to compressive stress and these changes are estimated as change in local solidosity and local permeability (k); these changes in cake compaction affect the flow of the liquid through the cake and therefore the cake growth rates.¹⁹ Dead end filtration can be studied by using different models, but the simplest model is the conventional cake filtration theory (Figure 3).²⁰

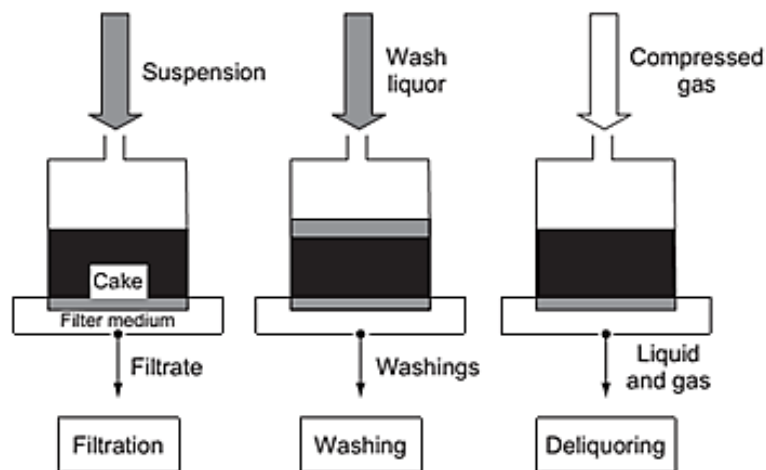


Figure 3 Different operations involved in cake filtration process: filtration, washing and deliquoring.¹¹

On the other hands, cross flow filtration is considered a continuous filtration operation because as shown in Figure 3 during one filtration cycle the slurry is filtered, the cake is washed, dried and discharged, and this process being repeated as the drum rotates.

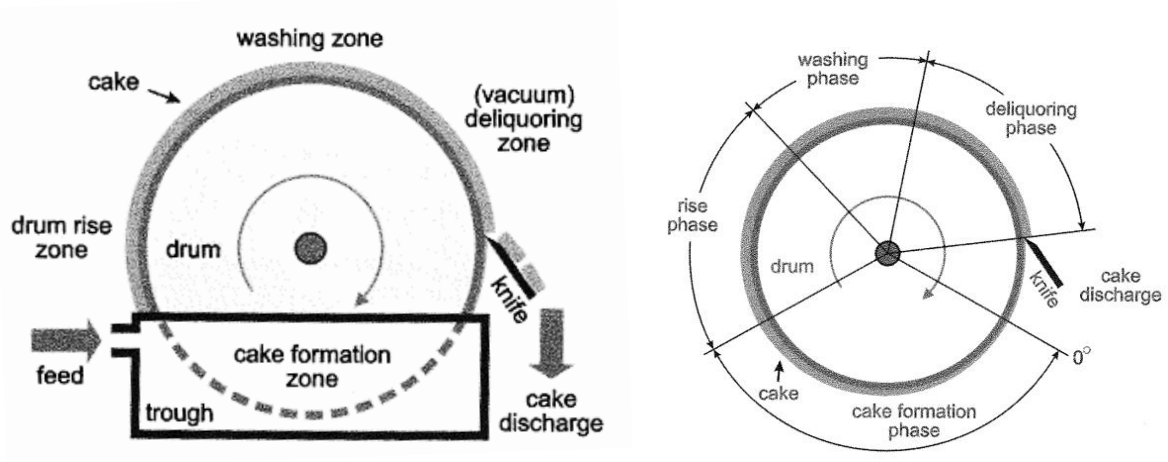


Figure 4 Crossflow filtration equipment schemes Figure on the left represent the evolution of cake formation during the different stages of filtration (cake formation zone, washing zone and cake discharge). Figure on the right represents the different stages of a crossflow filtration and cake thickness evolution.²¹

A drum filter is an example of a cross flow filtration unit, it is made of an inner filter encased in an outer cylinder. The process starts when slurry is conveyed into the outer cylinder where it is retained at a constant level by an offtake weir; the rate of flow from the source vessel is controlled such that the level is maintained by the offtake weir and there is always an overflow back to the source vessel and the flow in the system is sufficient to keep the particles suspended. Vacuum is applied to the inside of the rotating drum and this causes filtrate to flow through the medium where it is withdrawn to be collected in the filtrate waste solvent tank. Due to the combination of medium rotation and vacuum, solid is deposited on the medium surface whilst the medium surface is

submerged in the feed suspension. As the drum rotates the cake begins to deliquor and air or nitrogen passes through it. When cake reaches the wash station, a flow of wash solvent is gently distributed across cake surface, it is drawn through the cake in order to remove mother liquors which contain impurities that were rejected during crystallization. The wash solvent is removed by vacuum. Finally, the washed and partially dry cake encounters a blade which removes the solid from the medium.²²

2.2.1 Dead end conventional cake filtration

Conventional filtration theory describes the relevant continuity equations, the closing relationship and the appropriate initial boundary and moving boundary conditions^{23,24} of a filtration process. In Figure 5 schematic representation of mono-dimensional cake formation is evaluated, taking in consideration all the materials flows and variation of pressure due to the separation of solid and liquid phases and cake formation. The equation reported below (Tien, 2012) is derived in the approximation of a 2D approach and is widely used in classical filtration theory used to explain correlation of filtration parameters with cake and media resistance and filtration flow rate. The equation used in this work instead, reported in 2.6^{11, 20} are more suitable for the study presented here. Symbols reported in these equations will be defined in Table 2.

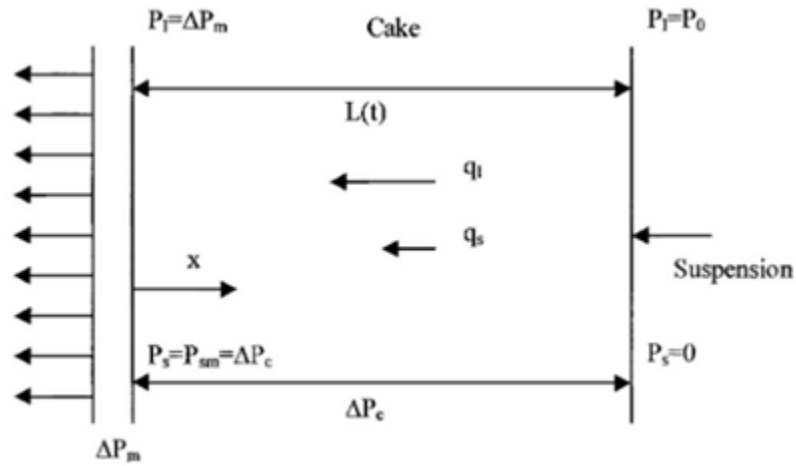


Figure 5 Scheme of cake filtration process.²⁰

The continuity equations of the liquid and particle phases are (Darcy's equation):

$$\frac{\partial q_l}{\partial x} = -\frac{d\varepsilon_s}{dt} \text{ for } 0 \leq x \leq L(t) \quad (2)$$

for liquid phase, and

$$\frac{\partial q_s}{\partial x} = -\frac{d\varepsilon_s}{dt} \quad (3)$$

for solid suspension phase.

The local fluid and solid superficial velocity, q_l and q_s are related by the following expression:

$$\frac{q_l}{1 - \varepsilon_s} - \frac{q_s}{\varepsilon_s} = \frac{1}{1 - \varepsilon_s} \frac{k dp_l}{\mu dx} \quad (4)$$

In a general case where the cake obtained during filtration is compressible, the cake structure (expressed by ε_s and k) are function of the compressive stress and to the pore liquid pressure:

$$\varepsilon_s = \varepsilon_s(p_s) \quad (5)$$

$$k = k(\varepsilon_s) \quad (6)$$

$$p_s = p_s(p_l) \quad (7)$$

Conventional filtration theory can produce a solution describing this system when certain assumptions related to liquid and solid flow and solid properties are met:

- The solid phase velocity (q_s) is negligible and the fluid velocity is constant throughout the cake at any instant
- Filter cake solidosity, permeability and specific cake resistance are functions of the compressive stress only, as mention in Equations 5 and Equation 6
- The moving boundary effect of the cake-suspension interface is negligible. Cake resistance, α , is dependent to p_s and this can be determined experimentally from filtration tests¹⁷ or by using the compression-permeability cell measurements.¹²

Both papers describe the relationship between the key filtration parameters ε_s , k and α , where these values are functions of some empirical constants related to the material characteristics:

$$\varepsilon_s = \varepsilon_s^0 \left(1 + \frac{p_s}{p_a}\right)^\beta \quad (8)$$

$$k = k^0 \left(1 + \frac{p_s}{p_a}\right)^{-\delta} \quad (9)$$

$$\alpha = \frac{1}{\varepsilon_s \rho_s k} = \alpha^0 \left(1 + \frac{p_s}{p_a}\right)^n \quad (10)$$

Where

$$\alpha^0 = (\varepsilon_s^0 k^0 \rho_s)^{-1} \text{ and } n = \delta - \beta \quad (11)$$

In general n and β are the parameter that evaluate the degree of compressibility; these two values can be used to determine cake deliquorability degree. Indeed, the literature reports three different level of cake compressibility that are defined based on the value of n :²⁵

- Low and moderately compressible, $n < 1$ ²⁶
- High compressible, $n > 1$ ²⁶
- Extremely compressible, $n \gg 1$.²⁷

The border between high and extreme compressibility is not well defined but n values for high compressible solid are typically reported in the interval of 1-2.^{28,29}

The empirical coefficient β is correlated to the degree of compressibility and it indicates the relative contribution of surface filtration to solid-liquid separation; in other words, the more concentrated the slurry, the smaller the contribution of surface filtration, while the higher the effect of cake thickness and the smaller β value are obtained.²⁵ In general pharmaceutical cakes are low-moderately compressible

- The filter cake is isotropic; this assumption is invalid where the cake behaves as an anisotropic system. Cake behaves differently in the bulk or near the walls: walls interact with cake sedimentation causing formation an anisotropic radial porosity that consequently influence the mean liquid flowability properties^{15, 29}

- Sum of cake liquid and solid pressure are equal to p_0 , that is the operating pressure

$$(P_0 = \Delta p_0 + \Delta p_m)$$

Liquid and solid velocity are evaluated as constant, as shown in Equation 12,

$$q_l + q_s = \text{const} \quad (12)$$

However, if the medium is permeable only by the liquid, q_{lm} is evaluated as the constant value

$$q_l + q_s = q_{lm} \quad (13)$$

Cumulative filtrate volume variation (m^3/m^2) with respect to time is evaluated as followed:

$$\begin{aligned} q_{lm} &= \frac{dV_{cum}}{dt} = \frac{\Delta p_c}{\mu s \rho (1 - m_{av} s)^{-1} \alpha_{av} V_{cum}} = \frac{\Delta p_m}{\mu R_m} \\ &= \frac{P_0}{\mu s \rho (1 - m_{av} s)^{-1} \alpha_{av} V_{cum} + \mu R_m} \quad (14) \end{aligned}$$

The value of m_{av} appearing in these equations are based on the average cake solidosity $\bar{\epsilon}_s$ where this parameter is defined as a function of cake thickness, or time.

Commonly solidosity profile is difficult to determine, therefore usually this value is approximated with the stress-average value of ϵ_s , that is $\bar{\epsilon}_s$

The conventional filtration theory can evaluate two mechanism of filtration:

- Constant-pressure filtration: where the operating pressure is constant during the process; this is the easiest mechanism of filtration, usually used during filtration

lab and large scale processes. For its simplicity this is the filtration mechanism used during this work

- Constant-rate filtration and variable pressure rate filtration are rarely encountered in the laboratory and are not very frequently encountered in industrial filtration. In this method the flow rate of the liquid removed during filtration is maintained constant during the filtration.^{30,31}

Conventional filtration theory does not fit well with experimental results in some circumstances. Therefore, different researchers have proposed alternative models to improve classical filtration theory's to match models with real data. For instance, different models were proposed (Table 1).

Table 1 Different models proposed in literature to improve filtration theory.

Model proposed	Reference
Estimate pressure drop across filter cake	20
Address the previous assumption that solid phase velocity is considered as negligible and liquid velocity is constant	20, 32, 33
Evaluate hydraulic-pressure distribution	20
Estimate solidosity profile, average solidosity and wet cake to dry cake mass ratio	19, 20, 34-36
Correlate filtrate volume vs t and thickness vs t	39-42
Estimate cake porosity or solidosity, and cake permeability	23
Estimate cake resistance	18, 43

Alternative method to determine filtration resistance	11, 37, 38
Characterise Wall friction	15, 29, 42
Estimate the effect of particle shape on the cake structure	37
Estimate the effect of fine particle penetration into the cake	44
Determine fine particle penetration into the filtration media	45
Consider clogging effects during filtration	23
Evaluate expression and compaction of cake during the deliquoring process	24, 27, 46

2.2.2 Cross flow conventional cake filtration

Tien described crossflow filtration performance based on the conventional cake filtration theory.¹¹ Filtration velocity is evaluated as follows, where the relationship of pressure between liquid and solid is evaluated as $dp_l + dp_s = 0$.

$$\frac{dV_{cum}}{dt} = \frac{p_0}{\mu[w(\alpha_{av})\Delta p_c + R_m]} \quad (15)$$

The major difference between dead end and crossflow filtration is that in dead end filtration all the particles in the suspension are going to be deposited onto the filter media, while for crossflow filtration only some of the particles in suspension will be deposited on the filter media. In general, this effect is dependent to the particle size: for smaller particles the flow of the liquid from the slurry to the filter media cause the anchoring of particles to the filter (convection forces, F_Y , and Van der Waals adhesion forces, F_A , higher

than drag forces, F_D , and lift forces, F_Y , responsible to particles removal from the filter).⁴⁷,

48

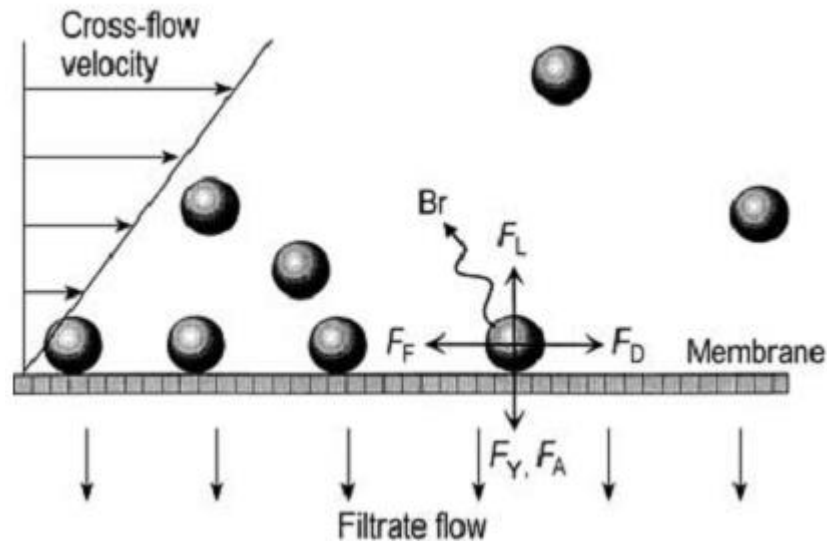


Figure 6 Forces and transport effects onto a particle in cross-flow filtration.⁴⁸

$$dV_{cum} = \frac{1 - s[(m - 1)\beta + 1]}{\beta s \rho} dw + \frac{w}{\beta s \rho} d(m - 1) \quad (16)$$

During the course of filtration, β cannot be a constant, but varies with time unless filtration proceeds with a filtration velocity less than the critical flux^b, which can be expected to

^b The flux of particles contacting the media at the beginning is not constant, but vary with time, unless the filtration velocity is less the critical flux. A threshold filtration velocity exists (critical flux), below which particle deposition is not occurring. This critical flux is the term that fix the beginning of the steady state and the beginning of cake formation on the filter media.

increase with the decrease of particle size. The steady-state filtration velocity $(dV_{cum}/dt)_{steady}$ that is the velocity of filtration at equilibrium condition is calculated as

$$\left(\frac{dV_{cum}}{dt}\right)_{steady} = \frac{p_0}{\mu s \rho(\alpha_{av}) \int_0^{t_c} \frac{\beta \left(\frac{dV_{cum}}{dt}\right)}{1 - s[(m-1)\beta + 1]} dt + \mu R_m} \text{ for } t > t_c \quad (17)$$

This theory does not fit well with experimental results when the input particle size is too different from the medium pore size. Indeed, when the particle size of the feed particles increase, the cake thickness increases. A higher solids throughput and deliquoring air flow rate, lower cake moisture contents, and more solutes and liquid in the discharged cake are obtained. Moreover, the smallest particles migrate during cake formation to be close to the filter medium, causing an increase in filter cake resistance and a decrease of filtration, washing and deliquoring rates. To verify cross flow filtration model different material PSD are evaluated.^c

Moreover, PSD shows a strong influence on filtration performance. According with the sedimentation theory bigger particles firstly deposit to filter medium, followed by the smallest particles that penetrate the cavity left by the cake formed with big particles and tend to migrate during cake formation near the filter medium, causing an increase in filter cake resistance and a decrease of filtration, washing and deliquoring rate. Smaller pore

^c In a concentrated suspension particles can directly interact with each other. Direct interactions influence the spatial distribution of particles. Another phenomenon related to direct interaction between particles is the build-up of stress when a bed of particles is compressed and subsequent release of stress when the pressure is removed. Particle network stress in a suspension is therefore evaluated as the sum of all the interaction that can occur between near particles.

size in a filter cake increase the capillary pressure in the cake, leading to the requirement of higher deliquoring pressures to displace liquid from the cake.³⁴⁻³⁶

In general specific cake resistance of a filter cake is defined as the resistance of fluid to pass through the cake; this parameter is inversely related to cake permeability:

$$\alpha_{av} = \frac{1}{\rho_s(1 - \varepsilon)k} \propto \frac{1}{x_{sv}^2} \quad (18)$$

Therefore cake resistance is inversely related to the square of particle size. In accordance to Carman-Kozeny equation, cake resistance is related also to cake porosity:

$$\alpha_{av} = \frac{180(1 - \varepsilon)}{\rho_s x_{sv}^2 \varepsilon^3} \quad (19)$$

Porosity is independent to particles size, but it is a function of particles size distribution, as explained above. Other approaches are used to determine cake resistance in accordance to the particles PSD and to the shape of particles.³⁴⁻³⁶

Particles shape primarily affects the volume and surface area of the particles, causing variations in cake permeability and fluid flowability (blinding or the filter).⁴⁹

The limit of the approximation used in these models are:

- Cake resistance is calculated using as particle size, the sauter mean value, while a real cake system is formed by particles that show a size distribution. This approach simplify the calculation of the cake resistance without considering that a cake formed with a system of particles presenting a size distribution (not mono-

dimensional particles size). This will result in a variation of cake resistance along the cake height due to migration of fines particles in proximity of the filter media during filtration. Fines migration generates a reduction of cake porosity with consequent increase of cake resistance.

- Carman Kozeny equation does not consider particles aspect ratio as parameter that affects cake resistance. As reported by Jim (2015),³⁶ shape and texture of particles can be represented by a fractal structure; considering the real texture and shape of particles bring to a more accurate evaluation of cake resistance. However, the use of fractal theory to determine shape of particles massively increases the computational time to calculate the real particle shape. Another approach to use to include particles aspect ratio is the use of the aspect ratio distribution instead of the use of the mean aspect ratio value proposed by Yelshin (2002)⁵⁰.

$$\alpha_{average} = \frac{36 k (1 - \varepsilon)}{\rho_s x_{sv}^2 \varepsilon^3} = \frac{36 k_0 T^2 (1 - \varepsilon)}{\rho_s x_{sv}^2 \varepsilon^3} \quad (20)$$

Symbols are summarized in Table 2, Table 3 and Table 4.

Table 2 Dead end filtration theory parameters.

Symbol	Parameter	Unit measure
X	distance away from the medium	m
T	time	s
ε_s	local cake solidosity	-
q_l	local fluid velocity	m/s
q_s	solid superficial velocity	m/s

k	local cake permeability	m^2
μ	fluid viscosity	$Kg/(ms)$
p_l	pore liquid pressure	$Kg/(ms^2)$
p_s	compressive stress	$Kg/(ms^2)$
$\varepsilon_s^0, k^0, \alpha^0, \beta, \delta$ and P_a	empirical constants related to the material characteristics	-
Δp_c	pressure drops across cake	$Kg/(ms^2)$
Δp_m	pressure drops across medium	$Kg/(ms^2)$
$P_0 = \Delta p_0 + \Delta p_m$	operating pressure	$Kg/(ms^2)$
q_{lm}	liquid permeation velocity	m/s
S	mass fraction of particles of the suspension	-
P	liquid density	Kg/m^3
$m_{av} = \frac{[\bar{\varepsilon}_s \rho_s + (1 - \bar{\varepsilon}_s) \rho]}{(\bar{\varepsilon}_s \rho_s)}$	average wet to dry cake mass ratio	-
ρ_s	particle density	Kg/m^3
$\bar{\varepsilon}_s = \frac{(\int_0^L \varepsilon_s dx)}{L}$	average cake porosity	-
$\bar{\varepsilon}_s = \frac{1}{\Delta p_c} \int_0^{\Delta p_c} \varepsilon_s dp_s$	stress-average value of ε_s	-
$\alpha_{av} = \frac{\Delta p_c}{\left[\int_0^{P_0 - \Delta p_c} \left(\frac{1}{\alpha} \right) \left(-\frac{dp_l}{dp_s} \right) dp_s \right]}$	average of specific cake resistance	m/kg

Table 3 Cross flow filtration theory parameters.

Symbol	Parameter	Unit measure
B	fraction of particles transported to the membrane surface	-
δt	time of feed mass treated	s
$\delta[(m - 1)w]$	increase of the filtrate entrained with the cake over time	-
m	wet to dry cake mass ratio	-
$s = \frac{\frac{dw}{\beta}}{\frac{dw}{\beta} + d[(m - 1)w] + \rho dV_{cum}}$	feed mass treated over time	-
dw	cake mass per unit medium area	Kg/m ²
t_c	critical time where steady state is reached	s

Table 4 Filtration theory parameters: particles parameters affecting filtration.

Symbol	Parameter	Unit measure
x_{sv}^2	Square Sauter mean diameter	m ²
T	Tortuosity of the cake	-
k_0	Shape coefficient	-

2.3 Sedimentation theory

During settling of a suspension of fine particles, different forces influence the sedimentation process: the gravitational force, the viscous drag force related to the suspension viscosity and particle network stress due to the particle-particle interactions.^{51,}

52

Researches has been undertaken on particle sedimentation and consolidation phenomenon because it offers a way to characterize porous media structure and interaction between particles and to quantify the final amount liquid trapped.

Tiller and Hsyung (1995)⁵³ tried to evaluate the effect of cake sedimentation prior filtration. This is a paper where the concepts of sedimentation prior/during filtration and the consequences this has for cake resistance are clarified.

One of the causes reported in literature of the deviation of the parabolic relationship between volume of filtrate collected during time is the sedimentation of cake prior filtration.^{54, 55}

Sedimentation is closely related to the solid concentration in slurry: settling velocity (u_{sR}) can be evaluated as $u_{sR} = u_s - u_L$. As the solid concentration ϕ_s increases, there is a point where larger particles sedimentation is obstructed by the small particles present and the sedimentation velocity of all the particles becomes identical, so particles sedimentation is evaluated as a zone process. In Figure 7 the relative settling velocities (left) and relative flux (right) are presented as a function of the concentration. Compare with the ideal concept of sedimentation, no real boundary is observed between diffusion and settling

zone in real sedimentation experiments. Sedimentation stops when the cake is fully formed, but the continuation of filtration maintains a compression of the cake.

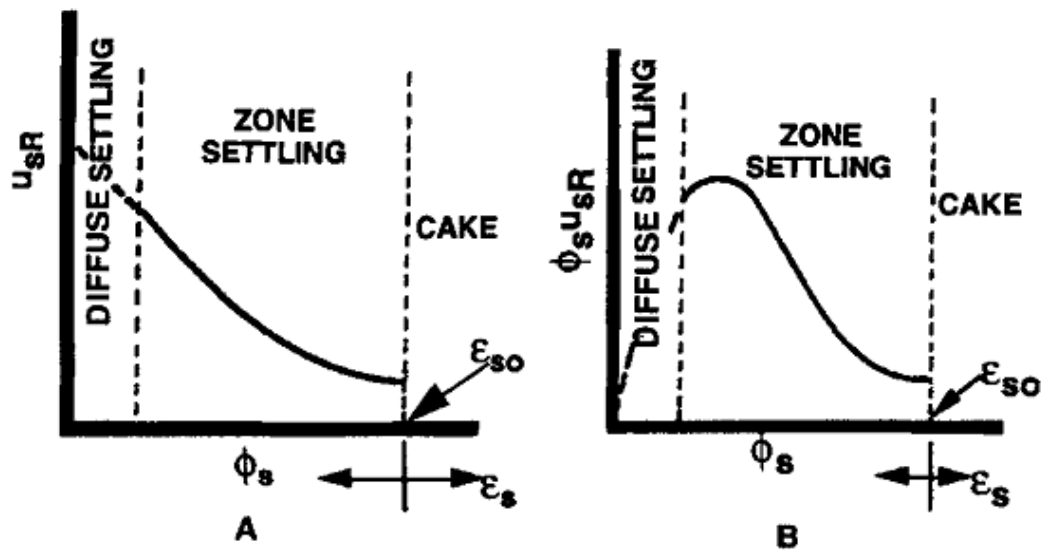


Figure 7 Relative settling velocities and relative flux as function of the solid concentration.⁵³

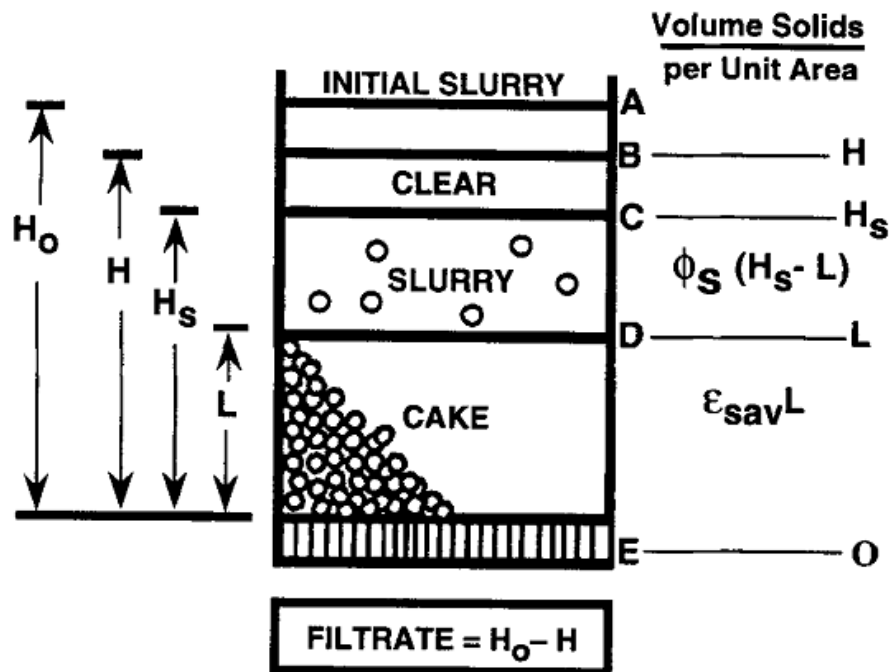


Figure 8 Scheme and quantities involved in filtration with sedimentation.⁵³

According to Tiller and Hsyung (1995)⁵³ filtration of a slurry in case of positive driving force can be evaluated as a series of stages (Figure 8):

- Slurry is introduced in the filtration chamber and pressure is applied on top of the slurry: initial slurry height is H_0
- By applying pressure, the liquid level drops to H and cake level is defined as H_s . From this observation, the classical filtration theory assumes that the solid velocity can be neglected. This fails to simulate a real filtration process; solidosity ϵ_s varies with distance and an average value can be evaluated, ϵ_{sav}
- As the cake builds on along the path ODC, cake resistance gradually increases; the slurry/clear surface interface can be evaluated as $H-H_s$, representing the relative settling velocity of the solid
- When H_s reaches D all the solid has settled and cake formation is completed.
- Clear liquid continues to pass through the cake until filtration is halted (dryland or breakthrough point); in this phase the liquid passage further compresses the cake increasing further the cake resistance until the filtration is completed.

In Tiller and Hsyung (1995)⁵³ study, relative settling velocities of liquid and solid during filtration were evaluated in real time by using X-ray tomography. From this analysis, the plot height vs filtration time of kaolin slurry was produced (Figure 9).

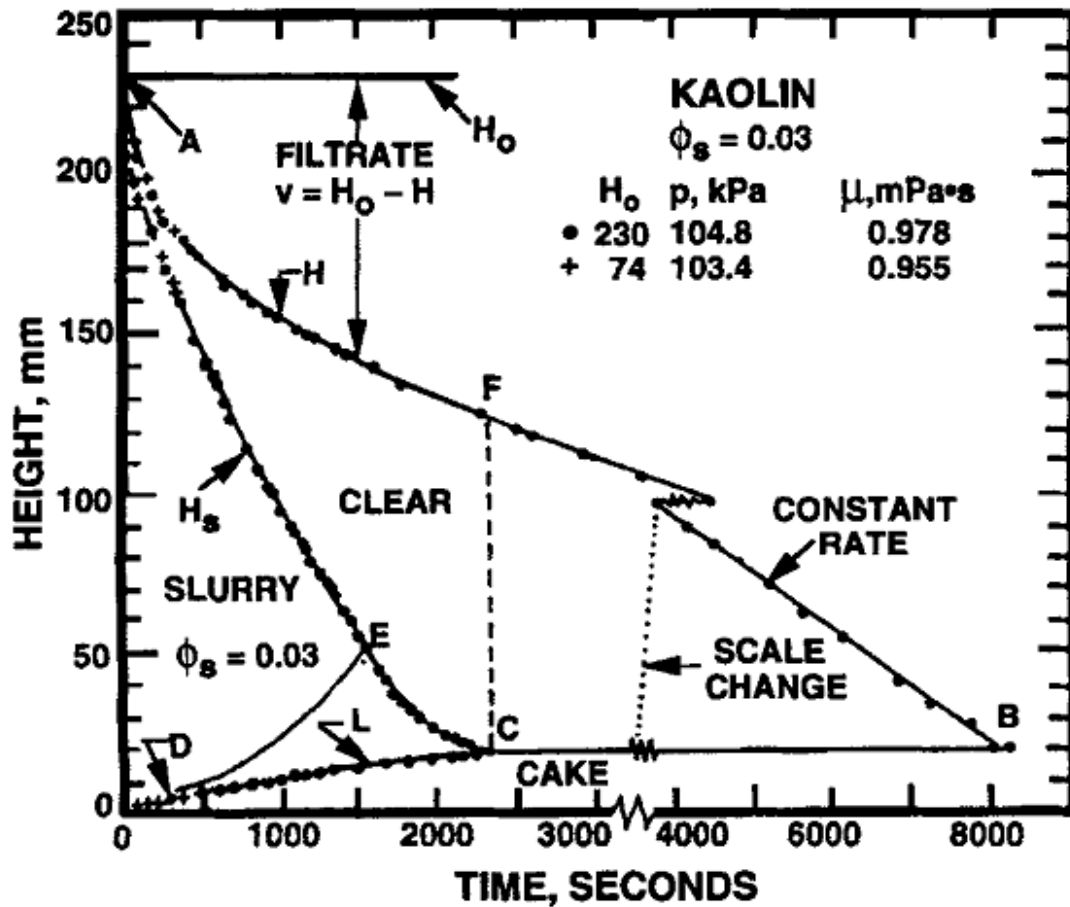


Figure 9 Filtration height versus filtration time of kaolin slurry measured with X-ray tomography.⁵³

From this detailed evaluation of cake sedimentation during filtration, a modified set of filtration equations was produced that include the velocity of cake sedimentation (Equation 21):

$$\frac{dV}{dt} = \frac{p}{\mu\alpha_{av}(V + u_{sR}t) + R_m} \quad (21)$$

This equation has not been used to describe the results obtained in the experiments reported in this work. Symbols are reported in Table 5.

Sedimentation prior/during filtration was also investigated by Yim (1999)⁵⁶, Rushton et al. (1973)⁵⁷ and Tarleton (2001)⁵⁸.

Yim (1999)⁵⁶ and Tarleton (2001)⁵⁸ proposed a methodology to quantify the contribution on the final cake resistance caused by pre-sedimentation and by pure filtration. As reported by Yim (1999)⁵⁶, cake resistance value calculated with the classical Darcy's filtration approach (Equation 1, chapter 1), gives inaccurate values in the case of concentrated suspensions. In fact, the cake resistance value obtained in our experiment is slightly different from the one calculated from Equation 1 (chapter 1), due to pre-sedimentation. The idea proposed by Yim (1999)⁵⁶ is to run a sedimentation experiment to get the cake height of the fully sedimented particles, then run filtration experiments of the cake without pre-sedimentation and to run a filtration experiment where the cake pre-sediment to compare cake height reduction and filtrate flow rate reduction. As result, he inferred that the Ruth-Darcy's equation (Equation 1, chapter 1) could also be used in case of filtration with sedimentation where the parameter c represents the contribution of filtrate density, S is the mass fraction of solid in suspension and S_c is the mass fraction of solid in the cake. However, as reported by Tiller and Hsyung (1995)⁵³, the boundary between full sedimented particles and the particles suspended is a fictitious concept and it is difficult to quantify. The definition and consequent measure of this boundary is strongly related to the judice of the operator and can lead to a bias error on the measurement of the overall media resistance.

Table 5 Sedimentation theory parameters.

Symbol	Parameter	Unit measure
---------------	------------------	---------------------

u_{sR}	settling velocity	m/s
u_S	solid relative velocities	m/s
u_L	liquid relative velocities	m/s
ϕ_s	solid concentration	kg/kg

2.4 Washing theory

During the filtration step the solid component is collected on the surface of the medium, while the liquid part, the filtrate, passes through the medium. In many slurries, the filtrate contains dissolved material, including impurities and dissolved product. After this step an amount of filtrate remains trapped inside the cake; if the filtrate retained in the filter cake is not removed before drying, the impurities present in solution will be incorporated into the product material and agglomeration/polymorph changes can occur. To remove impurities, and so to reduce the amount of solvent and dissolved impurities and solute trapped in the cake a washing step is used (Figure 10).⁵⁹

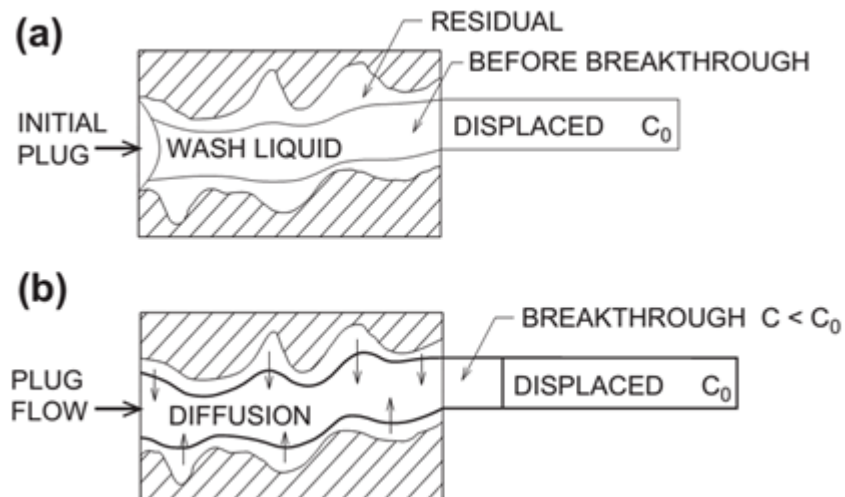


Figure 10 Schematic representation of cake washing.¹¹

Washing involves applying a clean wash liquid to displace the filtrate remaining within the cake. To measure cake washing, solute concentration as a function of time or wash liquid consumption is determined.

According to Rhodes (1934)⁶⁰, the conditions and variables that affect the washing curve are:⁶¹

- Flow rate of wash liquid through the cake
- Mother liquor and wash liquid properties
- Solute to solvent diffusivity
- Cake properties such as porosity, particles packing, initial saturation, homogeneity, and thickness
- Washing inefficiencies such as cake cracking, channelling, bypassing, and wash liquid maldistribution.

Different behaviors are observed according to the nature of mother liquor and wash solvent.^{62, 63} In general, it appears that when the mother liquor has a strong wetting preference for the solid the non-wetting fluid (wash solvent) tends to occupy the largest pores and the wetting fluid the finer ones. Thus, there may be two separate networks each containing its own fluid phase.

During washing, wash solvent enters the large pores in the cake and displaces the filtrate from the large pore network, then it penetrates in the immediate neighborhood cake porosity diffusing into the mother liquor and causing the dilution of the mother liquor and

transport of the liquor to the near bigger capillaries. Displacement is defined as the replacement of the fluid, which fill the porous media by another fluid. During displacement washing there is no capillary equilibrium in the system, but the pressure difference between the two sides of a meniscus has been assumed equal to the capillary pressure as predicted by Laplace's equation for the continuum (see capillary pressure section). During this process pressure, variation along a sequence of capillaries may be observed.⁶⁴ During this second washing phase, a combination of diffusion–dispersion process occurs.⁶⁵

To achieve perfect displacement, wash liquid has to penetrate in the entire cake pore without mixing with the original mother liquor of the initial suspension and plug flow must occur. Ideal displacement is never reached in a real situation; therefore, theory of ideal displacement washing has to be modified.

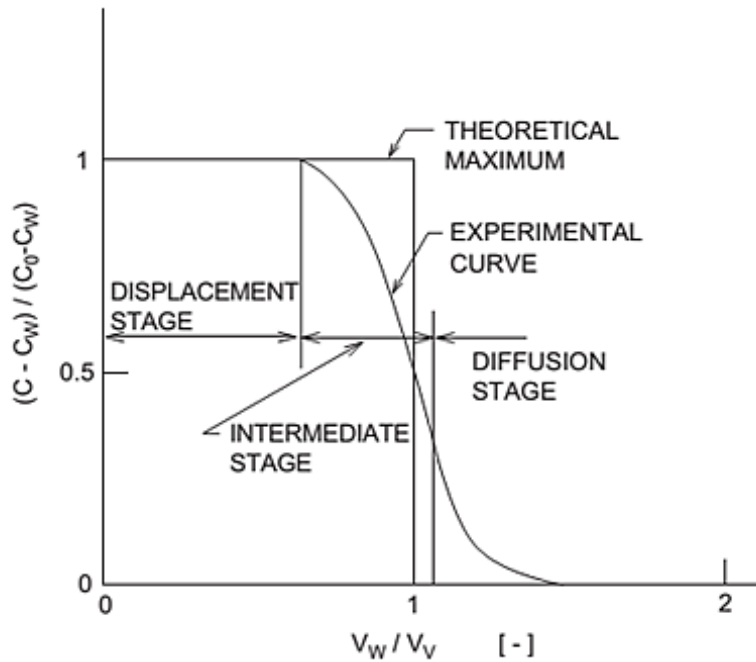


Figure 11 Wash curve of effluent concentration vs wash ratio.¹¹

The washing curve in Figure 11 has on the y axis the dimensionless solute concentration of the wash filtrate, this is plotted against the wash ratio, which is defined as the volume of the wash liquid used divided by the volume of the filtrate trapped in the cake at the initial point of the washing process.^{66, 67} The initial phase of a washing curve is a result of direct hydrodynamic displacement (see capillary pressure and wettability sections) of the residual liquor from the larger pores due to the wash liquid entering the cake. The second, intermediate stage occurs when there is direct displacement from the smaller flow pores in the cake; during this stage wash, solvent starts to dilute the filtrate from the larger pores in which a mass transfer process has started. In the third regime, the mass transfer stage, solute diffuses into the wash solvent this takes place over the entirety of the cake. The relative importance of each of these stages depends on the physical operating

conditions, the microstructures of the flow, the pores of the filter cake and the properties of the mother liquor and wash solvent.

Various researchers have tried to model the washing process.^{11, 21, 68}

The estimation of cake saturation and cake washing during the experiment is difficult to calculate. In this work no washing models were used and washing efficiency was mainly evaluated by HPLC/UV-vis analysis by determining the residual impurities concentration.

One widely used washing model is the main and side channel model⁶¹ that evaluates the cake void fraction as a system of blind side channels which retain mother liquor and which are not drained by diffusion and dilution washing, and a series of straight channels through which the wash liquor flows by displacement mechanism. This is a simple method used to mimic the results of real 3D channel structure. For a rigorous 3D channel structure analysis a simulation software (DEM and fluid dynamic model) requiring huge computational time is needed.

Main channels are defined as the channel created by pressure difference across the filter cake or created by excess liquid in the filter cake that is pushed out by the first passage of wash solvent. A general assumption is that in laminar flow conditions, wash solvent follows broadly straight channels along the main direction of wash flow without axial mixing, therefore no side channel mixing happens. Two basic equations are defined to describe the material balance: the side channel and the main channel equations. The analytical solution represents the concentration of solute in the wash liquor after a certain

period of washing. To solve this equation system different assumptions have to be considered:

- Less time is required to fill the main channels compared with the overall wash period.
- Side channels are the only places where residual filtrate solvent is present at the start of the mass transfer stage.
- Only diffusional displacement occurs during the mass transfer stage to remove filtrate from side channels.
- Filtrate is removed from side channels and leaves the cake by plug flow in the main channels.
- At the start of the mass transfer stage, the side channels are totally filled with residual filtrate.
- Part of the solute may be flushed out by initial charge of wash filling the main channels when the cake is fully saturated prior to the onset of washing.

The main and side channel model assumes that the solute concentration of the filtrate at the beginning in the cake is c_0 , while the wash solvent concentration is $(c_w)_I$ and the effluent concentration is $(c_w)_e$ and the amount of solute removed versus time t is given by Equation 22.¹¹

$$\int_0^t u_w [(c_w)_e - (c_w)_i] dt \quad (22)$$

Cake is considered completely washed when the cake becomes saturated with wash solvent and the solute concentration becomes $(c_w)_f$. The fraction of removable solute during the washing step, F is equal to:

$$F = \frac{\int_0^t u_w [(c_w)_e - (c_w)_i] dt}{[c_0 - (c_w)_i] L \varepsilon_{av}} = \int_0^w (c_w^*)_e dw \quad (23)$$

Washing efficiency is obtained as the final fraction of liquid trapped in the cake, R which is easily obtained from the wash curve, because the effectiveness of washing depends on the degree of displacement and to the degree of solute diffusion into the wash solvent.

$$R = 1 - F \quad (24)$$

When diffusion is the predominant mechanism in washing, solute concentration of the pore liquid is considered uniform and equal to c , therefore the mass balance is:

$$u_w [(c_w)_e - (c_w)_i] = L \varepsilon_{av} \frac{dc}{dt} \quad (25)$$

Where $(c_w)_e = \phi c$ where ϕ is a constant independent on time. Rhodes (1934)⁶⁰ therefore assumed that:

$$c_w^* = \frac{(c_w)_e - (c_w)_i}{c_0 - (c_w)_i} = e^{(-\phi W)} \quad (26)$$

$$R = 1 - F = \left(1 - \frac{1}{\phi}\right) + \frac{1}{\phi} e^{(-\phi W)} \quad (27)$$

This theory needs to be modified in cases where the API is soluble in mother liquor and wash solvent because product loss is an important parameter to consider.⁶⁹ During

washing the interaction between solid particles and solvent happens at the interface and solid/solvent interaction is determined as the sum of bonding forces between molecules, atoms and ions. Dissolution kinetics are also important, in the case of fast dissolution the wash liquor will be saturated by the product almost immediately after contact. On the other hand, when a system has slow dissolution kinetics, the product loss due to dissolution of the solids can be reduced by having a short contact time between the solids and wash liquid. The displacement process to eliminate impurities and mother liquor from the capillary system present in the porous structure by using wash solvent governs the effectiveness of cake washing.

To quantify the performance of washing the loading ratio X^* , is defined as the mass ratio between impurity loading in the product after (X) and before washing (X_0) is used.⁶⁹

$$X^* = \frac{X}{X_0} \quad (28)$$

The wash ratio W gives the specific volume of the added wash liquor V_w related to the cake pore volume V_p .

$$W = \frac{V_w}{V_p} \quad (29)$$

Cake saturation S , is defined as the ratio between the liquid volume V_l inside the cake pores (void areas between particles) and the total pore volume V_p and describes the cake solvent content.

$$S = \frac{V_l}{V_p} \quad (30)$$

At the beginning of a washing process, wash ratio is zero, because no wash solvent is added and cake is saturated with mother liquor (dryland). In case of deliquored cake a decrease of the amount of the residual liquid and therefore of the impurity present implies that the loading ratio is lower than one at $W = 0$.

Ideal washing is achieved by ideal displacement, when the entire quantity of mother liquor is replaced by the wash solvent. In a linear plot the ideal displacement curve is a line with a slope of minus one. In reality, when the solute is highly soluble in the wash solvent/mother liquor, a high level of product loss can be expected; in case of slow dissolution kinetics, reducing contact time between solvent and solute by modifying the pressure, can help to minimize product loss. However, sometimes particle surface dissolution can be useful for impurity removal.⁶⁹ If the surface during the washing step dissolves, the impurities remaining in stagnant interstitial areas, which are not accessible for the wash liquor can be set free as the areas are opened, so these impurities that usually are trapped in the particles structure can in this way easily be removed from the fine pores between crystals and the crystal surfaces.

Two way to reduce product loss arising from dissolution are to recover the solute or to use some kind of counter current washing.⁶⁹

Particle morphology can also affect washing performance, larger particles reduce the specific cake resistance and hence enable higher wash liquor flow rates, due to the larger size pores in the cake and the promotion of local turbulence that drastically increase mass transfer inside the cake. However, in the vast majority of practical cases the Reynolds

Number (and Peclet Number) are so small that mass transfer is determined by the rate of diffusion of the solute into the wash liquor.⁷⁰

2.4.1 Continuous filter cake washing by using rotary filtration

During washing, mother liquor and impurities are partially or completely removed by the wash solvent flowing through the cake volume. Ideal washing requires an amount of wash liquid equal to the pore volume of the cake; knowing the volume of wash solvent in relation to the pore volume used is crucial to determine washing efficiency.⁵⁹

Assuming that the primary filtrate has the same composition as the liquid present in the cake before washing, and that the pore volume remains constant during washing, it is, in principle, possible to derive equations to determine univocal quantity of wash solvent to use to remove impurities and mother liquor. For crossflow isolation, the washing equation is slightly different (Equation 31).²²

The theory shown below relates to the wash theory applied to the rotary drum filtration in continuous mode.

Considering a segment of filter media of rotary drum filtration unit at constant pressure with surface area equal to ΔA and cake resistance that increases with time, the mean filtrate rate is equal to

$$\frac{q}{T} = \frac{p \Delta A}{\mu \left(\frac{1}{1+n} \frac{k q^n}{\Delta A} + r \right)} \quad (31)$$

The filtrate removal rate that takes into account the rate of mother liquor and wash liquid flow is equal to

$$\frac{q_w}{q} = \frac{T_w}{T} \frac{\mu}{\mu^*} \frac{\frac{1}{2} \frac{kq}{A} + r}{\frac{kq}{A} + r} \quad (32)$$

The fraction of the original liquid removed in the primary filtrate is equal to O and is function of the amount of primary solvent used (mother liquor), solid content of the mixture to be separated and porosity of the cake:

$$\frac{q_w}{q_c} = x \frac{O}{1 - O} \quad (33)$$

$$\frac{q_w}{q_c} = x \left(\frac{1 - \varepsilon}{\varepsilon} S' - 1 \right) \quad (34)$$

Symbols related to the washing paragraph are reported in Table 6, Table 7 and Table 8.

Table 6 Dead end washing theory parameters.

Symbol	Parameter	Unit measure
c_0	solute concentration of the filtrate at the beginning in the cake filtration	mol/l
$(c_w)_I$	wash solvent concentration	kg/kg or V/V
$(c_w)_e$	effluent concentration	kg/kg or V/V
u_w	superficial wash liquid velocity	m/s
$[c_0 - (c_w)_i]L\varepsilon_{av}$	maximum solute that it is possible to remove by washing	-
u_w	cumulative wash liquid passing through the cake	m/s
u_v	cake void volume	-

$w = \frac{u_w t}{L \varepsilon_{av}} = \frac{u_w}{u_v}$	wash ratio	-
--	------------	---

Table 7 Washing theory parameters in case of cake desaturation.

Symbol	Parameter	Unit measure
X^*	washing loading ratio	g/g
X	impurity loading in the product after washing	g
X_0	impurity loading in the product before washing	g
W	wash ratio	-
V_W	wash liquor	m ³
V_P	cake pore volume	m ³
S	cake saturation	-
V_l	liquid volume	m ³

Table 8 Cross flow washing theory parameters.

Symbol	Parameter	Unit measure
q	volume of primary filtrate obtained in the filtration time	m ³
T	time	s
p	the pressure difference during the filtration process	kg/(ms ²)
μ	viscosity of the primary filtrate at filtration temperature	kg/(ms)
n	Generally equals to 1	-
k	specific filter cake resistance	m/kg

r	resistance of filter cloth per unit of surface area	1/m
T_w	time interval	s
μ^*	wash liquid viscosity	kg/(ms)
$\frac{k q}{A r} = \alpha$	ratio of cake and cloth resistance	-
$S' = \frac{1 - F + S}{F}$	ratio of liquid to solid in the slurry	-
F	solid content	kg/kg or V/V

2.5 Drying

Drying is defined as the process to separate volatile liquids from solid materials by vaporizing the liquid and remove the vapor from the solid phase. This process is the last step of the API isolation. After deliquoring, solid material is wet with a residual quantity of solvent (moisture content) deriving from washing or also even from residues of mother liquor. Drying is generally a thermal process, where the use of heat is applied to vaporize the residual solvent. The drying agent could be a gas, such as air, inert gas or superheated steam or the heat can be supplied by radiation, by hot surfaces, or by microwaves.

Drying process is the combination of three steps: removal of liquid phase from the surface of particles (interparticle solvent), removal of liquid from the particles capillaries (unbonded liquid, intraparticle solvent) and the third step that is occurring in presence of solvate or hydrate materials, the removal of bonded liquid from the crystal lattice (bonded solvent). Drying is often the bottle-neck in the API manufacture: other isolation steps,

such as extraction, crystallization and filtration require short residence time, for drying the process in some case can also prolong to hours or days.⁷¹

To reduce drying time, aggressive drying conditions are desirable to reduce the duration and hence cost of the manufacturing step. However, aggressive drying condition can adversely affect the properties of the final dried product by impacting particle properties, functionality and quality causing problems during the downstream processes. A particular concern being product degradation. A balance between drying time and preservation of product quality is needed. During drying several problems can arise from inappropriate selection of drying conditions, such as; formation of inhomogeneous dried material, formation of agglomerates and; lumps and particles breakage (attrition).⁷²

If the moisture content present in the solid during the drying process is defined as X, while Y is the moisture content of the drying agent (Equation 35)⁷³⁻⁷⁵:

$$X_A = \frac{M_A}{M_s} \text{ and } Y_A = \frac{M_A}{M_B} \quad (35)$$

The drying rate is defined as the change of moisture content during time (Equation 36):

$$\dot{m} = \frac{M_s}{A} \frac{dX_A}{dt} \quad (36)$$

Where M_s is the mass of dry solid and A is the exposed surface area of the particles subject to drying. The drying rate depends on the drying conditions that define the driving force and which in turn depend on the mode of drying (pressure exerted to drive a gas to flow through the wet material, temperature, humidity and so moisture content, radiation

temperature, microwave drying, or temperature of the hot surface, convective drying, intensity of microwave radiation, microwave drying, etc.). Other system characteristics, such as solvent properties and solvent interaction with the solid (bond or unbond) and the solid properties, such as PSD and particles morphology need to be considered. The drying rate curve (Figure 12) is the tool to evaluate the correlation between moisture content and drying rate.

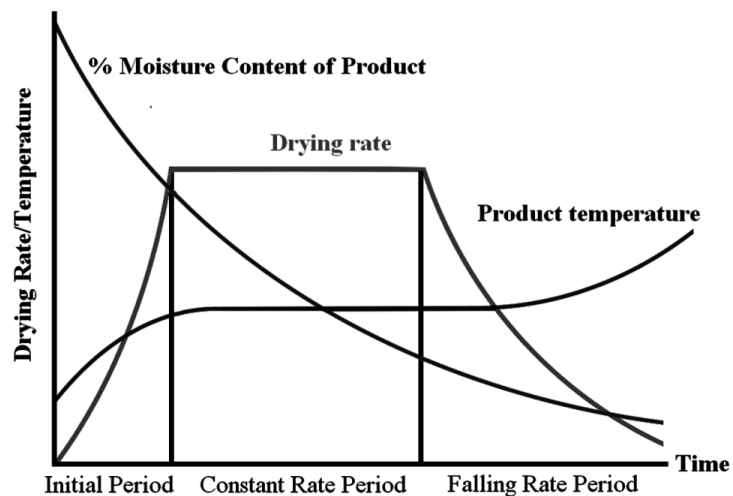


Figure 12 Drying curve.⁷⁴

From the drying curve three different drying stages are observed.⁷⁵

The first two stages of drying are called the initial period and the constant rate period; during this time liquid on the surface of solid and, trapped between particles is removed. During these stages the drying conditions which have most effect on the drying rate are the drying temperature and drying agent flow rate. The drying agent entering the drier is undersaturated with respect to the solvent to be removed but may be considered to be saturated with solvent vapor at the surface of the solid. Thus, the efficiency of

interparticulate solvent removal is seen in the difference in humidity of the unsaturated drying agent and the saturated one. This is related to the solvent enthalpy of vaporization and the heat capacities of the components.⁷³ During these two periods drying is relatively fast and an initial temperature reduction of the wet cake occurs (drying is an endothermic process). This is followed by subsequent increase in the product temperature. The endothermic cooling is due to the vaporization of the free solvent present between particles. In vacuum drying this initial vaporization may be rapid as the pressure is reduced such that the solvent may be above its boiling point at the reduced pressure. If drying is achieved by passage of nitrogen or air this evaporation process is usually slower. Solvent is removed in the exhaust gas stream. Evaporation starts from the exposed crystal faces on the bulk powder surface exposed to the drying medium, further solvent is then transported from the bulk by capillaries forces and a drying front is established and moisture content in the cake decreases linearly and it is limited just by the gas flow.

When the moisture content is reduced below a critical value X_{crit} , the surface of the solid dries out, and further evaporation continues to take place but the location moves to the interior of solid porosity. This condition represents the beginning of the third drying step called the falling rate period. The drying rate decreases with decreasing moisture content tending to the hygroscopic equilibrium moisture content (X_{eq}) which dependent on the system temperature and to the relative humidity (sample-ambient). In practice, the capillary forces struggle to keep up with the surface evaporation and diffusional drying occurs. The liquid-vapor interface no longer lies on the surface, but it shifts towards the particle interstices. Bonded moisture can be transported away from the solid by three main

mass transfer mechanisms: liquid diffusion, vapor diffusion, where liquid evaporates within the material and Knudsen diffusion where the diameter of the pore is comparable with the mean free path of the evaporating molecules, which is encountered when solvent molecules escape from a solvate such as a channel hydrate.

The initial stage (initial period) steady-state usually lasts for a very short period compared with the other two regimes, so the time required for this step is neglected. Drying time in constant rate period is calculated by (Equation 37):

$$t_1 = \frac{M_s(X_{A0} - X_{At})}{k_{UA}(Y_{Awet} - Y_A)} \quad (37)$$

During the falling rate period, the drying rate shows an exponential decay dependent to the residual moisture content (Equation 38):

$$t_2 = \frac{M_s}{A} \int_{X_{A0}}^{X_{At}} \frac{dX_A}{\phi_A} \quad (38)$$

To determine the level of dryness of the sample produced in chapter 6 and 7 at the end of the drying process the loss on drying is calculated as (Equation 39)

$$\begin{aligned} & \text{Loss on drying} \\ &= \frac{\text{initial wet sample weight} - \text{weight of sample after drying}}{\text{initial wet sample mass}} \times 100 \quad (39) \end{aligned}$$

Symbols of these equations are reported in Table 10.

2.5.1 Parameters affecting dried material size

The final size of particles after drying process can be influenced by a many particle and process properties, such as; particle size distribution and shape, initial moisture content (determined by deliquoring efficiency), solvent properties, such as viscosity API solubility, the presence of residual impurities or residual mother liquor, drying temperature and pressure, particle bed height and agitation mechanism, speed and duration.⁷⁵

Lekhal et al. (2003 and 2004)^{72, 77} investigated the role of these operating conditions and material parameters on the propensity for particle attrition or agglomeration measuring PSD and image analysis.

In Table 9 the role of operating parameters and material properties in influencing final particle size and morphology are tabulated.⁷⁸

Table 9 Operating parameters and material properties that affect final particle size and morphology of the dried material.

Parameter affecting dried product particle size	Main effect
Temperature ⁷²	<ul style="list-style-type: none">• If temperature increases, drying time is reduced and drying rate increases.• If temperature increases the tendency to form agglomerates increases and agglomerates become stronger (more material dissolved during drying leads to the formation of stronger particle-particle bridges.

	<p>(a)</p> <p>(b)</p> <p style="text-align: center;">T (°C)</p> <p><i>Figure 13 Effect of temperature on (a) final average diameter and (b) aspect ratio.⁷²</i></p>
Pressure ⁷²	<ul style="list-style-type: none"> • Using reduced pressure reduces heat transfer, but also reduces the solvent boiling temperature leading to faster drying increasing the tendency for agglomeration (even in case of low initial moisture content). • If drying pressure is high, even in case of low agitation rate, the agglomeration propensity increases. • If drying pressure is low, even in case of high agitation rate, the agglomeration propensity increases.

	<p style="text-align: center;"><i>Figure 14 Effect of pressure on final average diameter at different temperatures: (rhomb), 200Torr (square) and 80Torr (triangle).⁷²</i></p>
Particle bed height ^{78, 79}	<ul style="list-style-type: none"> • The thicker the bed the longer the drying time, the drying rate is reduced so the agglomeration tendency is also lower. • Bed flowability depends on bed height: if the bed height is small there is an increased probability of particle-particle collisions leading to the presence of spherical agglomerates in the bed and agglomerates migrate to the surface.
Initial moisture content ^{71, 77, 78}	<ul style="list-style-type: none"> • If the initial moisture content is high, the tendency for agglomeration increases (solvent dissolves product and deposits it on evaporation to act as a gluing agent) • If initial moisture content is low (less than the critical moisture content) there is increased possibility of attrition during agitation (higher particle-particle collision probability) • If initial moisture content exceeds critical moisture content higher agitation may increase particle-particle compaction, so increasing agglomeration propensity • If initial moisture content is high, solvent drips from condensation on the walls at the beginning of drying act to nucleate and promote growth of agglomerates.
Agitation speed ⁷⁷	<ul style="list-style-type: none"> • If agitation speed is high attrition increases (higher particle-blade and particle-wall collision intensity and frequency promotes causes particle breakage). This also reduces the aspect ratio as elongated particles are broken.

	<ul style="list-style-type: none"> • Slow agitation may promote agglomeration and reduction of the aspect ratio (agglomerated particles generally increase in sphericity) <p>Figure 15 consists of two plots, (a) and (b). Plot (a) shows the ratio of final average diameter to initial average diameter ($d_{final}/d_{initial}$) on the y-axis (ranging from 0 to 1.5) versus agitation speed N in rpm on the x-axis (ranging from 0 to 60). The data points are approximately: (10, 1.3), (20, 1.2), (30, 1.05), (40, 1.0), (50, 1.0). An inset graph shows $d_{final}/d_{initial}$ on the y-axis (ranging from 0.7 to 1.5) versus the number of revolutions N_{rev} on the x-axis (ranging from 500 to 2500). The inset data points are approximately: (500, 1.3), (1000, 1.2), (1500, 1.1), (2000, 1.0), (2500, 1.0). Plot (b) shows the Aspect ratio on the y-axis (ranging from 1 to 3) versus agitation speed N in rpm on the x-axis (ranging from 0 to 60). The data points are approximately: (10, 1.4), (20, 1.6), (30, 1.5), (40, 1.4), (50, 1.5).</p> <p>Figure 15 Effect of agitation on (a) final average diameter, small graph is the final average diameter respect the number of revolution and, (b) aspect ratio.⁷⁷</p>
Blow down time	Efficient deliquoring reduces residual solvent lowering the agglomeration tendency
Solvent ⁸⁰	<ul style="list-style-type: none"> • If API solubility is low the agglomeration tendency is low. • A high residual mother liquor content increases agglomeration tendency⁷⁶ • If the boiling point of the wash solvent is substantially lower than mother liquor, even if the residual mother liquor quantity is low, the agglomeration tendency increases due to enrichment of the less volatile solvent during drying (effect caused by re-dissolution of

	<p>product followed by interparticle bridge formation when the less volatile solvent evaporates)</p> <ul style="list-style-type: none"> • Solvent characteristics may impact agglomeration, for example an alcohol has less propensity for hydrogen bonds formation with the crystal surfaces than water, reducing particle-particle attraction and yielding softer agglomerates⁷⁸
Impurities	Impurities from residual mother liquor may be deposited on particle surfaces and promote agglomeration.
Particle morphology	Elongated particles, especially needles are easier to break (breakage direction across the smallest dimension of the particle due to the smaller energy required to break the particle) ⁸¹
Particle history	<ul style="list-style-type: none"> • If particles have already been subject to attrition, eg a wet milling process, the probability of attrition is low (energy used during milling to break particles already produced breakage along the cleavage plane)⁷⁸ • Small particles are less prone to attrition

McLeod et al. (2012)⁸¹ investigated the mechanism of particle attrition during agitated drying. Needle-shaped crystals were used to emphasize the effect of crystal morphology on particle breakage. To understand the mechanism of needle breakage during agitated drying a fracture model was developed, where two breakage mechanisms were evaluated: attrition when small particle fragments are removed from the edge of bigger crystals and the fracture of particles occurring when particles are broken into two main pieces with the formation of many smaller fragments. Muller (2009)⁸² calculated the yield strength in relation to the number of crystal-crystal junctions per unit area in a plane and the strength of these junctions. The critical stress required to break crystals were determined. When the stress applied to the system exceeds the critical stress, particles break along the length with higher propensity to break (slip plane). To further improve prediction of particle

breakage, a term to define the propensity for attrition to occur in semi-brittle materials was determined by calculating hardness and critical stress intensity factor of the API.

Many papers report agglomeration and examine possible causes.⁸³⁻⁸⁵ Tamrakar *et al.* for example investigated agglomeration tendency using a design of experiments approach to build a regime map to define the role of operating procedure (moisture content and composition, drying time and agitation) and their range, to design drying processes in relation to the API properties.⁸⁶ A common hypothesis suggests that if the solute is rather soluble in the wash solvent “sticky spots” form due to local API dissolution and subsequent redeposition and consequent formation of solid bridges after solvent evaporation occurs. One approach to reduce agglomeration is therefore to tailor the wash solvent composition to minimize concentration of the soluble component (product) during drying. Papageorgiou *et al* (2016)⁸⁴ investigated the potential for particles to undergo agglomeration by analyzing the effect of solvent selection and critical moisture content.⁸⁷ Well-designed solvent selection may have much more impact on particle clustering than particle size. This phenomenon will be evaluated in detail in chapter 4 of this thesis. Birch and Marziano (2013), Zhang and Lamberto (2013) and Tamrakar *et al.* (2016)^{76, 80, 86} studied the effect of solvent on drying analyzing the role of solvent polarity in the formation of strong granules. Generally, the higher the solubility of the product in the wash solvent, the greater the chance solid bridge formation. The reason for solid bridge formation is also the increased apparent viscosity of the thin liquid layer surrounding the particles.^{76, 78, 84, 87} They investigated the effect of surface tension on agglomeration using

different solvent mixtures, highlighting that surface tension of the saturated solution may be a good indicator of the cohesive force experienced in the wet cake.

Symbols related to drying sections are reported in Table 10.

Table 10 Drying theory parameters.

Symbol	Parameter	Unit measure
X_A	moisture content of solid	kg/kg
M_A	mass liquid	kg
M_S	mass dry solid	kg
Y_A	moisture content of drying agent	kg/kg
M_B	mass dry solid material	kg
\dot{m}	drying rate	-
A	surface area in contact with the drying agent	m ²
t_1	drying time at constant rate period	s
X_{A0}	moisture content of solid at time zero	kg/kg
X_{At}	moisture content of solid at time t	kg/kg
Y_{Awet}	moisture content of drying agent wet	kg/kg
K_U	mass transfer coefficient	-
t_2	drying time at falling rate period	s
ϕ_A	drying rate	kg/(m ² s)

2.6 How isoaltion parameters were calculated

Isolation parameters used to evaluate filtration, washing and drying efficiency in this work are:

- Filtrate flow rate (ml/s)
- Cake resistance (m/kg)
- Filter resistance (1/m)
- Cake permeability (1/m²)
- Cake porosity (-)
- Cake compressibility (-)
- Wet to dry mass or LOD (-, %)

To calculate filtrate flow rate, cake resistance, filter resistance and cake porosity; filtration time with respect to filtrate volume collected data were gathered. By plotting filtrate volume versus filtration time the evolution of the filtrate flow rate can be estimated and the calculation of the final filtrate flow rate is done as the ratio of the total filtrate volume collected (mL, m³) during the filtration/washing time (s) (Figure 17 and Figure 18).

It is important to state that filtration was running with a marginal pre-sedimentation (in real experiments it is not possible to start filtration without marginal pre-sedimentation).

As reported by Ripperger (2013)⁴⁸ (Figure 16), classical filtration model (reported in 2.2.1) can be used for a series of different filtration phenomena: ideal filtration with linear Darcy's plot (curve A); filtration where some solid is settled before the process starts (curve B); filtration where the starting point is not measured correctly and solid settled out

completely prior filtration (curve D); only coarse particles settled prior filtration (curve E) and fine particles block the filter (curve F).

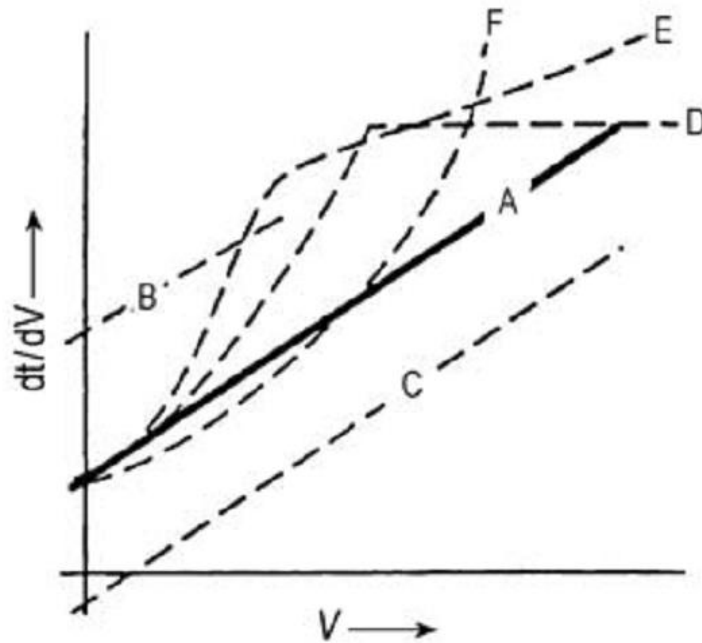


Figure 16 Plot showing how different secondary effects prior/during filtration can influence Darcy's plot.⁴⁸

In case of complete sedimentation prior filtration starts, the values of cake resistance can be consider null and the value of media resistance is the sum of the resistance of the medium and the resistance of the pre-settled cake. However, cake and media resistance values, as reported in Figure 69, are altered from the primary to the second filtration by two possible phenomena; consolidation of the cake (see 2.3) and/or cake breakage during the secondary filtration stage.

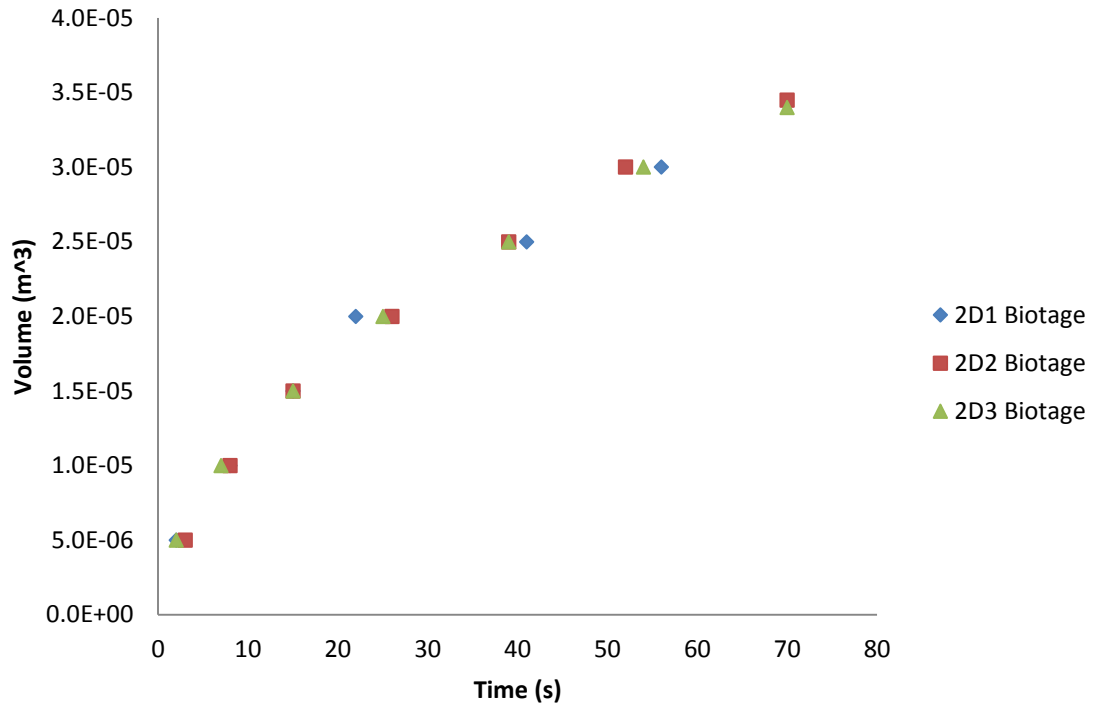


Figure 17 Example of filtration flow rate of a filtration experiment at constant pressure filtration in case of cake formation during filtration. Experiment 2d of chapter 8. P-value calculated with ANOVA statistic are (confidence level 95%); exp 2D1, intercept, 0.0129, x variable, 0.0012; exp 2D2, intercept, 0.0045, x variable, 8.9E-05; exp 2D3, intercept, 0.0031, x variable, 9.5E-05.

By plotting filtration time/filtrate volume versus filtrate volume a linear correlation is generated (Figure 18) where slope is correlated to cake resistance using the following equation (Equation 40):

$$\alpha = \frac{2 \text{ slope } A_f^2 \Delta p}{\mu c} \quad (40)$$

Where A_f is the filter tube area (m^2), Δp is the driving force (Kg/ms^{-2}), μ is the dynamic liquid viscosity (kg/ms)^d and c is the effective concentration of solids per volume of filtrate (kg/m^3).

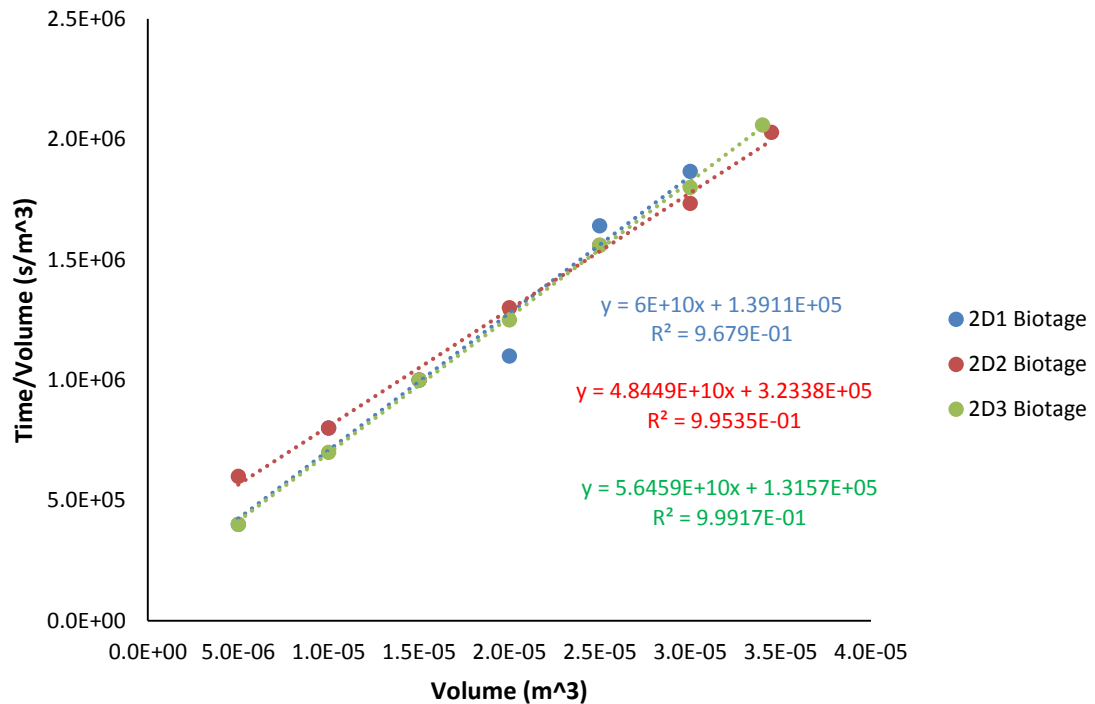


Figure 18 Example of Darcy's plot (time/volume of filtrate collected versus volume of filtrate collected during a constant pressure filtration experiment where the cake is forming during the filtration experiment. Experiment 2d of chapter 8. Average value of slope $5.4969E+10$ and standard deviation $5.9178E+09$. Average value of intercept $1.9802E+05$ and standard deviation $1.0863E+05$.

The intercept extracted from the linear plot is correlated to the filter media resistance (Equation 41):

^d To get more precise values the viscosity used during filtration step is the mother liquor viscosity. Cake resistance and filter resistance for the washing steps is not required because the cake is already settled on the filter and similar results as reported in chapter 7 are observed.

$$Rm = \frac{\text{intercept } A_f \Delta p}{\mu} \quad (41)$$

Cake porosity can be calculated using Equation 42:

$$\varepsilon = 1 - \left(\frac{\rho_s}{\rho_{true}} \right) \quad (42)$$

Where ρ_s is cake density and ρ_{true} is the paracetamol true density.

During washing the focus is to remove the mother liquor from the cake by replacing the mother liquor trapped in cake pores by the wash solvent. Generally, the solubility of the API in the crystallization solvent is substantially higher than the API solubility in wash solvent. Therefore, to avoid bridges formation during drying all the crystallization solvent needs to be displaced from the cake. A key parameter to be calculated is the wash volume quantity that corresponds to cake pore volume (Equation 43).

$$V_{void} = V_{cake} - V_{solid} = \frac{\pi d^2 h}{4} - \frac{m_s}{\rho_s} \quad (43)$$

Where d is equal to cake diameter (m), h is equal to cake height (m) and m_s corresponds to mass of the solid cake (kg).

As reported by Murugesen and Beckman^{34, 39} the amount of wash solvent required to completely remove the crystallization solvent from a filter cake is more than one cake void volume. In this work several washes each with a volume, corresponding to the void volume of the cake were used.

Cake permeability is defined as the capability of the liquid phase to pass through the cake.

Cake permeability is calculated as Equation 44:

$$k = \frac{\frac{\text{cake volume}}{\text{cake resistance}}}{\text{mass dry cake}} \quad (44)$$

Cake compressibility is defined as the capability of the cake to be squeezed by the driving force applied during the filtration step. As reported by Endo and Alonso (2001), Murugesan *et al.* (2012) and Rippenger *et al.* (2012)^{35, 34, 48} cake compressibility (n) is the slope of the linear fitting of the natural logarithm of different cake resistance values (calculated by using Equation 39) respect the natural logarithm of the driving forces used to determine those cake resistance, as seen in Equation 45:

$$\ln \alpha = n \ln \Delta p \quad (45)$$

2.7 Isolation solvents

Today, in the chemical industry, solvents are used in large quantities. In fine-chemical and pharmaceutical production, large amounts are used in manufacturing. Therefore, solvents represent a major part of the environmental performance of a process and also impact on cost, safety and health issues.

Most chemical reactions of organic substances need conventional organic solvents as reaction media. The use of simple organic solvents such as, toluene, methanol, ethanol and acetone in many industrial chemical processes is an issue of environmental concern. These solvents are characterized by high volatility and limited liquidus ranges (at atmospheric pressure, 85–200°C). As a result, about 20 million tons per year of volatile

organic compounds (VOCs) are discharged into the atmosphere by industrial processes,⁸⁸ contributing to global climatic changes, air pollution, and human health-related diseases.⁸⁹

Most classical solvents are toxic to some degree and are difficult to recycle. As a result pharmaceutical companies spend large sums of money buying, using and disposing solvents.⁹⁰

Over the past decade, there have been a variety of government and industry led efforts to eliminate, replace, recycle or minimize the use of solvents. This effort has been driven from a desire to reduce human health impacts, process safety risks, and multiple environmental impacts. Industry has responded through an ever-increasing system of regulations and voluntary efforts to consider reducing solvent use and to devise strategies to minimize use or mitigate their impact. Over time, it has become increasingly evident that further progress in reducing solvent use can only come through pollution prevention efforts that begin in the earliest phases of product development.⁹¹

Since the beginning of the Green Chemistry movement the need for alternative reaction solvents has been one of the major issues facing the chemical industry. Recognition of the need for new technology led to research evaluating new more eco-friendly solvents, such as ionic liquids, supercritical fluids, and fluorine solvents.⁹²

Green solvents offer potential advantages for instance the ease of production and recycling. The vision for “green” solvents expresses the goal to minimize the environmental impact resulting from the use of solvents in chemical production. Recently, four directions towards green solvents have been recommended:

- Substitution of hazardous solvents with those that show better EHS (environmental, health and safety) properties, such as increased biodegradability or reduced ozone depletion potential^{93, 94}
- Use of bio-solvents, these are solvents produced with renewable resources such as ethanol produced by fermentation of sugar-containing feeds, starchy feed materials or lignocellulosic materials
- Substitution of organic solvents either with supercritical fluids that are environmentally harmless (e.g. the use of supercritical CO₂ in polymer processing avoids the use of chlorofluorocarbons, and thus reduces ozone depletion)^{95, 96}
- Ionic liquids that exhibit low vapour pressure, and thus less emission to air.^{97, 98}

2.8 Correlation between chemical-physical slurry properties and filtration process

The filter cake may be considered as a porous media that increases in thickness during time. For a material to be a porous medium must satisfy two conditions:

- It contains small spaces between solid particles known as pores or voids, which are free of solids and imbedded in the solid or semisolid matrix. Usually these voids are filled with fluid
- It is permeable to a variety of fluids

All macroscopic properties of porous media are influenced by the pore structure. The most important macroscopic pore structure parameters are porosity, pore size, permeability, specific surface area, resistivity factor, and topology of pore structure and packing of particle.⁹⁹

2.8.1 Porosity and particle density

Porosity, ϕ , is the fraction of the bulk volume occupied by pore or void space.⁹⁹

Different pore types are defined in relation to the type of void space:

- Interconnected or effective pores, that is the porosity that allows transport of matter across the porous medium
- Non-interconnected or isolated pores.

Pore sizes is expressed as a pore size distribution. In general, a pore is defined as a space bounded by solid surfaces and by planes.

Considering a fluid passing through the pores in a cake, the capability of a fluid to flow through a porous medium is known as permeability. This parameter evaluates the conductivity of porous medium with respect to permeation by a Newtonian fluid, while specific permeability, k , is the permeability which depends on both fluid and flow properties. k is a term in Darcy's law (other expression of Darcy's law):

$$Q = \left(\frac{k A}{\mu}\right) \left(\frac{\Delta P}{L}\right) \quad (46)$$

Where A is the normal cross-sectional area of the sample, L is the length of the sample, ΔP is the hydrostatic pressure drop and μ is the fluid viscosity.

Another important parameter to be considered in a porous media is the surface area, defined as the total interstitial surface of the voids and pores per unit mass or unit bulk volume of the porous media.⁹⁹

In case of particles forming a porous medium, the packing state of particles inside a porous bed provides the 3D structure of the cake porosity. The combination of a series of porous structure properties, such as the shape of particle, PSD and wall effects need to be considered to identify the packing state of the particles. Particle packing is classified according to the level of packing organization: for instance when ordered spherical particles produce a porous bed, a regular array of particles forms, with each sphere touching other spheres at least in four different positions, while for random particle packing determine the number of contact between spheres is very complicated.⁹⁹

Another way to characterize a packing structure is to consider the particle arrangements: during processing of a spherical solid, breakage, sedimentation or flocculation occur, the original particles can form an open structure with regular arrangements but the attrition and breakage fragments can move freely into the structure; this arrangement is defined as a loose random arrangement.

Particle layer spacing or packing effects due to the interaction between wall and crystals are important parameters to consider because these two effects can produce an increase in particle packing randomness in localized areas of the cake (anisotropy of packing). In general, the base layer usually contains packing imperfections, which influence randomness in adjacent particle layers, while in regions adjacent to an external surface there are areas of higher porosity due to different radii of curvature of the wall and the particles.

2.8.2 Particles size, particles size distribution and particles shape

Measurement of particle size, size distribution and particle shape combine to provide a physical description of the powder product.¹⁰⁰ In this study particles size, size distribution and shape were conducted to evaluate process performance and to evaluate the extent of particle damage especially attrition and agglomeration during isolation.

Crystals are not spherical, so a series of different particles size definitions exist to allow comparison of particle sizes independently of shape, the most common being to identify equivalent diameters:^{101, 102}

- Feret diameter (D_f), defined as the distance between two parallel tangents placed at the opposites edges of the particle; particles are randomly oriented
- Martin diameter (D_M), defined as the diameter that divides a randomly oriented particle in two equal projected areas
- Breadth (B), equals to the min Feret diameter for a particle resting in a stable position
- Chord length (CL), that is the distance of intersection of particles with the laser source used to the determine the particles size in an FBRM (focus beam reflectance measurement)
- Thickness (T), height of the particle when resting in a stable condition.

An arbitrary particle can be described by defining an equivalent spherical diameter which is scaled by a factor to match a specific measured attribute. (as described in Figure 19).

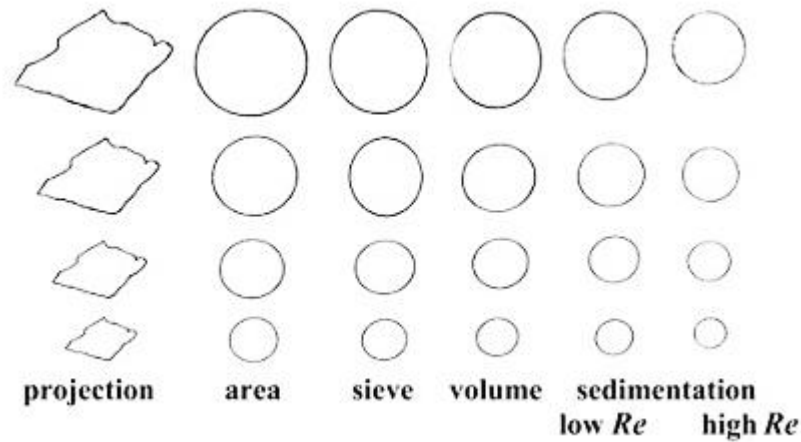


Figure 19 Equivalent sphere for arbitrary particles.¹⁰⁰

In general, the equivalent sphere diameter evaluated with one analytical approach is different from that determined using another analytical technique, thus two different particle size measurement approaches gives different particle size results for the same sample. The consequence of this is that particle sizes measured for different samples can be compared using the same analytical technique. Therefore, the concept of equivalent diameter can be classified in different way, in accordance with the measurement approach and the shape of the particle:

- Equivalent projected area diameter (D_A), that is the diameter of a circle having the same area as the particle's projection
- Equivalent surface area diameter (D_S): defined as the diameter of a sphere that has the same surface area of the particle analysed
- Equivalent volume diameter (D_V): that is the diameter of a sphere that has the same volume of the particle

- Equivalent sieve diameter (D_{Si}), defined as the diameter of an equivalent sphere that is just retained on the aperture of the sieve mesh; in general the sieve diameter is smaller than the other equivalent diameters for elongated particles because the particle orientation plays a key role in defining the pass/do not pass criteria (pass criteria is defined by the longest dimension perpendicular to the longest axis of the particle)
- Equivalent Stokes' diameter (D_{St}): defined as the diameter of the equivalent sphere that has the same settling rate as the particle under sedimentation conditions governed by Stokes' law^e; also this equivalent diameter is generally smaller than the other cases, due to the particle's surface area: for high surface area (porosity) the resistance to settling (drag force) increases.

Particle size distribution can be evaluated in three different ways and data are normalized:

- Cumulative distribution (Q,%): shows the probability that the variable (particle size) is smaller or larger than a value; from this representation the percentile PSD parameters, such median (D_{50}), D_{10} , D_{90} can be evaluated easily
- Distribution density (q,lg): using a logarithmic scale aids resolution of the particle size across size ranges

^e Discrete particle sedimentation is occurring when the concentration of particles in a suspension is so low that no particles interact during the sedimentation process (concentration lower than 2% V/V, as Kissa, 1999⁹⁹, reported). Velocity of particle settling is dependent from the diameter of the spherical particle (d_p) and to the density of particle (ρ_p) and fluid density ρ ($v = \frac{g(\rho_p - \rho)d_p^2}{18\mu}$).^{104, 105}

- Histograms are generally used for expressing particle size determined by sieving: it reports the amount of sample retained in each sieve (D_{Si}).

Other methods for describing particles size are used:

- Sauter mean diameter (SMD, $D[3,2]$) is a weighted mean diameter represented by the sum of the cubic equivalent diameters of particles divided by the sum of the square equivalent diameter (Equation 47) where n_i is the number of particles at a specific equivalent diameter and D_i is the equivalent diameter

$$SMD = \frac{\sum n_i D_i^3}{\sum n_i D_i^2} \quad (47)$$

- Volume mean diameter (VMD, $D[4,3]$) (Equation 48):

$$VMD = \frac{\sum n_i D_i^4}{\sum n_i D_i^3} \quad (48)$$

To define the shape of a particle the aspect ratio parameter is used. This is calculated as the ratio of maximum Feret and minimum Feret diameter taken perpendicularly to the maximum. Particles shape classification methodology are vary.¹⁰⁰

2.8.2.1 Solubility

The solubility is the maximum amount of the soluble substance, the solute, which can be dissolved in a solvent at a specific temperature.¹⁰⁶

From a thermodynamic analysis perspective the stages involved during creation of a solution from solid and solvent are; melting the solid, mixing the melted solid into the solvent to create a homogeneous mixture.

The solubility of ideal system, (systems where the enthalpy variation is only due to the melting of the solid, ΔH_f), x_{eq} , is given by:⁵

$$\ln x_{eq} = \frac{\Delta H_f}{R} \left[\frac{1}{T_f} - \frac{1}{T} \right] \quad (49)$$

In other systems the mixing process is accompanied by considerable change in enthalpy due to solvent-solute interactions (non-ideal systems); in these cases solubility variation with temperature is often described by using empirical constants a, b and c derived from experimental data.

$$\log x_{eq} = a + \frac{b}{T} + c \log T \quad (50)$$

The solubility is mostly a function of temperature and pressure, but also depends on the polarity of the components (solute and solvent) and to the presence of impurities.⁵

Solubility is a key parameter for isolation: the evaluation of washing efficiency, in terms of impurity removal capability and final yield, is related to the mutual solubility of API and impurities in the crystallization and wash solvents. Other effect influenced by the solubility of API and impurities during the isolation process are:

- During filtration, if the crystallization solvent selected exhibits high API and impurity solubility, reduction of yield is accompanied by improvement of impurity removal (This is exemplified in the results reported in chapter 5, chapter 6 and chapter 7)

- “Antisolvent” effects where the addition of the wash solvent leads to a large reduction in solubility of the API and impurities during the washing step and can cause the precipitation of fine particles of API and impurities. Washing efficiency is enhanced by promoting; displacement, diffusion and dilution washing. Selection of miscible crystallization and wash solvents is required. In order to improve washing efficiency and process yield, the use of wash solvents in which the product has very low solubility is required to minimise dissolution of the API. The solvent selected needs solubilise impurities readily respect to the API to promote removal of the impurities from the crystal surface and subsequent removal with the wash solvent. (results reported in chapter 7)
- Drying: incomplete washing can cause formation of solid particle-particle bridges in areas of the cake where residual crystallization solvent is trapped between particles; this leads to agglomerate formation in the isolated product. If the API shows solubility in the selected wash solvent, the same bridging effect is observed. (results reported in chapter 6 and 7). Symbols related to solubility section are reported in Table 11.

Table 11 Solubility theory parameters.

Symbol	Parameter	Unit measure
x_{eq}	Solubility	mol/mol
ΔH_f	enthalpy energy at melting temperature	J/mol
R	gas constant	$8.314\text{mol}^{-1}\text{K}^{-1}$
T_f	melting temperature	K

a,b	empirical constants	-
-----	---------------------	---

2.8.3 Particles morphology

The external shape of a crystal, also known as the crystal habit, is an important parameter in the isolation process because it influences the filtration and washing times and efficiency. During the drying stage morphology influences the drying rate and the overall drying time.¹ Polymorphic form and morphology, relate to the lattice arrangement of the atoms ions or molecules present.

The habit of crystals is mainly influenced by the symmetry of the internal structure, correlated to the symmetrical arrangement of molecules in the crystal lattice. The resulting energy of molecular/ionic attachment to the crystal surface influences the specific face growth rate. The surface chemical character of the crystal can also be influenced by external factors, such as the level of supersaturation of the solution, system temperature, solvent and by the solution purity.⁵

Crystal morphology depends on the crystal phase which nucleates, if the system is polymorphic and the mechanism of crystal growth.

Crystal growth is a kinetic process driven by the concentration exceeding the equilibration condition (temperature, composition, pressure).

According to Davey and Garside, (1999)¹ the important parameters which control crystallization are:

- Solubility and supersaturation

- Nucleation
- Growth

2.8.3.1 Solubility and Supersaturation

If the solute concentration is lower than the equilibrium solubility at that temperature (undersaturation), any crystals present in the system will dissolve. If the solution composition is above the equilibrium solubility crystals can grow. If the concentration is above the supersolubility curve (also known as the metastable zone boundary), crystal nucleation occurs spontaneously and crystal growth continues (Figure 20).

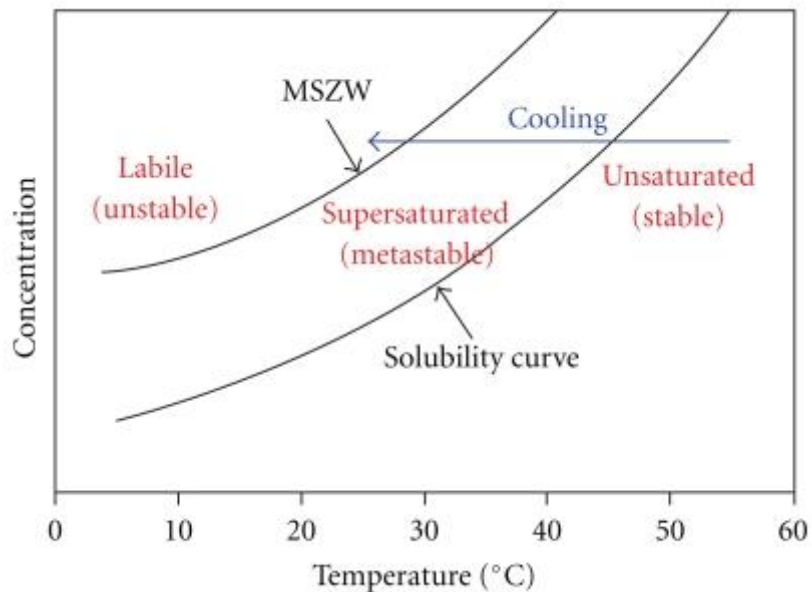


Figure 20 Solubility and supersolubility curves.¹⁰⁷

Supersaturation is defined thermodynamically as (Equation 51):

$$\sigma = \frac{(\mu_{ss} - \mu_{eq})}{kT} \approx \frac{(x_{ss} - x_{eq})}{x_{eq}} \quad (51)$$

Where μ_{ss} and μ_{eq} is the chemical potential of the system in its supersaturated and equilibrium conditions, k is the Boltzmann constant, T is the absolute temperature of the system and x_{ss} and x_{eq} are the solubility values at supersaturated and equilibrium conditions.

Nucleation¹⁰⁴ takes place via the formation of molecular clusters, some molecules become the bulk of the crystal nucleus (the number of these molecules is expressed as z_b), while others remain on the surface of the nucleus (z_s).

The free energy of a spherical cluster (g_z) is given by Equation 52:

$$g_z = z\mu_b + \beta\gamma z^{2/3} \quad (52)$$

Where γ is the interfacial tension between the cluster and the solution, the area of the cluster is defined as $z^{2/3}$ (z is the number of molecules forming the cluster) and β is the area shape factor depending to the nucleus shape and by the chemical potential of the molecules in the bulk of the cluster.

In the case of saturated solution, $x = x_{eq}$, Gibbs free energy is evaluated as (Equation 53):

$$\Delta G = -zkT \ln\left(\frac{x_{ss}}{x_{eq}}\right) + \beta\gamma z^{2/3} \quad (53)$$

Where μ_b is the bulk chemical potential that is evaluated as $\mu_b = \mu^0 + kT \ln x_{eq}$, and $\ln\left(\frac{x_{ss}}{x_{eq}}\right)$ is the supersaturation.

The free energy is function of the cluster size, z , as seen in Figure 21.

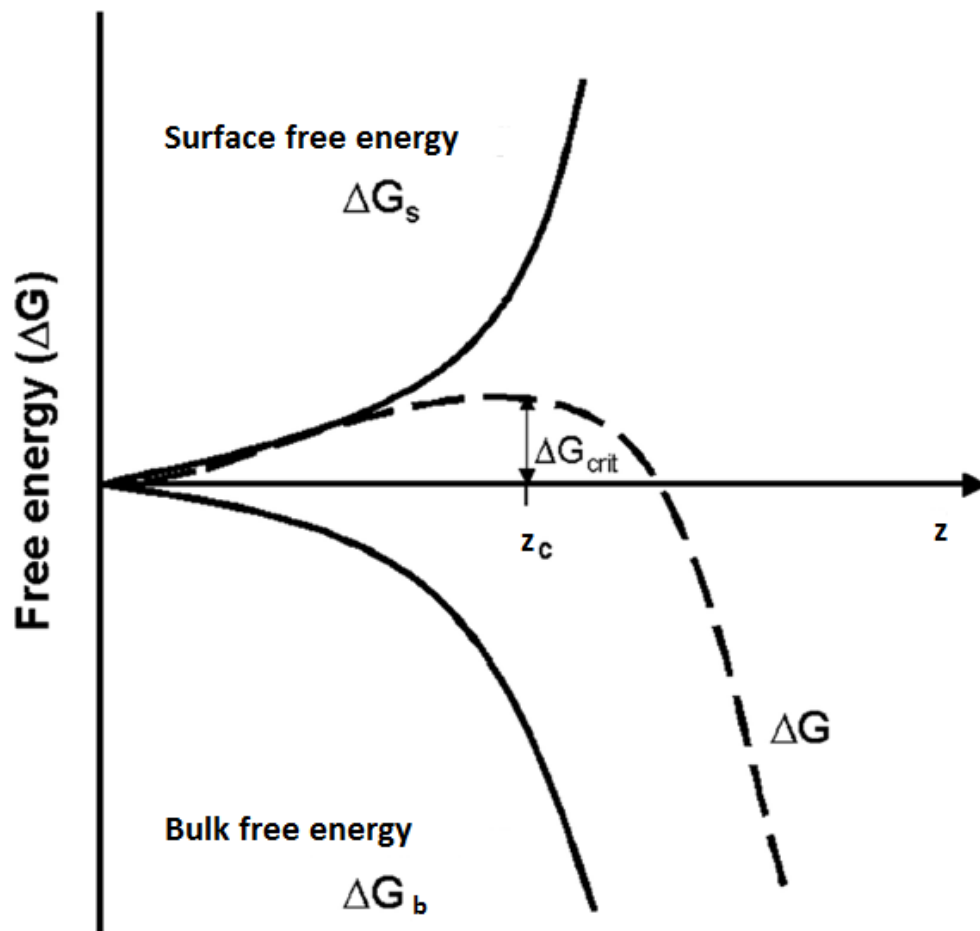


Figure 21 Free energy as function of the cluster size.⁵

In general:

- If a molecular cluster reaches the critical size , z_c , then further growth will lead to a reduction in the free energy of the system, while if the cluster size is smaller than z_c , the cluster will dissolve to reduce the system free energy
- Clusters of size equal to z_c are called critical nuclei: the formation of these nuclei is dependent to the size of the energetic barrier; as supersaturation increases the barrier is reduced and spontaneous nucleation occurs.

The rate of nucleation is related to the propensity for clusters to aggregate and it is related to the supersaturation, temperature and interfacial tension. Interfacial tension generally dominates at low supersaturation, where there is insufficient free energy available to create new surfaces. Increasing supersaturation to reach the critical supersaturation point, the nucleation propensity increases. Other factors may influence nucleation, such as the presence of impurities or catalyst (heterogeneous nucleation)¹⁰⁹⁻¹¹¹ or the presence of external agents, such as seeds, vessel walls, impeller and so on (secondary nucleation).

2.8.3.2 *Crystal growth*

When a crystal is exposed to a supersaturated solution that the flux of growth units approaching the surface is higher than the flux of the units that are leaving, therefore surface growth is always favored. In the bulk of the crystal lattice molecules are surrounded by other molecules and thus maximize their bonding interactions. While on a surface the number of interactions is reduced leading to a state of surface tension. In a simple 3D structure, the units are able to interact in up to 3 directions forming bonding interactions: a surface site where three bonds can be formed is called kinked or K face, a surface where maximum two bonds can be created is called stepped or S face, while in case of a surface with just 1 possible bond, the surface is called flat or F face. As the linear growth rate is proportional to the binding energy of a growth unit on a surface, the growth velocity order is kinked > stepped > flat face.

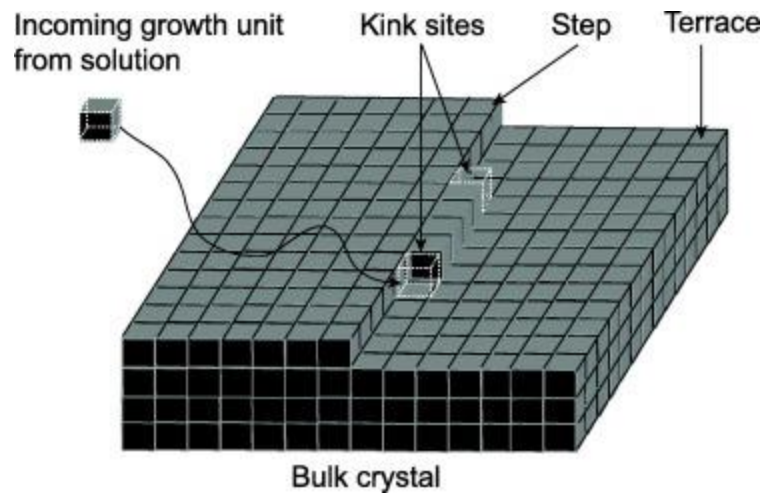


Figure 22 Kinked, stepped and flat facets during crystal growth.¹¹²

The α -factor is used to determine how easily a surface can form sites with multiple binding interactions and how the surface can grow (Equation 54):

$$\alpha = \frac{\Delta E}{kT} \quad (54)$$

Where ΔE is the energy change due to rearrangements of blocks during the crystal growth. In general, during crystal surface growth, two kind of block are presents, solid and fluid block. The fluid blocks are formed by the growth unit dissolved in solvent. During crystal growth, a growth unit in the bulk solution is fully solvated; reaching the crystal surface it looses some of its attached solvent molecules. This partially desolvated unit is then adsorbed on the crystal surface. This adsorbed unit may desolvate further and can diffuse on the surface until reaches a kink site: here the unit forms bonds at the kink site.

Different surface growth mechanisms can be observed: in the case of low α value, crystal surface is rich in kink sites such that all the growth units are able to connect

to the surface and generate a continuous growth. In the case of slightly higher α , surface roughness decreases and islands nuclei are formed on the surface. When α is high, kink sites on the surface are very rare and the surface of the crystal is really flat; in this case crystal growth can progress only if steps can be generated: in this case a spiral growth mechanism is obtained. Crystal growth equations symbols are reported in Table 12.

Table 12 Parameters related to crystal nucleation and growth theory.

Symbol	Parameter
σ	supersaturation
μ_{ss}	chemical potential of the system in supersaturated condition
μ_{eq}	chemical potential of the system in equilibrium condition
x_{ss}	solubility at supersaturated condition
g_z	free energy of a spherical cluster
z	number of molecules forming the cluster
μ_b	bulk chemical potential
β	area shape factor
γ	interfacial tension
ΔG	Gibbs free energy

2.8.4 Wettability

Porous systems are structures where particles of different size and shape are packed together to form a network of capillary pores with a 3D structure. In general, capillary systems are studied by evaluating their physical and mechanical properties, such as by

evaluating hydrostatic pressure, gravitational attraction and forces related to surface tension.

Surface tension and interfacial phenomenon have been widely studied in different scientific fields, in particular soaps and detergents.¹¹³ Young and Laplace firstly related the surface curvature of a liquid to the surface tension, and subsequently modelled this phenomenon with the Laplace equation (Figure 23).¹¹⁴

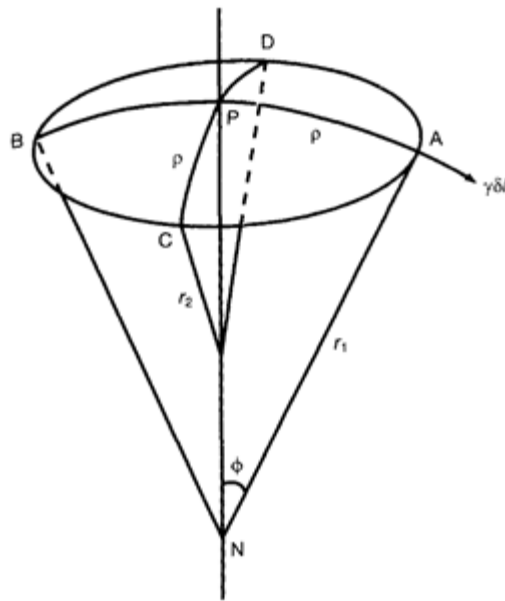


Figure 23 Schematic representation of isolated liquid surface for equilibrium analysis.⁹⁵⁻¹¹⁵

Considering a point P on a curved liquid surface, using it as the centre, and drawing a circle on the surface whose radius is ρ , the resulting liquid cap bounded by the circle is defined. An important assumption to consider is that, to reach mechanical equilibrium ρ tends towards zero. The radii of curvature of AB and CD lines are r_1 and r_2 . The length of the path along the liquid surface from P to any of A, B, C or D can be approximated by ρ ,

(ρ is very small). At point A on the circular boundary of the cap, a small element, δl , experiences a surface tension force of $\gamma\delta l$, where γ is the surface tension expressed in mN/m. Because ϕ is a small angle as ρ approaches zero, the component of this force along the line PN is

$$\gamma\delta l \sin \phi = \gamma\phi\delta l = \gamma \frac{\rho}{r_1} \delta l \quad (55)$$

If all four elements A, B, C, and D are considered, the combined force along PN is

$$\gamma\delta l \left(\frac{2\rho}{r_1} + \frac{2\rho}{r_2} \right) = 2\rho\gamma\delta l \left(\frac{1}{R_1} + \frac{1}{R_2} \right) \quad (56)$$

by Euler's theorem

$$\frac{1}{r_1} + \frac{1}{r_2} = \frac{1}{R_1} + \frac{1}{R_2} \quad (57)$$

where R_1 and R_2 refer to the principal radii of curvature.

$$\int_0^{\frac{\pi\rho}{2}} 2\rho\gamma \left(\frac{1}{R_1} + \frac{1}{R_2} \right) \delta l = \pi\rho^2\gamma \left(\frac{1}{R_1} + \frac{1}{R_2} \right) \quad (58)$$

To keep this isolated surface element in mechanical equilibrium, the surface tension force as shown in Equation 59 must be balanced by the hydrostatic force exerted on the surface.

Therefore

$$(P_2 - P_1)\pi\rho^2 = \pi\rho^2\gamma \left(\frac{1}{R_1} + \frac{1}{R_2} \right) \quad (59)$$

where P_1 and P_2 refer to the pressures within and outside the liquid surface. With $\Delta P = P_2 - P_1$, Equation 55 reduces to equation 56 the Laplace equation

$$\Delta P = \gamma \left(\frac{1}{R_1} + \frac{1}{R_2} \right) \quad (60)$$

From a mechanical consideration, equation 55 provides the first correct definition of surface tension.

2.8.4.1 *Contact angle*

Considering a drop of fluid placed on a smooth plane surface, the liquid may remain as a drop displaying a finite angle of contact θ between the two boundaries liquid/gas (air) and solid/liquid. The contact angle is therefore defined as the angle subtended by the tangent to the liquid/gas boundary constructed at a point on the three-phase line of contact and the tangent to the solid/liquid boundary constructed at the same point (Figure 24).

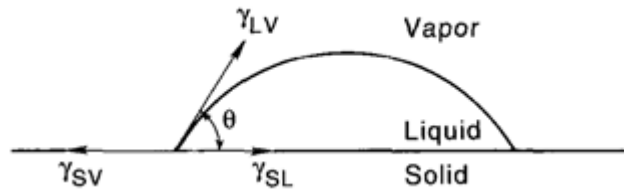


Figure 24 Liquid drop equilibrium on a flat and horizontal surface.^{99, 116}

Thus,

$$\gamma_{lv} \cos \theta = \gamma_{sv} - \gamma_{sl} \quad (61)$$

Where γ_{lv} and γ_{sv} are the surface tension of the liquid and solid respectively and γ_{sl} is the interfacial tension between the liquid and the solid. This equation was first reported by Young in 1805.¹¹⁴ The value of the contact angle may lie between 0 and 180°.

Equations have been developed for cases when surface is not smooth and plain. Wetting on rough surfaces may assume either of two regimes: homogeneous wetting,^{117, 118} where the liquid completely penetrates the roughness, or heterogeneous wetting,¹¹⁹ where air is trapped beneath the liquid inside the roughness.

2.8.4.2 Capillary pressure

Considering a single capillary filled with a wetting liquid at atmospheric pressure, the capillary is then connected to another cylinder containing a non-wetting fluid at atmospheric pressure: spontaneously the non-wetting fluid penetrate and displace the wetting liquid.⁹⁹

$$P_c = P'' - P' = \left(\frac{2\gamma}{R}\right) |\cos(\theta + \phi)| \quad (62)$$

As seen in Equation 56, $R/|\cos(\theta)|$ is the mean radius of curvature of the meniscus and it depends to the orientation of the solid surface with the angle ϕ (Figure 23), because the penetration of the non wetting fluid takes place in the direction of decreasing pore diameter. The pressure difference between the concave and the convex sides of the meniscus is named as capillary pressure and P_c is always a positive defined quantity.

Two different phenomena can be observed in accordance to the non-wetting fluid flow direction: wetting or dewetting.

If the displacement process is to be carried out in the reverse direction, where the wetting phase is displaying the non-wetting phase, then the capillary pressure must be decrease. This process is usually called as spontaneous imbibition or wetting.

Reversely, capillary pressure gradually increases during the non-wetting penetration, causing a variation of pressure inside the capillary (non-equilibrium condition). This phenomenon is called desaturation or dewetting.

2.8.5 Liquid transport in porous media

Three different cases can be evaluated:

- Single phase transport
- Multiphase flow of immiscible fluids
- Miscible displacement and dispersion.

2.8.5.1 *Single phase transport phenomena in porous media*

Darcy's law is the equation that define single phase fluid flow in porous media (Equation 63); fluid conductivity is evaluated using the specific permeability, k , of the medium.⁹⁹

$$v = -\frac{k}{\mu} \nabla \mathcal{P} = -\frac{k}{\mu} (\nabla P - \rho g) \quad (63)$$

Where \mathcal{P} is (Equation 64):

$$\mathcal{P} = P + \rho g z \quad (64)$$

Where z is the distance measured vertically upward from the arbitrary chosen datum level, P is the hydrostatic pressure, ρ is fluid density, g is the gravitational acceleration and v is the Darcy velocity.

An assumption, required to fit Darcy's model with experimental observations is, porous media consists of a network of small blocks and Darcy's law is applied to each block. These blocks must be small enough to get meaningful values for entire system.

In alternative to permeability, for porous media formed by beds of particles, the friction factor f_p is used to evaluate porous bed resistivity (Equation 65).

$$f_p = D_p \frac{\Delta \mathcal{P}}{\rho v^2} L \quad (65)$$

This parameter is considered as a function of the superficial or particle Reynolds number, Re_p (Equation 66):

$$Re_p = D_p v \frac{\rho}{\mu} \quad (66)$$

Where D_p is the average particle diameter (m), ρ is fluid density and L is the length of the bed in the macroscopic flow direction (m).

Different models have been developed to explain single phase flow, but phenomenological models are considered as particularly useful in the case fairly uniform and isometric particles packed together. These models relate the transport coefficients in the porous media to particle properties and packing structure.

This is exemplified in the Carman-Kozeny Equation 67^{70, 120}

$$k_{CK} = \left(\frac{D_{p2}^2}{180} \right) \left[\frac{\phi^3}{(1 - \phi)^2} \right] \quad (67)$$

Where

$$D_{p2} \equiv \frac{6 V_p}{S_p} = \phi_s D_v \quad (68)$$

Where ϕ_s is the sphericity that is the ratio of surface area of the equivalent sphere of the same volume to the actual surface area of the particle.

Often the relation between friction factor and Reynolds number is not linear because of changes in the direction of motion is great enough that the inertial forces become significant compared with viscous forces, therefore Darcy's law is considered no longer valid.

The main discrepancy between this model and reality is that the flow model for the bed of particles does not consider pores as an interconnected system. The Carman-Kozeny or mean hydraulic diameter model and bundle of capillary model can explain these interactions.

In Carman-Kozeny theory¹²¹⁻¹²⁴ a porous medium was assumed to be equivalent to a conduit, was assumed equivalent to a conduit, where its cross section has an extremely complicated shape, but, on the average, a constant open area. This theory evaluates a laminar flow. Channel diameter D_H (Equation 69) that is four times the hydraulic radius, governing the flow rate through the conduit.

$$D_H = \frac{4 * \text{void volume of medium}}{\text{surface area of channels in medium}} = \frac{4\phi}{S_0(1 - \phi)} \quad (69)$$

Where S_0 is the specific surface area (m^2) based on the solid's volume ($S_0 = \frac{6}{x_{SV}}$).⁷⁰

Hagen-Poiseuille equation gives the pore flow velocity (Equation 70):

$$v_p = \left(\frac{\Delta \mathcal{P}}{L_e}\right) \left(\frac{D_H^2}{k_0 16 \mu}\right) \quad (70)$$

Where L_e is the average path length of flow and k_0 is the shape factor. Pore velocity can be correlated with flow velocity in Darcy's law by using Equation 71

$$v_p = \left(\frac{v}{\phi}\right) \left(\frac{L_e}{L}\right) = v_{DF} \left(\frac{L_e}{L}\right) \quad (71)$$

Carman-Kozeny equation can be expressed therefore in two different ways (Equation 72):

$$k_{CK} = \frac{\phi D_H^2}{k_0 16 \left(\frac{L_e}{L}\right)^2} = \frac{\phi^3}{k_0 \left(\frac{L_e}{L}\right)^2 (1 - \phi)^2 S_0^2} \quad (72)$$

Where $\left(\frac{L_e}{L}\right)^2$ is usually called hydraulic tortuosity factor (Figure 25), Υ ,¹²⁵ that is not a property of the bed, but a model parameter. According to several experiments Carman proposed that the best value of $k' = k_0 \Upsilon$ for packed beds is 5, where k' is the Kozeny constant.

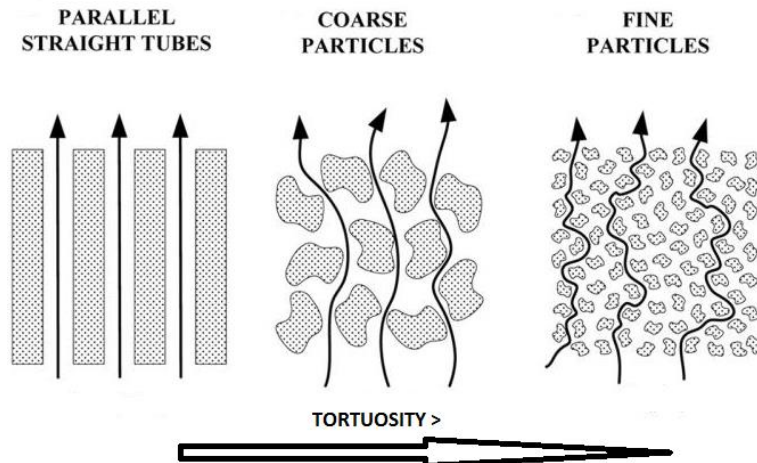


*Figure 25 Illustration of physical meaning of tortuosity.*⁹⁵

2.8.5.2 ***Multiphase flow of immiscible fluids in porous media***

Different researchers have evaluated the flow of immiscible fluids in porous media.¹²⁶⁻¹²⁸

The flow of immiscible fluids (both wetting and non wetting fluids) in porous media may be subdivided into two categories: steady state and unsteady state.

In the steady state flow of immiscible fluids contained in the system the flow is constant at all points and no displacement of any fluids is evaluated. On the other hand, in unsteady state the saturation at a given point in the system will change and in this case displacement can be observed.

Another distinction is made between co-current and counter-current flow. Co-current flow is defined as system where both phases flow in the same direction, while for counter-current flow the different phases flow in opposite direction.

2.8.5.3 ***Steady flow***

Two different fluids flow regimes are considered for immiscible fluids flowing inside capillaries.

The effect of wettability on relative permeabilities in uniform wetted systems at very small capillary numbers has been investigated by several authors.^{62, 63, 85, 129}

In general, the wetting phase preferentially occupies the smaller pores and it is present near the pore walls in those pores that have been penetrated by the non wetting phase. On the other hand, the non wetting phase preferentially occupies the central portion of the larger pores. In addition, viscosity of those two liquids interacts during the immiscible fluids flow.

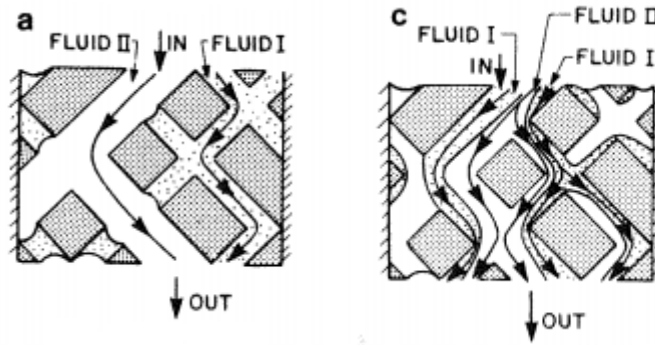


Figure 26 Representation of possible co-current steady two phase flow in porous media.⁹⁹

- In case a of Figure 26 each the wetting and non-wetting phase move through their own separate network of interconnecting channels; if the non-wetting phase saturation increases there is an increase in the number of channels carrying non-wetting phase and a corresponding decrease in the number of channels carrying the wetting phase. This model is called as the channel flow concept.
- When both a wetting and non wetting fluids are flowing simultaneously in all capillaries, the wetting phase covers the capillary surface, while the non wetting phase occupies the central portion of each capillary. This situation is the funicular flow regime regime in which case, increasing proportion of the non wetting phase implies an increase in the average diameter of the funicular entities of this phase (case c);

2.8.5.4 *Displacement*

Displacement occurs when a fluid that fills a porous media is forced by out another fluid.

During a displacement process the capillary equilibrium is disturbed, the pressure difference between the two sides of a meniscus at the fluid interface is assumed to equal

to the capillary pressure as predicted by Laplace's equation. During this process pressure variation along the capillaries are observed.⁶⁴

Due to complex pore morphology, the displacing phase tends to surround and cut off portions of the phase originally present in the pore space. Once cut off and isolated, these blobs of the phase to be displaced normally become stationary because of the interfacial forces that are too great to be overcome by the viscous or gravitational forces present.

As pores in real porous media shows irregular cross sections and rough surfaces the wetting phase is always trapped along the surface in grooves, edges and crevices.

When the flow rate of the displacing phase is increased and/or the value of the interfacial tension between the two phases is decreased sufficiently, the isolated blobs may start to flow along with the displaced phase and to be removed.

2.8.5.5 *Capillary rise and infiltration*

During infiltration liquid enters the porous material under the influence of capillary and gravity forces.

Experimental evidence has shown that the infiltration rate is very large initially and decreases eventually reaching a limiting value at large time. Initial infiltration rates result from capillary forces, while as infiltration proceeds, the relative role of capillary pressure is reduced and ultimately gravitational forces becomes dominant.⁹⁹

The simplest equation to model the rate of capillary penetration into a porous medium is attributed to Washburn (1921).¹³⁰

Together these methods give different insights into the behavior and characteristics with influence flow in porous media (Dang-Vu and Hupka, 2005):¹³¹

- Pore dimension
- Contact angle between liquid phases and the porous solid phase
- Surface free energy of the system
- Capillary penetration behaviour.

A simplifying assumption is that porous media comprise as a bundle of uniform capillary tubes.

The Washburn method is a capillary rise method where a liquid phase (with known properties) penetrates into the porous bed driven by capillary forces.

The penetrating fluid flow inside capillaries is laminar and is governed by the Hagen-Poiseuille Equation 73⁹⁹

$$dV = \frac{r^4 \Delta P \pi}{8\mu h} dt \quad (73)$$

Where dV is the infinitesimal volume (m^3), r is the capillary radius (m), μ is the liquid viscosity, h is defined as the liquid rise inside the capillaries and ΔP is the pressure drop inside the porous bed.

The pressure drop is defined as the difference between capillary pressure and hydrostatic pressure (Equation 74):

$$\Delta P = P_c - P_h = \frac{2\gamma_L}{r} \cos \theta - g\rho h \quad (74)$$

Considering all the above equations, capillary rise height is determined:

$$\frac{dh}{dt} = \frac{r^2}{8\mu h} \left(\frac{2\gamma_L}{r} \cos \theta - g\rho h \right) \quad (75)$$

Assuming that hydrostatic pressure is negligible for a flow where capillary pressure is dominant ($P_c > P_h$),

$$h \frac{dh}{dt} = \frac{r\gamma_L \cos \theta}{4\mu} \quad (76)$$

Assuming also that the initial condition $h = 0$ at $t = 0$, Washburn equation is determined:¹³⁰

$$h^2 = \frac{r\gamma_L \cos \theta}{2\mu} t \quad (77)$$

Where γ_L is the liquid surface tension and θ is the contact angle between liquid and porous media solid (°).

The Washburn equation describes a linear correlation between the capillary rise height squared and time and could be considered valid when:

- The liquid which penetrates the porous bed is in steady state with laminar flow
- No shear is taking place at the interface
- No external pressure is applied
- Gravitational forces are negligible
- There is no crystal dissolution in the wetting solvent.

Tortuosity and porosity of the porous bed can affect the rate and extent of liquid capillary rise and consequently cause experimental errors. Measuring the mass increase vs time

during the capillary rise process can reduce effect of these factors (Equation 78, used in chapter 6).¹³²

$$m = \pi R_c^2 h \rho \varepsilon$$

$$m^2 = \left[\frac{r(\pi R_c^2)^2 \varepsilon^2}{2} \right] \frac{\rho^2 \gamma_L \cos \theta}{\mu} t$$

$$m^2 = \frac{K \rho^2 \gamma_L \cos \theta}{\mu} t \quad (78)$$

Where K is a geometrical parameter that depends to the radius of porous bed (R_c), to the porous bed porosity (ε) and to the capillary radius (r).

The linear correlation between the square of mass and time is vulnerable to a range of incorrect experimental procedures:¹³¹

- Inhomogeneity of bed packing
- Different PSD
- Different radius of capillaries inside the porous bed.

To correlate the chemical properties of porous media (solid) with the fluid phase used for capillary penetration, a thermodynamic approach proposed by Van Oss-Chaudhury-Good (OCG)¹³¹ is considered to be one of the most promising methods to determine surface free energy and surface tension.

The surface tension of a solid can be split in different components that are related to the different interaction between the solid porous media and the fluid and to the intrinsic solid properties.¹³³⁻¹³⁵

$$\gamma_i = \sum_i \gamma_i^j \quad (79)$$

Where j is related to the different surface tension components:

- Dispersive interactions
- Dipolar interactions
- Inductive interactions
- Hydrogen bonding.

A simple way to represent the surface tension components is to gather all different interactions in two main groups: non polar, where Lifshitz-Van der Waals (γ_i^{LW}) interaction are included and polar interactions, where Lewis acid-base components are evaluated (Equation 80).¹³⁶⁻¹³⁹

$$\gamma_i = \gamma_i^{LW} + \gamma_i^{AB} \quad (80)$$

Considering that $\Delta G_{ii} = -2\gamma_i$ Equation 79 can be replaced by

$$\Delta G = \Delta G^{LW} + \Delta G^{AB} \quad (81)$$

Where ΔG^{LW} is the variation of free energy due to Lifshitz-Van der Waals interactions and ΔG^{AB} is the variation of free energy caused by Lewis acid-base interactions. Fowkes and Oss proposed the same method to break up surface tension also for interfacial energy.

$$\Delta G_{SL} = \Delta G_{SL}^{LW} + \Delta G_{SL}^{AB} \quad (82)$$

Where ΔG_{SL}^{LW} is the free energy variation (J) due to Lifshitz-Van der Waals interactions and ΔG_{SL}^{AB} is the free energy variation for Lewis acid-base interactions.

Considering a system where only non polar interaction taking place, polar interaction parameter is considered to be as negligible.¹⁴⁰

$$\Delta G_{SL}^{LW} = -2\sqrt{\gamma_L^{LW}\gamma_S^{LW}} \quad (83)$$

Van Oss (1986, 1987, 1989),¹³⁷⁻¹³⁹ studied the Lewis acid-base interaction theory proposed by Fowkes (1962,1963,1964),¹³³⁻¹³⁵ demonstrated a peculiar behavior between electron-donating interactions (Lewis acid) and electron-acceptor interactions (Lewis base);

$$\Delta G_{SL}^{AB} = -2\sqrt{\gamma_L^+\gamma_S^-} - 2\sqrt{\gamma_L^-\gamma_S^+} \quad (84)$$

γ^+ is the acid component while γ^- is defined as the base component of the interfacial polar tension.

Combining Equation 82, 83 and 84 interfacial free energy equation for solid-liquid system is obtained.

When a drop of liquid is in contact with a surface, interaction between solid and liquid tension is taking place, as shown in Figure 27

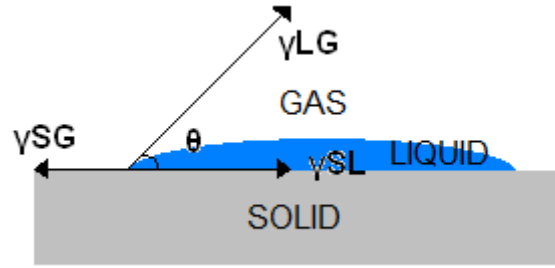


Figure 27 Contact angle that taking place during liquid and surface contact. Picture rearranged from Ottoboni et al.(2013).¹⁴⁰

The equation describing the behavior of liquid drop in contact with a solid is the Young equation.

During drop adhesion also the variation of the Gibbs energy can be determined by using Duprè equation (Equation 85).

$$\Delta G_{SL} = \gamma_{SL} - \gamma_S - \gamma_L \quad (85)$$

Combining Duprè and Young equation, the Young-Duprè equation is obtained (Equation 86):

$$-\Delta G_{SL} = \gamma_L(1 + \cos \theta) \quad (86)$$

By using the thermodynamic approach proposed by Van Oss-Chaudhury-Good (OCG)¹²⁷ different components of solid surface tension are determined.

$$\gamma_L(1 + \cos \theta) = 2 \left(\sqrt{\gamma_L^{LW} \gamma_S^{LW}} + \sqrt{\gamma_L^+ \gamma_S^-} + \sqrt{\gamma_L^- \gamma_S^+} \right) \quad (87)$$

This relation allows us to determine the different component of cake surface energy ($\gamma_S^{LW}; \gamma_S^-; \gamma_S^+$) by measuring with the Washburn method three different contact angles obtained with three different testing liquids with known surface tension components.

2.8.5.6 *Miscible Displacement and Dispersion*

When two immiscible fluids, one with a strong wettability preference are pumped together through a porous medium, they tend to flow in separate channels and maintain their identity.

Other differences between immiscible and miscible fluids used in displacement washing are; washing using immiscible fluids is generally incomplete, while for miscible fluids, displacement eventually asymptotes to completion with no residual mother liquor remaining. Moreover, in displacement washing with miscible fluids the fluids mix, the transition from pure displaced to pure displacing phase tends to become more gradual at increasing flow rate.

Two distinct approaches to displacement have been developed; dispersion in a tubular capillary and dispersion in a porous medium.

Considering dispersion in capillaries^{99, 141} a tracer injected into a stream of water in laminar flow or into quiescent water spreads out in a symmetrical manner with the average flow velocity due to molecular diffusion. Taylor (1953, 1954)^{99, 142, 143} observed that under flowing conditions this phenomenon appears because fluid inside the capillary shows a laminar flow and in the centre of the capillary it moves with twice the mean speed of flow and the tracer moves at the same speed

If a tracer fluid is injected into a homogeneous and isotropic porous medium, saturated with another fluid that is stagnant the tracer diffuses in all directions. On the other hand, if fluid is flowing, the tracer will spread faster in the direction of flow rather than in the perpendicular direction, resulting in a plume of tracer shaped as shown in Figure 28

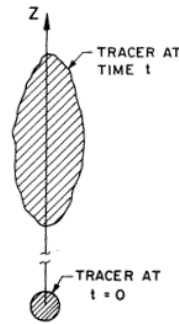


Figure 28 Hydrodynamic dispersion in porous media.⁹⁹

Two different dispersion coefficients can be considered: one that is in the direction of flow and the other one that is in the transverse direction, D_L and D_T , respectively.

A feature of dispersion in porous media is that the stream in capillaries which cross the axis of flow the medium are characterized by differential tracer velocities in relation to the tube that it is streaming. As a result, in the direction of the macroscopic pressure gradient there would be a spreading of the tracer front in the form of micro-fingers, the magnitude of which is proportional to the time elapsed from the moment of starting inject the tracer, this is illustrated in Figure 29.^{99, 144}

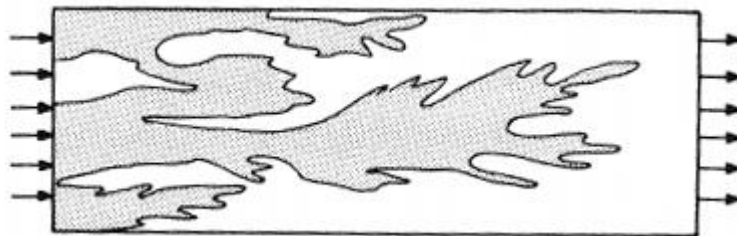


Figure 29 Micro-fingers displacement.⁹⁹

However, in the real case, molecular diffusion will result in a dilution of the tracer moving ahead in pores of high velocity, whereas the tracer lagging behind in pores or that shows less level of conductance, as seen in Figure 30

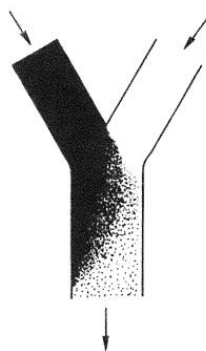


Figure 30 Mixing of two streams by molecular diffusion.⁹⁹

2.8.6 Solvent properties

A number of liquid properties are evaluated in this work; density, viscosity, boiling point and enthalpy of vaporization. All of those properties depend significantly on temperature.

The density a pure liquid is easily available in chemical data handbooks however, the density of solutions need to be determined experimentally.

Viscosity is another important property. Apparent viscosity, expressed in centipoise (cP), equivalent to 1 mNsm^{-2} , tends to decrease with increasing temperature. Kinematic viscosity is the ratio of absolute viscosity and the density is measured in stokes, (St, equals m^2s^{-1}).

Boiling temperature is defined as the temperature at which the pressure exerted by the surroundings upon a liquid is equaled by the pressure exerted by the liquid vapour.¹⁴⁵

During a phase change, a quantity of heat is transferred between the substance and the surrounding media. The enthalpy changes linked to phase changes are; enthalpy of transition from solid 1 to solid 2, (ΔH_t), enthalpy of fusion, from liquid to solid (ΔH_{fus}), enthalpy of sublimation from solid to gas, (ΔH_s) and enthalpy of vaporization from liquid

to gas, (ΔH_v). The relationship between enthalpy change, temperature, volume and pressure system parameter is defined by the Clapeyron equation (Equation 88):

$$\frac{dp}{dT} = \frac{\Delta H}{T \Delta V} \quad (88)$$

Where the dp/dT is the rate of change of vapor pressure with respect to the absolute temperature and ΔV is the variation of volume of the substance during the phase transition. For vaporization the change in vapor pressure of the liquid is due to an increase in temperature. The variation of enthalpy due to a temperature change is defined by the Clausius equation (Equation 89):

$$\frac{d\Delta H}{dT} = -\frac{\Delta H}{T} = c_2 - c_1 \quad (89)$$

Where c_1 and c_2 are the molar heat capacity of the liquid at different temperature ($\text{JK}^{-1}\text{mol}^{-1}$).

In general, the enthalpy of vaporization of a liquid at temperature 1 can be calculated as (Equation 90):

$$\Delta H_{v_1} = \Delta H_{v_2} \left(\frac{T_c - T_1}{T_c - T_2} \right)^{0.38} \quad (90)$$

Where T_c is the critical temperature of the liquid.

2.9 Abbreviations

API, Active Pharmaceutical Ingredient, PSD, particle size distribution, VOCs, volatile organic compounds, D_f , Feret diameter, D_{Mm} Martin number, B, breadth, CL, chord

length, FBRM, focus beam reflectance measurement, T, thickness, D_A , equivalent projected area diameter, D_S , equivalent surface area diameter, D_V , equivalent volume diameter, D_{Si} , equivalent sieve diameter, D_{St} , equivalent Stoke's diameter, Q%, cumulative distribution, q, distribution density, SMD, Sauter mean diameter, VDM, volume mean diameter, D_H , hydraulic diameter, OCG, Van Oss-Chaudhury-Good method.

References

1. Davey, R., J., Garside, J., From Molecules to Crystallizers, Oxford University Press, 2000.
2. Mersmann, A., Crystallization Technology Handbook, CRC Press, 2001.
3. Kaialy, W., Nokhodchi, A., 2012. Antisolvent crystallisation is a potential technique to prepare engineered lactose with promising aerosolisation properties: effect of saturation degree. *Int. J. Pharm.*, 57.
4. Sangwal, K., 2010. On the interpretation of metastable zone width in anti-solvent crystallization. *Cryst. Res. Technol.*, 909
5. Mullin, J., W. Crystallization. Elsevier Science, 2001.
6. Chow, R., Blindt, R., Chivers, R., Povey, M., 2003. The sonocrystallisation of ice in sucrose solutions: primary and secondary nucleation. *Ultrason.*, 595.
7. Kiani, H., Zhang, Z., Delgado, A., Sun, D.-W., 2011. Ultrasound assisted nucleation of some liquid and solid model foods during freezing. *Food Res. Int.*, 2915.
8. Khamskii, E., V., Chemical Process Equipment, 2nd edition, Butterworth-Heinemann, 1969.
9. Garside, J., 1985. Industrial crystallization from solution. *Chem. Eng. Sci.*, 3.
10. Lawton, S., Steele, G., Shering, P., 2009. Continuous Crystallization of Pharmaceuticals Using a Continuous Oscillatory Baffled Crystallizer. *OPR&D*, 1357.
11. Tien, C. Principle of Filtration. Elsevier, 2012.
12. Grace, H., P., 1953. Resistance and compressibility of filter cakes. *Chem. Eng. Prog.*, 18.
13. Tiller, F., M., 1953. The Role of Porosity in Filtration: I. Numerical Methods for Constant Rate and Constant Pressure Filtration Based on Kozeny's Law. *Chem. Eng. Prog.*, 467.
14. Tiller, F., M., 1955. The Role of Porosity in Filtration: II. Analytical Equations for Constant Rate Filtration. *Chem. Eng. Prog.*, 282.
15. Tiller, F., M., 1958. The role of porosity in filtration part 3: Variable-pressure variable-rate filtration. *AIChE J.*, 170.

16. Tiller, F., M., Cooper, H., 1962. The role of porosity in filtration: Part V. Porosity variation in filter cakes. *AIChE J.*, 445.
17. Shirato, M., Murase, T., Ivitari, E., Tiller, F., M. Filtration in the chemical process industry. In M. J. Matteson & C. Orr (Ed.), *Filtration: Principles and practices*, 2nd edition, New York: Marcel Dekker, 1987.
18. Ruth, B., F., 1946. Correlating Filtration Theory with Industrial Practice. *Ind. Eng. Chem.*, 564
19. Stamatakis, K., Tien, C., 1991. Cake formation and growth in cake filtration. *Chem. Eng. Sci.*, 1917.
20. Tien, C., Bai, R., 2003. An assessment of the conventional cake filtration theory. *Chem. Eng. Sci.*, 1323.
21. Tarleton, E., S., Wakeman, R., J. *Solid/liquid separation: equipment selection and process design*. 1st edition, Oxford: Butterworth-Heinemann, 2007.
22. Mondria, H., 1951. Continuous filtration: Calculation of cake impurity and liquid yield. *Chem. Eng. Sci.*, 20.
23. Tien, C., 2002. Cake filtration research—a personal view. *Powder Technol.*, 1.
24. Wakeman, R., J., Sabri, M., N., Tarleton, E., S., 1991. Factors affecting the formation and properties of wet compacts. *Powder Technology, A Special Volume Devoted to the Second Symposium on Advances in Particulate Technology*, 283.
25. Tiller, F., M., Kwon, J., H., 1998. Role of porosity in filtration: XIII. Behavior of highly compactible cakes. *AIChE J.*, 2159.
26. Tiller, F., M., Yeh, C., S., 1987. The role of porosity in filtration. Part XI: Filtration followed by expression. *AIChE J.*, 1241.
27. Sørensen, P., B., Hansen, A. 1993. Extreme Solid Compressibility in Biological Sludge Dewatering. *Water Sci. Technol.*, 133.
28. Tiller, F., M., Green, T., C., 1973. Role of porosity in filtration IX skin effect with highly compressible materials. *AIChE J.*, 1266.
29. Tiller, F., M., Lu, W.-M., 1972. The role of porosity in filtration VIII: Cake nonuniformity in compression–permeability cells. *AIChE J.*, 569.
30. Shirato, M., Aragaki, T., Iritani, E., Funahashi, T., 1980. Constant rate and variable pressure-variable rate filtration of power-law non-newtonian fluids. *J. Chem. Eng. Jpn.*, 473.
31. Mahdi, F., M., Holdich, R., G., 2013. Laboratory cake filtration testing using constant rate. *Chem. Eng. Res. Des.*, 1145.
32. Lee, D., J., Ju, S., P., Kwon, J., H., Tiller, F., M., 2000. Filtration of highly compactible filter cake: variable internal flow rate. *AIChE J.*, 110.
33. Smiles, D., E., 1970. A theory of constant pressure filtration. *Chem. Eng. Sci.*, 985.
34. Murugesan S., Sharma P., K., Tabora J., E. *Design of Filtration and Drying Operations in Chemical Engineering in the Pharmaceutical Industry: R&D to Manufacturing*. Wiley New York, 2010
35. Endo, Y., Alonso, M., 2001. Physical Meaning of Specific Cake Resistance and Effect of Cake Properties in Compressible Cake Filtration. *Filtr. Sep.*, 42.

36. Jin, Y., Zhu, Y., B., Li, X., Zheng, J., L., Dong, J., B., 2015. Scaling Invariant Effects on the Permeability of Fractal Porous Media. *Trans. Porous Media*, 433.
37. Lu, W.-M., Hwang, K.-J., 1993. Mechanism of cake formation in constant pressure filtrations. *Sep. Technol.*, 122.
38. Ni, L., A., Yu, A., B., Lu, G., Q., Howes, T., 2006. Simulation of the cake formation and growth in cake filtration. *Miner. Eng.*, 1084.
39. Bai, R., Tien, C., 2005. Further work on cake filtration analysis. *Chem. Eng. Sci.*, 301.
40. Tien, C., Teoh, S., K., Tan, R., B., H., 2001. Cake filtration analysis—the effect of the relationship between the pore liquid pressure and the cake compressive stress. *Chem. Eng. Sci.*, 5361.
41. Fathi-Najafi, M., Theliander, H., 1995. Determination of local filtration properties at constant pressure. *Sep. Technol.*, *Progress in Separations and Waste Reduction*, 165.
42. Tiller, F., M., Haynes, S., Lu, W.-M., 1972. The role of porosity in filtration VII effect of side-wall friction in compression-permeability cells. *AIChE J.*, 13.
43. Teoh, S.-K., Tan, R., B., H., Tien, C., 2006. A new procedure for determining specific filter cake resistance from filtration data. *Chem. Eng. Sci.*, 4957.
44. Tien, C., Bai, R., Ramarao, B., V., 1997. Analysis of cake growth in cake filtration: Effect of fine particle retention. *AIChE J.*, 33.
45. Lee, D., J., 1997. Filter medium clogging during cake filtration. *AIChE J.*, 273.
46. Bürger, R., Concha, F., H. Karlsen, K., 2001. Phenomenological model of filtration processes: 1. Cake formation and expression. *Chem. Eng. Sci.*, 4537.
47. Stamatakis, K., Tien, C., 1993. *AIChE J.*, 1292.
48. Ripperger, S., Gösele, W., Alt, C., Loewe, T. *Filtration*, 1. Fundamentals. Ullmann's Encyclopedia of Industrial Chemistry, Major Reference Works, 2013.
49. Beckmann, W. 14, *Downstream Processes in Crystallization: Basic Concepts and Industrial Applications*. 1st ed. Weinheim, Germany: Wiley-VCH, 2013.
50. Mota, M., Teixeira, J., A., Yelshin, A., 2002. Influence of cell-shape on the cake resistance in dead-end and cross-flow filtration. *Sep. Purif. Technol.*, 137.
51. Buscall, R., White, L., R., 1987. The consolidation of concentrated suspensions. Part 1.—The theory of sedimentation. *J. Chem. Soc., Faraday Trans. 1*, 873.
52. Kynch, G., J., 1952. A theory of sedimentation. *Trans. Faraday Soc.*, 166.
53. Tiller, F., M., Hsyung, N., B., Cong, D., Z., 1995. Role of porosity in filtration: XII Filtration with sedimentation. *AIChE J.*, 1153.
54. Sperry, D., R., 1917. The principle of filtration: II. *Chem. Met. Eng.*, 161.
55. Bockstal, F., Fourarge, L., Hermia, J., Rahier, G., 1985. Constant Pressure Cake Filtration With Simultaneous Sedimentation. *Filtr. Sep.*, 255.
56. Yim, S.S., 1999. A Theoretical and Experimental Study on Cake Filtration with Sedimentation. *Korean J. Chem. Eng.*, 308.
57. Rushton, A., Rushton, A., 1973. Sedimentation effects in filtration. *Filt. Sep.*, 267. (cited from 58)

58. Research gate website [cited 2018-09-15]. <https://www.researchgate.net/publication/48353340> The influence of sedimentation during downward cake filtration.
59. Kuo, M., T., Barrett, E., C., 1970. Continuous filter cake washing performance. *AIChE J.*, 633.
60. Rhodes, F., H., 1934. *Ind. Eng. Chem.*, 1331.
61. Wakeman, R., J., Rushton, A., 1974. A structural model for filter cake washing. *Chem. Eng. Sci.*, 1857.
62. McCaffery, F., G., Bennion, D., W., 1974. *J. Can. Pet. Technol.*, 42.
63. Yadav, G., D., Dullien, F., A., L., Chatzis, I., Macdonald, I., F., 1987. *SPE Reservoir Engineering*, May.
64. Calvo, A., Paterson, I., Chertcoff, R., Rosen, M., Hulin, J., P., 1990. *Fundamentals of Fluid Transport in Porous Media*. May 14-18, Arles, France.
65. Dullien, F., A., L., 1988. *Chem. Eng. And Tech. II*, 407.
66. Ruslim, F., Nirschl, H., Stahl, W., Carvin, P., 2007. Optimization of the wash liquor flow rate to improve washing of pre-deliquored filter cakes. *Chem. Eng. Sci.*, 3951.
67. Huhtanen, M., Salmimies, R., Kinnarinen, T., Häkkinen, A., Ekberg, B., Kallas, J., 2012. Empirical Modelling of Cake Washing in a Pressure Filter. *Sep. Sci. and Technol.*, 1102.
68. Michaels A., S., Baker W., E., Bixler H., J. and Vieth W., R., *Z. E. C. Fund*, 1967, 33.
69. Ruslim, F., Hoffner, B., Nirschl, H., Stahl, W., 2009. Evaluation of pathways for washing soluble solids. *Chem. Eng. Res. Des.*, 1075.
70. Wakeman, R., 2007. The influence of particle properties on filtration. *Sep. Purif. Technol.*, 234.
71. Murru, M., Giorgio, G., Monomoli, S., Ricard, F., Stepanek, F., 2011. Model-bases scale-up of vacuum contact drying of pharmaceutical compounds. *Chem. Eng. Sci.*, 5045.
72. Lekhal, A., Girard, K., P., Brown, M., A., Kiang, S., Khinast, J., G., Glasser, B., J., 2004. The effect of agitated drying on the morphology of l-threonine (needle-like) crystals. *Int. J. Pharm.*, 263.
73. Tsosas, E., Metzger, T., Gnielinski, V., Schundler, E. *Ullmann's Encyclopedia of Industrial Chemistry*. 11th ed. Weinheim: Wiley-VCH, 2012
74. Simurda, M. MSc thesis: Solvent selection for isolation of pharmaceutical products. Dept. of Chemical Engineering, University of Chemistry and Technology Prague 2017.
75. Intelvi, M. MSc thesis: Contact drying of particulate pharmaceuticals: modelling and simulation. Dept. of Chemical Engineering Principles and Practice "I. Sorgato, University of Padova, Padova, Italy, 2010.
76. Kougoulos, E., Chadwick, C., E., Ticehurst, M., D., 2011. Impact of agitated drying on the powder properties of an active pharmaceutical ingredient. *Powder Technol.*, 308.

77. Lekhal, A., Girard, K., P., Brown, M., A., Kiang, S., Glasser, B., J., Khinast, J., G., 2003. Impact of agitated drying on crystal morphology: KCl–water system. *Powder Technol.*, 119.
78. Lim, H., L., Hapgood, K., P., Haig, B., 2012. Understanding and preventing agglomeration in a filter drying process. *Powder Technol.*, 146.
79. Sahni, E., K., Chaudhuri, B., 2012. Contact drying: A review of experimental and mechanistic modelling approaches. *Int. J. Pharm.*, 2012, 334-348.
80. Birch, M., Marziano, I. Understanding and Avoidance of Agglomeration During Drying Processes: A Case Study. *OPR&D*, 1359.
81. MacLeod, C., S., Muller, F., L., 2012. On the Fracture of Pharmaceutical Needle-Shaped Crystals during Pressure Filtration: Case Studies and Mechanistic Understanding. *OPR&D*, 425.
82. Muller, F., L., 2009. On the Rheological Behaviour of Batch Crystallisations. *Chem. Eng. Res. Des.*, 627.
83. Lamberto, D., J., Cohen, B., Marencic, J., Miranda, C., Petrova, R., Sierra, L., 2011. Laboratory methods for assessing API sensitivity to mechanical stress during agitated drying. *Chem. Eng. Sci.*, 3868.
84. Papageorgiou, C., D., Langston, M., Hicks, F., am Ende, D., Martin, E., Rothstein, S., Salan, J., Muir, R., 2016. Development of Screening Methodology for the Assessment of the Agglomeration Potential of APIs. *OPR&D*.
85. Chatzis, I., Dullien, F., A., L., 1983. Dynamic immiscible displacement mechanisms in pore doublets: theory versus experiments. *J. Colloid Interface Sci.*, 199.
86. Tamrakar, A., Gunadi, A., Piccione, P., M., Ramachandran, R., 2016. Dynamic agglomeration profiling during the drying phase in an agitated filter dryer: Parametric investigation and regime map studies. *Powder Technol.*, 109.
87. Zhang, S., Lamberto, D., J., 2014. Development of New Laboratory Tools for Assessment of Granulation Behavior During Bulk Active Pharmaceutical Ingredient Drying. *J. Pharm. Sci.*, 152.
88. Brennecke J., F, Maginn E., J., 2001. Ionic liquids: innovative fluids for chemical processing. *AIChE J.*, 2384.
89. Sheldon R., A., 2001. Catalytic reactions in ionic liquids. *Chem. Comm. (Camb)*, 2399.
90. Henderson, R., K., Jiménez-González, C., Constable, D., J., C., Alston, S., R., Inglis, G., G., A., Fisher, G., Sherwood, J., Binks, S., P., Curzons, A., D., 2011. Expanding GSK's solvent selection guide – embedding sustainability into solvent selection starting at medicinal chemistry. *Green Chem.*, 854.
91. Curzons, A., D., Constable, D., C., Cunningham, V., L., 1999. Solvent selection guide: a guide to the integration of environmental, health and safety criteria into the selection of solvents. *Clean Technol. Env. Policy*, 82.
92. Clark, J., H., Tavener, S., J., 2007. Alternative Solvents: Shades of Green. *OPR&D*, 149.
93. Tucker, J., L., 2006. Green Chemistry, a Pharmaceutical Perspective. *OPR&D*, 315.

94. Sheldon, R., A., 2012. Fundamentals of green chemistry: efficiency in reaction design. *Chem. Soc. Rev.*, 1437.
95. Leazer, J., L., Gant, S., Houck, A., Leonard, W., Welch, C., J., 2009. Removal of Common Organic Solvents from Aqueous Waste Streams via Supercritical CO₂ Extraction: A Potential Green Approach to Sustainable Waste Management in the Pharmaceutical Industry. *Environ. Sci. Technol.*, 2018.
96. Perrut, M., 2000. Supercritical Fluid Applications: Industrial Developments and Economic Issues. *Ind. Eng. Chem. Res.*, 4531.
97. Smith, K., B., Bridson, R., H., Leeke, G., A., 2011. Solubilities of Pharmaceutical Compounds in Ionic Liquids. *J. Chem. Eng. Data*, 2039.
98. Swarloski, R., P., Holbrey, J., D., Rogers, R., D., 2003. Ionic liquids are not always green: hydrolysis of 1-butyl-3-methylimidazolium hexafluorophosphate. *Green Chem.*, 361.
99. Dullien, F., A., L., Porous media fluid transport and pore structure, second edition. Academic press inc., 1992.
100. Merkus, H., H. Particle Size Measurements. Springer, 2009.
101. Terence Allen Particle Size Measurement, Volume 1 5th edition. Chapman and Hall Dordrecht, Netherlands, 2012.
102. Research gate website [cited 2018-09-15]
https://www.researchgate.net/profile/Ioan_Tanu/post/What_is_the_meaning_of_D4_3_and_D0_5_values_in_grain_size_analysis_and_how_is_it_calculated/attachment/59d63265c49f478072ea189a/AS%3A273632960417813%401442250590500/download/Basic_principles_of_particle_size_analysis_MRK034.pdf
103. Kissa, E. Dispersions: Characterisation, Testing and Measurement. In *Dispersions: Characterisation, Testing and Measurement*. New York: Marcel Decker, 1999.
104. Patwardhan, S. (2012). CP405 - Environmental Technology Course Notes. Glasgow: University of Strathclyde.
105. Quispe, J., Concha, F., Toledo, P., G., 2000. Discrete sedimentation model for ideal suspensions. *Chem. Eng. J.*, 135.
106. Abolghasem, J. Handbook of Solubility data for pharmaceuticals. CRC Press, Taylor & Francis Group, NW, 2010.
107. Panagiotou, T., Fisher, R., J., 2011. Enhanced Transport Capabilities via Nanotechnologies: Impacting Bioefficiency, Controlled Release Strategies, and Novel Chaperones. *J. Drug Delivery*, 1.
108. Aulton, M., E. Aulton's Pharmaceuticals: The Design and Manufacture of Medicines, 5th edition. Elsevier health, 2018.
109. Hendriksen, B., A., Grant, D., J., W., Meenan, P., Green, D., A., 1998. Crystallisation of paracetamol (acetaminophen) in the presence of structurally

- related substances. *J. Cryst. Growth*, 629.
110. Hendriksen, B., A., Grant, D., J., W., 1995. The effect of structurally related substances on the nucleation kinetics of paracetamol (acetaminophen). *J. Cryst. Growth*, 252.
 111. Kuvadia, Z., B., Doherty, M., F., 2013. Effect of Structurally Similar Additives on Crystal Habit of Organic Molecular Crystals at Low Supersaturation. *Cryst. Growth Des.*, 1412.
 112. Li, J., Tilbury, C., J., Kim, S., H., Doherty, M., F., 2016. A design aid for crystal growth engineering. *Prog. Mater. Sci.*, 1.
 113. Mittal, K., L. *Advances in Contact Angle, Wettability and Adhesion*, Volume 1. Wiley, 2013.
 114. Ip, S., W., Toguri, J., M., 1994. The equivalency of surface tension, energy and surface free energy surface. *J. Mater. Sci.*, 688.
 115. Defay, R., Prigogine, I. *Surface Tension and Adsorption*. Longmans, Green and Co. Ltd., London, 1966.
 116. Craig, F., F., Jr., 1971. *The Reservoir Engineering Aspects of Waterflooding*. Society of Petroleum Engineers of AIME, Monograph, Vol. 3, Dallas, Texas.
 117. Wenzel, R., N., 1936. *Ind. Eng. Chem.*, 988.
 118. Wenzel, R., N., 1949. *J. Phys. Coll. Chem.*, 1466.
 119. Cassie, A., B., D., Baxter, S., 1944. Wettability of porous surfaces. *Trans. Faraday Soc.*, 546.
 120. Svarovsky, L., *Solid-Liquid Separation*, 4th edition. Elsevier, 2001.
 121. Carman, P., C., 1937. *Trans. Inst. Chem. Eng.*, London, 150.
 122. Carman, P., C., 1938. *J. Soc. Chem. Ind.*, 225.
 123. Carman, C., M. *Flow of Gases Through Porous Media*. Butterworths, London, 1956. (from ref 95)
 124. Kozeny, J., 1927. *Royal Academy of Science, Vienna, Proc. Class I*, 3127.
 125. Bear, J. *Dynamics of Fluids in Porous Media*. Elsevier, New York, 1972. (from ref 95)
 126. Muskat, M. *The flow of homogeneous fluids through Porous Media*. McGraw-Hill, New York, 1937. (from ref 95)
 127. Scheidegger, A., E. *Then Physics of flow through Porous Media*. Univ. of Toronto Press, 1974. (from ref 95)
 128. De Wiest, R., J., M. *Flow through Porous Media*. Academic Press, New York, 1969. (from ref 95)
 129. Owens, W., W., Archer, D., L., (1971), *J. Pet. Tech.*, 873. (from ref 95)
 130. Washburn, E., W., 1921. *The Dynamics of Capillary Flow*. *Phys. Rev.*, 273.
 131. Dang-Vu T., Hupka, J., 2005. Characterization of porous materials by capillary rise method. *Physicochem. Probl. Mi.*, 47.
 132. Siebold, A., Walliser, A., Nardin, M., Oppliger, M., Schultz, J., 1997. Capillary rise method for thermodynamic characterization of solid particle surface. *J. Colloid Interface Sci.*, 60.

133. Fowkes, F., M., 1962. Determination of interfacial tensions, contact angles, and dispersion forces in surfaces by assuming additivity of intermolecular interactions in surfaces. *J. Phys. Chem.*, 382.
134. Fowkes, F., M., 1963. Additivity of intermolecular forces at interfaces. I. Determination of the contribution to surface and interfacial tensions of dispersion forces in various liquids. *J. Phys. Chem.*, 2538.
135. Fowkes, F. M., 1964. *Ind. Eng. Chem.* 40.
136. Mittal, K., L., *Physicochemical aspects of polymer surfaces*. Plenum Press, 1983. (from ref 95)
137. Oss, C., J., V., Ju, L., Chaudhury, M., K., Good, R., J., 1986. The role of van der Waals forces and hydrogen bonds in “hydrophobic interactions” between biopolymers and low energy surfaces. *J. Colloid Interface Sci.*, 378.
138. Oss, C., J., V., Ju, L., Chaudhury, M., K., Good, R., J., 1987. Monopolar surfaces. *Adv. Colloid Interface Sci.*, 35.
139. Oss, C., J., V., Ju, L., Chaudhury, M., K., Good, R., J., 1989. Estimation of the polar parameters of the surface tension of liquids by contact angle measurements on gels. *J. Colloid Interface Sci.*, 313.
140. Ottoboni, S., Paterno', V., A., Gronchi, P., 2013. Determinazione della bagnabilità delle polveri. *Trattamenti e Finiture*, 44.
141. Griffith, A., 1911. *Proc. Phys. Soc., London*, 190. (from ref 95)
142. Taylor, L., 1953. *Proc. R. Soc., London Ser. A*, 186.
143. Taylor, L., 1954. *Proc. R. Soc., London*, 857.
144. Collins, R., E. *Flow of Fluids through Porous Materials*, Van Nostrand-Reinhold Princeton, New Jersey, 1961. (from ref 95)
145. Green, D., Perry, R. *Perry's Chemical Engineers' Handbook*, 8th edition. McGraw-Hill, New York, 2008.

3 Aims and thesis structure

The research program focused on solid-liquid separation using cake formation assisted by; vacuum, cake washing, cake deliquoring and drying. Many parameters influence both isolation process performance and the final product characteristics:

- **CRYSTAL PROPERTIES:**
 - Particles size and size distribution
 - Crystal shape, polymorphic form and surface structure
 - Surface wettability
 - Particle porosity
 - Particles sedimentation and packed bed porosity.
- **FLUID DYNAMIC PARAMETERS:**
 - System viscosity and density
 - Pressure
 - Slurry flow characteristics
 - Particle rheology
- **SOLVENT:**
 - Chemical characteristics of the solvent (polarity, solubility, density, viscosity, propensity to evaporate)
 - Process safety, health and environment (SHE) (use of green solvents vs traditional solvents).
- **EQUIPMENT:**
 - Mechanism of filtration, washing and drying
 - Product recovery

- Filtration, washing and drying efficiency
- Final product properties dependency on process parameters.

These parameters play a fundamental role in the study of an isolation process: they account for microscopic and macroscopic properties of the system and it is necessary to consider the role of those properties in each step of the isolation process.

Studying the microscopic interaction between chemical species present during an isolation step deepens our understanding of how:

- To select solvents to increase system purity. In chapter 5 alternative analytical techniques to determine API-related impurities and their interaction during crystallization is discussed. The evaluation of impurity adsorption mechanisms during crystallization and the location of impurity deposition on API crystal faces is fundamental to determine which solvent characteristics to select in designing the washing strategy.
- To design new isolation equipment (chapters 6 and 7); the evaluation of particles chemical, physical and mechanical properties are useful for designing a flexible and versatile isolation system able to rapidly filter particles, whilst avoiding particle breakage, achieving the required purity and maintaining unaltered the particle properties obtained during crystallization.

This work illustrates how by changing the chemical and physical slurry properties and process parameters, the isolation performance and product particle quality can be influenced.

By using a well characterized API as a model compound, it is possible to use data available from previous research and so focus on the specific research questions targeted in this thesis. For this reason, paracetamol was selected as the API candidate. A series of crystallization and wash solvents were chosen to evaluate the effect of solvent properties on isolation performance. Paracetamol related impurities were used to investigate filtration, washing and isolation efficiency. To improve the eco-sustainable characteristics of isolation green solvents were used during the washing stage to evaluate the impact of these alternative solvents on final product characteristics and process efficiency (chapter 6).

The mind map shown in Figure 31 illustrates the key aspects of the research summarized in the discussion above.

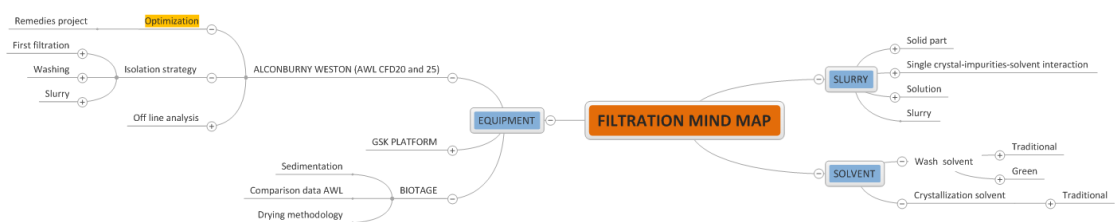


Figure 31 Reduced continuous isolation program mind map.

This project has focused on creating a consistent evaluation method to:

- Determine how impurity molecules-interact with both API and solvent(s) during the crystallization process to improve the washing strategy
- Evaluate the feasibility of alternative analytical techniques to quantify API-impurity interactions after crystallization process

- Determine the role of crystals and their chemical and physical properties in defining filtration, washing and drying performance.
- Evaluate the use of green solvents during the washing to determine their capability to remove related impurities; determine their impact on the whole isolation process (including washing and drying).
- Understand how wash solvents interact with impurities and API particles and API dissolved in the mother liquor during the washing process (addressing impurity removal, impurity and / or API precipitation and API dissolution during washing)
- Develop new analytical techniques to investigate how particle properties change during the isolation process; evaluate the washing and drying efficiency with respect to particle size, size distribution and mechanical properties of single crystals, small agglomerates and large agglomerates.
- Develop and test new isolation equipment designed to move the lab scale isolation from batch to continuous processing.
- Compare batch and continuous filtration process to determine benefits and drawbacks of continuous filtration.

4 Materials and methods

4.1 Material: paracetamol

The compound used for all the experimental work is paracetamol, ($C_8H_9NO_2$). This project has many questions related to equipment capability, chemical and physical material interactions during isolation that the use of a well-researched compound is needed to facilitate both experimental work and data interpretation.¹⁻³

Paracetamol, also known as acetaminophen, is a molecular organic compound and an active pharmaceutical ingredient (API) that shows analgesic and antipyretic effects (cold relief). It is considered as relatively safety medicine, even if in high dosage it has toxic effects.⁴ Common synthesis methods are reported by (Ellis, 2002).⁴

Paracetamol consists of a benzene ring core, substituted by one hydroxyl group and the nitrogen atom of an amide group in the para position (Figure 32).^{5, 6} The amide and hydroxyl groups can act as hydrogen bond donors, the carbonyl and hydroxyl groups acts as intramolecular hydrogen bond acceptors. The combination of these hydrogen bond donors and acceptors allow the formation of a hydrogen bonded network in the crystal lattice (this characteristic bonding behaviour is sometimes described as a push-pull molecule). The $C = O \cdots HO$ and $OH \cdots NH$ molecules of successive layers form a head to tail sequence of hydrogen bonds.

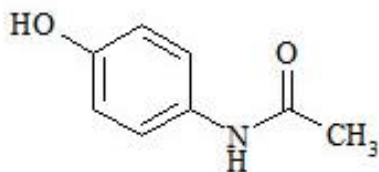


Figure 32 Molecular structure of paracetamol.

In Table 13 the crystallographic and thermal properties of the three main paracetamol polymorphs are summarized.

Table 13 Crystallographic and thermal properties of different paracetamol polymorphisms.

Polymorph	Lattice	Thermal properties	Advantages/disadvantages
Form I	-Monoclinic centrosymmetric crystal structure with space group P21/n ⁷ -Crystallizes with 4 molecules in a unit cell dimensions a=11.709Å, b=9.375Å, c=7.104Å and β =97.42°	-Melting temperature 169°C ⁸ - Glass transition at 23°C ⁸	-Thermodynamically stable at room temperature; -Poor compaction behaviour ^{1, 10-12}
Form II	Orthorhombic structure ⁷	Melting temperature 157°C ⁹	-Metastable - Parallel hydrogen-bonded sheets along the <i>c</i> axis, giving slip planes which allow plastic deformation ¹³
Form III			- Very unstable ^{14, 15}

The habit of paracetamol form I crystals can vary from hexagonal to needle-like depending on the crystallization conditions. The calculated principal facets of paracetamol (using BFDH modelling) are shown in Figure 33 and paracetamol functional groups exposed on each facet are summarised in Table 14.^{2, 16}

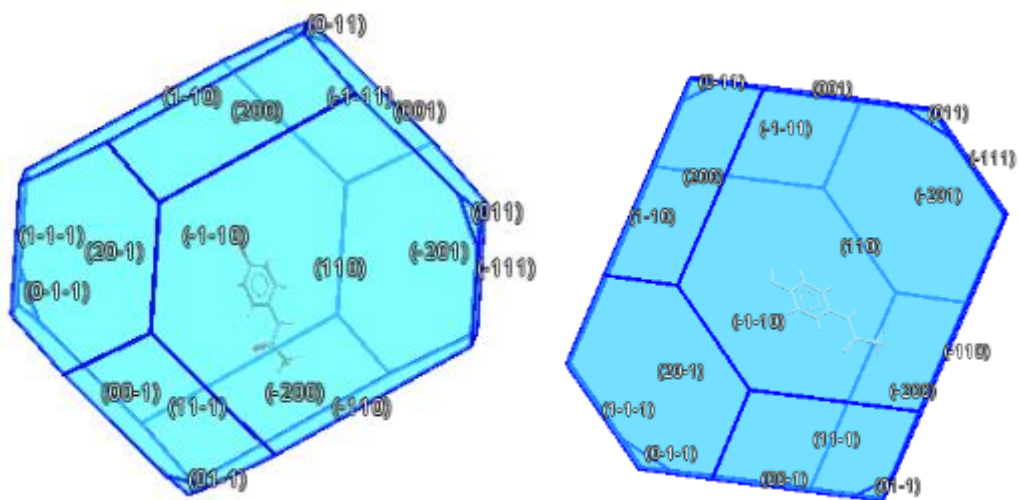
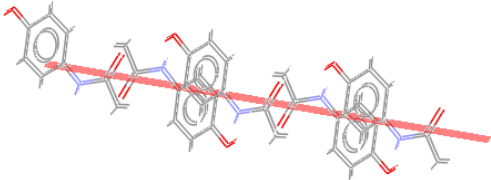
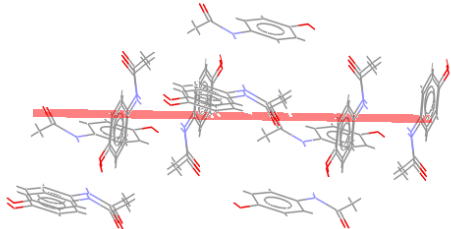
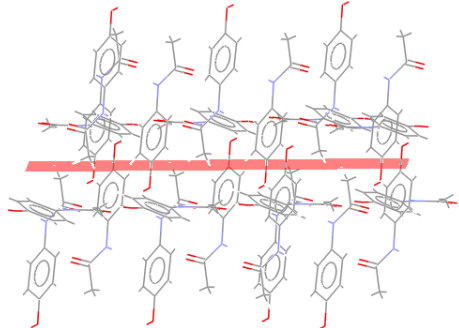
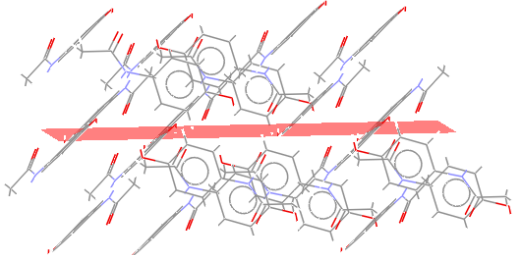


Figure 33 Main faces of paracetamol form I. Paracetamol predicted morphology using the Bravais-Friedel-Donnay-Harker (BFDH) method assuming that the relative growth rates R_{hkl} of the crystal faces is inversely proportional to the inter-planar spacing d_{hkl} , without taking account of the chemical nature of the crystal, molecular packing arrangement or crystallising environment.

Table 14 Molecular packing diagrams based upon the crystallographic structures: the (001) face showing more polar surface with exposed $-OH$ and $-NHCOCH_3$ groups in various directions; the (20-1) face showing mainly the $-OH$ and $-C=O$ groups exposed from the surface; the (011) face shows $-NHCOCH_3$ group exposed; the (-110) face showing less polar with less functional groups $-OH$ and $-NHCOCH_3$ exposed. The molecules can be seen to be arranged alternatively nearly parallel and perpendicular to the surface. Face (11-1) shows $-NHCOCH_3$ group exposed; the (200) face showing $-OH$ and $-NHCOCH_3$ exposed. The red shadow represents a crystal plane. Depth of the slice 10\AA , Area of the slice 20\AA .

Facet	Functional group exposed on each facet
(001) main facet	
(20-1)	

	
(0-11), (011) and (1-10)	
(-110) and (-1-10)	
(11-1)	
(200)	

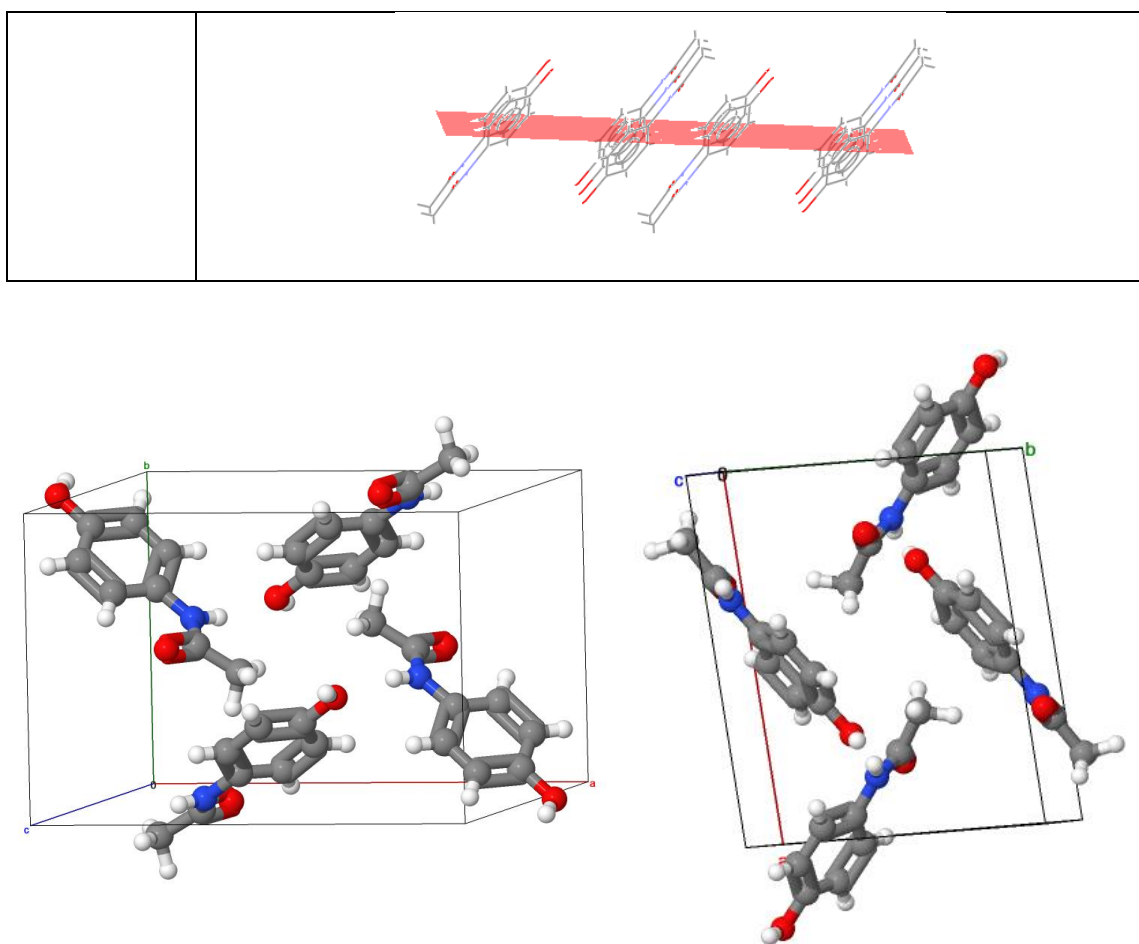
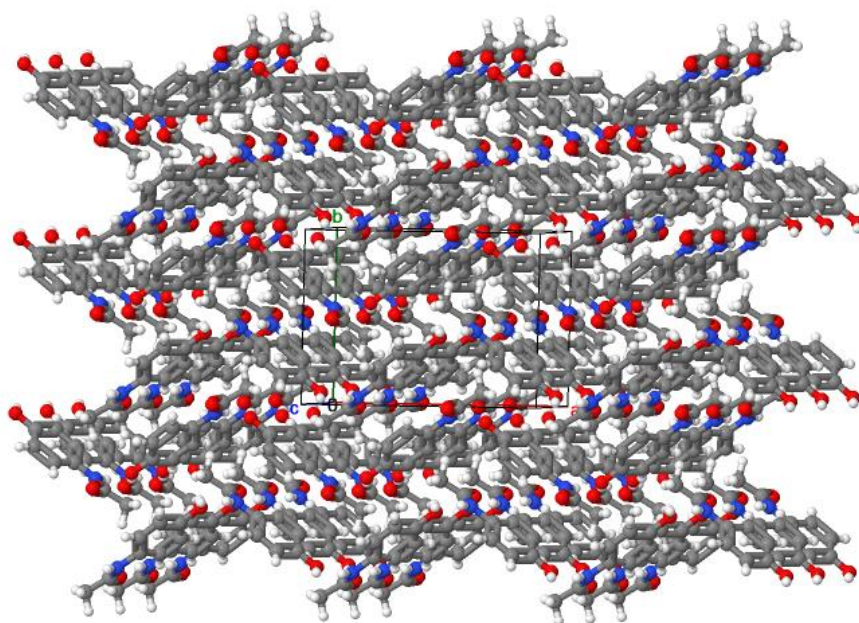
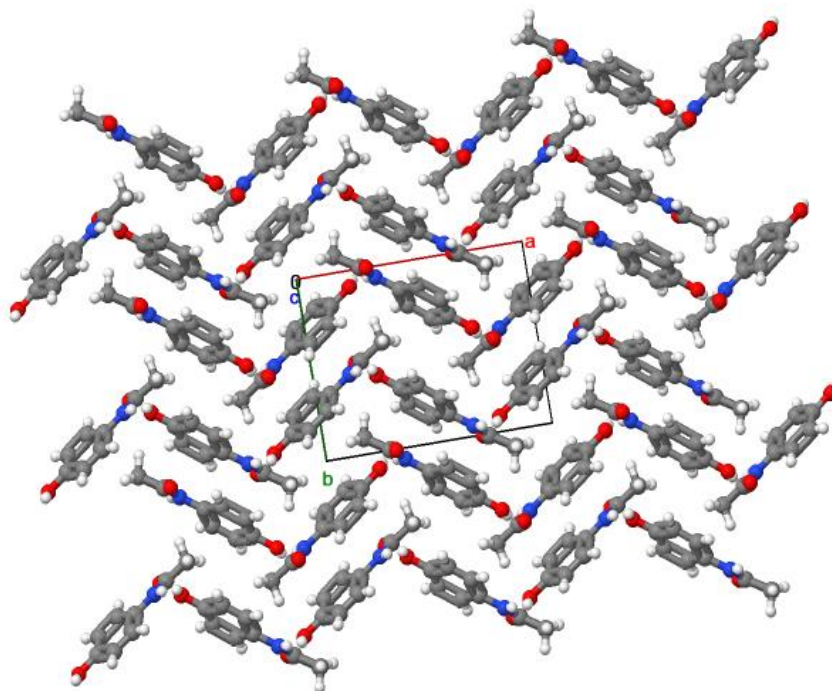


Figure 34 Space distribution and orientation in crystal lattice of paracetamol form I molecules.





*Figure 35 Space distribution and orientation in crystal lattice of paracetamol form I molecules.3*3 packing structure.*

Paracetamol molecules pack in a corrugated hydrogen bonded sheet stacked in the (010) direction. Consecutive stacks are held together by van der Waals interactions (Figure 34 and Figure 35).⁶ Hydrogen bond strength is approximately equal to $8.31 \text{ kcal mol}^{-1}$,² which corresponds to approximately 30% of the total lattice energy.¹ In general, the strength of hydrogen bonding is affected by the strength of hydrogen bonding with solvents.⁵

Other chemical and physical properties of paracetamol are listed below:

- Infrared spectroscopy (Table 15)

Table 15 IR frequency of paracetamol functional groups for three polymorphic forms of paracetamol.¹⁴

Form I	Form II	Form III	Related functional groups
3329	3330	3328	N-H of amidic group
1650	1673	1656	C=O of amidic group
1564	1559	1569	C-N of amidic group
1516	1510	1510	C-N of amidic group
1260	1280	1275	C-N and N-H of amidic group
1610	1628	1614	C-C of aromatic group
1510	1510	1510	C-C of aromatic group
1442	1462	1462	C-C of aromatic group
1173	1169	1173	C-H of aromatic group
1110	1110	1110	C-H of aromatic group

- Wettability: Heng et al. (2006)^{17, 18} studied the wettability of paracetamol form I using the sessile drop technique and by employing different liquid probes, such as diiodomethane, water ethylene glycol and formamide. His research group observed the following contact angles and surface energy, using the Owens-Wendt analytical method (Table 16 and Table 17).

Table 16 Values of advancing (θ_a), receding (θ_r) and contact angle hysteresis ($\Delta\theta$) of different paracetamol facets with different test liquids.^{17, 18}

Facet	Di-iodiomethane			Water			Ethylene glycol	Formamide
	Advancing contact angle θ_a (°)	Receding contact angle θ_r (°)	Hysteresis contact	Advancing contact angle θ_a (°)	Receding contact angle θ_r (°)	Hysteresis contact	Advancing contact angle θ_a (°)	Advancing contact angle θ_a (°)
(201)	48.8 ± 2.2	26.9 ± 5.7	22	38.1 ± 4.6	22.6 ± 3.6	16	-	13.3 ± 1.2
(001)	49.8 ± 3.2	26.4 ± 5.3	23	15.9 ± 3.1	0	16	-	-
(011)	50.7 ± 2.9	30.4 ± 4.3	20	28.8 ± 5.7	23.7 ± 6.0	6	10.9 ± 2.5	14.5 ± 2.5
(110)	50.2 ± 2.4	23.8 ± 3.0	26	50.8 ± 4.9	17.5 ± 3.0	33	15.7 ± 3.0	17.6 ± 3.0
(010)	27.8 ± 2.5	13.4 ± 2.0	14	67.7 ± 2.5	26.4 ± 4.5	41	42.5 ± 3.2	46.9 ± 2.4

Table 17 Surface energy values of paracetamol facets determined by Owens-Wendt analysis.^{17, 18}

Facet	Dispersive surface energy γ^d (mJ/m ²)	Polar surface energy γ^p (mJ/m ²)	Surface energy (sum of γ^d and γ^p) γ (mJ/m ²)	Polar character γ^p/γ (mJ/m ²)
(201)	34.9	27.5	62.4	0.44
(001)	34.4	38.0	72.4	0.53
(011)	33.9	32.7	66.5	0.49
(110)	34.2	20.2	54.4	0.37
(010)	45.1	7.0	52.1	0.13

Diiodiomethane is a purely dispersive Van der Waals liquid probe, whilst water, ethylene glycol and formamide are polar liquids that interact with the crystals via paracetamols

surface exposed polar functional groups. Advancing contact angles determined with polar solvents show different results for the different facets. The wetting behavior of both ethylene glycol and formamide on the (001) face would indicate that this surface interacts strongly with these polar test liquids, while on face (201) the interaction is weaker, as only ethylene glycol wets this surface. Diiodomethane shows similar advancing and receding contact angles due to the strongest van der Waals dispersive interactions on the facet (highest value of γ^d).

On the other hand, the θ_A of all the polar probe liquids on facet (010) was much higher than those observed for the exposed facets; this is due to its higher hydrophobicity.

On the basis of these results, a hydrophilicity order for paracetamol form I facets was proposed:¹⁸

$$(001) > (011) > (201) > (110) > (010)$$

From the contact angle data for diiodomethane, an order of the van der Waals interactions was be generated:¹⁸

$$(010) > (001) = (011) = (201) = (110)$$

- Mechanical properties: Paracetamol crystal hardness were measured using a Vickers indenter, hardness values are in the range 297–358MPa⁶. Finnie *et al.* (2001) and Beyer *et al.* (2001) have reported the hardness, Young's modulus, and fracture toughness values of paracetamol single crystals as 421MPa, 8.3Gpa, and 0.05(MPam)^{1/2} respectively.^{6, 13}

Micronised, conventionally crystallized (powder) and special granular pharmaceutical paracetamol grades were supplied by Mallinckrodt Inc., Raleigh, N.C., Micronised, batch number 042213E407, Powder (typical crystalline material) batch number 637514D001 and Granular, batch number 161713J561 were used throughout the work reported here except where highly purified paracetamol was required in which case Bioextra grade paracetamol from Sigma Aldrich was used. The paracetamol used is of polymorphic form I. The particle size distributions for the three materials expressed as; x_{10} , x_{50} and x_{90} , the Sauter mean diameter (SDM) the volume mean diameter (VMD) and true density were measured experimentally and are reported in Table 18.

Table 18 Material characteristics of the three paracetamol grades. True density values were determined with Helium pycnometer, x_{10} , x_{50} and x_{90} , SMD and VMD were determined using a QICPIC particle size analyser^f.

Micronised Batch 042213E407	Powder Batch 637514D001	Granular Batch 161713J561
True density (g.cm⁻³)*		
1.1914 ± 0.0067	1.2417 ± 0.0020	1.2675 ± 0.0016
Particle size distribution (averaged with 3 replicas) †		
$x_{10} = 9.58 \mu\text{m}$	$x_{10} = 23.85 \mu\text{m}$	$x_{10} = 273.91 \mu\text{m}$
$x_{50} = 24.55 \mu\text{m}$	$x_{50} = 64.03 \mu\text{m}$	$x_{50} = 363.58 \mu\text{m}$
$x_{90} = 51.11 \mu\text{m}$	$x_{90} = 179.14 \mu\text{m}$	$x_{90} = 462.26 \mu\text{m}$
SMD = 18.66 μm	SMD = 46.35 μm	SMD = 299.30 μm
VMD = 34.73 μm	VMD = 86.01 μm	VMD = 360.03 μm
Specific surface area BET (m²/g) with Octane		
0.725	0.276	0.056

^f * Helium pycnometer: AccuPyc 1330 V1.30

[†] QICPIC Particle Size Analyser (Sympatec VIBRI/L), Sympatec GmbH System-Partikel-Technik

Paracetamol Bioextra (LOT SLBM5923V) was supplied by Sigma Aldrich ($\geq 99\%$). Particles size of paracetamol Bioextra are; 29.45 μm (x10), 79.57 μm (x50), 220.47 μm (x90), 57.24 μm (SMD) and 104.92 μm (VMD).

4.2 **Materials: paracetamol related impurities**

An impurity in a drug substance is defined as any component that is not the chemical entity defined as the drug substance and it affects the purity of active ingredient, in accordance with the International Conference on Harmonisation (ICH) Guidelines.²⁰ Most of the active pharmaceutical ingredients (API) are produced by organic chemical synthesis. Non-API components remaining in the final API, are considered as impurities. These impurities can be classified as; organic impurities, inorganic impurities and residual solvents.^{21, 22}

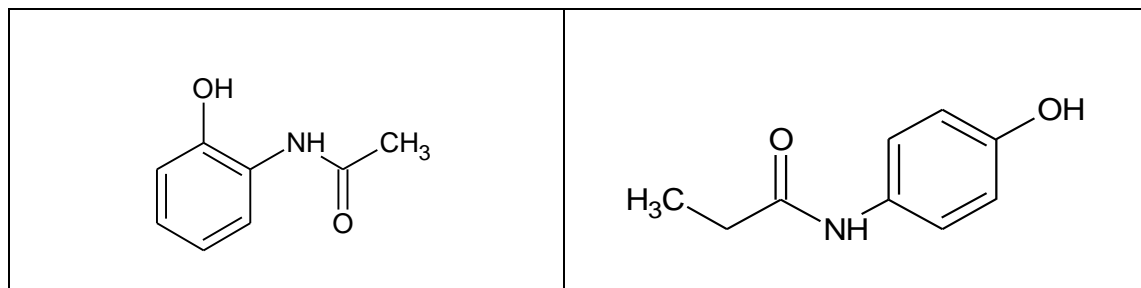
Potential API impurities are starting materials, reaction by-products and residual solvents from the API synthesis, degradants formed during the process and on long-term storage, contaminants from packaging components and other drug products manufactured in the same facility. Stringent efforts are made to monitor and control impurities in APIs.

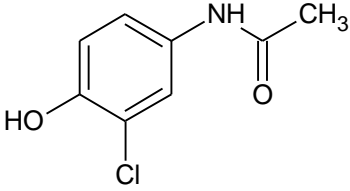
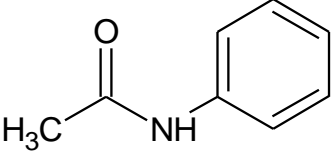
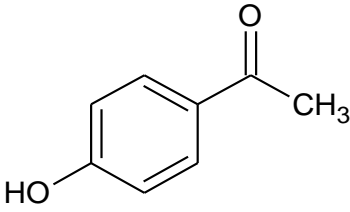
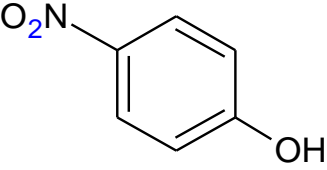
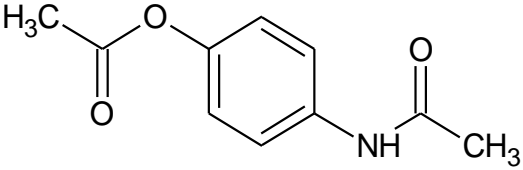
Impurity formation on storage can be promoted by the effect of heat, light, residual solvents and oxidants (including air) or by the presence in the product or traces of metal impurities (catalyst) that can promote degradation, a notable degradation pathway involves bonding between multiple molecules of the product to form dimers, trimers and oligomers.

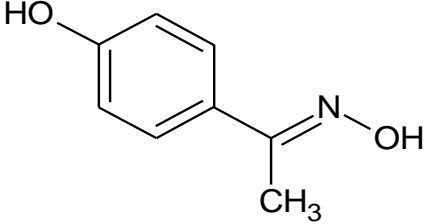
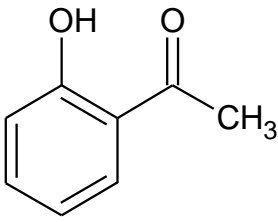
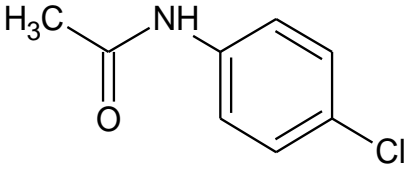
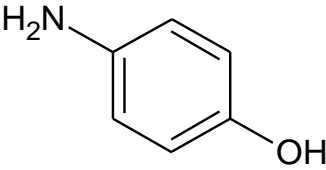
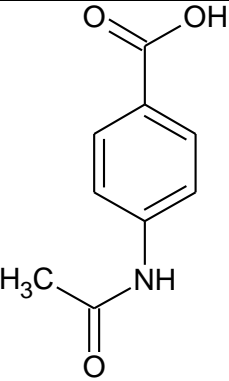
When the solubility of these impurities are similar to the API solubility in a specific solvent, their elimination by washing may be difficult due to the dissolution of the API, reducing process yield.²³ Some of these impurity molecules can modify the API solubility, its nucleation and crystal growth kinetics changing crystal habit. The mechanism of impurity incorporation in the crystal lattice and on the crystal surface will be examined in chapter 5.

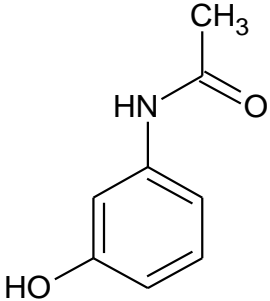
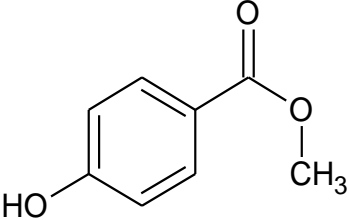
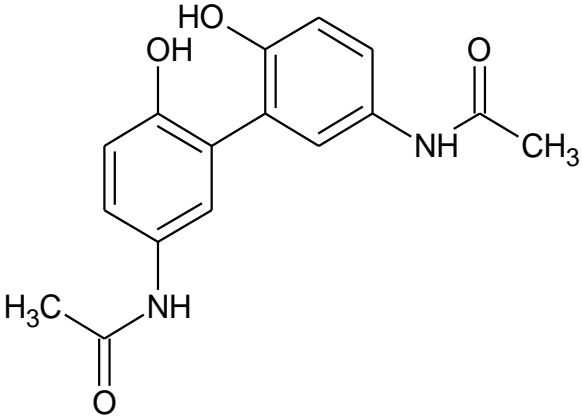
The main paracetamol related impurities of synthesis are listed in Table 19 (those in bold are the impurities used during this project and all of them available from chemical suppliers). In chapter 5, these impurities were selected to show the sensitivity of the TOF-SIMS to detect the location of those impurities on crystal surface. In chapter 7, acetanilide and metacetamol were selected as impurities to show the capability of washing to remove related impurities from the mother liquor, because of their different solubility respect to the paracetamol in crystallization and in wash solvent. Acetanilide, as seen in Table 19, does not contain in the molecular structure the hydroxyl group that reduce solubility in solvents, while metacetamol is the meta isomer of paracetamol showing lower solubility respect to the paracetamol. Orthocetamol is contained in the raw paracetamol.

Table 19 Major paracetamol impurities and their main properties.^{2, 4}



Paracetamol impurity A: Orthocetamol (CAS: 614-80-2), by-product of reaction	Paracetamol impurity B: Parapropamol (CAS: 1693-37-4)
Molecular weight: 151.16g/mol Functional groups: hydroxyl, phenylene, amide	Molecular weight: 165.19g/mol Functional groups: hydroxyl, phenylene, amido
	
Paracetamol impurity C (CAS: 3964-54-3)	Paracetamol impurity D: Acetaminophen related compound D or Acetanilide (CAS: 103-84-4), by-product of reaction
Molecular weight: 185.6g/mol Functional groups: hydroxyl, phenylene, chloro, amido	Molecular weight: 135.16g/mol Functional groups: phenyl, amido
	
Paracetamol impurity E: 4-hydroxy acetophenone (CAS: 99-93-4), intermediate of reaction	Paracetamol impurity F: 4-nitrophenol (CAS: 100-02-7), reagent
Molecular weight: 136.15g/mol Functional groups: hydroxyl, phenylene, carbonyl	Molecular weight: 139.11g/mol Functional groups: nitro, phenylene, hydroxyl
	

	
<p>Paracetamol impurity: 4-hydroxyacetophenone oxime (CAS: 34523-34-7)</p>	<p>Paracetamol impurity H: N,O-Diacetyl-4-aminophenol or acetaminophen acetate (CAS: 2623-33-8), by-product of reaction</p>
<p>Molecular weight: 151.17g/mol Functional groups: hydroxyl, phenylene, ketoxime</p>	<p>Molecular weight: 193.2g/mol Functional groups: acetate, phenylene, amido</p>
	
<p>Paracetamol impurity I: 2'-hydroxyacetophenone (CAS: 118-93-4)</p>	<p>Paracetamol impurity J or 4-chloro acetanilide (CAS: 539-03-7), intermediate of reaction</p>
<p>Molecular weight: 136.2g/mol Functional groups: hydroxyl, phenylene, carbonyl</p>	<p>Molecular weight: 169.61g/mol Functional groups: amido, phenylene, hydroxyl</p>
	
<p>Paracetamol impurity K: 4-aminophenol (CAS: 123-30-8), reagent</p>	<p>Paracetamol impurity: 4-acetamido benzoic acid (CAS: 556-08-1), by-product of reaction</p>
<p>Molecular weight: 109.1g/mol</p>	<p>Molecular weight: 179.17g/mol</p>

Functional groups: amino, phenylene, hydroxyl	Functional groups: carboxyl, phenylene, amido
	
Paracetamol impurity: metacetamol (CAS: 621-42-1), by-product of reaction	Paracetamol impurity : methyl-4-hydroxy benzoate (CAS: 99-76-3), by-product of reaction
Molecular weight: 151.16g/mol Functional groups: amido, phenylene, hydroxyl	Molecular weight: 152,15g/mol Functional groups: methyl, carboxyl, phenylene, hydroxyl
	
Paracetamol dimer (CAS: 98966-14-4)	
Molecular weight: 300.31g/mol	

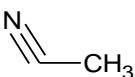
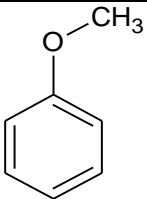
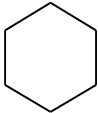
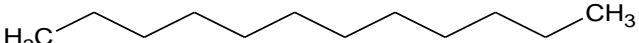
In each chapter material suppliers and the important properties of the related impurities used for the investigation are reported. In chapter 7, an organic dye was used to mimic

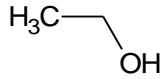
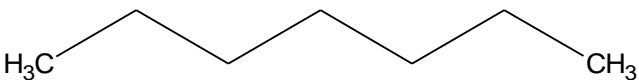
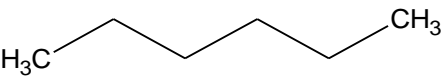
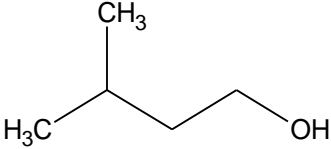
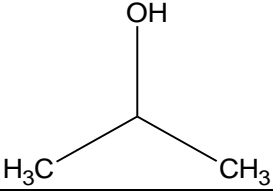
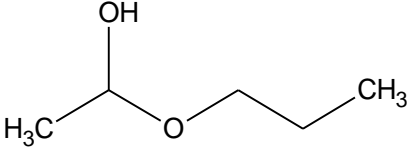
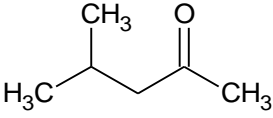
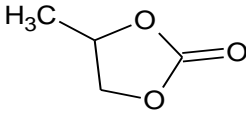
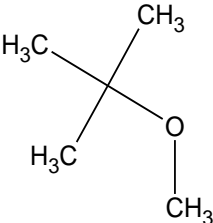
impurity to better visualize impurity removal during isolation. Further information about the dye are reported in chapter 7.

4.3 Materials: solvents

A series of crystallization and wash solvents were used in this work. Four solvents were selected as crystallization solvents for paracetamol: ethanol, isopropanol, isoamyl alcohol and water.^{1, 4, 24} A series of wash solvents were chosen based on presenting low/very low paracetamol solubility and different miscibility with the selected crystallization solvents (Table 20 and Table 21).

Table 20 Solvent used during this work.^{25, 26, 27, 28}

Solvent	Structure	Crystallization (C)/wash solvent (W), if wash solvent, miscible with C?
Acetonitrile		W, miscible with ethanol, isopropanol, isoamyl alcohol*
Anisole (methoxybenzene)		W, miscible in ethanol, isopropanol*, isoamyl alcohol*
Cyclohexane		W, miscible with ethanol, isopropanol, isoamyl alcohol*
n-dodecane		W, not miscible with ethanol, isopropanol, isoamyl alcohol*

Ethanol		C
n-heptane		W, miscible with ethanol, isopropanol, isoamyl alcohol*
n-hexane		C
Isoamyl alcohol (3-Methyl-1-Butanol)		C
Isopropanol (propan-2-ol)		C
Iso-propyl acetate		W, miscible in ethanol, isopropanol, isoamyl alcohol*
MIBK (4-Methyl-2-pentan-2-ol)		W, miscible in ethanol, isopropanol, isoamyl alcohol*
Propylene carbonate		W, miscible in ethanol, isopropanol, isoamyl alcohol* (green solvent)
Tert-butyl-methyl-ether (TBME)		W, miscible with ethanol, isopropanol, isoamyl alcohol*

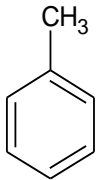
Toluene (methyl benzene)		W, miscible with ethanol, isopropanol, isoamyl alcohol*
Water	H ₂ O	W, miscible with ethanol

Table 21 Main properties of the solvent used during this ^{work29-33}

Solvent	Boiling point (°C)	Enthalpy of vaporization (kJ/mol)	Viscosity (cP) (Temperature °C)	Density (g/ml) (Temperature °C)	Surface tension (mN/m) (Temperature °C)
Acetonitrile	81.6	33.2	0.36 (20)	0.79 (15)	29.4 (20)
Anisole	155	46.84	1.52 (15)	0.99 (18)	35 (20)
Cyclohexane	80.7	33.06	0.98 (20)	0.78 (20)	24.98 (20)
N-dodecane	216.3	61.52	1.5 (25)	0.75 (20)	25.35 (20)
Ethanol	78.4	38.58	1.26 (20)	0.79 (20)	21.99 (20)
n-heptane	98.4	31.77	0.397 (25)	0.68 (20)	19.7 (20)
n-hexane	68.7	28.85	0.29 (25)	0.66 (25)	17.94 (20)
Isoamyl alcohol	132	55.2	3.74 (25)	0.81 (15)	24.77 (15)
Isopropanol	82.2	39.85	2.1 (25)	0.78 (25)	21.4 (20)
Isopropyl acetate	88.5	37.2	0.52 (25)	0.87 (20)	22.3 (20)
4-methylpentan-2-one	116.1	40.61	0.59 (20)	0.8 (20)	24 (20)

Propylene carbonate	241.7	55.2	2.5	1.2 (20)	40.9 (25)
TBME	55.2	27.94	0.35 (20)	0.76 (25)	18.5 (20)
Toluene	111	38.01	1.16 (25)	0.86 (20)	27.73 (25)
Water	100	43.99	0.89 (25)	0.999 (25)	72.7 (25)

4.4 Methods

A range of different analytical techniques were used to investigate different aspects of the final product. Raw materials, prior the experiments were also characterized to evaluate the effect of the specific experiments on final product.

Analytical characterizations are subdivided by category:

- Physical characterization (PSD, density, viscosity, solubility)
- Surface characterization (OM, SEM, Raman Microscope, AFM, wettability)
- Chemical analysis (TOF-SIMS, HPLC, UV-vis spectroscopy, NMR)
- Mechanical characterization (extent of agglomeration, ABI index)

The specific methodologies used during this research are reported in this chapter.

4.4.1 Physical characterization techniques

4.4.1.1 *Particle size, size distribution and aspect ratio*

In chapter 6 and 7, the particle characteristics of the different paracetamol grades were determine using a Sympatec QICPIC particle size analyser with VIBRI/L setup at a feed pressure of 0.5 bar, a feed rate of 25% and 0.5mm gap width. The same methodology was used to analyse product PSD after drying. Agglomerated particles with a size smaller than 1 mm were analysed in this way. Approximately 1g of sample was used for the PSD

characterization. For the filtration and washing DoEs the sample feed rate was firstly set to 0.5bar to allow comparison with the data of the input paracetamol. The measurement was then repeated with a feed pressure of 2 and 4 bar to evaluate particle breakage due to shear stress (chapter 6).

Density

Bulk density was determined in this project by gently filling a 10mL pre-weighed glass cylinder with the material, without shaking or tapping the cylinder to avoid powder compaction, noting the volume and measuring the mass of the sample and container. The experiment is repeated three times.

True density of the paracetamol grades was determined with the Accupyc 1330 V1.30 Helium pycnometer. Ten replicas for each compound were run.

4.4.1.2 Solubility

The solubility of paracetamol and related impurities were measured in the series of solvents reported in the material section were determined by isothermal equilibration and dry residues method.

Pre-weighed suspensions of in crystallization/wash solvents were prepared and placed in an incubator (Incubator S160D, Stuart) on a multi-position stirrer plate and held isothermally at the selected equilibration temperatures of 25, 40 and 55°C, and equilibrated with agitation for 24 hours. Once the 24-hour equilibration period was completed 1mL samples were taken and the mass recorded. The samples were then left without lids in a fume hood for 24 hours to allow the solvent to evaporate. After 24 hours,

the sample vials were weighed and their mass recorded. Finally, the sample vials were placed in a vacuum oven (Gallenamp) for 24 hours at room temperature and (20mbar) prior to recording the final dry residue mass which was used to calculate the solubility of each compound.

4.4.2 Surface characterization techniques

4.4.2.1 *Optical Microscopy*

Optical microscopy is the primary method used to examine material microstructure.

In this work transmitted light optical microscopy, stereomicroscopy and diffraction interference contrast (DIC) optical microscopy were used.

In chapter 5 a stereomicroscope (Brunel microscopes ltd, BMDZ zoom stereomicroscope) was used to evaluate single crystal morphology and identify the main macroscopic features. A Leica DM6000M microscope was used in differential interference contrast (DIC) mode to analyse the surface texture of the crystals.

4.4.2.2 *Scanning electron microscopy*

In chapter 5, a Hitachi TM-1000 version 02-11 scanning electron microscope was used to evaluate the micro surface texture and features of the crystals. The operating conditions for the SEM experiments were: back scattered detector, accelerating voltage 15000V, magnification 200x, working distance 6700 μ m, emission current 57.4mA, scan speed slow, vacuum conditions 15.0kV.

4.4.2.3 *Atomic force microscopy*

Atomic Force Microscopy (AFM) reported in chapter 5 was carried out using a Bruker AFM with Icon Scanner system and Scan Asyst in air experiment mode, equipped with a

MPP-12120-10 tip. The dimensions of the scan area were 50x50 μm for each of the samples studied.

4.4.2.4 *Raman microscopy in imaging mode*

A Horiba Raman Xplora microscope was used to perform the Raman mapping reported in chapter 5. A 532nm laser source coupled with a 50x objective (1.23 μm spatial beam width), 50 μm slit, and 100 μm aperture was used to collect the Raman spectra over the range 50 to 3500 cm^{-1} at room temperature. Data acquisition time was 2s with averaging over 2 spectra with a delay of 2s. A 25% filter was used to reduce the effects of interaction of the laser with the sample. The characteristic Raman peaks for paracetamol and 4-nitrophenol were evaluated from published sources^{34, 35} coupled with our own measurements of the individual Raman spectra of paracetamol (PP) and 4-nitrophenol (PN) crystals. The main 4-nitrophenol Raman peak has a characteristic frequency of 1111 cm^{-1} which is related to -CN stretching of the nitro group.³⁵ Based on this characteristic peak, 2-dimensional maps were created for 20x20 μm or 10x10 μm sampling areas by calculation of the intensity ratio between peak and baseline intensity; this was performed using Origin software. Measurements were conducted on crystals obtained from the three different crystallization conditions.

4.4.2.5 *Surface tension and contact angle*

Washburn method is a capillary rise method where a liquid phase (with known properties) penetrate into the porous bed thanks to capillary forces.³⁶

Fluid penetration flow inside capillaries is a laminar flow that is governed by the Hagen-Poiseuille equation.³⁷ Measuring the mass increase vs time during the capillary rise penetration can be used to determine contact angle value (Equation 91).³⁸

$$m^2 = \frac{K\rho^2\gamma_L \cos\theta}{\mu} t \quad (91)$$

Where K is a geometrical parameter that depends to the radius of porous bed (R_c), to the porous bed porosity (ϵ) and to the capillary radius (r). Constant K has to be determined separately using a reference solvent which shows high wetting capabilities, thus the contact angle θ can be assumed as 0° ($\cos\theta = 1$). The geometric constant K of the reference solvent is then used to determine the contact angle θ of the studied liquids. To determine contact angle of paracetamol in different solvents a saturated solution was created to avoid paracetamol dissolution during capillary rise.

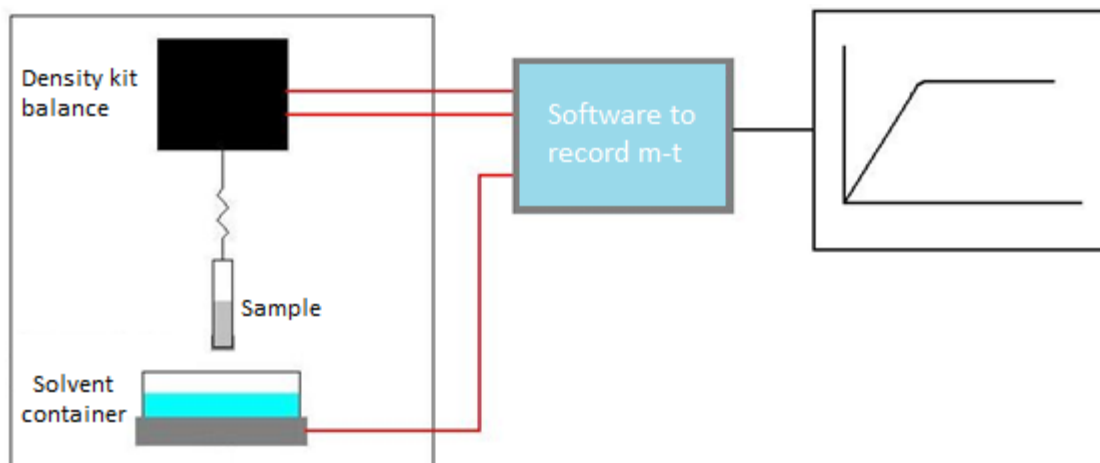


Figure 36 Schematic representation of the Washburn method.³⁹

The setup developed uses a Sartorius Quintix balance (Sartorius) logged to a recording excel datasheet, where mass over time is recorded (Figure 36 and Figure 37). Around 1g

of Bioextra paracetamol (powder) was filled into a Biotage 6mL double frit tube. Powder packing, done to homogenize the capillary radius in the bed, is done by tapping the sample with the autotap system (Quantachrome instrument) for 700 time.

The holder and scaffolding are from the Sartorius Density Measuring Kit Analytical; Balance YPK03 was set up as shown in Figure 37.

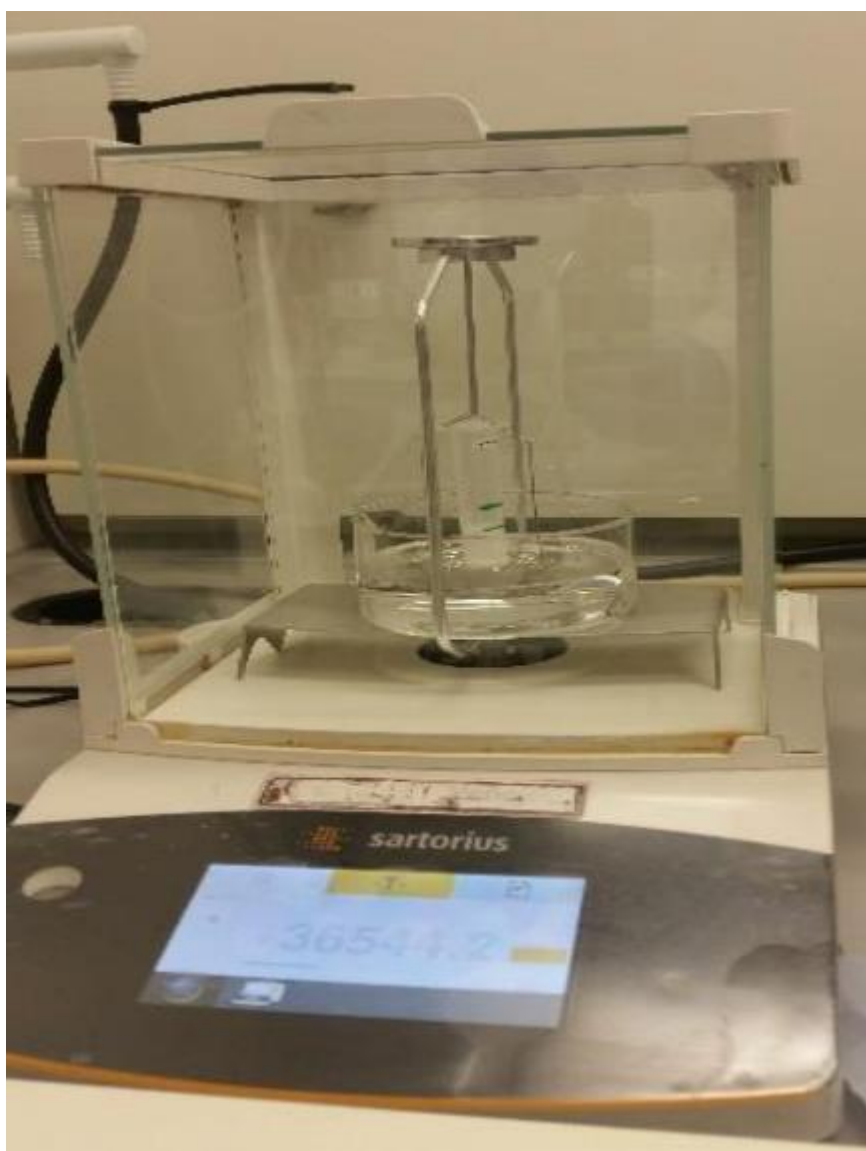


Figure 37 Washburn method setup with the Sartorius balance and density kit.

A series of replica of each capillary rice sample-solvent combination are required.

4.4.3 Solid state

4.4.3.1 SC-XRD and PXRD

X-ray diffraction was used in the work described in chapter 5 to evaluate the solid state properties of pure paracetamol and material prepared by immersing a paracetamol crystal

in a paracetamol solution containing 4% mol/mol of 4-nitrophenol. X-ray diffraction intensities were collected on a Bruker APEX 2 diffractometer coupled with an Incoatec IuS Mo microsource (0.71073 Å) operating at room temperature (293 K). A total of 780 frames were collected using three angular settings with a scan width of 0.5° in omega. Two crystals from each crystallization experiment were face-indexed to assign the Miller indices.

4.4.4 Chemical analysis

4.4.4.1 TOF-SIMS

The TOF-SIMS instrument used in chapter 5 was a TOF-SIMS 5 from IONTOF Germany. Data were collected in both positive and negative polarity modes for all prepared samples. Negative polarity was selected as the preferred mode due to enhanced molecular polarizability of the 4-nitrophenol fragments. All images were collected using the Bi₃⁺⁺ ion source with settings adjusted towards high lateral resolution (30keV base setting, due to double charge effective 60keV, 100ns pulse width, 0.05nA beam current). All crystals were analyzed with a field of view of 100x100µm. While the PP and PN crystals were recorded at 256x256px raster size, P4%N was recorded at 1024x1024px raster size. The total dose densities recorded were 4e+11 ions/cm² for the PP and PN crystals and 9e+11 ions/cm² for the P4N crystal. A total dose density of below 1e+12 ions/cm² ensured the experiment remaining within the static SIMS limit. To aid the assignment of all mass fragments the software tools NIST 08 MS Demo and AMDIS 2.6 were used. In combination, a mass spectroscopy analysis done with the TOF-SIMS was done on the pure compounds.

4.4.4.2 *UV-vis spectroscopy*

UV-vis spectroscopy mythology is reported in chapter 7.

4.4.4.3 *HPLC*

The chemical composition of single crystal samples of paracetamol with nitrophenol investigated in chapter 5 were analysed using HPLC-MS approach. An Agilent 1290 UPLC, 6530 Q-TOF using an internal standard method. An Agilent Poroshell 120 EC-C18 (3.0 x 50 mm, 2.7 micron) column was used. The analysis was performed at 25°C, using a 1.5mL/min flow rate recording the absorbance at 230nm. The mobile phase was 20:80 methanol: water. The samples were prepared by dissolving the selected crystals in 100 mL of a 5% w/w methanol/water solution. A calibration curve for the 4-nitrophenol impurity was prepared using 5µL solutions containing 0.14 mg/mL paracetamol spiked with 5-15% (w/w) of 4-nitrophenol. Samples were analyzed in triplicate. This chemical composition analysis is destructive in the sense that the crystal is dissolved and so was performed as the final analytical technique in the characterization sequence.

In chapter 7, HPLC was used to quantify impurity content of filter cakes and filtrates, calibration curves for pure paracetamol, acetanilide, metacetamol and orthocetamol (an impurity present in the raw paracetamol) were gathered using a multilevel calibration method. An Agilent 1260 Infinity II system with diode array and RI detector was used. The column was an Agilent Poroshell 120 EC-C18 4.6 x 100mm 4µm operated at 40°C, with a flow rate of 1ml/min. The injection volume was 5µL, wavelength: 243 and 230.5 nm, the mobile phase was 80% water and 20% methanol.

4.4.4.4 ¹H-NMR

NMR was used to determine the solvent identities and quantities remaining after drying. An AVII+600 NMR Spectrometer, Bruker Avance 2+ (Bruker, UK) were used to collect proton NMR spectra. A few mg of cake was dissolved in 0.75ml of DMSO-d. To determine number of scans a T1/T2 relaxation time evaluation was performed for all the solvent combinations (process parameters: frequency axis F1 equals to 32, pulse program t1ir, 4 scans, 2 replicas of T1/T2 analysis to evaluate T1 relaxation). In the light of this wet cake, samples were analysed using 64 scans, corresponding to approximately 5 time T1. The time determined from the T1/T2 relaxation time test (5T1) is required to maximize signal to noise intensity and so detect very small proton signals from solvent traces. Each sample was analysed in duplicate.

4.4.5 Mechanical characterization techniques

4.4.5.1 *Extent of agglomeration and friability test to determine ABI index*

Defining when an aggregate is considered an agglomerate, lump or remains an aggregate is not well defined in the literature. Birch and Marziano⁴⁰ arbitrarily defined agglomerates as particle aggregates that were retained by a 1mm sieves.

The extent of agglomeration was defined as in Equation 92:

$$\text{Extent of agglomeration} = \frac{\text{mass of agglomerates above 1mm}}{\text{mass of total cake}} \quad (92)$$

A 1mm sieve (Endecotts Ltd) was used to separate particles at the 1mm size boundary.

The sieves were shaken by hand to avoid breakage of particles.

This analytical methodology was used in chapter 6 and 7.

4.4.5.2 *Mechanical properties of agglomerates*

Birch and Marziano³⁶ developed a qualitative technique to calculate an agglomerate brittleness index (ABI) related to the strength of agglomerates. Approximately 500mg of sample were shake in a sieve column (1mm and pan, pre-weighted) using a Variable Speed Mini Vortex Mixer (Fisherbrand™) at 2800rpm for 1 minute. After the shaking the sieve and pan were weighted to determine the fraction of sample in each class, the test was repeated 4 times. The mass loss of the upper retained fraction recorded within each cycle was then plotted using a power law curve, the power of the fitted curve describing the mechanical properties as agglomerate brittleness index (ABI). This indicates the agglomerate hardness, the higher the index, the softer the agglomerates (Figure 38).

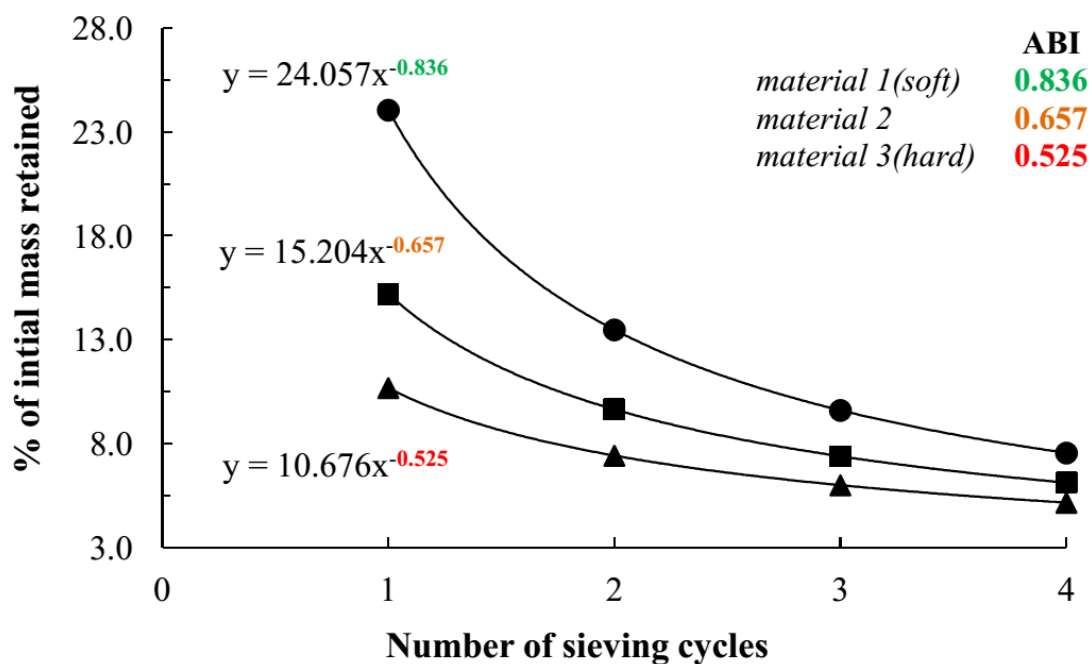


Figure 38 Example of three ABI indexes of a soft, middle hard and hard dried cakes.

In Figure 39 the mass loss per each cycle was recorded

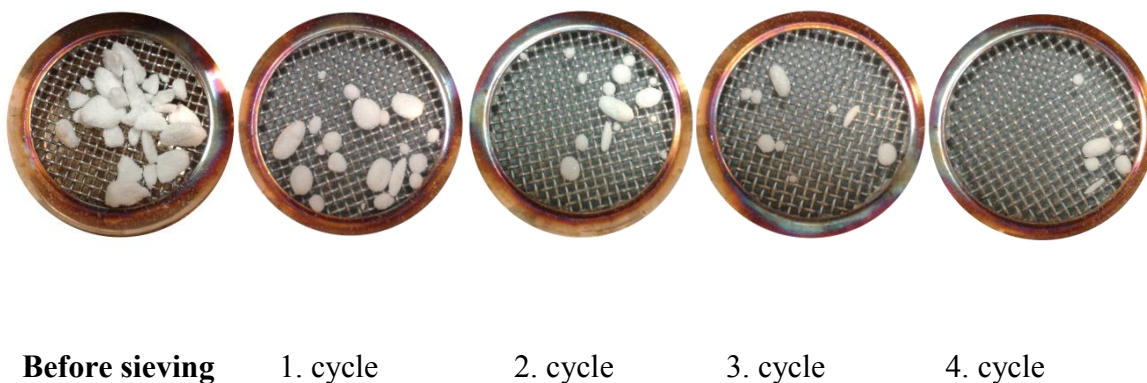


Figure 39 Visual fragmentation of agglomerates within each shaking cycle.

This analytical methodology was used in chapter 6 and 7.

4.4.6 Isolation units

4.4.6.1 *Biotage manual filtration system overview*

A modified Biotage VacMaster and a V850 vacuum controller (BÜCHI) was used to filter and wash the paracetamol suspensions using manual best practice (Figure 40).

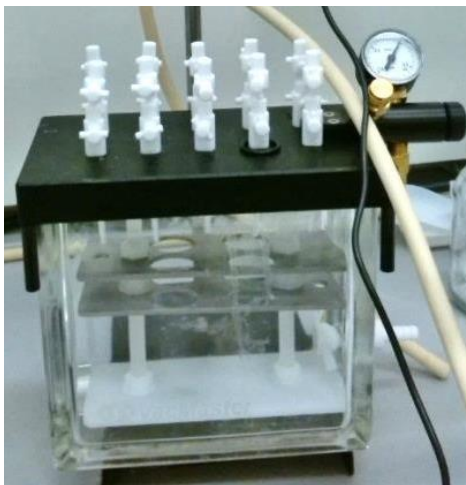


Figure 40 Biotage filtration unit setup.

The rack inside the filter chamber was modified to accommodate maximum 4 shortened 50mL graduated cylinders, the valve assembly on the chamber lid comprised a pair of PTFE valves. One valve remained with the filter tube to prevent leakage during transfer and weighing steps, the other prevented ingress of air when the filter tube was removed. The pressure driving force was controlled using a Buchi V850 vacuum controller.

Biotage ISOLUTE 70mL single fritted polypropylene reservoirs with 5, 10 and, 20 μ m pore size were used to filter, wash and deliquor the cake. The pre-weighed filter tube was connected to the PTFE valves on top of the tank. Inside the tank pre-weighed glass

graduated cylinders were positioned to collect filtrate, wash liquors and final deliquoring residue prior to drying.

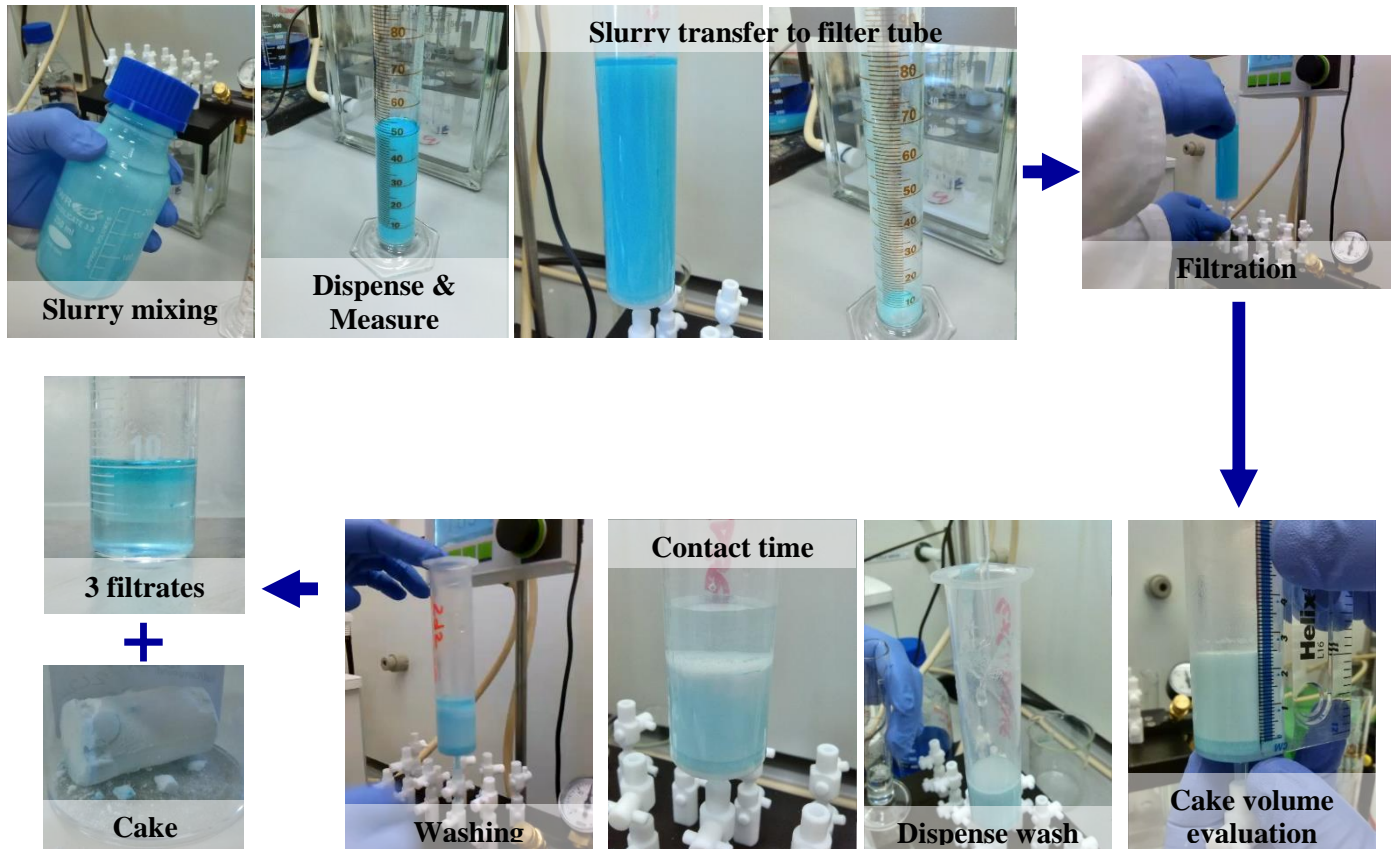


Figure 41 Biotage experimental procedure.

A new filter tube was used for each experiment. 50 mL of sample slurry was transferred to the filter tube and if necessary, some liquor was transferred back to the slurry vessel to allow quick back-rinsing to achieve as complete a slurry transfer as possible without delaying which would allow the particles to settle in the filter. The required level of vacuum inside the glass tank was confirmed on the V850 and the valve below the filter tube was opened to allow filtrate to flow through the medium into the graduated cylinder.

Simultaneously a stopwatch was started to time the filtrate flow; time taken to accumulate 10, 20, 30 and 40 mL of filtrate being noted. On reaching dryland, or if specified breakthrough, both PTFE valves were closed. The filter tube and the upper PTFE valve were removed and the mass of tube and filter cake was measured along with the filter cake thickness. The tube was then placed on the next valve on the top of the filter chamber in preparation for washing.

The required quantity of wash solvent was transferred to the top of the cake by slowly running the wash down the wall of the filter tube using a disposable pipette. Great care was taken to minimize disturbance of the filter cake surface and mixing of the clean wash liquor with the mother liquors in the cake. The same procedure used to measure the primary filtration rate was employed. This complete procedure was repeated for each washing step, if more than one was required.

Moving the filter tube in another position with empty glass cylinder was then possible to run deliquoring using the same vacuum set for filtration and washing step. Deliquoring stopped when bubble point is reached and air freely passed the cake and filter media.

4.4.6.2 *CFD20 and 25 continuous filtration, washing and drying system overview*

The CFD20 and 25 are a dead end filtration unit able to filtrate, wash and dry API cakes in manual, semi-automated or even continuous mode.

The CFD20 unit shown on the left of Figure 42 allows filtration followed by up to two washing steps with two different solvents, deliquoring and drying. The unit is controlled through a touch-screen panel (HMI). The system implements the same workflow described above using the Biotage unit.

Different components forms the CFD20/25 (Figure 42):

- A slurry tank where the slurry is mixed by an agitator to allow homogeneous mixing of the slurry
- A vacuum system used to transfer the slurry to the isolation carousel. The carousel is made of 10 different position where filtration, multiple washing stages, deliquoring and drying is done. Each position consists to a 90ml glass cylinder with inner diameter 20mm for the CFD20 and 24.4mm for the CFD25. These tubes rotate above a base with ten filter apertures, nine of which contain a BOPP Poremet 20 μ m filter mesh (G. BOPP & CO.). The filter chambers are formed when the carousel is compressed against the base plate with each glass tube located above a filter.

Position 1 of the carousel is used for slurry feeding and filtration, position two and three can be used for multiple washing steps, position four can be used for additional washing or deliquoring step, while position five to nine is used for drying. In position ten the filter media is missing to allow the dried cake removal by using a piston that mechanically ejects the cake.

- Two wash solvent container are connected to the washing positions. To prevent disturbance of the cake surface, wash solvent is dispensed on top of the cake using solvent atomizer
- Connected to the bottom of each carousel position a receiver is used to collect the liquid phase removed to analyze the impurity content in each filtrate phase

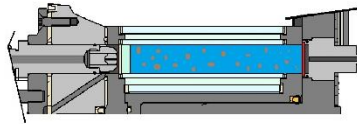
- Static drying process is done under vacuum built in the receiver container to allow the flow of room temperature air to flow through the cake.

Three different operating approaches can be used: fully manual, semi-automated, called “optimisation mode”, and fully continuous mode, called “production mode”. Manual mode is used when the operator requires full control of each step of isolation; this method uses the maximum available vacuum (900mbar) to filter the cake and as the camera cannot be used to halt filtration at dryland the operator must manually stop the filtration step. In addition, the operator may manually control wash quantity, wash solvent deliquoring and drying. Optimisation mode is used when cakes are processed one at a time: this mode is recommended for process development. To set filtration, washing and drying parameters a setup screen is used to program the unit. In optimization mode, drying is done just in port five. Production mode is fully automated and can simultaneously process a cake in each port and so isolate multiple aliquots of slurry, this mode is used once the process has been optimised and allows for maximum throughput. To allow continuous cake processing, drying is divided through port five to nine and drying time is dependent to filtration time (longest isolation step).

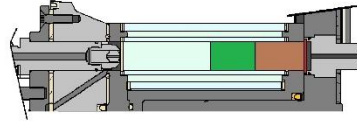


Figure 42 CFD20 Carousel filtration unit on the left and CFD25 on the right (detail of the modified carousel and camera).

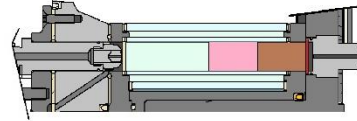
Port 1:
Suspension
feed and
filtration



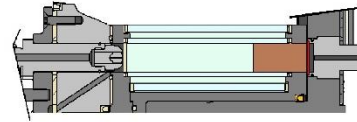
Port 2: first
washing



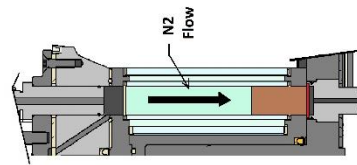
Port 3: second
washing



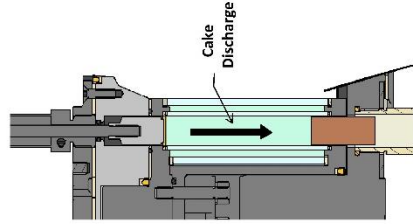
Port 4:
deliquoring



Port 5:
convective
drying (in
optimization
mode); in
productin mode
drying is
subdivided
from port 5 to 9



Port 10: cake
discharge



KEY






-  CAKE
-  SLURRY
-  WASH
-  SOLVENT EXCHANGE
-  FILTER DISC

Figure 43 AWL CFD20 schematic operative procedure.

During operation of the CFD20, a selected volume of slurry was transferred into the first glass filter tube using a vacuum slurry transfer system. Filtration was performed at a set pressure by modulating a vacuum valve. Filtrate was collected in a receiver on a load-cell allowing the filtration rate to be logged. In the updated system (CFD25), the volume of filtrate is recorded using the vision system; the system is calibrated to convert camera pixels in volume (

Figure 44).

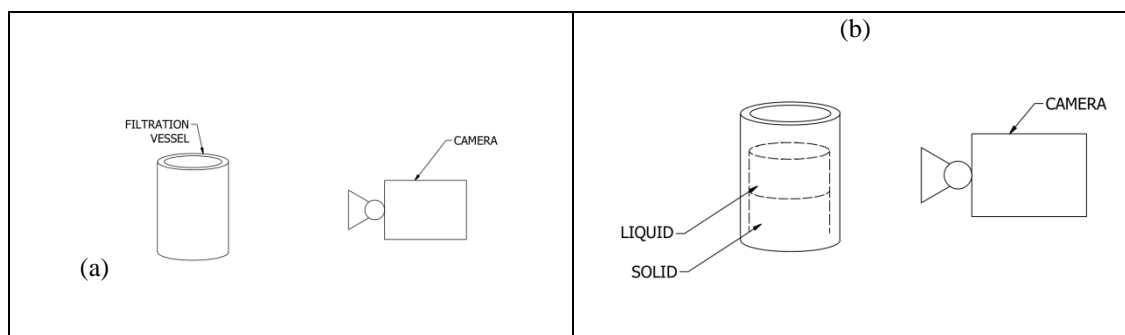


Figure 44 Schematic of the camera arrangement for the vision system. a. The camera looks through the side of the glass tube (filtration vessel) b. The liquid and solid interfaces are visible to the camera.

The filtration was either halted at dryland by a vision system, or allowed to continue to breakthrough by bypassing the automatic control and stopping the filtration manually.

After filtration, the carousel was rotated taking the filter cake along with it. Once in position above the second filter plate, the carousel was again compressed against the base plate to form a seal. This second position was then used for the first washing. A set volume of solvent was dispensed onto the cake by using an atomizer to dispense the solvent

without disturbing the cake surface, and then driven through the cake in a similar manner to the first filtration. The wash liquid was collected in a separate receiver. Separate receivers allowed samples of mother liquor and wash liquor to be recovered for analysis. A subsequent wash may be applied in the third position (port 3) of the carousel.

After the filtration and washing steps were completed, the filter cake was thoroughly deliquored by applying vacuum for 300 seconds (fixed duration experiments undertaken with CFD20). For experiments conducted using the CFD25 a range of drying times were used, in accordance with the design of experiment. The filter carousel was then rotated to its final position and a piston ejected the filter cake as product. Cake is collected in sample vials, while filtrates of port 1 to 3 are collected separately in different individual glass bottles.

4.4.7 Design of experiment approach

Design of experiments (DoE)⁴¹ is a statistical tool used in many sector of industry and research to investigate multi-variable problematic by using the minimum number of experiments to maximize the amount of relevant information.

In general, to investigate a multivariable problem a huge quantity of experiments is required. Considering a set of experiments in the COST approach, if y is the result needed and x is the factor investigated to check the evolution of y in function of x , a minimum set of 3 experiments is required to understand the kind of correlation between x and y . If the problem shows a series of variables and a series of results that are important to check to get the solution of the problem, the number of experiments to run increase exponentially as also the time required to run all the experiments.

With the DoE approach a series of steps are required:

- Define the input conditions
- Define the number of factor that may influence the results of the problem; it is important also to define the range of each factor
- Define the number of responses required to fully solve the problem
- Define the objective of the investigation: is the investigation done to optimize a manufacturing process, an analytical methodology, to screen and identify key parameters, to design a new set of experiments or to validate a method or product.

In the DoE approach the first step is the screening step that is used to predict the responses values from all the possible combinations of factor that may affect the problem. Evaluating how each factor influences the responses selected and its variability and how the experiment was done (experimental noise) by using regression coefficient plot and response contour plot, the selection of factors that mainly influence the selected responses and their extent (quantity) is done. These new information are then used to test the robustness of the method developed and define the correct procedure to solve the problem. A series of empirical models can be selected to screen, optimize and validate the factors affecting the selected responses. Those models are related to the quality of factor selected, to the number of experiment used for each stage of the problematic evaluation and to the number of replica used to define the robustness of the model (centre points). Factor can be defined as quantitative, so that a range can be estimated or qualitative, where a series of attributes can be defined.

The great advantage of using DoE is that it provides an organized approach to investigate a multi variable problem. Another advantage done by the use of DoE is the possibility to visualize clearly variables-responses correlations.

As first stage the selection of factor, nature of factors (qualitative, quantitative, quantitative multilevel, etc.) and the selection of responses and nature of responses need to be done to select the design space and centre points. During this work a D-Optimal design space approach was used. This design space approach is recommended in case several qualitative factors are used. During the design space development, the operator can select the model to fit the experimental data and that is used to interpret the correlation between factors and responses. There are a series of model that can be selected using MODDE: linear models, interaction models, quadratic models, partial least squares (PLS), etc. During this work PLS fitting model was used. This fitting model is used in case several responses were measured and the model is used to simultaneously represent the variation of all the responses to the variation of factors. This fitting model contains the linear regression of a matrix Y (response variables) and a matrix X (factor variables), expressed as $Y=XB+E$. X matrix consider the predictor variables and their square and/or cross term. In other term, PLS crates new variables, called X-scores that are the weighted combinations of the original X-variables. Those X-score are used to model the responses. The same is done also for the Y-responses, with the creation of a Y-scores. Better explanation of this fitting model is reported in literature.^{42, 43} The evaluation of the quality of raw data obtained during the experiments needs to be done (consider to repeat some experiments that show wrong results). First, the replicate of data is used to evaluate the raw data quality. In this plot, the measured values of a response are plotted against the

unique number of each experiment. Statistical parameters[§] used to evaluate the goodness of fit (R^2), goodness of prediction (Q^2), model validity and reproducibility are used to show where data shows problems of repeatability or problems related to the selection of the right model (Figure 45 Summary of fit of some of the responses selected for the DoE approach presented in chapter 7).

When the goodness of the model selected to fit the experimental data is done, then the model can be interpreted. Tools used to interpret interactions between factor and responses are the regression coefficient of the model for the selected response and the response contour plot. Regression coefficient plot is used to evaluate which factors affect the response selected or if the interaction is meaningless (examples are reported in chapter 6 and 7, ex. Figure 66). As reported by the user-guide manual of MODDE “the coefficient plots provide graphical presentation of the significance of the model terms. A significant term is one with a large distance from $y=0$ as well as having an uncertainty level that does not extend across $y=0$. A non significant model term is a model term close to $y=0$ and with an uncertainty level that crosses $y=0$ ”. The error bar expresses the 95% confidence interval that is related to the coefficient. The regression coefficient plot presented in chapter 6 and 7 on the Y axis (responses), present the expression “extended”. If a term in the model comprises a qualitative factor, C , with k levels, there will be $k - 1$ expanded terms associated with that term for the regular option, while in the expanded option all the levels

[§] R^2 identify how the regression model fit with data. Q^2 estimate the predictive power of the model. model validity show the goodness of the model selected during the DoE design. Reproducibility show how the data vary across the entire design. To discriminate if the model selected is good, those statistical model performance indicators should be: $R^2-Q^2 < 0.2-0.3$, $Q^2 > 0.5$, model validity > 0.25 and reproducibility > 0.5 .

are correlated with the selected response. For example considering crystallization solvent as qualitative factor, there are three levels, ethanol, isopropanol and isoamyl alcohol. In the regular option for presenting the qualitative coefficients, MODDE is plotting isopropanol and isoamyl alcohol, while the expanded option is plotting all the three levels.

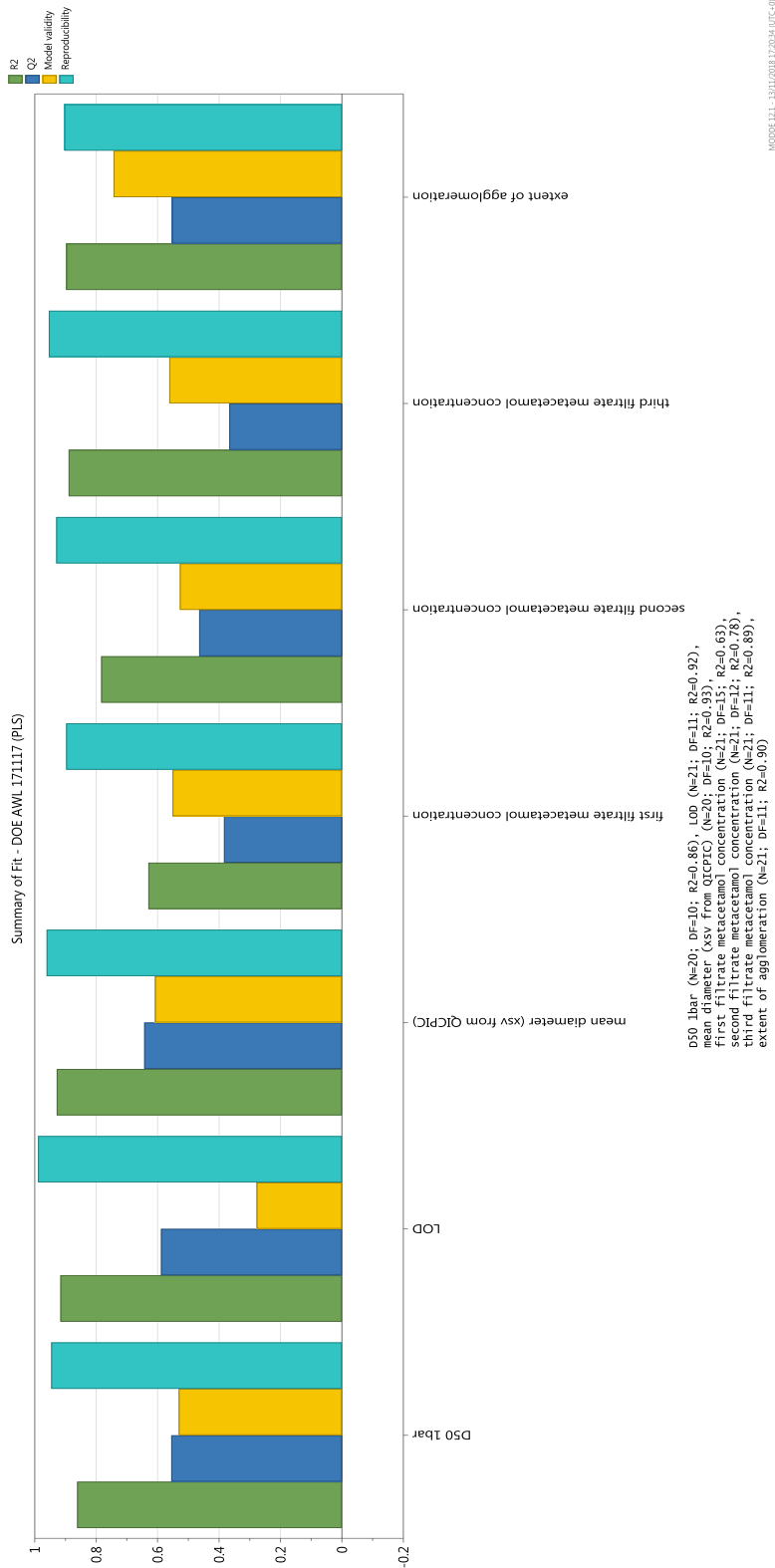


Figure 45 Summary of fit of some of the responses selected for the DoE approach presented in chapter 7.

Another tool used to evaluate correlation between factors and responses is the contour plot (Figure 67). As reported by the user-guide manual of MODDE “the 4D Contour plot displays the predicted response values for the selected response, spanned by two factors, in 9 response surface contour plots in a 3x3 grid and spanned by another two factors”. This tool is used to define the region of factor on the X and Y axis where the response show a minimum and a maximum value. This tool is used to get a qualitative evaluation of the experimental space where the selected response shows its best conditions.

The approach used during this work can be defined as “qualitative” use of MODDE. The PLS fitting model was used to qualitative understand how the different factors affected the responses, by using regression coefficient plots and 4D contour plots. The fitting model was not used to get the optimum design space for the responses.

4.5 Abbreviations

API, Active Pharmaceutical Ingredient, BFDH, Bravias-Friedel-Dannay-Harker model, SMD, Sauter mean diameter, VMD, volume mean diameter, ICH, International Conference on Harmonisation, MIBK, methyl-isobutyl-ketone, TBME, tert-butyl-methyl-ether, OM, optical microscopy, SEM, scanning electron microscopy, AFM, atomic force microscopy, TOF-SIMS, time of flight secondary ion mass spectrometry, HPLC, high performance liquid chromatography, UV, ultra violet, NMR, nuclear magnetic resonance spectrometry, ABI, agglomerate brittleness index, DIC, differential interference contrast, PP, pure single crystal of paracetamol crystallized by cooling crystallization method, PN, pure single crystal of 4-nitrophenol crystallized by cooling crystallization method, SC-XRD, single crystal X-ray diffractometry, PXRD, powder X-ray diffractometry, P4%N,

single crystal of paracetamol crystallized in presence of 4%mol/mol of 4-nitrophenol by cooling crystallization method, NIST, National Institute of Standards and Technology, HPLC-MS, high performance liquid chromatography with mass spectroscopy, CFD20, continuous filter dryer version 1, CFD25, continuous filter dryer version 2, DoE, design of experiment, COST, change one separate factor at a time.

References

1. Thompson, C.; Davies, M., C., Roberts, C., J., Tendler, S., J., B., Wilkinson, M., J., 2004. The effects of additives on the growth and morphology of paracetamol (acetaminophen) crystals. *Int. J. Pharm.*, 137.
2. Hendriksen, B., A., Grant, D., J., W., Meenan, P., Green, D., A., 1998. Crystallisation of paracetamol (acetaminophen) in the presence of structurally related substances. *J. Cryst. Growth*, 629.
3. Prasad, K., V., R., Ristic, R., I., Sheen, D., B., Sherwood, J., N., 2001. Crystallization of paracetamol from solution in the presence and absence of impurity. *Int. J. Pharm.*, 29.
4. Ellis, F. Paracetamol: A Curriculum Resource; Royal Society of Chemistry, 2002.
5. Sudha, C., Srinivasan, K., 2014. Understanding the effect of solvent polarity on the habit modification of monoclinic paracetamol in terms of molecular recognition at the solvent crystal/interface. *Cryst. Res. Technol.*, 865.
6. Finnie, S., Prasad, K., V., R., Sheen, D., B., 2001. Sherwood, Microhardness and Dislocation Identification Studies on Paracetamol Single Crystals. *J. N. Pharm Res.*, 674.
7. Haisa, M., Kashino, S., Kawai, R., Maeda, H., 1976. The Monoclinic Form of p-Hydroxyacetanilide. *Acta Cryst B*, *Acta Cryst Sect B*, *Acta Crystallogr B*, *Acta Crystallogr Sect B*, *Acta Crystallogr B Struct Crystallogr Cryst Chem*, *Acta Crystallogr Sect B Struct Crystallogr Cryst Chem.*, 1283.
8. Sibik, J., Sargent, M., J., Franklin, M., Zeitler, J., A., 2014. Crystallization and Phase Changes in Paracetamol from the Amorphous Solid to the Liquid Phase. *Mol. Pharmaceutics*, 1326.
9. Granberg, R., A., Rasmuson, Å., C., 1999. Solubility of Paracetamol in Pure Solvents. *J. Chem. Eng. Data*, 1391.
10. Femi-Oyewo, M., N., Spring, M., S., 1994. Studies on paracetamol crystals produced by growth in aqueous solutions. *Int. J. Pharm.*, 17.
11. Garekani, H., A., Ford, J., L., Rubinstein, M., H., Rajabi-Siahboomi, A., R., 2000. Highly compressible paracetamol: I: crystallization and characterization. *Int. J. Pharm.*, 87.
12. Garekani, H., A., Ford, J., L., Rubinstein, M., H., Rajabi-Siahboomi, A., R., 2000. Highly compressible paracetamol: II: Compression properties. *Int. J. Pharm.*, 101.

13. Beyer, T., Day, G., M., Price, S., L., 2001. The Prediction, Morphology, and Mechanical Properties of the Polymorphs of Paracetamol. *J. Am. Chem. Soc.*, 5086.
14. Martino, P., D., Conflant, P., Drache, M., Huvenne, J.-P., Guyot-Hermann, A.-M., 1997. Preparation and physical characterization of forms II and III of paracetamol. *J. Therm. Anal.*, 447.
15. Saleemi, A., Onyemelukwe, I., I., Nagy, Z., 2013. Effects of a structurally related substance on the crystallization of paracetamol. *Front. Chem. Sci. Eng.*, 79.
16. Shekunov, B., Y.; Aulton, M., E.; Adama-Acquah, R., W., Grant, D., J., W., 1996. Effect of temperature on crystal growth and crystal properties of paracetamol. *J. Chem. Soc., Faraday Trans.*, 439.
17. Heng, J., Y., Y., Bismarck, A., Lee, A., F., Wilson, K., Williams, D., R., 2006. Anisotropic Surface Energetics and Wettability of Macroscopic Form I Paracetamol Crystals. *Langmuir*, 2760.
18. Heng, J., Y., Y., Williams, D., R., 2006. Wettability of Paracetamol Polymorphic Forms I and II. *Langmuir*, 6905.
19. Good, R., J. Contact angle, wetting and adhesion: A critical review. In *Contact Angle, Wettability and Adhesion*. Utrecht, The Netherlands, 1993; p 3-36.
20. U. S. Department of Health and Human Services, Food and Drug Administration, Center for Drug Evaluation and Research (CDER), Center for Biologics Evaluation and Research (CBER). Q3D Elemental Impurities, Guidance for Industry. ICH, 2015
21. Prabu, S., L., Suriyaprakash, T., N., K., 2010. Impurities and its importance in pharmacy. *Int. J. Pharm. Sci. Rev. Res.*, 66.
22. Witschi, C., Doelker, E., 1997. Residual solvents in pharmaceutical products: acceptable limits, influences on physicochemical properties, analytical methods and documented values. *Eur. J. Pharm. Biopharm.*, 215.
23. Kuvadia, Z., B., Doherty, M., F., 2013. Effect of Structurally Similar Additives on Crystal Habit of Organic Molecular Crystals at Low Supersaturation. *Cryst. Growth Des.*, 1412.
24. Murugesan S., Sharma P., K., Tabora J., E. *Design of Filtration and Drying Operations in Chemical Engineering in the Pharmaceutical Industry: R&D to Manufacturing*. Wiley New York, 2010
25. Csustan website [cited 2018-11-02]
https://www.csustan.edu/sites/default/files/groups/Chemistry/Drake/documents/solvent_miscibility_table.pdf
26. Sigma Aldrich website [cited 2018-11-02]
https://www.sigmaaldrich.com/content/dam/sigma-aldrich/docs/Sigma/Product_Information_Sheet/a4405pis.pdf
27. Erowid website [cited 2018-11-02]
<https://erowid.org/archive/rhodium/pdf/solvent.miscibility.pdf>
28. Huntsman website [cited 2018-11-02]
https://www.huntsman.com/performance_products/Media%20Library/a_MC348531CFA3EA9A2E040EBCD2B6B7B06/Products_MC348531D0B9FA9A2E040

EBCD2B6B7B06/Carbonates_MC348531D1109A9A2E040EBCD2B6B7B06/files/miscibility_chart.pdf

29. Wypych, A., Wypych, G. Databook of solvents. ChemTec Publishing, 2014
30. PubChem website [cited 2018-05-15]
<https://pubchem.ncbi.nlm.nih.gov/compound/>
31. Accudynet website [cited 2018-05-15]
https://www.accudynetest.com/visc_table.html
32. Physical chemistry website [cited 2018-07-02]
<https://physicalchemistryrosamonte.wordpress.com/enthalpy-of-vaporization-of-water>
33. Surface tension website [cited 2018-07-02] <http://www.surface-tension.de/>
34. Al-Zoubi, N., Koundourellis, J., E., Malamataris, S., 2002. FT-IR and Raman spectroscopic methods for identification and quantitation of orthorhombic and monoclinic paracetamol in powder mixes. *J. Pharm. Biomed. Anal.*, 459.
35. Vijayalakshmi, S., Kalyanaraman, S., Ravindran, T., R., 2014. Raman investigation with group theoretical method on structural polymorphism of the nonlinear optical hexamine: p –nitrophenol cocrystals. *Phys. Scr.*, 95501.
36. Duncan-Hewitt, W., Nisman, R., 1993. Investigation of the surface free energy of pharmaceutical materials from contact angle, sedimentation, and adhesion measurements. *J. Adhes. Sci. Technol.*, 263.
37. Dullien F., A., L. Porous media fluid transport and pore structure, 2nd ed. Academic press inc.; 1992.
38. Siebold, A., Walliser, A., Nardin, M., Opploger, M., Schultz, J., 1997. Capillary Rise for Thermodynamic Characterization of Solid Particle Surface. *J. Colloid Interface Sci.*, 60.
39. Ottoboni, S., Paterno', A., V., Gronchi, P., 2013. Determinazione della bagnabilita' delle polveri. *Trattamenti e Finiture*, 44.
40. Birch, M., Marziano, I., 2013. Understanding and Avoidance of Agglomeration During Drying Processes: A Case Study. *OPR&D*, 1359.
41. Eriksson, L., Johansson, E., Kettaneh-Wold, N., Wikstrom, C., Wold, S. Design of Experiments, Principle and Applications. 3rd revised and enlarged edition. Umetrics Academy, 2016.
42. Metabolomics website [cited 2018-11-14]
http://www.metabolomics.se/Courses/MVA/DOE_Handouts_Exercises_Solutions_Wed.pdf
43. Eriksson, L., Johansson, E., Wikstrom, C., 1998. Mixture design-design generation, PLS analysis, and model usage. *Chemom. Intell. Lab. Syst.*, 1.

5 The impact of paracetamol impurities on face properties: investigating the surface of single crystals using TOF-SIMS.

The work reported in this chapter is published as The impact of paracetamol impurities on face-specific properties: investigating the surface of single crystals using TOF-SIMS, Sara Ottoboni, Michael Chrubasik, Layla Mir Bruce, Hien Nguyen, Blair Johnston, Alastair Florence, Chris Price, *Crystal Growth and Design* (DOI: 10.1021/acs.cgd.7b01411). The text contains small amplifications to extend the samples prepared and evaluated.

5.1 Introduction

This chapter focuses on the interactions occurring between API, impurities and crystallization and wash solvent at a microscopic scale. This investigation uses modelling and analytical tools to determine the interaction of species on the crystal surface and to understand how to design the isolation process to avoid impurities attaching to the crystal surface without possibility of removal during the washing step. In this work impurities are defined as; the related impurities that are produced during the synthesis step, by-products, residual reagents and crystallization solvent left after the washing step. In this chapter, a small group of related impurities were investigated.

Previous attempts to investigate the role of impurities and residual solvent to modify crystal morphology and surface texture are reported in Chapter 2. Several analytical techniques have been used to evaluate the role of structurally related impurities on crystal surface texture and crystal morphology; No single technique can extract all the information about both the chemical and topographic character of individual crystal faces. Combining a series of techniques has allowed the interpretation of the effect of these impurities on the crystal morphology and surface properties to be investigated. In this work two alternative analytical techniques, Raman mapping and Time of Flight Secondary Ion Mass Spectrometry (TOF-SIMS), were used to evaluate their effectiveness and sensitivity to simultaneously detect impurity distribution on the crystal surface and surface modification caused by the structurally related impurities. To investigate the sensitivity of those techniques to determine spatial distribution of 4-nitrophenol (paracetamol starting material), crystals were produced using different crystallization approaches to achieve different impurity content and location (cooling crystallization, drop deposition of impure

solution on crystal surface and epitaxial impurity growth on pure single crystal surface). The first step of the work highlighted the capability of TOF-SIMS to detect presence of 4-nitrophenol even at low impurity concentration, while Raman mapping required a higher impurity content to resolve the impurity peak from the spectra baseline. The second step of the work addressed the detectability of other paracetamol related impurities on single crystal, grown by cooling crystallization, to determine whether impurities show face specific adsorption preferences or they uniformly deposit on the entire crystal surface. A combination of TOF-SIMS and classical analytical techniques were used to give a complete assessment of the single crystal properties.

5.2 Background

Active pharmaceutical ingredients (API) are typically produced by chemical synthesis. Various components, including residual solvents, trace amounts of inorganic and organic compounds including unreacted starting materials and by-products are typically present at the end of the synthesis and are removed to a large extent by crystallization. All remaining substances in the final API product are defined as impurities. Impurities related to the synthesis can be classified as intermediate, penultimate intermediate and by-products that are produced during the different synthesis steps. These typically have chemical structures which are to some degree similar to the API, just as any degradation products.¹

Structurally related substances can change API crystallization behavior. When the solubility of these substances is similar to or less than the API solubility, elimination of these substances may be difficult. Furthermore, these impurity molecules have the

capability to modify API solubility, nucleation and crystal growth resulting in changes in crystal morphology and crystallization kinetics.

Paracetamol, also known as acetaminophen, is a molecular organic compound and an active pharmaceutical ingredient (API) that shows analgesic and antipyretic effects.² It consists of a benzene ring core, substituted by one hydroxyl group and a methylamide group in the para position.^{3,4} The amide and hydroxyl groups act as hydrogen bond donors whereas the carbonyl and hydroxyl groups act as acceptors.

Hendriksen and Grant (1995)⁵ showed that some substances, which are structurally related to paracetamol, such as acetanilide and metacetamol inhibit the primary nucleation of paracetamol in aqueous solution. They also suggested that the nucleation rate is modified through a mechanism similar to that previously reported for crystal growth modification by structurally related additives. Hendriksen *et al.* (1998)⁶ and then Kuvadia and Doherty (2013)⁷ have proposed that structurally related additives may influence the nucleation and growth of crystals in three principal ways:

- Blocking adsorption of solute molecules onto the crystal surface and therefore inducing morphological changes;^{6,8} for example 4-acetoxyacetanilide acts as a blocking impurity inhibiting crystal growth on the (110) facet;
- Docking onto the surface and become incorporated into the crystal lattice without significantly affecting the arrival of further API molecules;⁶ metacetamol operates in this way;

- Disrupting the emerging nucleus to inhibit the nucleation process;⁶ metacetamol is also described as a disrupting impurity.

Various experimental methodologies to evaluate the role of structurally related impurities on crystal surface texture and crystal morphology are reported in the literature.^{6, 8-12} Optical (OM) and scanning electron microscopy (SEM) are useful to investigate crystal morphology, aspect ratio, and, to provide some information about surface texture. Saleemi (2013)¹² reported the influence of metacetamol on paracetamol crystal morphology whereby the habit was altered from a tabular to columnar with increasing metacetamol content during crystallization. The authors also analysed the variation of induction time, crystal size distribution (PSD) and solution concentration during paracetamol crystallization; these were enabled by the use of *in-situ* UV spectroscopy and Focused Beam Reflectance Measurements (FBRM)

Prasad *et al.* (2001)¹¹ and Chow *et al.* (1985)¹⁰ examined the role of 4-acetoxyacetanilide solution concentrations and supersaturation levels on the transition of paracetamol crystals from columnar to plate-like habits. In addition to this they were able, using scanning and optical microscopy, to investigate, shape and strain/defect content, as well as quantification of 4-acetoxyacetanilide incorporation into paracetamol crystals.

Optical and electron microscopy and atomic force microscopy (AFM) allow surface roughness and crystal growth mechanism to be explored. For example Thompson *et al.* (2004)⁸ investigated how the morphology and chemical properties of the (001) face of paracetamol can be affected by the presence of different structurally related impurities.

One of the challenges faced in previous investigations was extracting information about both the chemical and topographic character of individual crystal faces using a single technique. In this work we have explored alternative analytical tools such as Raman mapping and Time of Flight Secondary Ion Mass Spectrometry (TOF-SIMS) in order to evaluate their effectiveness and sensitivity when used to simultaneously detect impurity distribution on the crystal surface and surface modification caused by the structurally related impurities.

TOF-SIMS is a surface-sensitive analytical technique that is extensively used in material science¹³⁻¹⁷ and has, in recent years, seen a rise in pharmaceutical applications.¹⁸⁻²³ The technique utilizes a pulsed ion beam to release molecules from the outer-most layers of a sample surface resulting in the emission of both neutral and charged species (atoms and molecules), with the charged species termed secondary ions.^{24, 25} These ions, in turn, are extracted into a time of flight mass analyser for detection and quantification. Moving the ion beam across the sample surface enables elemental and molecular surveying of the sample surface.

This study focuses on the API paracetamol and 4-nitrophenol as a paracetamol related impurity. 4-nitrophenol was chosen as the representative impurity as it is a precursor in the synthesis of paracetamol and hence could be present as an impurity during the crystallisation process. We investigate the limit of detection for this impurity on crystal surfaces by preparing samples using three different crystallization techniques: cooling crystallization; surface deposition via solvent drop evaporation; and epitaxial growth. The solubility of both compounds in the different solvents (ethanol and hexane) was investigated to control the supersaturation through prediction methods using

COSMO*Therm* and through experimental measurement by isothermal equilibration. Further investigations were performed using additional paracetamol related impurities and is reported in appendix (chapter 9). Cooling crystallizations of single crystals of paracetamol in ethanol were undertaken in the presence of the other related impurities. The two main facets of each crystal were analysed to evaluate face-specific impurity absorption during the crystal growth process. For this stage of the investigation, surface and 3D chemical mapping were performed using the TOF-SIMS. Optical microscopy (OM) and scanning electron microscopy (SEM) were used in tandem to evaluate crystal morphology, surface character and aspect ratio. AFM was used to study crystal surface topography; the solid state and chemical composition were determined by single crystal X-ray diffraction (SC-XRD) and HPLC respectively.

5.3 **Materials and method**

5.3.1 Materials

Paracetamol (4-acetamidophenol, Bioextra, $\geq 99\%$), 4-nitrophenol ($\geq 99\%$), methyl-4-hydroxybenzoate (97%), 4-acetamido benzoic acid ($\geq 98\%$), 4'-chloroacetanilide (97%), acetanilide (99%), 4-hydroxy acetophenone (99%), orthocetamol (97%), 4-aminophenol (98%), metacetamol ($\geq 99\%$), absolute ethanol (GC grade $\geq 99.8\%$) and n-hexane ($\geq 95\%$) were purchased from Sigma Aldrich. Acetaminophen acetate (99%) was supplied by Tokyo Chemical Industries.

5.3.2 Methods

To test the sensitivity limit for impurity detection on crystal faces three different crystallization methods were implemented.

5.3.2.1 Cooling crystallization from impure solution

A single crystal of paracetamol containing 4-nitrophenol as an impurity was obtained by preparing a supersaturated solution of paracetamol (0.88g) in absolute ethanol (5g) by the addition of 4% mol of 4-nitrophenol (0.029g). The solution was heated to 50°C and allowed to cool to room temperature and then further to 5°C in a refrigerator. A suitable single crystal of paracetamol with 4-nitrophenol (P4%N) of size exceeding 1mm was then isolated from the solution. In a similar way the other single crystals containing different related paracetamol impurities were produced. For each combination two single crystal were produced to compensate the lack of mobility of the TOF-SIMS sample holder. One crystal was used to examine large face 1 and the second to analyse large face 2 of the crystal. The two crystal were grown using the exact same crystallization conditions. In Table 22 the mass of solvent, paracetamol and impurities are reported, as well as the supersaturation used for the cooling crystallization.

Table 22 Cooling crystallization of single crystals with the different impurities: supersaturation, mass of paracetamol, solvent and impurities used relative to 1mg of paracetamol.

Single crystal name	Sample code	Supersaturation	Mass solvent (g)	Mass impurity (mg)
Paracetamol with 4% mol of 4 acetamido benzoic acid in ethanol	P4%AMBA-EtOH	1.5	5	55.50
Paracetamol with 4% mol of 4 aminophenol in ethanol	P4%AP- EtOH	1.5	5	30.71
Paracetamol with 4% mol of 4-hydroxy acetophenone in ethanol	P4%HA- EtOH	1.5	5	38.32

Paracetamol with 4% mol of 4-chloroacetanilide in ethanol	P4%CA- EtOH	1.5	5	47.74
Paracetamol with 4% mol of Acetanilide in ethanol	P4%A-EtOH	1.5	5	38.05
Paracetamol with 4% mol of 4-Methyl hydroxyl benzoate in ethanol	P4%MHB-EtOH	1.5	5	42.82
Paracetamol with 4% mol of Acetaminophen acetate in ethanol	P4%AA-EtOH	1.5	5	54.38

5.3.2.2 *Paracetamol crystal with 4-nitrophenol deposited by evaporation*

Paracetamol single crystals with a surface deposit of 4-nitrophenol (PDN) were prepared by growing pure paracetamol single crystals (PP) using the same cooling crystallization procedure outlined above but in the absence of the impurity. After the pure crystals were isolated and dried at room temperature, a room temperature saturated solution of 4-nitrophenol in ethanol was prepared (1500mg/g ethanol). A drop of this solution was dispensed onto the dominant face of the PP crystal using a micro syringe. The solvent was allowed to evaporate at ambient temperature producing a layer of 4-nitrophenol crystals on the paracetamol crystal surface.

5.3.2.3 *Crystal with 4-nitrophenol epitaxially deposited*

Epitaxial deposition of 4-nitrophenol (PEN) onto the surface of a paracetamol crystal was achieved by growing a pure paracetamol single crystal (PP) using the procedure described earlier followed by immersion in a saturated solution of 4-nitrophenol in hexane at room temperature. The crystal and solution were then cooled to 5°C. Hexane was selected as

solvent for the 4-nitrophenol solution due to the relatively high solubility of paracetamol in ethanol, which may have caused slight dissolution of the single crystal during the preparation of the earlier sample. Given the much larger quantity of solvent to be used in this preparation it was considered prudent to use an alternative solvent. Very fine needle-like 4-nitrophenol crystals were formed on the surface of paracetamol crystal and in the surrounding solution.

To provide a comparator to allow chemical and physical changes to be identified pure crystals of paracetamol and 4-nitrophenol were prepared from an ethanol solution using the method described earlier.

Table 23 Crystallization procedure for single crystals prepared in this work.

Crystallization method	Preparation	Single crystals obtained
Cooling crystallizations	<p>Raw material: Supersaturated solution of paracetamol with 4% mol of impurity</p> <p>Temperature profile: Dissolution= 50°C Cooling= 50°C down to 5°C Isolation= 5°C</p>	<ul style="list-style-type: none"> • Pure paracetamol (PP) • Pure 4-nitrophenol (PN) • Paracetamol crystal with the presence of 4% mol 4-nitrophenol (P4%N) • P4%AMBA-EtOH • P4%AP-EtOH • P4%HA-EtOH • P4%CA-EtOH • P4%A-EtOH • P4%MHB-EtOH • P4%O-EtOH • P4%M-EtOH • P4%AA-EtOH
Crystal with drop of 4-nitrophenol	<p>Raw material: paracetamol single crystal grown by the method above, 4-nitrophenol solution (1500mg/g ethanol)</p> <p>Procedure: dropping 4-nitrophenol solution on a flat dominant surface of PP and</p>	Layer of 4-nitrophenol crystals deposited on the surface of the paracetamol crystal surface (PDN)

	allowing the solvent to evaporate	
Crystal with 4-nitrophenol deposit grown epitaxially.	<p>Raw material: paracetamol single crystal grown by the method above, saturated solution of 4-nitrophenol in hexane</p> <p>Temperature profile: Immersion= room temperature Cooling= room temperature down to 5°C Isolation= room temperature</p> <p>Procedure: immersing the PP crystal in the saturated solution of 4-nitrophenol and allowing 4-nitrophenol crystals to grow on the paracetamol crystal surface</p>	Very fine needle-like 4-nitrophenol crystals were crystallised on the surface of paracetamol crystal and in the solution (PEN)

5.3.2.4 *Solubility experiments*

The solubility of paracetamol in ethanol was taken from the literature;²⁶ its solubility and that of 4-nitrophenol in ethanol and hexane were compared with predictions made using COSMO*Therm* and with experimental measurements made by isothermal equilibration. Solubility of 4-acetamido benzoic acid, 4-aminophenol, 4-hydroxy acetophenone, 4'-chloroacetanilide, acetanilide, metacetamol, 4-methyl hydroxyl benzoate, orthocetamol and acetaminophen acetate in ethanol were as well compared with predictions made using COSMO*Therm* and with experimental measurements made by isothermal equilibration.

5.3.2.5 *Solid state and composition analysis*

The chemical composition of single crystal samples of paracetamol with nitrophenol were analyzed using HPLC-MS approach. Solid-state analysis of the pure paracetamol and cooling crystallized paracetamol single crystal in presence of 4% mol/mol of 4-nitrophenol were done by SC-Xray diffractometry technique.

5.3.2.6 *Chemical character and surface texture evaluation*

A stereomicroscope (Brunel microscopes ltd, BMDZ zoom stereomicroscope) was used to evaluate single crystal morphology and identify the main macroscopic features. A Leica DM6000M microscope was used in differential interference contrast (DIC) mode to analyse the surface texture of the crystals. Scannign electron microscopy methodology is reported in method section.

Raman microscopy in mapping mode and TOF-SIMS were used to investigate the distribution of impurities on the crystal faces.

Raman microscopy may be operated in mapping mode to analyse localized regions of samples by vibrational micro-spectroscopy.²⁷⁻³⁰ Mapping involves the sequential measurement of the Raman spectra of adjacent regions of a sample by moving each region of the surface of the sample into the focal point of a Raman microscope.

The TOF-SIMS instrument used in this study was a TOF-SIMS 5 from IONTOF Germany which has four different operational modes; surface spectroscopy, surface imaging, depth profiling and 3D-imaging. Of these modes, surface spectroscopy and surface imaging were the main approaches used.

Atomic Force Microscopy (AFM) was carried out to get single crystal facets texture information.

5.4 **Results and discussions**

Solubility predictions were made for paracetamol and 4-nitrophenol in ethanol and hexane using COSMO*Therm*. The enthalpy of fusion and melting temperature of paracetamol and 4-nitrophenol used in the solubility predictions were taken from the literature.^{31, 32} The

predicted solubilities are shown in Figure 46 along with values obtained from the literature and measured by equilibration.

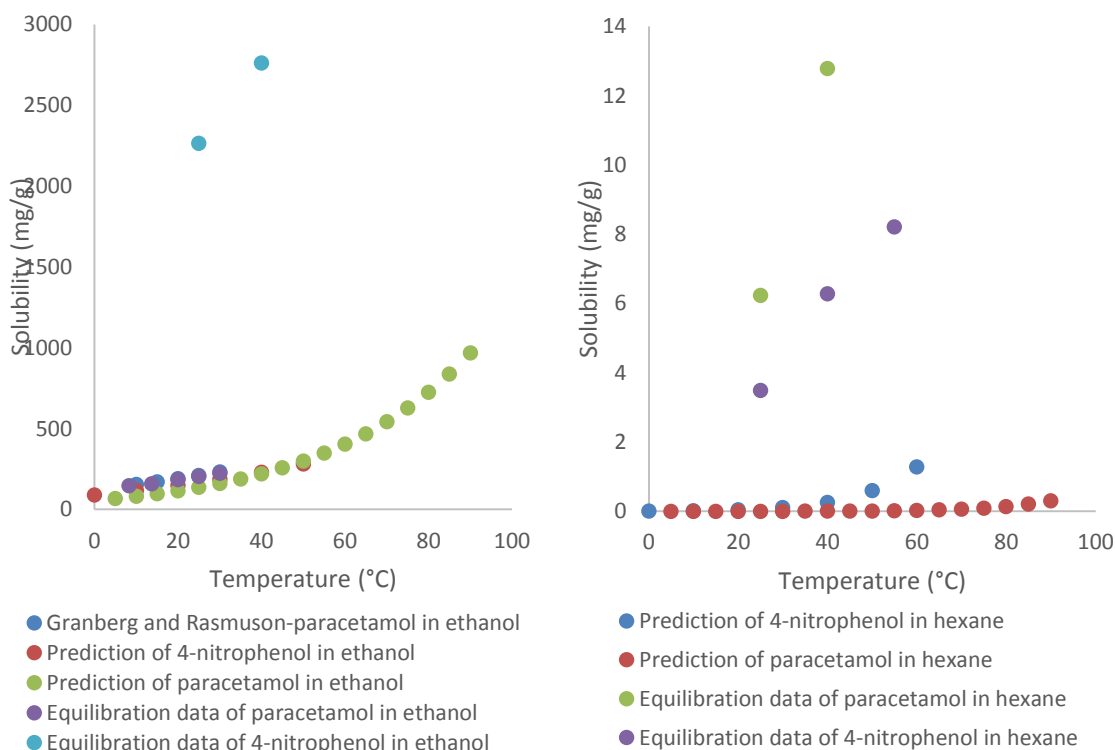


Figure 46 Solubility curve of paracetamol in ethanol (left hand side) and hexane (right hand side) in mg/g of solvent predicted by using COSMOTherm, evaluated from literature and measured by equilibration method.^{26,31} Solubility measurements were replicated three times. Standard deviation values are reported in chapter 9.

Figure 46 indicates that the predicted solubility data substantially underestimated the experimentally determined values. The solubility of paracetamol in ethanol determined by equilibration shows good agreement with published data.³¹ No published solubility data is available for paracetamol in hexane or for 4-nitrophenol in either solvents. Very low solubility values predicted for both paracetamol and 4-nitrophenol in hexane across the anticipated range of temperatures typically used in processing.

The solubility values of the other impurities in ethanol are reported in Table 24.

Table 24 Solubility of paracetamol related impurities used in this work in ethanol at 25, 40 and, 55°C.

Impurity	Solubility at 25°C (mg/g) predicted with COSMOTerm/by experimental approach	Solubility at 40°C (mg/g) predicted with COSMOTerm/by experimental approach	Solubility at 55°C (mg/g) predicted with COSMOTerm/by experimental approach
4-acetamido benzoic acid in ethanol	2.3/38.5	5.2/58.8	11.1/71.2
4-aminophenol in ethanol	21.4/25.2	40.3/40.2	73.1/48.4
4-hydroxy acetophenone in ethanol	1091.0/1134.8	1703.9/2095.0	2639.8/2240.7
4'-chloro acetanilide in ethanol	7.9/9.8	17.9/23.9	38.4/62.7
Acetanilide in ethanol	252.0/332.2	461.9/472.2	866.0/654.3
Metacetamol in ethanol	339.8/294.4	515.8/410.3	777.9/549.1
4-methyl hydroxyl benzoate in ethanol	611.4/555.8	977.6/664.4	1487.3/1801.9
Orthocetamol in ethanol	5.2/18.4	8.9/27.5	14.7/29.3
Acetaminophen acetate in ethanol	38.5/43.5	64.3/67.8	105.4/118.4

5.4.1 Chemical character and surface texture evaluation

The SC-XRD of the pure crystals were concordant with the literature values for form I (monoclinic) of paracetamol³³⁻³⁵ and the alpha form of 4-nitrophenol.³ The lattice parameters of P4%N suggest that 4-nitrophenol modifies the paracetamol crystal lattice

without causing a polymorphic change however it is known that the errors calculated from X-ray data are overoptimistic given the area-detector and the systematic errors in data collection (Table 25).^{36,37}

Table 25 Crystal lattice parameters, volume and lattice systems for PP, PN and P4%N.

Sample	Lattice parameters a, b, c (Å)	Lattice parameters α , β , γ (°)	Lattice volume (Å ³)	Lattice system
PP	7.0962 ± 0.004, 9.3856 ± 0.007, 11.7073 ± 0.006	90, 97.435 ± 0.004, 90	774	Monoclinic P
PN	6.1582 ± 0.0011, 8.8945 ± 0.0019, 11.74 ± 0.003	90, 103.234 ± 0.0015, 90	626	Monoclinic P
P4%N	7.116 ± 0.005, 9.412 ± 0.007, 11.75 ± 0.009	90, 97.403 ± 0.007, 90	780	Monoclinic P

Observation reveals a new crystal face and changes in face shapes on the paracetamol crystal grown in the presence of 4-nitrophenol compared with the crystals grown from pure solution. The change in morphology associated with the incorporation of 4-nitrophenol in the paracetamol lattice is presumed to be due to the reduced capability of the nitro group to form hydrogen bonds compared with the amide. This indicates that the 4-nitrophenol though present in small quantities acted as crystal face modifier (Figure 47).

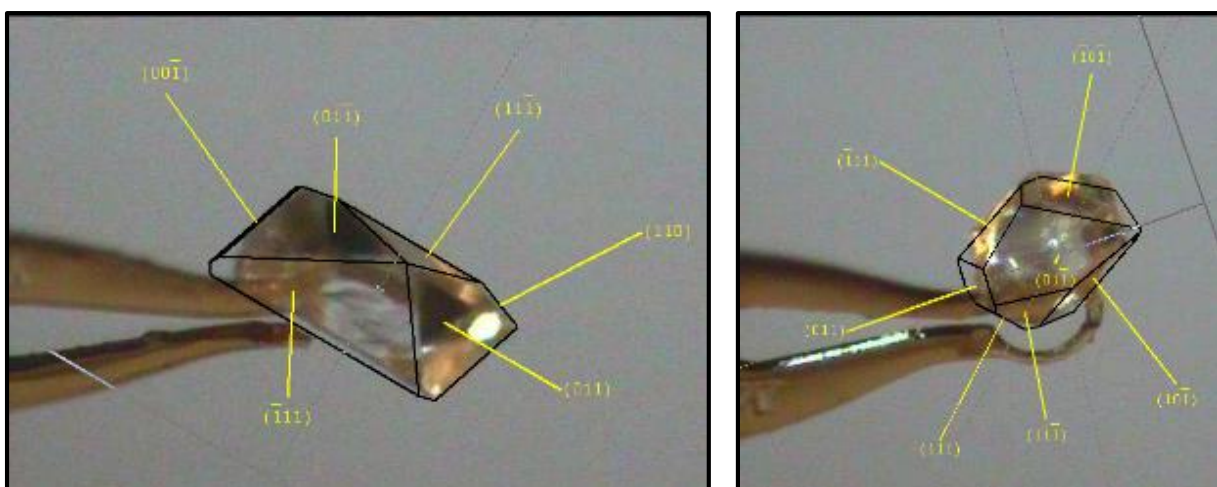
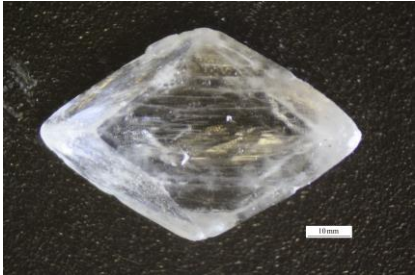


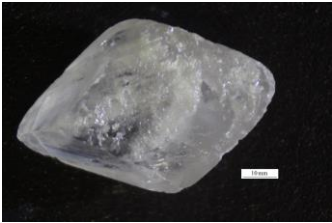
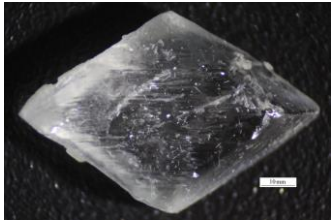


Figure 47 SC-XRD images of PP crystal (on the left) and P4%N crystal (on the right).

OM in DIC mode, SEM images and AFM images were examined to assess surface texture characteristics of pure paracetamol (PP), pure 4-nitrophenol (PN) and the three different impure crystals P4%N, PDN and PEN. Comparing pure paracetamol and pure 4-nitrophenol single crystals surface texture differences and different edge shapes were observed: PP crystal shows characteristic edge steps, while rounded and shorter steps are visible on the PN crystal (Table 26). None SC-XRD, either Raman microscopy analysis in mapping mode were run for the other crystals generated by cooling crystallization with the other related impurities.

Table 26 Stereomicroscopic images of the different crystal examined in this work: paracetamol crystal (PP), 4-nitrophenol crystal (PN), cooling crystallization crystal of paracetamol in presence of 4-nitrophenol (P4%N), pure paracetamol crystal with drops of 4-nitrophenol solution (PDN) and pure paracetamol crystal with 4-nitrophenol crystal epitaxial growth (PEN). Scale bar corresponds to 10mm

			
(PP)		(PN)	
			
(P4%N)	(PDN)	(PEN)	

Examination of the OM and SEM images indicates that 4-nitrophenol added as impurity during growth acted as a texture modifier, increasing the number of steps and other surface defects; this is consistent with the observation of Prasad and Thompson (Figure 48, Figure 49 and Figure 50).^{8, 11}

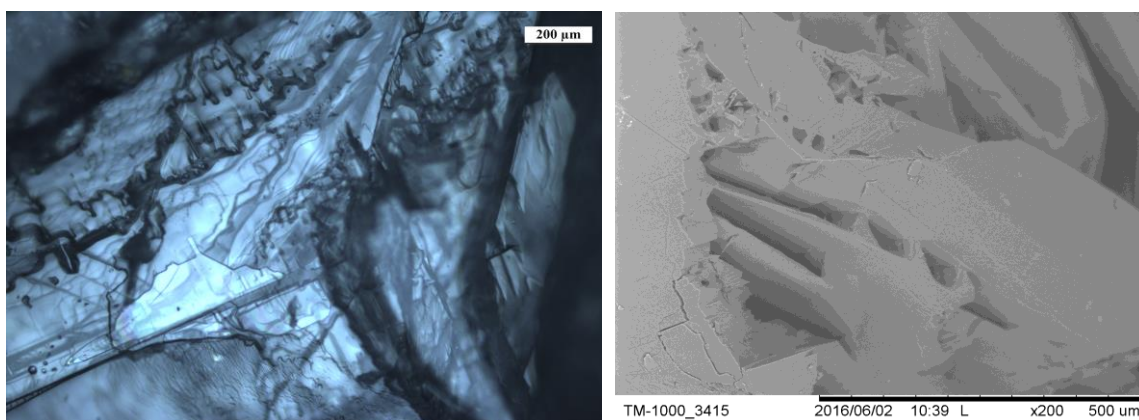


Figure 48 OM image in DIC mode, 10X, and SEM image of paracetamol crystal (PP). SEM operating conditions: distance 7210um, emission current 58.9mA, WD 7.21mm. Paracetamol surface texture is observed in OM and SEM image, with the characteristic edge steps.

AFM observations of the same crystal suggest that the surface of individual terraces adjacent to steps are relatively smooth (Figure 49). These crystal surface characteristics are consistent with those reported by Thompson *et al.* (2004)⁸ who used electron microscopy. In this case steps are higher than Thompson *et al.* (2004)⁸ observed due to growth at higher supersaturation ($S=1.5$ vs $S=0.44$). The PP crystal showed steps ranging in the height from 10 to 30 nm. Topographic analysis using AFM confirmed the microscopic characterization of the pure paracetamol and pure 4-nitrophenol crystals.

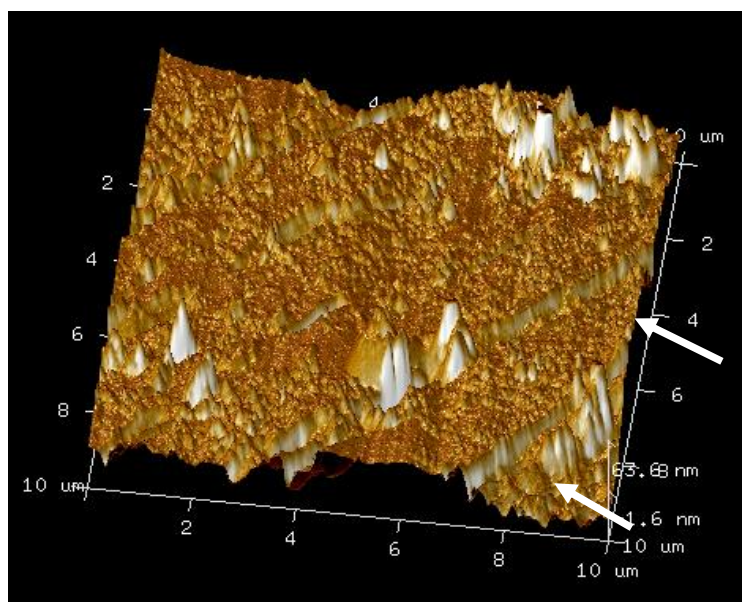


Figure 49 AFM map of PP crystal collected in air using Scan Asyst mode, the area of detection is 10x10 μ m. Topography shows roughness of PP crystal and the typical crystal step growth of PP crystal with step ranging in the height from 10 to 30 nm (see white arrows).

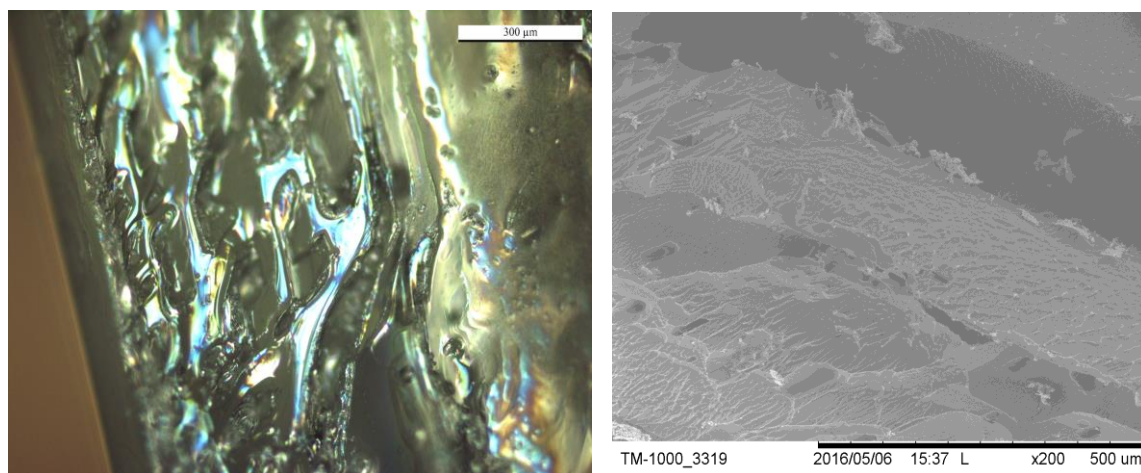


Figure 50 OM image in DIC mode, 10X, and SEM image of 4-nitrophenol crystal (PN). SEM operating conditions: distance 6220 μ m, emission current 57.9mA, WD 6.22mm. 4-nitrophenol characteristics rounded steps are observed in OM and SEM image.

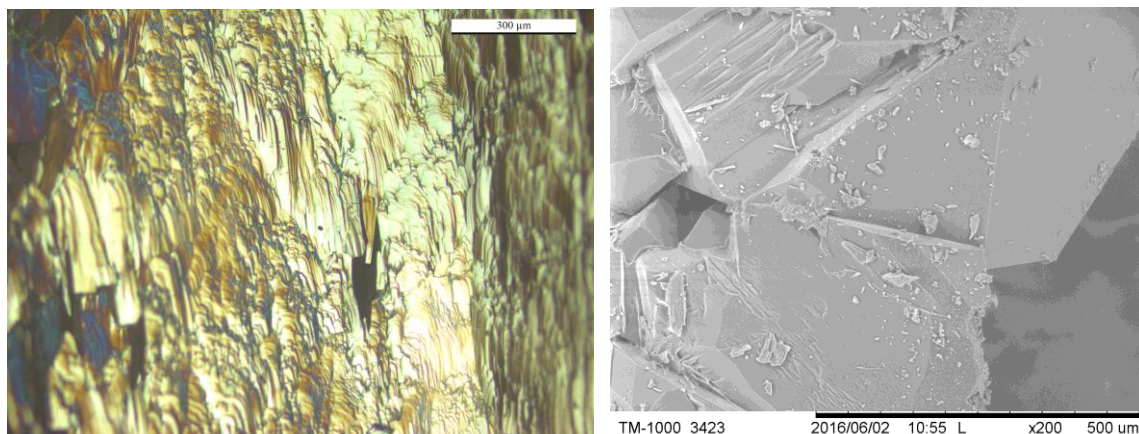


Figure 51 OM image in DIC mode, 10X, and SEM image of cooling crystallization crystal (P4%N). SEM operating conditions: working distance 6700um, emission current 57.4mA, WD 6.7mm. Increase frequency of surface defects are apparent in OM and SEM images and are associated with the presence of the impurity 4-nitrophenol (see the arrow).

The paracetamol crystal grown from a solution containing 4% mol of 4-nitrophenol (P4%N) shown in Figure 51 has a very rough surface texture characterized by nano-steps. The terrace edges of the P4%N crystal are small and curved quite different to the PP crystal which has larger terraces with straight edges. Examination of the OM and SEM images indicates that 4-nitrophenol added as impurity during growth acted as a texture modifier increasing the number of steps and other surface defects (Figure 51 and Figure 52). This is consistent with the observation of Prasad *et al.* (2001) and Thompson *et al.* (2004).^{8, 10} The AFM analysis reveals widespread nano-roughness and is consistent with the SEM and OM images.

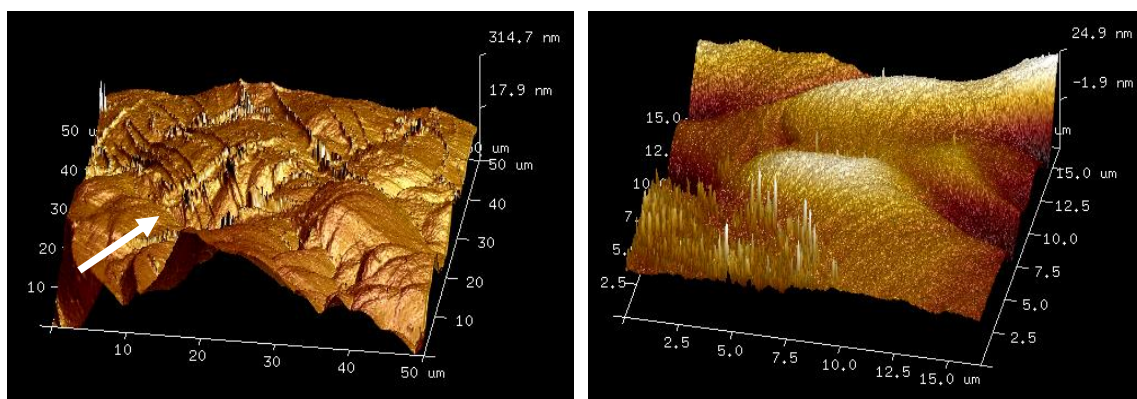


Figure 52 Two different AFM maps of P4%N crystal obtained in air with Scan Asyst mode, scan area respectively 50 and 15μm. From these two AFM topographic maps rough surface with nanometric steps can be evaluated (white arrow).

PDN crystal were examined within the perimeter area of the evaporated 4-nitrophenol saturated drop. Needle like crystals of 4-nitrophenol were randomly distributed in the core area of the drop, while at the perimeter they were aligned in the direction of spread. Areas not covered by the spreading drops of 4-nitrophenol solution showed characteristic paracetamol surface texture (Figure 53). The 4-nitrophenol crystals grown on the paracetamol crystal surface by rapid solvent evaporation exhibit a needle like morphology that is quite different to the slowly grown 4-nitrophenol crystal grown for the SCXRD. This may be due to rapid growth by evaporation or alternatively could be due to the formation of the beta polymorph of 4-nitrophenol³⁸ which have a needle-like morphology (the 4-nitrophenol crystals were too small to determine their crystal form).

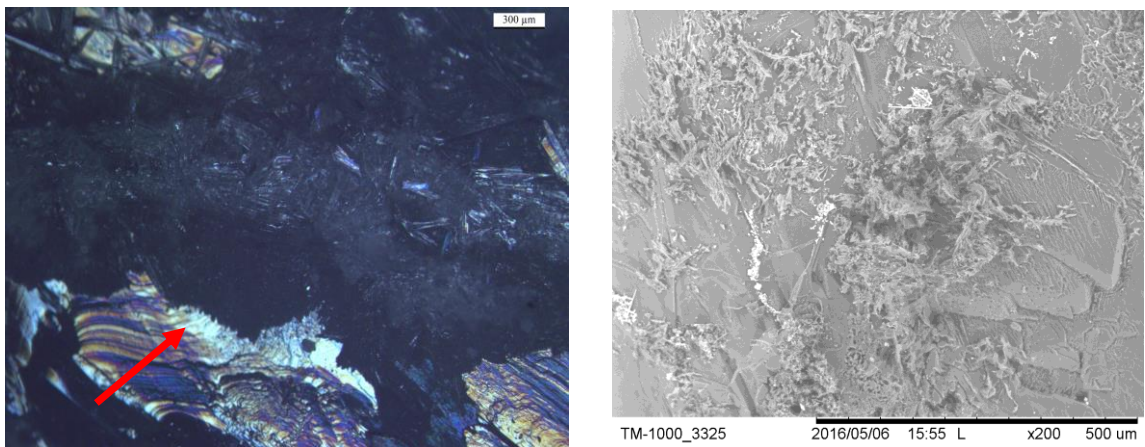


Figure 53 OM image in DIC mode, 10X, and SEM image of drop crystal (PDN). Red arrow highlight the drop perimeter. SEM operating conditions: working distance 6360um, emission current 58.7mA, WD 6.36mm. Needle shape 4-nitrophenol crystals are observed in the drop area both in OM and SEM images (see the arrow).

The PDN crystals were analysed by atomic force microscopy (Figure 54) however, the 4-nitrophenol crystals formed during rapid evaporation were not strongly bonded to the paracetamol substrate crystal surface as a consequence of this they were easily detached during the AFM analysis and became attached to the AFM tip. Therefore only boundary areas of the drop have been analysed by AFM.

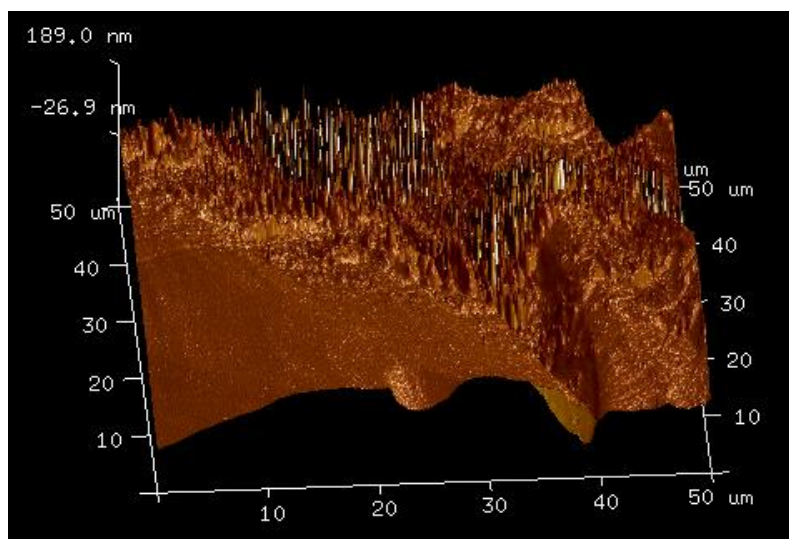


Figure 54 AFM maps of PDN crystal obtained in air with Scan Asyst mode, scan area 50 μ m. The perimeter drop can be observed. On the left side of the image the surface is smooth with macro roughness characteristic of paracetamol, while on the right side the increase of micro roughness is due to the needle like 4-nitrophenol crystal randomly orientated is observe.

The epitaxially grown crystals include both micrometer and nanometer size crystals of 4-nitrophenol on the paracetamol crystal surface are seen in the OM image (Figure 55). These crystals showed the same needle like shape observed when 4-nitrophenol was deposited by evaporation of a drop of ethanol saturated solution.

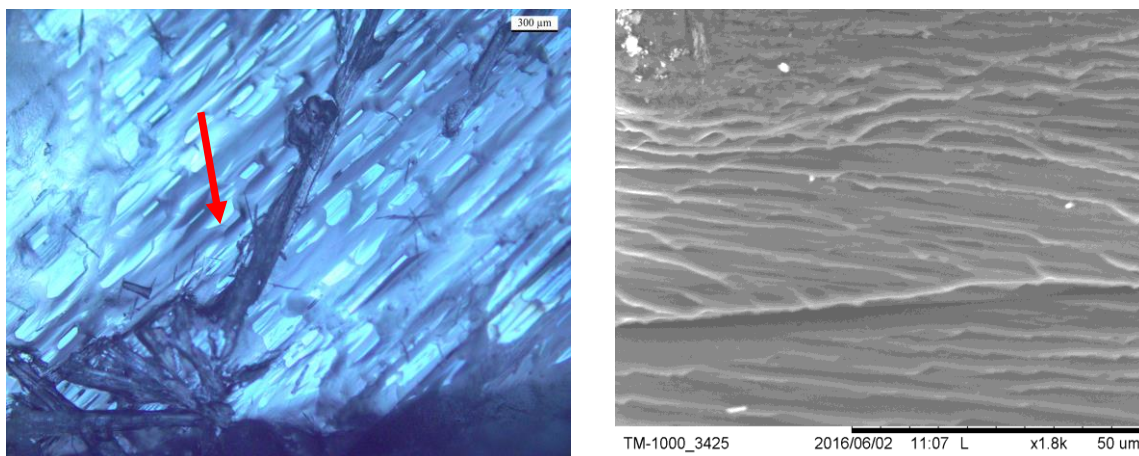


Figure 55 OM image in DIC mode, 10X, and SEM image of epitaxial crystal (PEN). Needle shape epitaxially growth 4-nitrophenol crystals are observed (arrow). SEM operating conditions: working distance 5820um, emission current 57.7mA, WD 5.82mm. Paracetamol steps substrate texture is seen from SEM image.

This observation suggests that the needle like habit of 4-nitrophenol occurs both during rapid evaporation of ethanol or more controlled epitaxial growth from heptane. This is in marked contrast to the slow solution grown crystals of pure 4-nitrophenol used to determine lattice parameters, as seen in Table 26 which have a more diamond prism like habit. Paracetamol stripe step texture was visible on OM and SEM images (Figure 48). Micro and nano roughness have been detected with AFM (Figure 56). 4-nitrophenol crystals on paracetamol surface increase sample roughness. Micro roughness appears to be linked to 4-nitrophenol crystal epitaxial growth on paracetamol crystal surface, while nano roughness was probably linked the proximity of multiple 4-nitrophenol crystals.

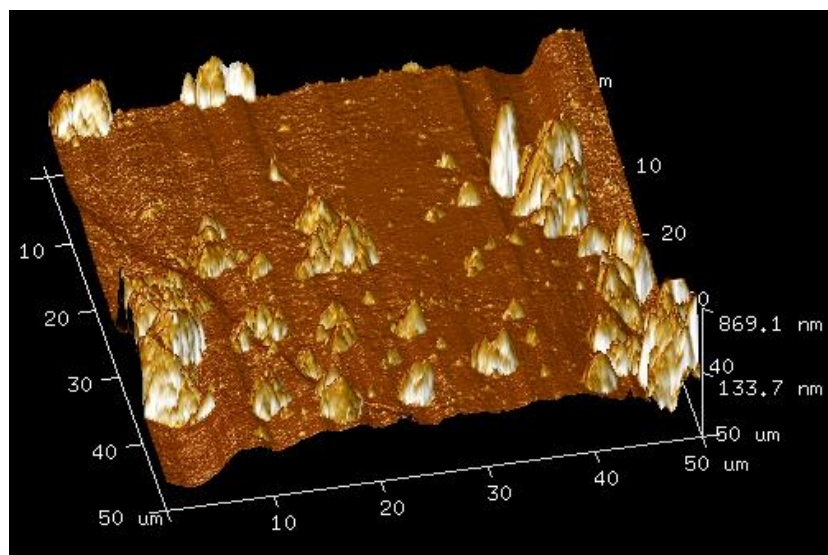


Figure 56 AFM maps of PEN crystal obtained in air with Scan Asyst mode, scan area respectively 50μm. Nano and micro roughness can be observed.

5.4.2 Raman and TOF-SIMS analysis

Raman microscopy in mapping mode and TOF-SIMS were evaluated as complimentary techniques, both have the potential to allow the distribution of 4-nitrophenol on the crystal surface to be determined. As described previously three different crystallization

techniques were used to prepare samples containing both paracetamol and 4-nitrophenol with which to evaluate the sensitivity of these two analytical tools to investigate concentration and distribution. Raman spectra of the pure PP and PN crystals were collected to establish the differences in the spectra between the two compounds to identify characteristic Raman bands so that the local composition could be mapped.

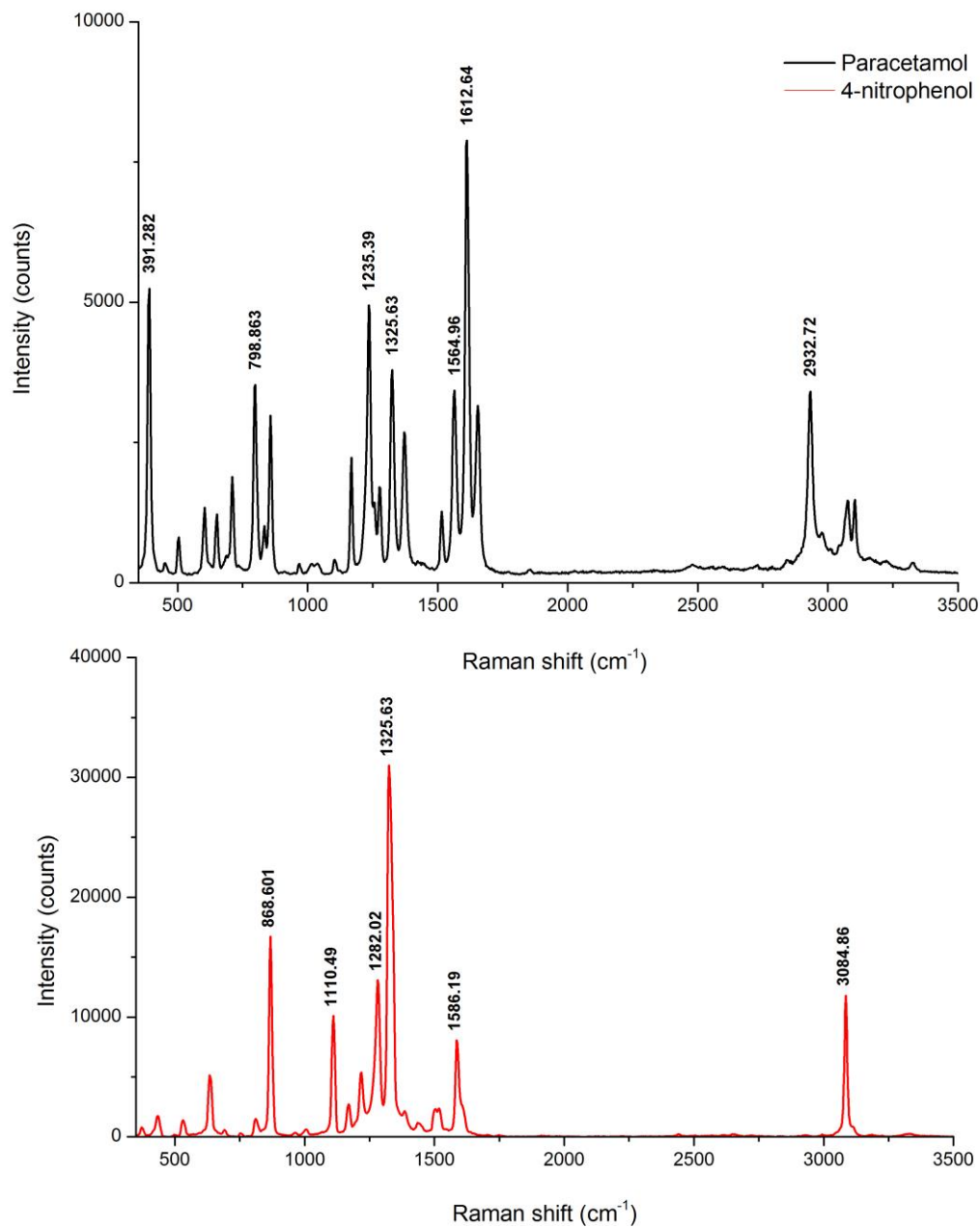


Figure 57 Raman spectra of paracetamol (PP) (top) and 4-nitrophenol (PN) bottom spectrum.

Anitha and co-workers (2015)^{39, 40} reported the assignment of spectral bands for paracetamol whilst Vijayalakshmi et al. (2014)³¹ reported the assignment of the Raman bands for 4-nitrophenol. Characteristic 4-nitrophenol Raman peaks were 303cm⁻¹, 869cm⁻¹

¹, 1110cm⁻¹, 1586cm⁻¹ and 3085cm⁻¹. Due to the absence of overlapping features in the spectral region the CN stretching peak at 1111cm⁻¹ was selected for evaluating the presence of 4-nitrophenol on the paracetamol crystal surface (Figure 57). The Raman maps presented in Figure 58 and Figure 59 were obtained by tracking this characteristic peak of 4-nitrophenol with respect to the difference between the maximum peak intensity and baseline intensity. By processing the spectra in this way, concentration contour maps were generated.

Regions of the crystal surfaces were selected to maximise the probability of detecting the 4-nitrophenol. In the case of the crystal grown from paracetamol solution containing 4% mol 4-nitrophenol, P4%N, the Raman map was constructed across a growth step (Figure 58), In the case of the epitaxially deposited 4-nitrophenol, PEN, the map centred on an area rich in needle like 4-nitrophenol crystals (Figure 59). Comparing Raman maps of P4%N and PEN crystals only the PEN crystal showed a significant difference between peak and baseline intensity, in some areas the peak intensity to baseline intensity ratio at the selected characteristic wavelength exceeded 10. This indicates that, under favourable conditions, Raman microscopy may be used in mapping mode to evaluate the distribution of chemical species.

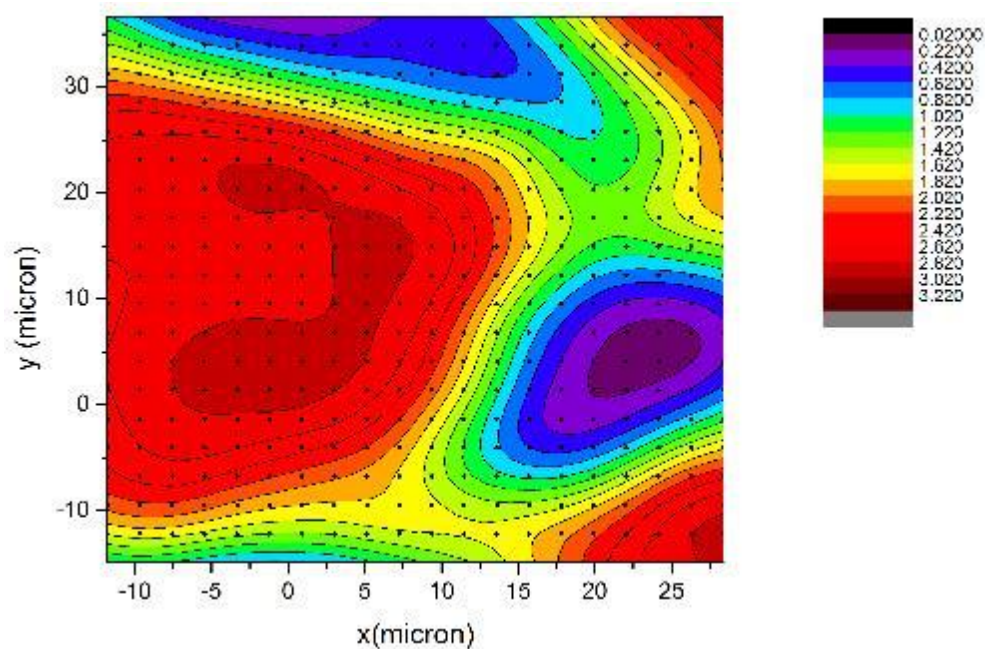


Figure 58 Raman map of P4%N crystal. Crystal was analysed in a step area. Area of detection 20x20 μm . Black dots on the map correspond to the position of the laser detection. Scale is related to the intensity of 4-nitrophenol peak within respect to the baseline.

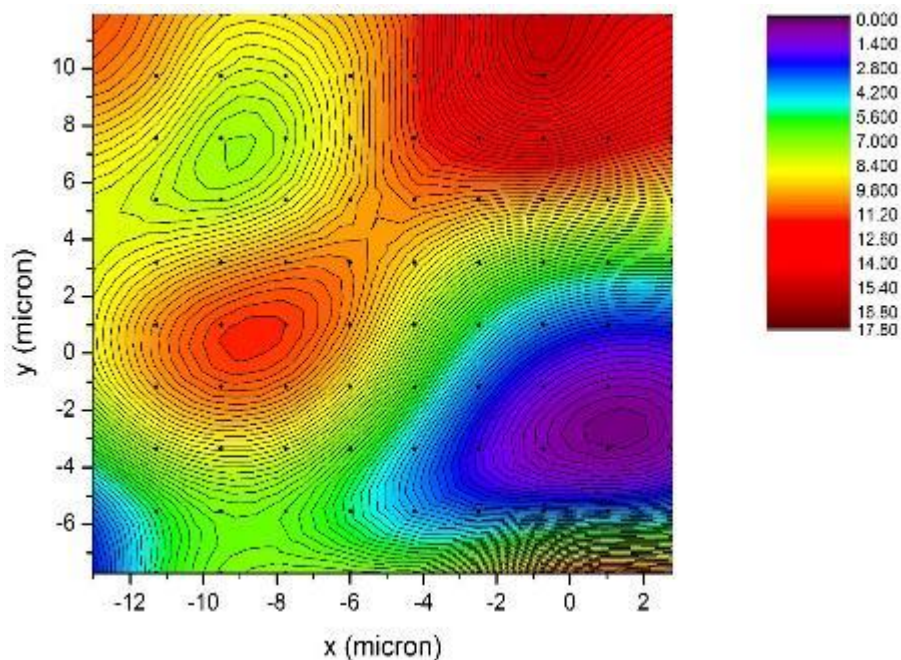


Figure 59 Raman map of PEN crystal. The area of the crystal analysed was in an area where 4-nitrophenol needle like crystals were concentrated. Area of detection 10x10 μm . The black dots on the map correspond to the centres of the spectrum collections. Scale is related to the intensity of 4-nitrophenol peak within respect to the baseline.

The TOF-SIMS mass spectra and ion maps of the three different crystals were obtained in a similar way to the Raman maps. The pure PP and PN crystals were analysed to obtain mass spectra of these two pure crystals in order to identify the characteristic mass fragment ions.

To verify the mass spectra obtained and to confirm the fragmentation ion identities two software tools were used; NIST 08 MS Demo and AMDIS 2.6 from NIST. The 10 largest molecular fragment peaks from paracetamol and 4-nitrophenol are listed and their mass ion identified in Table 27.

Table 27 Characteristic neutral fragment mass spectra peaks of paracetamol and 4-nitrophenol taking from NIST 08 MS Demo and AMDIS 2.6.

Paracetamol fragment mass	Intensity (counts)	Fragment assignment	4- nitrophenol fragment mass	Intensity (counts)	Fragment assignment
109	999	C ₆ H ₇ NO	65	999	C ₄ H ₃ N
151	440	Paracetamol	139	803	4- nitrophenol
43	153	CHNO	39	645	C ₂ HN
80	126	C ₅ H ₄ O	109	580	C ₅ H ₃ NO ₂ or C ₆ H ₅ O ₂
108	115	C ₆ H ₄ O ₂ or C ₆ H ₆ NO	81	286	C ₅ H ₆ O
81	90	C ₅ H ₆ O	63	241	CH ₅ NO ₂ or C ₄ HN
110	79	C ₅ H ₄ NO ₂ or C ₆ H ₆ O ₂	93	233	C ₆ H ₅ O
53	62	C ₃ H ₃ N	53	140	C ₃ H ₃ N

52	46	C ₃ H ₂ N	38	130	C ₂ N
152	40	Paracetamol	62	115	C ₄ H ₅ NO ₃

The distinctive molecular fragments for 4-nitrophenol were 38 m/z, 63 m/z, 65 m/z and 139 m/z. Analysing fragment mass images at 139 m/z, which corresponds to the 4-nitrophenol monoisotopic mass, allowed the distribution of 4-nitrophenol to be determined.

TOF-SIMS negative polarity mass fragment images for the P4%N crystal suggest a homogeneous distribution of 4-nitrophenol (138 m/z) across the crystal surface. The step surface texture of the crystal can be seen in Figure 60, which is consistent with SEM and OM images also obtained.

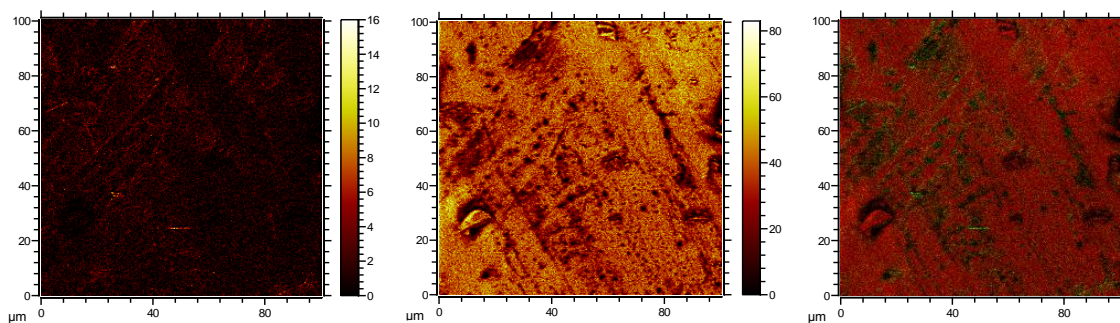


Figure 60 Paracetamol with 4% (mol/mol) of 4-nitrophenol. From left to right, 4-nitrophenol molecular ion image at 138 m/z (maximum counts = 16), paracetamol molecular ion image at 150 m/z (maximum counts = 83) and RGB overlay of paracetamol (red) with 4-nitrophenol (green).

TOF-SIMS mass fragment images of the PDN crystal (Figure 61) allow the investigation of the evaporated 4-nitrophenol solution drop on top of the paracetamol crystal. The images show a layer of 4-nitrophenol (138 m/z) covering a large area of the crystal with only small areas of paracetamol (150 m/z) still remaining exposed.

From these images, it appears that the 4-nitrophenol drop spread across the surface leaving a covering layer of 4-nitrophenol behind, the image does not however reveal the shape of the individual impurity crystals.

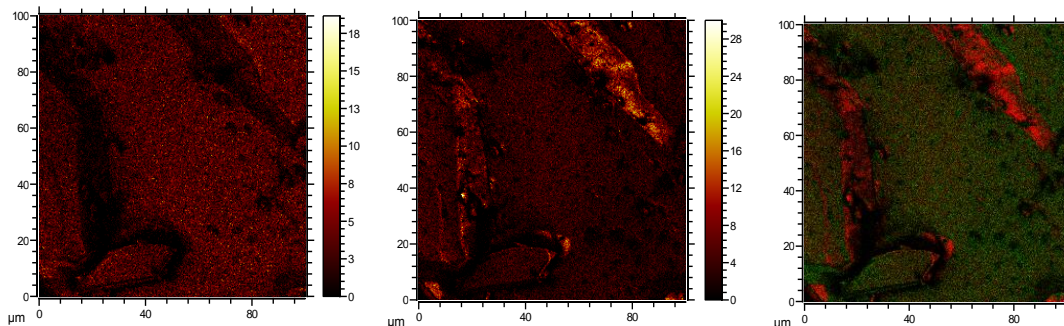


Figure 61 Paracetamol crystal with drop of 4-nitrophenol applied. From left to right, 4-nitrophenol molecular ion image at 138 m/z (maximum counts = 19), paracetamol molecular ion image at 150 m/z (maximum counts = 30) and RGB overlay of paracetamol (red) with 4-nitrophenol (green).

Figure 62, shows the TOF-SIMS mass ion fragment images of the PEN crystal. A needle shaped 4-nitrophenol crystal is clearly seen at 138 m/z. The corresponding image for the molecular ion fragment of paracetamol (150 m/z) shows the uniform spread of paracetamol, the area covered by the 4-nitrophenol appears darker as the surface of the paracetamol crystal is not accessed by the ionization beam. This sequence of figures (Figure 60, Figure 61, Figure 62) demonstrates the capability of TOF-SIMS to evaluate the distribution of different chemical species on crystal surfaces.

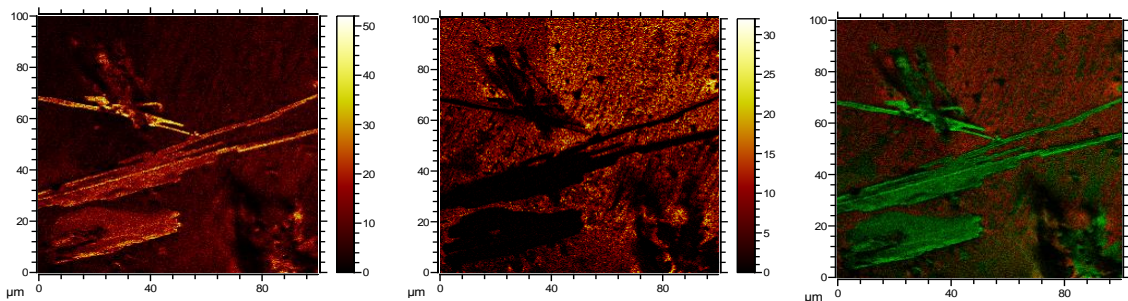


Figure 62 Suggested paracetamol with 4-nitrophenol Epitaxy. From left to right, 4-nitrophenol molecular ion image at 138 m/z (maximum counts = 52), paracetamol molecular ion image at 150 m/z (maximum counts = 32) and RGB overlay of paracetamol (red) with 4-nitrophenol (green).

Results related to single crystals crystallized in presence of other paracetamol related impurities are reported in the appendix (chapter 9).

5.5 Conclusions

Three different approaches, epitaxy, droplet evaporation and cooling crystallization were used to create paracetamol crystals with molecules of 4-nitrophenol present on the crystal surface. The methods were used to study the effectiveness of different analytical techniques, to investigate the quantity and spatial distribution of the impurity on crystal surfaces and to identify any associated morphological and surface texture changes.

TOF-SIMS is a relatively unused technique for pharmaceutical material characterization and allows the presence of 4-nitrophenol to be verified by the distribution of the secondary-ion fragments.

The presence and spatial distribution of 4-nitrophenol crystals generated epitaxially are observed.

SEM, AFM, Raman Microscopy and TOF-SIMS were evaluated to assess the level at which the impurity 4-nitrophenol can be detected.

Raman Microscopy mapping reveals the impurity location when the main peak intensity ratio is more intense than the baseline, for example the intensity difference in Figure 59 is substantially greater than in Figure 58.

OM, SEM and AFM show crystal epitaxial growth on pure paracetamol crystal surface, they reveal surface texture changes and allow the distribution of small crystal agglomerates to be observed. These techniques can be used as complementary analytical tools to address changes in surface texture due to presence of impurity in the crystal lattice and on the crystal surface.

From the results gathered from the 4-nitrophenol impurity, a series of other related impurities of paracetamol were used to determine if TOF-SIMS was able to detect other chemical related species. However, TOF-SIMS cannot be used to accurately quantify chemical species in the sample because of the following effects:^{41, 42, 43}

- Topography effect: TOF-SIMS images can be affected by surface topography features. In particular, the electron field intensity in insulating materials varies with surface height, causing the secondary ion signal to vary even when there is no chemical variation. To address this problem it is important to select an area of the sample that is as flat as possible or compare SIMS images from several types of secondary ions.
- Matrix effect: TOF-SIMS uses energized primary particles to bombard the surface area of the solid under investigation to induce sputtering of secondary

particles. These secondary particles generated can be electrons, neutral species of atoms or molecules (majority of emitted particles) and ions. Only generated secondary ions are used for the chemical analysis. In general, only a very small percentage of the secondary particles produced are analysed (approximately 1% of the secondary particles are ions). The ionization probability of each ion is partially dependent on the surrounding environment defined as “the matrix”. The yield of the same chemical species located in two different chemical environments may be different.

- Fragment overlapping effect: TOF measurements cannot discriminate secondary ion mass/charge ratio for fragments of different molecular species preventing an accurate quantitative analysis for a single molecular species.
- Mass resolution of the TOF-SIMS: as shown in this work, the surface of the crystals was made up from molecules with similar molecular structure: the related compounds of paracetamol. The related compounds are fragmented by the primary ion source in similar ways to paracetamol, as observed in the mass spectra in chapter 9, making very difficult to assign a particular mass/charge ion peak of a fragment to a singular specific molecular species. With advanced chemometric analysis methods and more method development time such challenges could possibly be overcome.

A cooling crystallization approach was used to grow single crystals in ethanol in presence of 4% mol/mol paracetamol related impurities. Two crystals for each combination were grown. Optical microscopy in DIC mode was used to evaluate morphological variations

caused by the presence of related impurities. Comparisons with the morphology of pure paracetamol crystals grown using cooling crystallization in ethanol with the same crystallization conditions were performed. In detail, the two main largest faces of single crystals were analyzed to determine if any of the related impurities of paracetamol show face specific adsorption propensity. TOF-SIMS surface imaging and 3D depth profiles of the chemical species were used to evaluate whether the related impurities were deposited only on the crystal surface or if they were also present in sub-surface layers.

As observed from the data gathered (see appendix, chapter 9), mainly 4-nitrophenol and 4-acetamido benzoic acid show distinctive ion fragmentation peaks in mass spectra that are specific to the impurities. The other related impurities show largely overlapping ion fragment peaks with pure paracetamol mass spectra in negative and positive mode, making them very difficult to analyze.

P4%AMBA-EtOH face 1 and 2 show non-homogeneous layer formation on top of the crystal surface. Analyzing the 3D depth profile results, it is possible to infer that the impurity is located in high concentration at the crystal surfaces.

This work also highlighted issues determining the depth of the 3D analysis craters. AFM and optical microscopy were used to determine the depth of the sputtered area but only optical microscopy was able to give usable results. AFM, on the other hand, was used to evaluate the texture of the area outside and inside the crater.

This work demonstrates that TOF-SIMS analysis allowed investigation of both chemical and topographic character of crystal faces and in combination with other complementary techniques proves to be a valuable addition to the analysis of crystals and their impurities.

To better evaluate the effect of impurities and solvent as crystal growth modifiers, a series of crystal growth kinetic investigation is required. SC-XRD can be possibly used as well to identify new faces formation. To investigate the impurity content in single crystals where the impurity present is not detectable with TOF-SIMS, the use of HPLC is required; however, this technique is only able to provide the total impurity content without showing the distribution of the species on different crystal facets.

5.6 Abbreviations

SIPBS, Strathclyde Institute of Pharmacy & Biomedical Sciences, SEM, scanning electron microscopy, XPS, X-ray photoelectron spectroscopy, TOF-SIMS, time of flight secondary ion mass spectrometry, OM, optical microscopy, HPLC, high performance liquid chromatography, XRD, X-ray diffractometry, API, Active Pharmaceutical Ingredients, EDX, energy-dispersive X-ray spectroscopy, PSD, particle size distribution, FBRM, focused beam reflectance measurement, AFM, atomic force microscopy, SC-XRD, single crystal X-ray diffractometry, P4%N, paracetamol crystal with the presence of 4%mol 4-nitrophenol made by cooling crystallization, PDN, paracetamol crystal with drop of 4-nitrophenol, PEN, paracetamol crystal with epitaxially grown 4-nitrophenol, PP, pure paracetamol crystal made by cooling crystallization, PN, pure 4-nitrophenol made by cooling crystallization, P4%AMBA-EtOH, paracetamol crystal with the presence of 4%mol 4-acetamido benzoic acid made by cooling crystallization, P4%AP- EtOH, paracetamol crystal with the presence of 4%mol 4-aminophenol made by cooling crystallization, P4%HA- EtOH, paracetamol crystal with the presence of 4%mol 4-

hydroxy acetophenone made by cooling crystallization, P4%CA- EtOH, paracetamol crystal with the presence of 4%mol 4'-chloroacetanilide made by cooling crystallization, P4%A-EtOH, paracetamol crystal with the presence of 4%mol acetanilide made by cooling crystallization, P4%MHB-EtOH, paracetamol crystal with the presence of 4%mol 4-methyl hydroxyl benzoate made by cooling crystallization, P4%AA-EtOH, paracetamol crystal with the presence of 4%mol acetaminophen acetate made by cooling crystallization, WD, working distance, RTD, real time data.

References

1. Prabu, S., L., Suriyaprakash, T., N., K., 2010. Impurities and its importance in pharmacy. *Int. J. Pharm. Sci. Rev. Res.*, 66.
2. Ellis, F. Paracetamol: A Curriculum Resource; Royal Society of Chemistry, 2002.
3. Finnie, S., Prasad, K., V., R., Sheen, D., B., Sherwood, J., N., 2001. Microhardness and Dislocation Identification Studies on Paracetamol Single Crystals. *J. N. Pharm. Res.*, 674.
4. Sudha, C., Srinivasan, K., 2014. Understanding the effect of solvent polarity on the habit modification of monoclinic paracetamol in terms of molecular recognition at the solvent crystal/interface. *Cryst. Res. Technol.*, 865.
5. Hendriksen, B., A., Grant, D., J., W., 1995. The effect of structurally related substances on the nucleation kinetics of paracetamol (acetaminophen). *J. Cryst. Growth*, 252.
6. Hendriksen, B., A., Grant, D., J., W., Meenan, P., Green, D., A., 1998. Crystallisation of paracetamol (acetaminophen) in the presence of structurally related substances. *J. Cryst. Growth*, 629.
7. Kuvadia, Z., B., Doherty, M., F., 2013. Effect of Structurally Similar Additives on Crystal Habit of Organic Molecular Crystals at Low Supersaturation. *Cryst. Growth Des.*, 1412.
8. Thompson, C., Davies, M., C., Roberts, C., J., Tendler, S., J., B., Wilkinson, M., J., 2004. The effects of additives on the growth and morphology of paracetamol (acetaminophen) crystals. *Int. J. Pharm.*, 137.
9. Shekunov, B., Y., Grant, D., J., W., Latham, R., J., Sherwood, J., N., 1997. In Situ Optical Interferometric Studies of the Growth and Dissolution Behavior of Paracetamol (Acetaminophen) Crystals. 3. Influence of Growth in the Presence of p-Acetoxyacetanilide *J. Phys. Chem. B*, 9107.
10. Chow, A., H.-L., Chow, P., K., K., Zhongshan, W., Grant, D., J., W., 1985. Modification of acetaminophen crystals: influence of growth in aqueous solutions

- containing p-acetoxyacetanilide on crystal properties. *Int. J. Pharm.*, 239.
11. Prasad, K., V., R., Ristic, R., I., Sheen, D., B., Sherwood, J., N., 2001. Crystallization of paracetamol from solution in the presence and absence of impurity. *Int. J. Pharm.*, 29.
 12. Saleemi, A., Onyemelukwe, I., I., Nagy, Z., 2013. Effects of a structurally related substance on the crystallization of paracetamol. *Front. Chem. Sci. Eng.*, 79.
 13. Winograd, N., 2003. Prospects for imaging TOF-SIMS: from fundamentals to biotechnology. *Applied Surface Science, Secondary ion mass spectrometry SIMS. Appl. Surf. Sci.*, 203.
 14. Verlinden, G., Gijbels, R., Geuens, I., Keyzer, R., D., 1999. Surface analysis of halide distributions in complex AgX microcrystals by imaging time-of-flight SIMS (TOF-SIMS). *J. Anal. At. Spectrom.*, 429.
 15. Rutten, F., J., M., Roe, M., J., Henderson, J., Briggs, D., 2006. Surface analysis of ancient glass artefacts with ToF-SIMS: A novel tool for provenancing? *Appl. Surf. Sci.*, 7124.
 16. Park, J., S., Kim, H., 2009. Surface characterization of plasma-modified resist patterns by ToF-SIMS analysis. *Applied Surface Science, Proceedings of the Symposium on Surface Science. Appl. Surf. Sci.*, 1604.
 17. Marques, A., F., A., Scott, S., D., Sodhi, R., N., S., 2011. Determining major and trace element compositions of exposed melt inclusions in minerals using ToF-SIMS. *Surf. Interface Anal.*, 436.
 18. Belu, A., M., Davies, M., C., Newton, J., M., Patel, N., 2000. TOF-SIMS Characterization and Imaging of Controlled-Release Drug Delivery Systems. *Anal. Chem.*, 5625.
 19. Muster, T., H., Prestidge, C., A., 2002. Face specific surface properties of pharmaceutical crystals. *J. Pharm. Sci.*, 1432.
 20. Prestidge, C., A., Barnes, T., J., Skinner, W., 2007. Time-of-flight secondary-ion mass spectrometry for the surface characterization of solid-state pharmaceuticals. *J. Pharm. Pharmacol.*, 251.
 21. Malmberg, P., Jennische, E., Nilsson, D., Nygen, H., 2011. High-resolution, imaging TOF-SIMS: novel applications in medical research. *Anal. Bioanal. Chem.*, 2711.
 22. Koch, S., Ziegler, G., Hutter, H., 2013. ToF-SIMS measurements with topographic information in combined images. *Anal. Bioanal. Chem.*, 7161.
 23. Iuraş, A., Scurr, D., J., Boissier, C., Nicholas, M., L., Roberts, C., J., Alexander, M., R., 2016. Imaging of Crystalline and Amorphous Surface Regions Using Time-of-Flight Secondary-Ion Mass Spectrometry (ToF-SIMS): Application to Pharmaceutical Materials. *Anal. Chem.*, 3481.
 24. Barnes, T., J., Kempson, I., M., Prestidge, C., A., 2011. Surface analysis for compositional, chemical and structural imaging in pharmaceuticals with mass spectrometry: A ToF-SIMS perspective. *Int. J. Pharm.*, 61.
 25. Wiley: Materials Characterization: Introduction to Microscopic and Spectroscopic Methods, 2nd Edition - Yang Leng <http://eu.wiley.com/WileyCDA/WileyTitle/productCd-3527334637.html> [cited 2016-09-01].

26. Granberg, R., A., Rasmuson, Å., C., 1999. Solubility of Paracetamol in Pure Solvents. *J. Chem. Eng. Data*, 1391.
27. Morris, D., M. In *Emerging Raman Applications and Techniques in Biomedical and Pharmaceutical Fields*; Matousek, P., Morris, M. D., Eds.; Biological and Medical Physics, Biomedical Engineering; Springer Berlin Heidelberg, 2010; pp 347–364.
28. Gordon, K., C., McGoverin, C., M., 2011. Raman mapping of pharmaceuticals. *Int. J. Pharm.*, 151.
29. Pyatski, Y., Zhang, Q., Mendelsohn, R., Flach, C., R., 2016. Effects of permeation enhancers on flufenamic acid delivery in Ex vivo human skin by confocal Raman microscopy. *Int. J. Pharm.*, 319.
30. Al-Zoubi, N., Koundourellis, J., E., Malamataris, S., 2002. FT-IR and Raman spectroscopic methods for identification and quantitation of orthorhombic and monoclinic paracetamol in powder mixes. *J. Pharm. Biomed. Anal.*, 459.
31. Vijayalakshmi, S., Kalyanaraman, S., Ravindran, T., R., 2014. Raman investigation with group theoretical method on structural polymorphism of the nonlinear optical hexamine: p –nitrophenol cocrystals. *Phys. Scr.*, 95501.
32. Xu, F., Sun, L., X., Tan, Z., C., Liang, J., G., Zhang, T., 2006. Adiabatic calorimetry and thermal analysis on acetaminophen. *J. Therm. Anal. Calorim.*, 187.
33. Perrin, M.-A., Neumann, M., A., Elmaleh, H., Zaske, L., 2009. Crystal structure determination of the elusive paracetamol Form III. *Chem. Commun.*, 3181.
34. Nichols, G., Frampton, C., S., 1998. Physicochemical Characterization of the Orthorhombic Polymorph of Paracetamol Crystallized from Solution. *J. Pharm. Sci.*, 684.
35. Druzhbin, D., A., Drebuschak, T., N., Min'kov, V., S., Boldyreva, E., V., 2015. Crystal structure of two paracetamol polymorphs at 20K: a search for the “structure-property” relationship. *J. Struct. Chem.*, 317.
36. Kulkarni, G., U., Kumaradhas, P., Rao, C., N., R., 1998. Charge Density Study of the Polymorphs of p-Nitrophenol. *Chem. Mater.*, 3498.
37. Wójcik, G., Mossakowska, I., 2006. Polymorphs of p-nitrophenol as studied by variable-temperature X-ray diffraction and calorimetry: comparison with m-nitrophenol. *Acta Cryst B, Acta Cryst Sect B, Acta Crystallogr B, Acta Crystallogr Sect B, Acta Crystallogr Struct Sci, Acta Crystallogr Sect B Struct Sci, Acta Crystallogr B Struct Sci Cryst Eng Mater*, 143.
38. Coppens, P., Schmidt, G., M., 1965. The crystal structure of the metastable (β) modification of p-nitrophenol. *Acta Crystallogr.*, 654.
39. Gandhimathi, R., Dhanasekaran, R., 2013. Third order nonlinear studies and other characterization of 4-nitrophenol (4-NP) single crystals. *IOP Conf. Ser.: Mater. Sci. Eng.*, 12004.
40. Anitha, R., Gunasekaran, M., Kumar, S., S., Athimoolam, S., Sridhar, B., 2015. Single crystal XRD, vibrational and quantum chemical calculation of pharmaceutical drug paracetamol: A new synthesis form. *Spectrochim. Acta, Part A*, 488.
41. Iida, S.-i., Sanada, N., Bryan, S., R., Suzuki, M., 2008. Extraction of

- inhomogeneous chemical species from TOF-SIMS images with topographic artifacts by using correlation coefficient mapping. *Appl. Surf. Sci.*, 1603.
42. Ziegler, G., Hutter, H., 2012. Correction of topographic artefacts of TOF-SIMS element distributions. *Surf. Interfact Anal.*, 457.
 43. Scarazzini, R., PhD thesis: TOF-SIMS characterization of fragile materials used in microelectronic and microsystem devices: validation and enhancement of the chemical information, 2016.

6 Effect of filtration, washing and drying on the isolated product: Paracetamol case study.

The work reported in this chapter was submitted as Understanding effect of filtration and washing on the dried product. Paracetamol case study, Sara Ottoboni, Martin Simurda, Samantha Wilson, Andrew Irwin, Fraser Ramsay, Chris Price, OPR&D.

6.1 Introduction

One of the key challenge that pharmaceutical industry faces is to maintain particle properties across the entire purification and isolation process. Substantial effort has been made during the last decade to generate particles in suspension of the required size, habit, purity and other attributes by crystal engineering. However, the task of maintaining these particles properties during the downstream drug isolation has received less attention. Active Pharmaceutical Ingredient (API) isolation by filtration, washing and drying still poses significant challenges if practitioners are to avoid breaking or granulating the crystals or precipitating dissolved product or impurities.

This research focuses on the effect of slurry properties, wash solvent, filtration and washing mechanism on API agglomeration/granulation during isolation and the impact on product physical properties. In this investigation, each isolation step was analysed to identify factors that have the potential to affect the final product qualities. A multivariate statistical design of experiments approach was used. The model compound used in this study was paracetamol. Slurry properties, such as solids loading, particle size distribution (PSD) and crystallization solvents were investigated to examine the impact of filtration on drying. The role of washing was scrutinised by analysing the effect of different primary crystallization solvents, the quantity and identity of wash solvent used and number of washing steps. The effect of halting filtration and washing at dryland (i.e. maintaining a fully saturated filter cake) or breakthrough (deliquoring the filter cake) on the properties of final dried product was also studied. Different drying methodologies were used to examine the effect of heat on the attributes of the dried product. Filtration and drying kinetics were measured in each experiment. Proton nuclear magnetic resonance (^1H -

NMR) was used to determine cake washing efficiency in terms of removing the primary solvent. The isolated product was also analysed to characterize mechanical properties, the extent of agglomeration and the PSD.

The design of experiments approach was used to provide a basis to develop a procedure to reduce agglomeration during drying. Combining all the findings, the combination of factors which were most detrimental in increasing particle agglomeration were found to be the particle size of the input material, the quantity and quality of wash solvent and the drying mode. Parameters that tended to reduce agglomeration were also considered to aid the selection of wash solvent based on properties, such as viscosity, density, surface tension and API solubility and their effect on particle agglomeration. Low boiling aliphatic hydrocarbons (cyclohexane and n-heptane) are shown to be desirable final wash solvents if the objective is to reduce the extent and strength of particle cementing to produce soft agglomerates.

6.2 Background

Typically, the Critical Quality Attributes (CQAs) which must be established during API isolation are purity and particle size distribution. Both are achieved principally by the upstream process of crystallization in which particles of the required size and purity are generated in suspension in impure mother liquors.¹ Filtration, washing and drying steps are necessary to isolate the API and ideally should accomplish this without breaking or granulating the crystals or precipitating dissolved product or impurities on the crystal surfaces. In order to develop an isolation strategy it is necessary to consider the different materials and processing steps to identify conditions which allow production of dried

particles with the PSD obtained during primary crystallization and simultaneously meet the purity requirements consistent with use as a drug substance (i.e. consistent with regulatory guidance e.g. ICH).² According to Murugesan et al and Beckmann^{3,4}, typical industrial practice is to wash a filter cake with at least three cake volumes of solvent, which approximates to between 5 to 7 mL of solvent per gram of API produced. Improving wash efficiency would reduce solvent use and improves environmental metrics.

Solvent selection and variability in particle properties significantly affect the efficacy and operation of each individual processing step during filter cake processing. Finding a suitable sequence of steps and combination of parameters may help to achieve consistent product quality and increase equipment utilization.

Isolation can be divided in five stages: cake formation (sometimes called sedimentation), filtration, washing, deliquoring and drying.⁵⁻⁸ At the end of final washing step, a common industrial practise is to introduce a deliquoring step, which is conducted to mechanically displace as much as possible of the remaining liquor phase trapped in cake pore structure. Mechanical displacement can be conducted by using pressure, vacuum or by physical compression using a piston all with the objective of displacing solvent residues from the inter-particle voids. Subsequently, a thermal drying process is conducted to remove any residual intra-particle solvent further reducing the solvent content to achieve a target level of dryness.⁹ Drying is the activity within the isolation step that is most frequently responsible of particle size variation (breakage or agglomeration) and in extreme cases even lump formation.¹⁰⁻¹⁴ Washing, on the other hand, has an essential role in delivering

cake purity. By selection of filtration and washing strategies drying can be improved to facilitate production of pure particles with comparable size as to the crystallized material.

Considering which properties are likely to affect slurry filterability, the liquid phase properties and particle properties have the most marked effect. For example, Wakeman investigated the influence of particle properties on filtration.¹⁵ From Darcy's theory of filtration at constant pressure, the volumetric flow rate (dV/dt), the filtrate is related to the resistance of the cake and the resistance of the medium, as shown in the Equation 93:

$$\frac{dV}{dt} = \frac{A^2 \Delta P}{\mu (\alpha_{av} cV + AR_m)} \quad (93)$$

Where ΔP ($\text{kg m}^{-1} \text{s}^{-2}$) is the pressure drop along the filter axis, A (m^2) is the filter area, μ ($\text{kg m}^{-1} \text{s}^{-1}$) is the filtrate viscosity, α_{av} (m kg^{-1}) the specific cake resistance is related to the cake filterability, R_m (m^{-1}) is the filter medium resistance and c (kg m^{-3}) is the dry cake mass per unit volume of filtrate. From Carman-Kozeny equation cake resistance is correlated with cake porosity and the square of the particle size (Equation 94):

$$\alpha_{av} = \frac{180}{\rho_s x_{av}^2} \frac{1 - \varepsilon}{\varepsilon^3} \quad (94)$$

Therefore, reducing particle size¹⁶ and/or widening particle size distribution increases the resistance of the cake, reducing filterability of the system and increasing the probability of trapping higher quantities of mother liquor between particles. As reported by Wakeman¹⁴ and later by Beckmann⁴, particle shape affects filtration rate, cake porosity and cake resistance. Beckman reports as the particle shape becomes more elongated; from

rectangular plates, to needles to filaments the specific cake resistance increases from $5 \cdot 10^{10} \text{ m}^{-2}$, $8 \cdot 10^{11} \text{ m}^{-2}$ to $2 \cdot 10^{14} \text{ m}^{-2}$.

Filterability^h of slurries is also affected significantly by the physical properties of liquid phase. A low viscosity mother liquor encounters less resistance when passing through cake pores than a more viscous mother liquor. This influences both filterability and filtration time. Mass transfer for a viscous liquid is reduced due to its difficulty in overcoming capillary forces in order to penetrate the smallest capillaries in the cake. This can be seen in the Hagen-Poiseuille equation¹⁷ (Equation 95) that is used to describe the fluid flow within capillaries:

$$dV = \frac{r^4 \Delta P \pi}{8 \mu h} dt \quad (95)$$

where dV (m^3) is the infinitesimal volume, r (m) is the capillary radius, μ ($\text{kg m}^{-1} \text{ s}^{-1}$) is the liquid phase viscosity, h (m) is defined as the liquid rise inside a capillary and ΔP ($\text{kg m}^{-1} \text{ s}^{-2}$) is the pressure drop inside the porous bed.^{15,18}

^hThe term filterability, expresses the sum of the slurry and process properties that allow the slurry filtration or that impede it. The first author to outline the concept of filterability was Ruth (1933).³⁰ As reported by Yukseler et al. (2007)³¹ filterability can be evaluated by the filtrate flow rate (or as it called sludge filtration capillary suction time) and by the specific cake resistance. For example, Spark (2012)³² suggested a series of slurry and process parameters that may affect the performance of a filtration process, such as slurry density, evaluated as the solid content, temperature that reduce liquid viscosity or the use of additive, that can modify pH or causes particles to agglomerate. The evolution of media resistance due to filter blockage influences the specific cake resistance.³² Using the same material presenting the same PSD value and the same experimental conditions, but changing the pore size of the filter media, a change in filtration flow rate and maximum flux (dt^2/dV^2 vs dt/dV) was observed. After an initial increment of the flux, a steeper slope is observed indicating the blockage of the filter resulting in a higher resistance to filter. From this finding, a revised filtration relation was produced where a new parameter, called cake filtration constant show the resistance component that is independent to the filter medium (initial stage of filtration).

API particle size and mother liquor properties also affect the cake washing process. Different approaches are used across the pharmaceutical industry. Some use the same solvent or solvent mixture attained at the end of the crystallization step, others select wash solvents with lower viscosity compare with the crystallization solvent, which along with dissolved API and impurities composes the mother liquor.¹⁹ In general, less viscous wash liquors tend to be more effective in entering small capillaries and favour effective solvent displacement and diffusion washing.

Miscibility of crystallization and wash solvent is another critical parameter to consider when seeking to improve washing efficiency. Various researches have undertaken work to evaluate flow of immiscible fluids in porous media.²⁰⁻²³

At the start of the washing process, wash solvent enters the largest pores in the cake and displaces the filtrate from the connected network of large pores and channels, once this has occurred filtrate in adjacent network of fine pores held up between the product crystals may diffuse into the wash liquid, thus solvent and solute transport occurs due to axial dispersion.

During displacement washing there is no capillary equilibrium in the system, but the pressure difference between the two sides of a meniscus at any microscopic point in the system has been assumed to be equal to the capillary pressure as predicted by Laplace's equation for the continuum existing at that point. During this process pressure variation along a sequence of capillaries may be observed.²⁴ During this second washing phase, a combination of diffusion and dispersion processes occur.²⁵ To achieve a perfect

displacement wash, the wash solvent has to penetrate the entire cake pore network without mixing with the original mother liquor and thus plug flow must occur. In this idealised displacement washing, the washing process is completed when a wash solvent volume corresponding to the cake void volume is flushed through the cake.²⁶ Ideal displacement in a real situation is never reached because of the wide range of dimensions of interparticulate pores within the filter cake. In fact a combination of displacement and diffusion is required to enhance cake purity, so a combination of miscible crystallization and wash solvent is required to form a uniform front of washing phase, as Burisch and Peuker report.²⁶ Solvent miscibility, as described by Burisch and Peuker leads to variations in the wettability of the liquid phase on the product crystals as the solvents mix during penetration of the filter cake; a knowledge of liquid surface tension and system wettability is needed to understand the mechanism of washing.²⁷⁻²⁹ In general, it appears that when the wettability of crystallization and wash solvent with respect to the particles (which form the porous bed) is different, the wetting phase covers the capillary surface, while the non-wetting phase occupy the central portion of the capillary. This effect is observed in big capillaries, while in small capillaries only the wetting liquid occupies the space between particles. This effect is emphasized in the presence of liquids with different viscosities.¹⁷ The results obtained in this situation is that a huge amount of non-wetting solvent (wash solvent) is required to wash out the wetting solvent (crystallization solvent). In case of miscible solvents, the wash solvent diffuses into the crystallization solvent and gradually dilutes the crystallization solvent favouring the removal of residual mother liquor even in small capillaries.

API particle solubility is another important property to consider during washing. Making a solvent switch between the crystallization solvent and wash solvent is a frequently used strategy in pharmaceutical industry. For example switching to a more volatile solvent in which the API has low solubility aids drying. This procedure needs to be carefully designed to minimise the formation of particle aggregates.³³ The strength and friability of such granules (or aggregates) significantly vary depending on the choice of solvent and the solubility of the solute in the solvent. In general, the more soluble the API in the final solvent, the greater the extent of granule formation and the harder the final granules. As a first approximation, the more polar the wash solvent the greater the probability of robust granules (this is because most APIs contain multiple polar functions). When granules are formed during isolation further processing to disrupt the granules and attain the desired size distribution is usually necessary, typically this is accomplished by introducing a milling step.¹⁴ Wash solvent selection can also lead to dissolution of small particles and consequently narrowing of PSD and/or reducing isolation yield. This may occur either because the API has appreciable solubility in the wash solvent or in mixtures of the wash solvent and the crystallization solvent. Such phenomenon of a maximum solubility being reached in mixtures of solvents is relatively common for example.³⁴⁻³⁵ In case of slurry containing API related impurities, the wash solvent has to show higher impurities dissolution respect to the API. Anyway, the solubility has to be non null to allow the removal of those impurities that are adsorbed on the crystal surface, as reported in chapter 5.

Drying performance and the impact of drying on product attributes is influenced by both particle and process properties including; particle size distribution and crystal shape, the flow rate of the drying gas (nitrogen) through the cake, the residual solvent content and composition, the heat applied and the design and operation of the drying device.^{10-14, 36}

Numerous papers have reported and examined possible causes of agglomeration during drying.^{33, 36, 37} Common hypotheses suggest that if the API solubility in the wash solvent is high and sufficient solvent is present inter-particle bridges of polycrystalline material are deposited due to the evaporation of solvent saturated with dissolved API depositing product at the points of contact between particles. One approach to reduce agglomeration is therefore to tailor the wash solvent composition to minimize concentration of the solute during the drying operation. Papageorgiou *et al.*³⁸ investigated the propensity of particles to undergo agglomeration analysing the effect of solvent selection and the amount of residual solvent present.³⁹ An appropriate solvent selection can have a larger impact on particle clustering than particle size. Birch and Marziano (2013)³⁵, Zhang and Lamberto (2013)⁴⁰ and Tamrakar *et al.* (2016)¹⁴ have all studied the effect of solvent choice on drying, analysing the role of solvent polarity in the formation of strong granules. Generally, the higher the solubility of the product in the wash solvent, the greater the chance of solid bridge formation. In addition to solubility, another reason for the increased formation of inter-particle bridges with polar solvents is the increased viscosity of the thin liquid layer surrounding the particles.¹⁴ Lim *et al.* (2016)³⁹ and Zhang and Lamberto (2013)⁴⁰ investigated the effect of surface tension on agglomeration using different solvent

mixtures highlighting that surface tension of the saturated solution can be a good indicator of the cohesive force experienced in the wet cake.

Wakeman¹⁵, reports that particle size and shape play a noticeable role in deliquoring performance. Increasing particle size shortens deliquoring time when blowing nitrogen through the cake due to increased gas flow rate through the cake. Solvent removal during constant-rate period of drying is controlled in part by the accessible particle surface area, while internal particle morphology (e.g. for agglomerated material) limits drying kinetics during the falling-rate period.^{9, 41-44} Moreover, PSD also affects heat transfer: as a composite particle (agglomerate) dries, the outer layers insulate the core shielding it from further heat propagation. It also forms a diffusion barrier. This is seen in case of large porous particles, removing all the solvent from the core requires extra drying time. Thus, in the case of material containing agglomerates, the larger ones extend the drying time required to meet a target residual solvent content. Dryer geometry and impeller design and agitation strategy can significantly change the mixing patterns and mixing intensity and so affect the ultimate product size distribution. Agitators and orbiting elements serve to induce attrition and increase particle collisions resulting in attrition and breakage changing both particle size and shape.¹² The same agitation can also be responsible of lump formation. Typically, agglomeration occurs in agitated dryers when the material with a relatively high level of residual solvent is very intensively agitated.⁴⁵

Other parameters affecting drying are the drying temperature, pressure, agitation speed, solid loading, length of blow-down period and height of solid bed.^{10-14, 46, 47}

Although the fundamental mechanism of agglomeration is fairly well understood, there are only general guidelines available on addressing this issue during drying. Typical industrial practice includes avoidance of agitation in the initial stages of drying. An alternative practiced in other industry sectors is to use surfactants as agglomeration inhibitors. However, such additives may not be acceptable in pharmaceutical manufacturing.^{10, 48} The addition of an extra functional component is regarded “adulterating” the API in primary processing, and the resulting material is considered as intermediate drug product. This would require the modified material to comply with the regulatory controls associated with drug product manufacture.

The goal of this paper is to provide useful guidance on how to minimise agglomeration during API isolation by developing optimal filtration and washing strategies and by analysing different drying strategies to evaluate the impact of key factors that affect the properties of final dried product. The API selected for this investigation is paracetamol (acetaminophen), used as a widely studied model compound with an extensive range of background data facilitates interpretation of the experimental results.⁴⁹⁻⁵³ This has allowed the project to focus on questions related to equipment capability, chemical and physical interactions of the API and the solvents during filtration, washing and drying. A further objective of the experimental work was to examine the effect of particle size on API filtration and washing with a focus on the selecting suitable wash solvents and washing regimes to minimise particle agglomeration during filtration and washing and to decouple this from granule formation during drying. The extent of granule formation during drying was determined and linked with friability analysis the dried particles.

Solvent combinations were selected to investigate the effect washing by switching between a crystallization solvent and wash solvent. In particular, analysing the consequence of solvent switching on the tendency for particles to agglomerate during drying. Mass loss on drying and residual solvent content were used as parameters to evaluate the roles of crystallization and wash solvent and of wash quantity on agglomeration tendency. Three distinct populations of paracetamol particles were used in the experiments; micronised, typical powder and rather larger granular material. This allowed the effect of particle size to be evaluated over a broad range of processing conditions. A multivariate design of experiments (DoE) was used to allow the combined impact of multiple factors to be evaluated in terms of the tendency to form agglomerates/granules during both filtration and washing and drying, and to understand the impact of cake washing on the robustness of resulting agglomerates. Solubility of the drug substance in the wash solvent, the viscosity of the wash solvent and wettability of the API with crystallization solvent and wash solvent, the mother liquor/solvent hold up in the wet filter cake were selected as some of the system variables.

Different dryer configurations are used in pharmaceutical industry. Dryers are classified by the dominant mechanism of heat transfer, the principle distinction as being conductive or convective. Three different convective static drying combinations were investigated. Static drying took place in a vacuum oven which was used without heat or moving the particles. The other two experiments used flowing gas (nitrogen); at ambient temperature and at 60°C. From Figure 63 the overview of the experimental workflow used for this work is described.

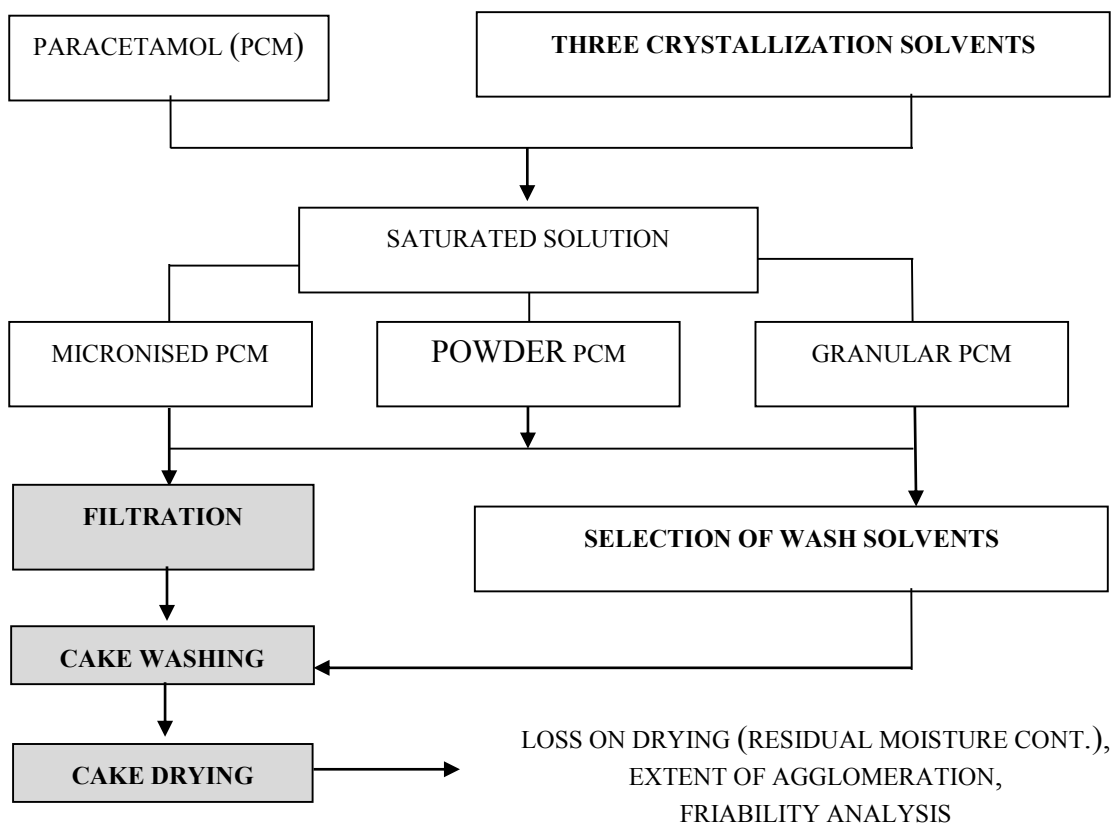


Figure 63 Experimental workflow. Three different paracetamol grades were selected, micronised, powder and granular. Slurries were prepared by creating a saturated solution and then pouring the solid load required to build the cake with the selected paracetamol grade. Filtration was then performed to form the cake for the washing step. The selection of wash strategy for each experiment was set using DoE approach. After the drying process, the final material was analysed to evaluate loss on drying, residual solvent composition and quantity, extent of agglomeration and agglomerate strength using a friability analysis.

An optimisation test was run to calculate a single combination of factors minimizing agglomerate hardness, extent of agglomeration and particle size. The same set of parameters were used to analyse the impact of wash solvent characteristics on drying.

Material attributes such as the particle size distribution of the different grades of paracetamol, the solubility of paracetamol in the different wash solvents were examined, and mother liquor viscosity were determined experimentally.

The final dried product was characterised in order to quantify the effect of filtration, washing and drying methodology on the product. Specifically, the loss of mass on drying and the composition and quantity of residual solvents were measured as well as the extent of agglomeration and the friability of any isolated agglomerated were measured.

6.3 Materials

Micronised, conventionally crystallized (powder) and special granular as pharmaceutical grade paracetamol ($C_8H_9NO_2$) were supplied by Mallinckrodt Inc., Raleigh, N.C., USA. Micronised batch number 042213E407, powder batch number 637514D001 and granular batch number 161713J561 were used throughout the work reported here. The basis for selecting these three grades of material is that; the micronised material is challenging to filter, wash and dry because of its small particle size; it shows wide size distribution and damaged particle surfaces; the conventional powder represents typical API and the special granular material poses a challenge because of its large particle size. In pharmaceutical industry, these three grades are generally used. The polymorphic form, x_{10} , x_{50} and x_{90} , the Sauter mean diameter (SMD), the volume mean diameter (VMD) and true density were measured experimentally and are reported in chapter 4 (Table 18).

The crystallization solvents selected for this study were ethanol (purity $\geq 99.8\%$ (GC), from Sigma Aldrich), isopropanol (IPA) (purity $\geq 99.5\%$ (GC), from Sigma Aldrich) and isoamyl alcohol, commonly called isoamylalcohol (purity $\geq 99.5\%$ (GC), from Sigma Aldrich). All three solvents are appropriate crystallization solvents for paracetamol.⁴⁹ The wash solvents selected were n-heptane (purity 99%, from Alfa Aesar), isopropyl acetate (purity 99+ %, from Alfa Aesar), toluene (purity 99%, from Alfa Aesar), anisole (purity

99%, from Alfa Aesar), n-dodecane (purity 99%, from Alfa Aesar), tert-butyl-methyl ether (TBME) (purity 98%, from Sigma Aldrich), cyclohexane (purity 99+ %, from Alfa Aesar), 4-methylpentan-2-one (purity $\geq 99.5\%$ (GC), from Sigma Aldrich), propylene carbonate (purity 99%, from Alfa Aesar) and acetonitrile (ACN) (purity 99.5%+, from Alfa Aesar). Each of the wash solvents listed above were selected for their different chemical and physical properties (surface tension, density, viscosity and paracetamol solubility) and their miscibility with the chosen crystallization solvents.

6.4 Method

In order to investigate the propensity of different grades of paracetamol to agglomerate under different process conditions, the experimental procedure was divided into a series of consecutive steps: filtration to recover suspended solid material, filter cake washing and product drying, as seen in Figure 63.

A multivariate design of experiment (DoE) approach was used to investigate the combined effects of these key parameters on the quality of the final dried material because of the complexity of the interactions between material and process parameters in this multi stage process. The ultimate aim is to use the data to identify an isolation strategy, which is effective and reproducible in reducing particle agglomeration. Thus, parameters spanning through different stages within the isolation process including; solid loading, filtration pressure, number of washes, volume of wash solvent and drying mechanism were examined simultaneously. MOODE Pro V11.0.1 developed by MKS Umetrics⁵⁴ was selected as DoE software to build a statistical model to identify how the selected responses can be correlated with the multi-variate parameters. The range of values explored for each variable were selected to lie within the range of conditions typically employed during

isolation. A linear D-Optimal approach was used to reduce number of experiments from 2048 (full factorial) to 31 experiments with 3 centre points used to determine the reproducibility of the experimental procedure.

The D-Optimal approach is appropriate in this case because the experimental variables investigated comprise of a combination of quantitative and qualitative factors.^{55, 56} A number of potential factors were held constant and were not included in the DoE; those potential variables are intrinsically related for example to the nature of solvent or grade of the paracetamol used. Those properties include the solubility of paracetamol in the solvent investigated, other examples include the, viscosity of the pure solvent, the viscosity of mother liquor, the density of the pure solvent, density of the saturated solution (mother liquor) and tapped and bulk density of the paracetamol samples, surface tension and contact angle of paracetamol with different solvents. Other fixed parameters not included as factors are process parameters: pore size of the filter used for the isolation, (nominal pore size 10 μ m; for settling test 5 μ m, 10 μ m and 20 μ m filter media pore size were used), the temperature of the suspension and wash solvent during filtration and washing was held at 20°C. Finally, cake height was treated as a fixed parameter, because it is strictly related to the solid loading of the slurry; cake compressibility was also excluded from design factors, because cake compressibility index is a parameter strictly defined by the slurry attributes imparted by the other factors. Based on the preliminary characterization of the paracetamol cake obtained during constant pressure filtration experiments, the different slurries all show partially compressible behaviour ($n < 1$).^{9, 15, 16, 57}

<p>Number of washes (abbreviation: Num)</p> <ul style="list-style-type: none"> • 1x, 2x 	<p>(friability test to evaluate ABI index)</p>
<p>Wash solvent (abbreviation: Was)</p> <ul style="list-style-type: none"> • n-heptane • isopropyl acetate <ul style="list-style-type: none"> • toluene • anisole • n-dodecane • TBME • cyclohexane • 4-methylpentan-2-one • propylene carbonate <ul style="list-style-type: none"> • acetonitrile 	<p>Residual solvent content (abbreviation: Res)</p> <p>(vacuum oven to determine wet to dry mass and ¹H-NMR for residual solvent composition)</p>
<p>Drying mechanism (Dry)</p> <ul style="list-style-type: none"> • vacuum • RT, dry nitrogen • 60°C, dry nitrogen 	<p>Particle size distribution (abbreviation : Par)</p> <p>(Particle size analyser, QICPIC)</p>

To evaluate the pre-settling of the cake prior filtration, another DoE was produced. In Table 29, the list of variables and responses is reported. The raw data related to each experiment are reported in chapter 9.

Table 29 Table of factor for pre-settling DoE (second DoE).

Variables	
Factors (abbreviation)	Range and Units
Driving force (Pre)	500-900mbar
Filter pore size (Fil)	5, 10, 20µm
Solid material (PCM)	Micronised and powder
Crystallization solvent (sol)	ethanol, isopropanol and isoamyl alcohol
Methodology (Met)	Settling and reload, filter and reload
Solid load (so2)	10-30% V/V
Responses	
Responses (abbreviation)	Units
Cake resistance step 1 (cak)	1/kg
Medium resistance step 1 (med)	1/m
Cake height step 1 (ca2)	m
Filtration time to dryland step 1 (fi2)	S
Cake resistance step 2 (ca3)	1/kg
Medium resistance step 2 (me2)	1/m
Filtration time to dryland step 2 (fi3)	S
Cake height step 2 (hei)	m

A third DoE used to understand the effect of wash solvent on the dried material was designed (Table 30), based on the optimal values of parameters determined in the first DoE (optimum parameters are reported in Table 42).

The values of several parameters were intentionally modified from the optimal parameters gathered from the first DoE. Micronised paracetamol was chosen as the mechanical properties of agglomerates generated can be more readily studied by sieving than in agglomerates formed from the larger crystalline material. Four cake void volumes were selected as the initial amount of wash solvent to be used and evaluated by ¹H NMR analysis. This quantity of wash solvent was chosen to be enough to remove the mother liquor from the cake. The isolated dry material from each experiment was then analysed by using the same analytical methods as in all DoE.

Table 30 Fixed parameters and variables of the third DoE.

Fixed parameters	
Parameters and Units	Set points
Driving force (mbar)	500
Solid load (% V/V)	30
Material	Micronised
Crystallization solvent	Isopropanol
Filtration and washing endpoint	Dryland
Volume of wash solvent	2 void cake volumes
Number of washing	2
Drying mechanism	Room temperature, flowing nitrogen (dynamic drying)

Variables	
Wash solvent	n-heptane, isopropyl acetate, toluene, anisole, n-dodecane, TBME, cyclohexane, 4-methylpentan-2-one, acetonitrile

6.4.1 Preliminary characterization

The three different paracetamol grades were characterized to determine raw material particle size distribution, x_{10} , x_{50} and x_{90} , SMD, VMD, paracetamol solubility was measured in the solvent used, the contact angle of paracetamol with the different solvents and the density and viscosity of paracetamol saturated solutions (mother liquor in each crystallization solvent).

The particle size distributions of the different grades of paracetamol were determined using Sympatec QICPIC particle size analyser⁵⁸ with VIBRI/L setup at feed pressure of 0.5bar, feed rate of 25% and 0.5mm gap width. The same methodology was used to analyse the sub 1mm particles isolated after drying. The mass of sample used for the PSD characterization was around 1g. The feed rate was initially set to 0.5bar to allow comparison with the input paracetamol. The test was then repeated with a feed pressure of 2 and 4bar to evaluate particle breakage due to shear stress.

The solubility of paracetamol in the different solvents was determined by equilibration. Pre-weighed suspensions of paracetamol in each solvent were prepared and placed in an incubator (Incubator S160D, Stuart, UK) on a multi-position stirrer plate (CamLab, UK) and held isothermally at the selected equilibration temperature of 25°C, and equilibrated

with agitation for 24 hours. At the end of the 24 hours equilibration period 1ml samples were taken, the mass recorded and the samples were then placed in a fume hood for 24 hours for the solvent to evaporate. After 24 hours the sample masses were recorded and the sample vials were placed in a vacuum oven (Gallenamp, UK) for 24 hours at room temperature and (20mbar) prior to determining the final dry residue mass which was used to calculate the solubilities (Table 31 and Table 32).

Table 31 Paracetamol solubility in the three different crystallization solvent used for this work.

Crystallization solvent	Solubility of paracetamol at 25°C (g/g solvent)	Solubility of paracetamol at 20°C (g/g solvent)
Ethanol	0.2056	0.1840
Isopropanol	0.1243	0.1088
isoamyl alcohol	0.5487	0.0469

Table 32 Paracetamol solubility in the different wash solvent used for this work.

Wash solvent	Solubility of paracetamol at 25°C (g/g solvent)
n-heptane	0.0001
Isopropyl acetate	0.0075
Toluene	0.0002
Anisole	0.0005
n-dodecane	0.0007
t-butyl-methyl-ether (TBME)	0.0028
Cyclohexane	0.0005
4-methylpentan-2-one	0.0166

Acetonitrile	0.0294
Propylene carbonate	-

The contact angle of paracetamol with the different solvents was determined using the Washburn capillary rise method in which a liquid phase (with known properties) migrates through the pore network of a packed bed of sample particles due to capillary forces.

Fluid flow through the capillaries is considered as laminar flow and is governed by the Hagen-Poiseuille equation.¹⁷ Measuring the mass increase of the powder sample vs time during the capillary rise process allows the contact angle to be determined (Equation 85 in chapter 4).⁵⁹

The capillary constant K of the reference solvent is then used to determine the contact angle θ of the solvents under investigation. To determine contact angle of paracetamol in ethanol, IPA and isoamyl alcohol, saturated solutions of each solvent were created to avoid paracetamol dissolution during capillary rise measurements, the data are presented in Table 33.

Table 33 Geometric coefficient K and contact angle for the three saturated solutions of crystallization solvent. The contact angles for ethanol and 2 propanol where calculated using the K value determined for isoamyl alcohol solution.

Saturated solution	K value (m⁵)	Contact angle θ (°)
ethanol	7.87×10^{-16}	59.29
isopropanol	5.95×10^{-16}	67.31
isoamyl alcohol	1.54×10^{-15}	Reference

The true density of the three grades of paracetamol were determined using a helium pycnometer AccuPyc 1330 V1.30 and are reported in Table 34, three replicate measurements were made.

Table 34 True density value of micronised, powder and granular paracetamol.

Paracetamol grade	True density (g/ml)	Standard deviation (g/ml)
Micronised	1.1914	0.0067
Powder	1.2417	0.0020
Granular	1.2675	0.0016

The viscosities of the saturated solutions were determined by using a GV500 viscometer (Hydramotion UK). Comparison of the mother liquor viscosity with pure solvent viscosity data shows the importance of measuring the viscosity of the mother liquor, rather than using published viscosity values for pure solvents. The data are compared in Table 35 and viscosity plots are available in chapter 9.

*Table 35 Pure solvent density and viscosity (*Detherm database⁶⁰) and mother liquor viscosity calculated with the GV500 viscometer.*

Solvent	Density (g/ml)	Density saturated solution at 20°C (g/ml)	Viscosity (Ns/m²)	Viscosity mother liquor (Ns/m²)
Ethanol	0.789	0.824	0.0011*	0.0016
Isopropanol	0.786	0.817	0.002*	0.0029
isoamyl alcohol	0.810	0.827	0.0037*	0.0048

6.4.2 Filtration and washing procedure

A modified Biotage VacMaster⁶¹ was used for conducting filtration and washing of the paracetamol suspensions using manual best practice.

The paracetamol suspensions evaluated in this study were prepared by first saturating the solvent with paracetamol at 20°C. The quantity of paracetamol required to saturate the solution was calculated from the solubility data in each of the crystallization solvents. In order to produce paracetamol suspensions with 10, 20 or 30% by volume of undissolved paracetamol respectively 3, 6 or 9g of paracetamol was added to the saturated solution. By preparing the particle suspensions in this way and filtering, washing and drying them immediately the particle size distributions of the different grades of paracetamol were preserved into the filtration experiments.

To determine the effect of pre-settling cake on top of the filter medium prior to filtration, a set of experiments using 10-30% V/V of solid load in slurry was prepared using; micronised, powder or special granular paracetamol and using; ethanol, isopropanol or isoamyl alcohol as crystallization solvent and three pressure driving forces (300, 500 and 900mbar) were conducted to evaluate the effect of sedimentation on final cake and media resistance. Those experiments were performed using three different Biotage filter tube media grades; 5, 10 and 20µm. Two sets of experiments were conducted: filter and reload, and, settle and reload. The filter and reload experiments were performed using 30ml of slurry that were poured into the filter tube with care to avoid slurry wetting the tube walls with slurry. The filtration was then halted at dryland and the filtrate removed from the

cake was re-dispensed onto the top of the cake without disturbing the cake surface. A second filtration was then run. The settle and reload experiments were performed by dispensing the slurry into the filter tube with care to avoid leaving slurry on the walls, the suspension was then allowed to settle pre-forming a cake, the filtration was performed and the collected filtrate was re-dispensed onto the top of the cake without disturbing the surface and re-filtered again. The collection of filtration flow rate was conducted for both the steps to allow comparison of the cake and medium resistance in the two steps for filtration through cake comprised from the same source material but formed in different ways.

6.4.3 Drying methodologies

Three different static drying approaches were evaluated in this investigation: The first drying method was vacuum driven using a vacuum oven (Gallenamp) at room temperature and 20mbar. The static drying process allowed moisture evaporation by thermodynamic equilibrium of vapour pressure in the closed system of the vacuum oven. Two static drying experiments with flowing gas were also used; room temperature flowing nitrogen and 60°C flowing hot nitrogen. The drying apparatus took nitrogen from the 5bar fumehood gas distribution system, the gas pressure was lowered to 2bar and controlled using a pressure reducer. The nitrogen flow rate was adjusted using a rotameter capable of adjusting the nitrogen flow rate from 0.1L/min up to a maximum of 1.0L/min. To allow the drying rate of the more volatile solvents, to be determined, the nitrogen flow rate of 0.3L/min was selected. Nitrogen flow rate was fixed at 0.3 L/min for both the drying setups. In the case of the experiments conducted at 60°C, nitrogen flowed through a coil

of copper pipe to allow thermal equilibration as the entire experiment was held in an incubator.

The filter tube containing the wet cake was connected to the nitrogen supply by a tube fixed to the open end of the filter tube by a rubber stopper such that the nitrogen flowed through the cake in the same direction as the filtrate and wash can pass through the filter medium. A schematic figure of the dynamic drying apparatus is shown in Figure 64. For drying with heated nitrogen the incubator temperature was controlled by thermocouples placed in different positions in the incubator to allow system temperature to be monitored and controlled. One of the thermocouples penetrated the stopper in the filter tube to allow the temperature of the nitrogen to be measured just above the surface of the wet cake to ensure the gas was heated to the required temperature (Figure 65).

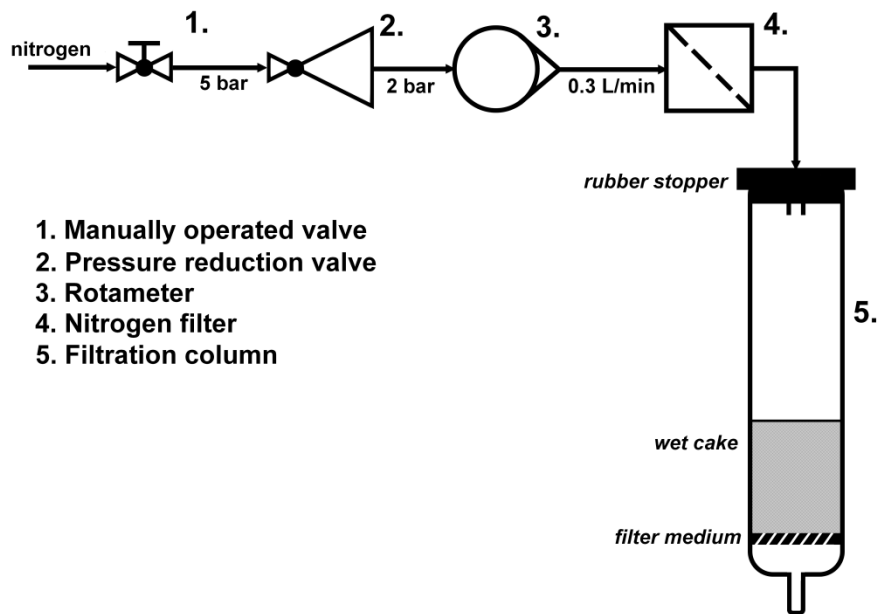


Figure 64 Scheme of static drying with flowing nitrogen apparatus at room temperature.

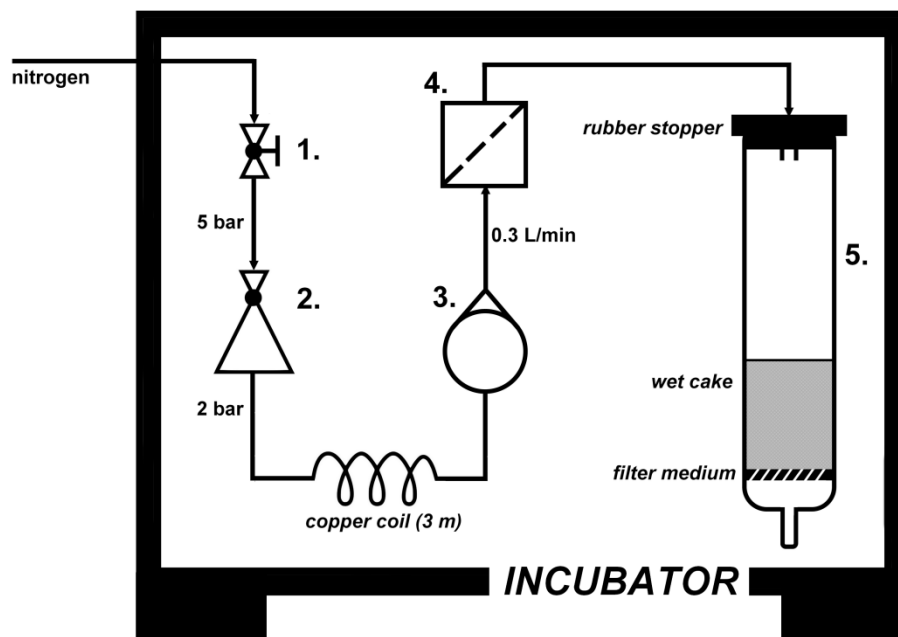


Figure 65 Scheme of flowing N₂ drying apparatus at 60°C temperature.

Loss on drying was monitored periodically by closing valve 1, removing the stopper from the filter tube and determining the wet mass of the filter cake.

6.4.4 Offline characterization

Cakes were dried to stable mass in vacuum oven (Gallenkamp) to determine moisture content (LOD %).

To determine composition of moisture content, % of residual crystallization and wash solvent NMR analytical technique was used (method described in chapter 4).

Extent of agglomeration and ABI index methods are reported in the method chapter, mechanical characterization analysis part.

6.5 Results and discussions

6.5.1 Parameters affecting filtration

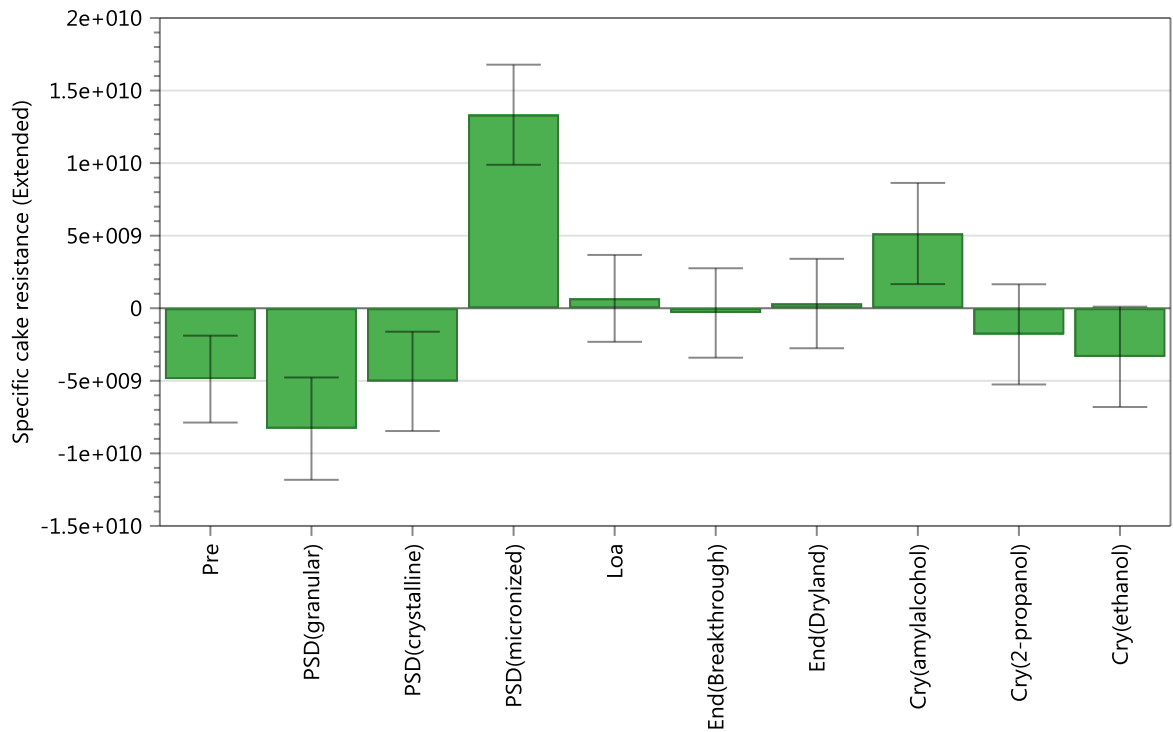


Figure 66 DoE variables affecting cake resistance during filtration.

Figure 66 shows the overview plot of factors affecting the cake resistance during filtration. PSD, the nature of the crystallization solvent and the pressure driving force (Pre) mainly affect the resistance to the flow of the liquid phase passing through the cake.

Analysing the two extremes of the paracetamol PSD, micronised and special granular, it can be inferred that using small particles with broad particle size distribution results in increased filtration time, reduction of filtrate flow rate and increase of cake resistance. As reported by Wakeman^{15, 63}, during the course of filtration, finer particles migrate through the filter cake toward the filter medium, depositing in close proximity to the filter medium, causing an increase of cake tortuosity in the proximity of the filter medium. This migration of fine particles impacts the cake resistance resulting in a gradient of alpha along the axis of the cake^{64, 65}, slowing washing and deliquoring step and potentially leading to increased

solvent retention in the deliquored cake. Conversely, the special granular paracetamol has a large particle size and contains large interparticles pores, it has low surface area and narrow PSD which both result in negligible cake resistance and results in the highest observable filtrate flow rate.

The identity and characteristics of the crystallization solvent are the second main contributions affecting filtration performance. Ethanol and isopropanol show similar properties in terms of solubility, density and viscosity, while isoamyl alcohol has a higher viscosity. As seen from Figure 66, Figure 67, Figure 68 and, Figure 69 ethanol and isopropanol exhibit similar cake resistances, while an increase of cake resistance is obtained using isoamyl alcohol³⁶: hence the data confirm that faster flow rate and lower cake resistance are observed for less viscous solvents.

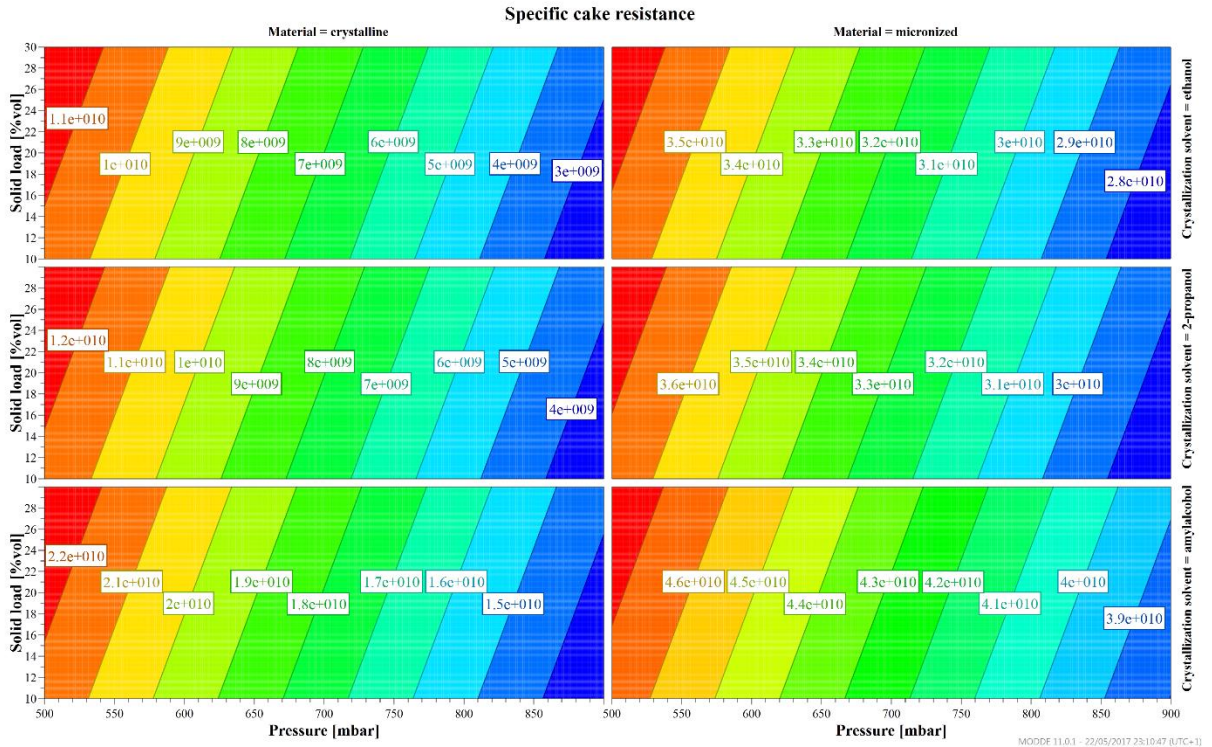


Figure 67 4D contour plot of the effect of solid load and driving force on cake resistance for slurry prepared with ethanol as crystallization solvent.

Analysing Figure 67, the effect of cake height (solid load) and driving force (pressure difference) can be observed: a high solid loading in the feed material yields high cake resistance. Applying a high driving force (high pressure difference) leads to increased pressure drop through the solid bed and therefore reduce resistance due to paracetamol even if there is cake compression¹⁵ (micronised paracetamol compressibility index calculated to be 0.2327 compared with 0.3976 for typical crystalline paracetamol).

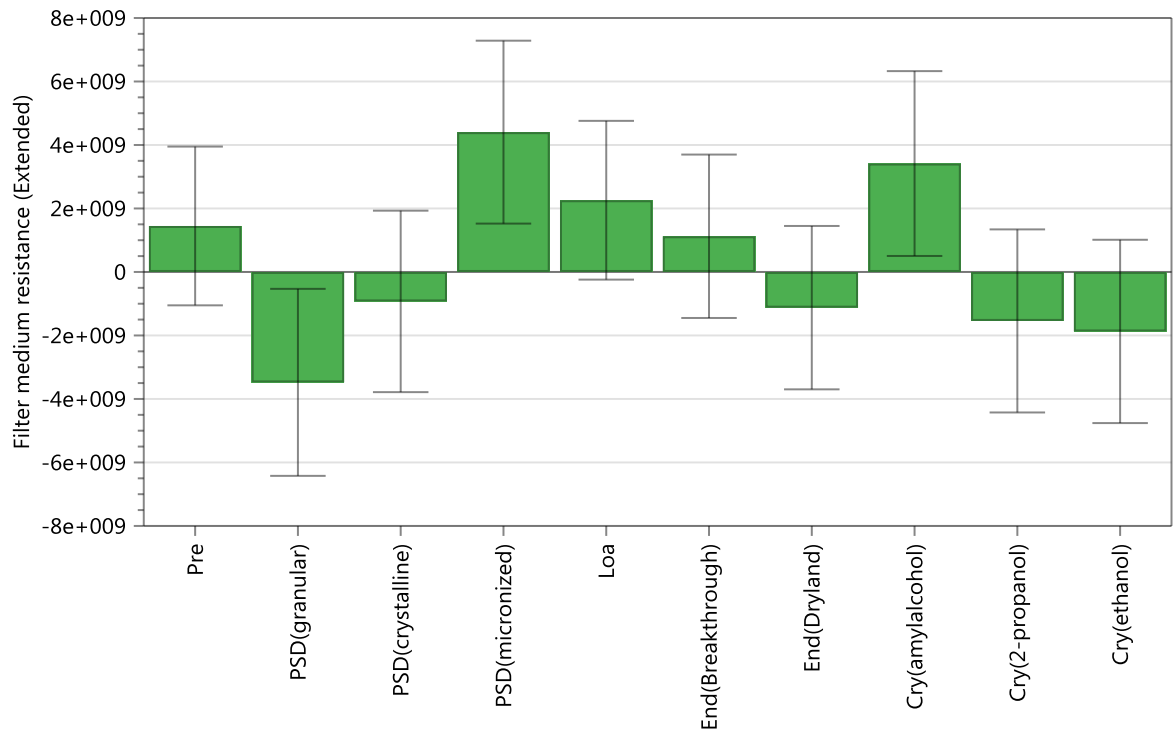


Figure 68 DoE variables affecting media resistance during filtration.

Figure 68 shows the relative importance of the filtration parameters which affect filter medium resistance: a large variance in the collected data has been observed, this may probably be attributed to the solid particles sedimentation behaviour where the settled particles contribute extra resistance to filtrate flow which is typically represented as increased.^{9, 66, 67} To verify this hypothesis, a DoE was run to test the effect of pre-settling to form a cake prior filtration and to compare this with the effect of forming a filter cake conventionally and reload the filtrate on top of the cake to re-filter it again. Figure 69 shows the difference between the Darcy plots arising from these different approaches. The filtration time for the primary filtration is shorter than the secondary filtration due to the increase of resistance to the filtrate flow. During the first filtration, cake resistance increase during cake formation, reaching its maximum value when filter cake was

completely formed. This contrasts with filtering the pre-formed cake arising from settling; the cake resistance is constant throughout the filtration process. The filtration rate for both secondary filtrations is relatively constant throughout the secondary filtration process which is consistent with filtration taking place on an already formed, in contrast with the primary filtration rate which decreases with increasing time. The effect of filtering, reloading the filtrate and then re-filtering the filtrate on medium resistance is shown in Table 36. Cake resistance from step 1 and 2 slightly increase, while medium resistance from step 1 to step 2 increases by an order of magnitude. This effect is caused by the already formed cake acting as a “second filter medium” increasing resistance to the flow of the filtrate.

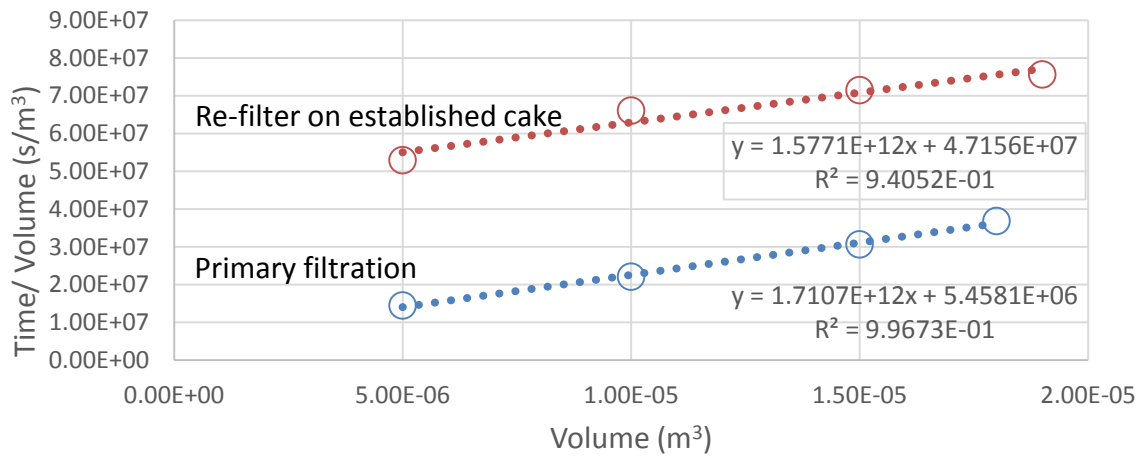


Figure 69 Filtration and reload experiment performed using a slurry made with 30% V/V of micronised paracetamol in isopropanol and filtered at 900mbar driving force.

Table 36 Cake resistance and medium resistance for experiments where filtration followed by reloading the filtrate and filtering using a slurry made with 30% V/V of micronized paracetamol in isopropanol and filtered at 900mbar driving force (the data correspond to the Darcy plot shown in Figure 9).

Stage of the experiment	Cake resistance (1/kg)	Medium resistance (1/m)
Filter	1.0154E+10	1.0154E+10
Reload and filter	1.1250E+10	1.1250E+11

Comparison of the 4D contour plots of cake resistance in the first and second steps of settling and reload and filter and reload experiments, with ethanol as crystallization solvent, are reported below in Figure 70-Figure 75. No major difference in cake resistance was seen between steps 1 and 2 of the settling, reload, filter, and reload experiments. The effect of filter pore size is clearly visible: the smaller the pore size of the filter medium, the more pronounced the variation of cake resistance from step 1 to 2. A similar effect is seen using both the micronised and powder grades of paracetamol with the overall change in cake resistance from 5×10^9 to 1×10^{10} .

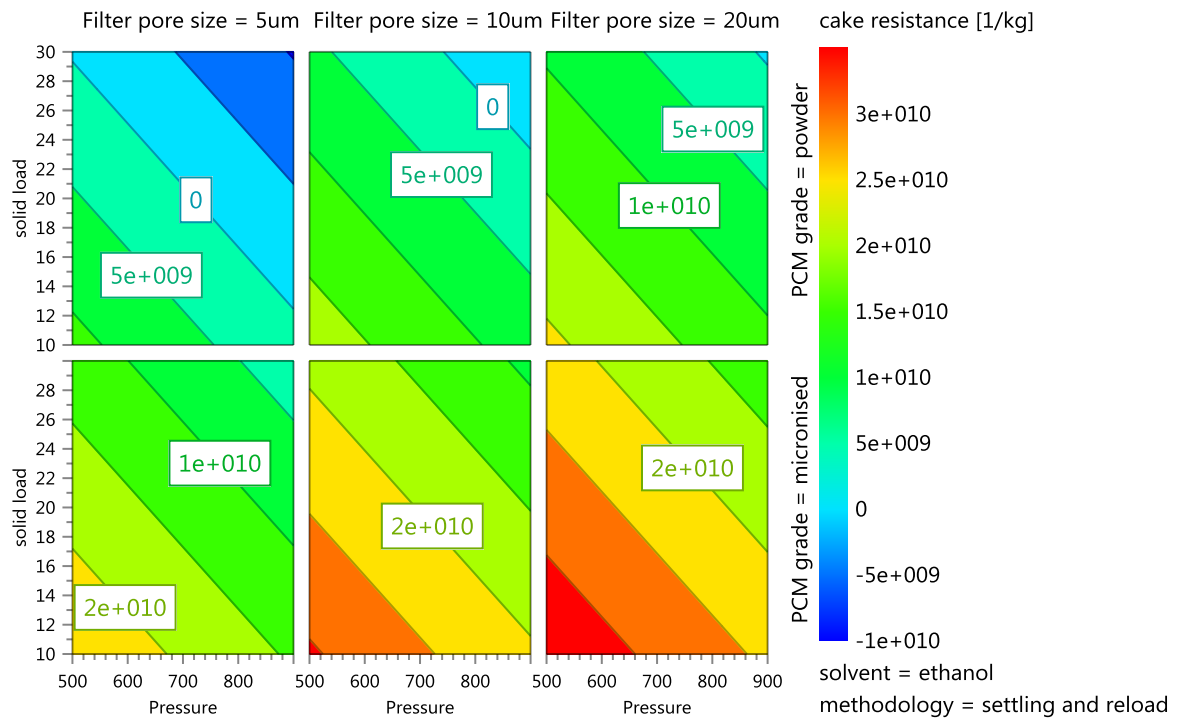


Figure 70 4D Response contour plot of cake resistance in step 1 (settled and then filtered) in the DoE addressing solids loading, driving force, filter medium pore size and paracetamol particle size range (powder and micronised) where the crystallization solvent was ethanol.

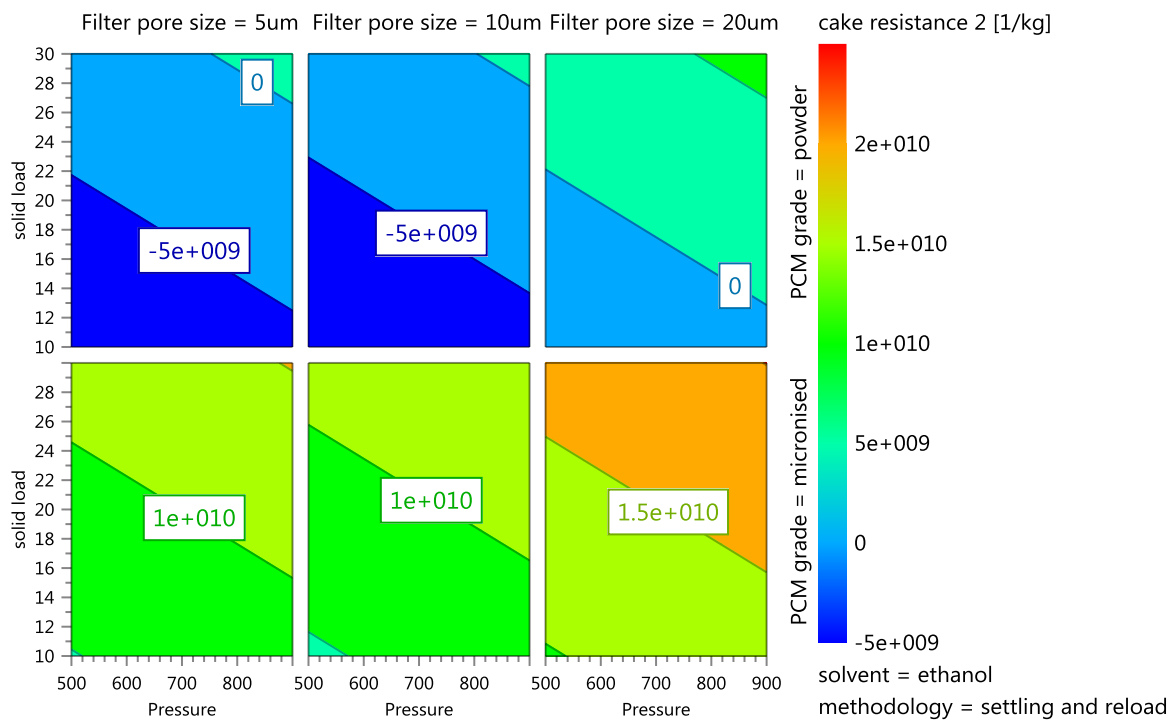


Figure 71 4D response contour plot of cake resistance in step 2 (reload and filtered) in the DoE range of solid load and driving force, crystallization solvent ethanol, comparison of different filter medium pore size and powder and micronised paracetamol.

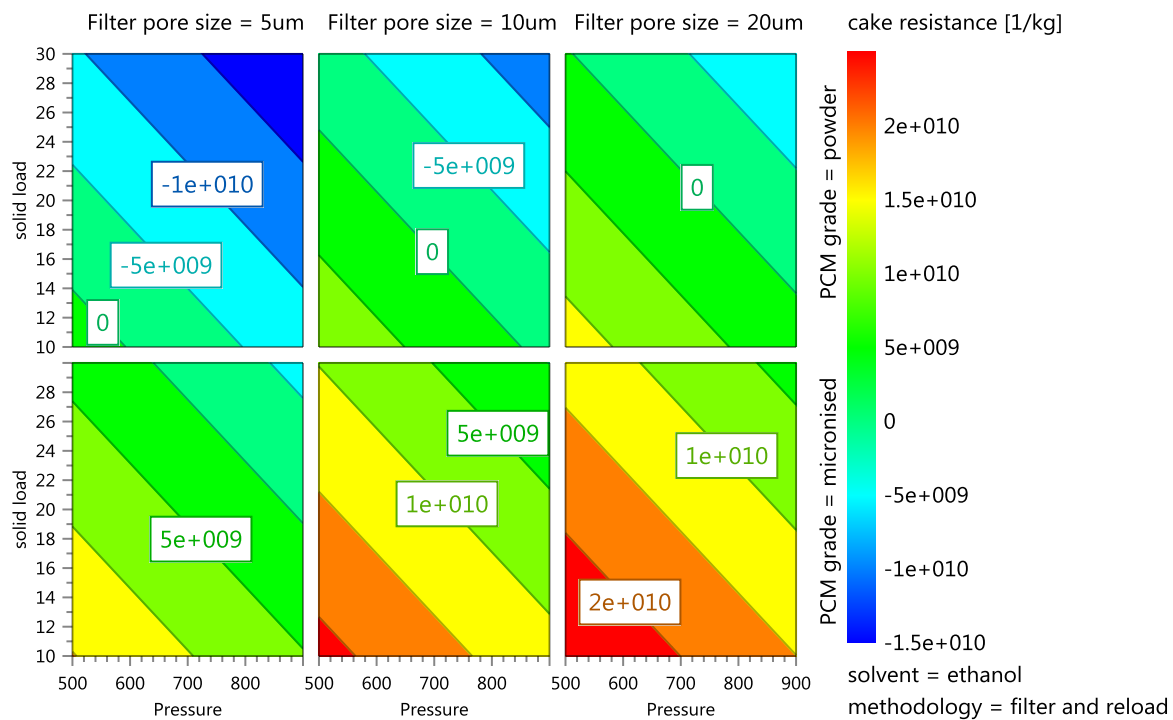


Figure 72 4D response contour plot of cake resistance in step 1 (filtered) in the DoE range of solid load and driving force, crystallization solvent ethanol, comparison of different filter medium pore size and powder and micronised paracetamol.

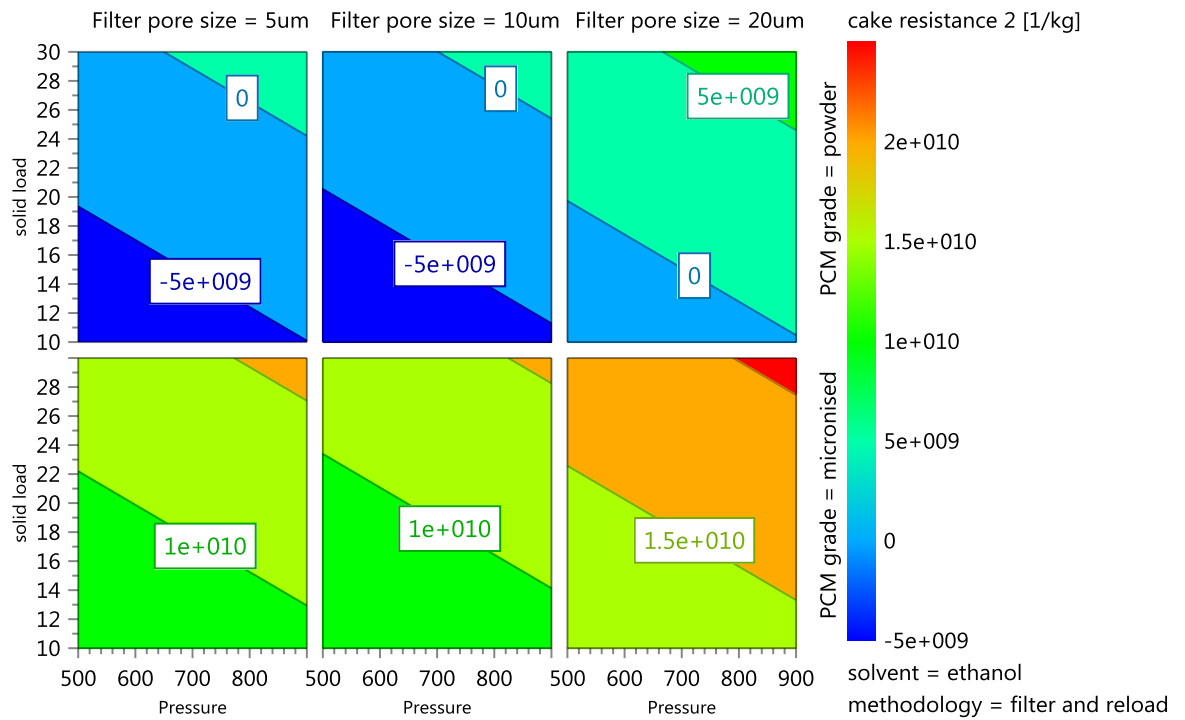


Figure 73 4D response contour plot of cake resistance in step 2 (reload and filtered) in the DoE range of solid load and driving force, crystallization solvent ethanol, comparison of different filter medium pore size and powder and micronised paracetamol.

The effect of viscosity of the crystallization solvent can be seen comparing Figure 70- Figure 73 with Figure 74 and Figure 75. Higher the solvent viscosity higher the cake resistance.

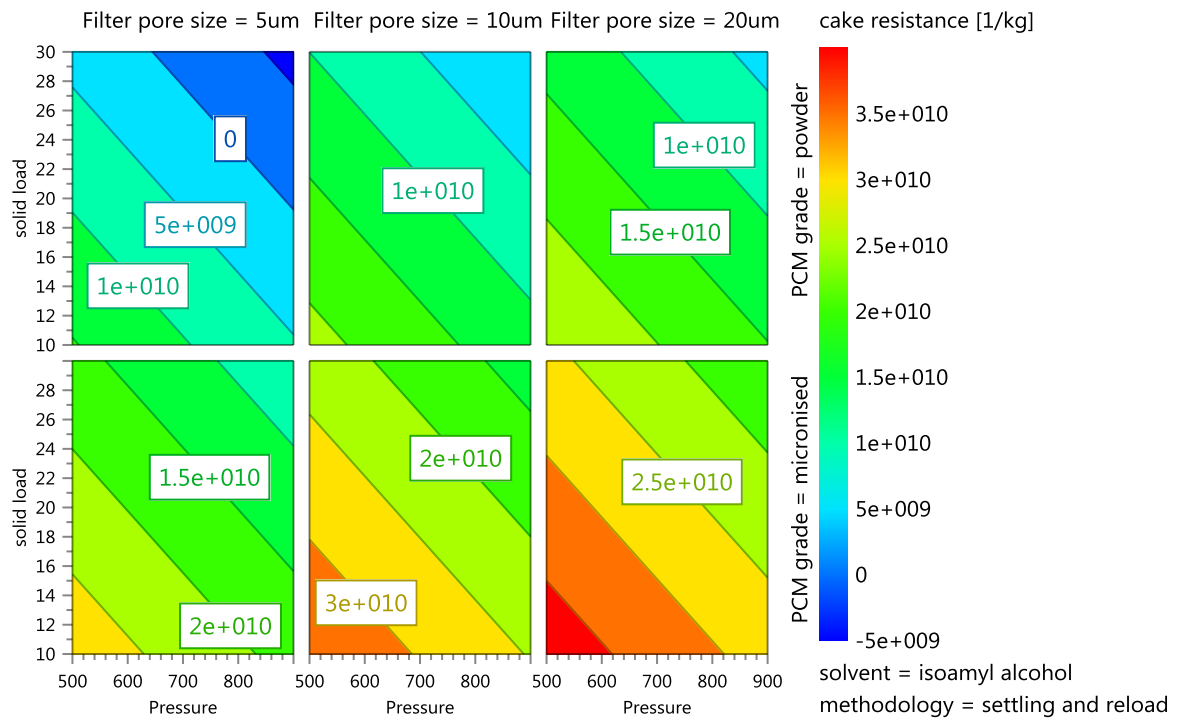


Figure 74 4D response contour plot of cake resistance in step 1 (settled and then filtered) in the DoE range of solid load and driving force, crystallization solvent isoamyl alcohol, comparison of different filter medium pore size and powder and micronised paracetamol.

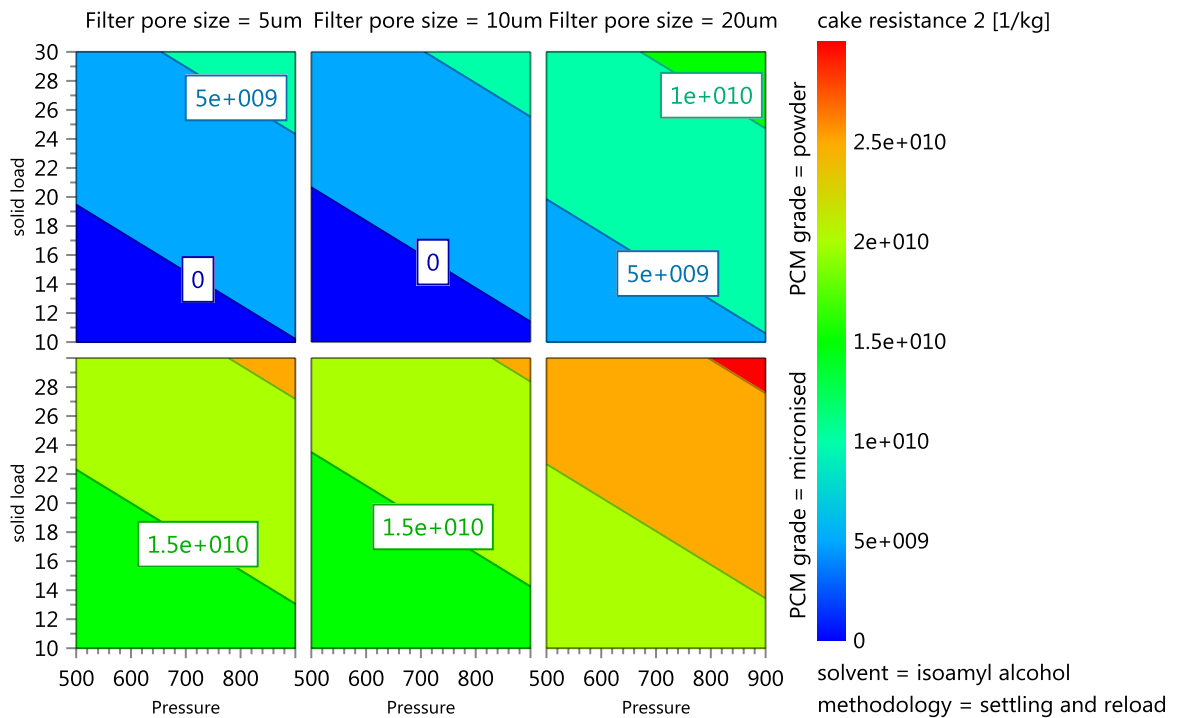


Figure 75 4D response contour plot of cake resistance in step 1 (reload and filtered) in the DoE range of solid load and driving force, crystallization solvent isoamyl alcohol, comparison of different filter medium pore size and powder and micronised paracetamol.

Two extremes of filtration behavior were encountered in this DoE:

- Very rapid filtration was challenging to record manually; this was encountered when filtering granular paracetamol slurry with a low solids content and employing a high driving force. In this case rapid filtration is likely to be accompanied by rather inefficient cake washing due to the very short contact time between the wash solvent and the filter cake; however the low particle surface area associated with the large particles compensates for this due to the lower mother liquor hold up in the filter cake.
- Very slow filtration arising from the combination of high solids loading, low driving force using micronised paracetamol suspended in isoamyl alcohol as

mother liquor. In this case, the filtration time increased from a few of minutes (a typical time for a laboratory filtration) to over an hour. The prolonged filtration involved extended contact between the mother liquors and the crystals. This extended contact time may enable changes to occur to the particle size distribution for example by the formation of interparticle solid bridges, i.e. agglomerate formation.

6.5.2 Parameters affecting washing

The DoE was not focused particularly on washing and as consequences, there were few responses, which correlate to the washing step, which makes evaluation of possible parameters affecting washing difficult. Nevertheless, a few observations can be made:

- In few cases where a second washing step was included, the duration of the second washing step was noticeably shorter than for the first wash step. This effect may be caused by the reduction of solvent viscosity between the mother liquor to the pure wash solvent (see Table 35). During the first wash, a major portion of mother liquor is displaced from the cake, predominantly the mother liquor that was occupying the network of large pores in the filter cake. During the second wash further residual mother liquor is removed from the cake⁶⁸⁻⁷⁰, however when the second wash is removed from the cake it is principally composed of wash solvent in which some paracetamol is likely to have dissolved depending on the identity of the wash solvent and the contact time.
- During filter cake washing with propylene carbonate an unusual process of filter cake disturbance was observed. Propylene carbonate density is higher than the

mother liquor (1.21 g/mL), causing the floating on mother liquor on top of the wash solvent with consequence disturbance of the cake for the liquids movements. This buoyancy driven movement of mother liquors was observed to disturb the upper layers of the cake.

- In all cases, cake washing was immediately followed by cake deliquoring which was allowed to continue for around 10 seconds after the bubble point was detected and a break in the steady flow of filtrate was observed.

Other effects of the wash solvents on the dried cake properties are discussed in the model optimization section.

6.5.3 Parameters affecting drying

Static drying was conducted in vacuum oven at ambient temperature at a reduced pressure of 20mbar or it was done using nitrogen flow at ambient temperature and 60°C, to study the effect of temperature on the dried material. All the three drying methodologies were conducted with cakes after few seconds of deliquoring using the Biotage unit. After drying, the cake was gently removed from the tube to avoid breakage of agglomerates or lumps to determine the effect of the different variables considered in the DoE on the final dried cake quality.

From Figure 76, the parameters which have the larger effect on the residual solvent content after drying, are the grade of the particles forming the cake (the lower the particle size the higher the quantity of solvent retained), the identity of the wash solvent, the number of washes (and hence the quantity of crystallization solvent remaining in the cake prior to

drying), the stopping point of the filtration (dry land or break through), the solid quantity (cake thickness) and the drying methodology.

The boiling point, enthalpy of vaporization and viscosity of solvents are all important parameters affecting the residual solvent content after drying. The boiling point and enthalpy of vaporization of the wash solvent affect the ease of solvent removal during drying, while higher viscosity may be associated with an increase in the extent of solvent retention in the cake. From Figure 76, it is apparent that solvents with high boiling points require longer drying times to be removed, such as n-dodecane, anisole and propylene carbonate. Anisole, n-dodecane extended the drying times from hours to days. Propylene carbonate showed an extremely slow evaporation rate, drying being complete after almost 75 days.

Analyzing the effect of crystallization solvent; isoamyl alcohol resulted in an increased in the residual moisture content of the deliquored cake due to its high viscosity. Literature values of; boiling point, enthalpy of vaporization, viscosity, density and surface tension of the different solvents used in this investigation are reported in Table 37.

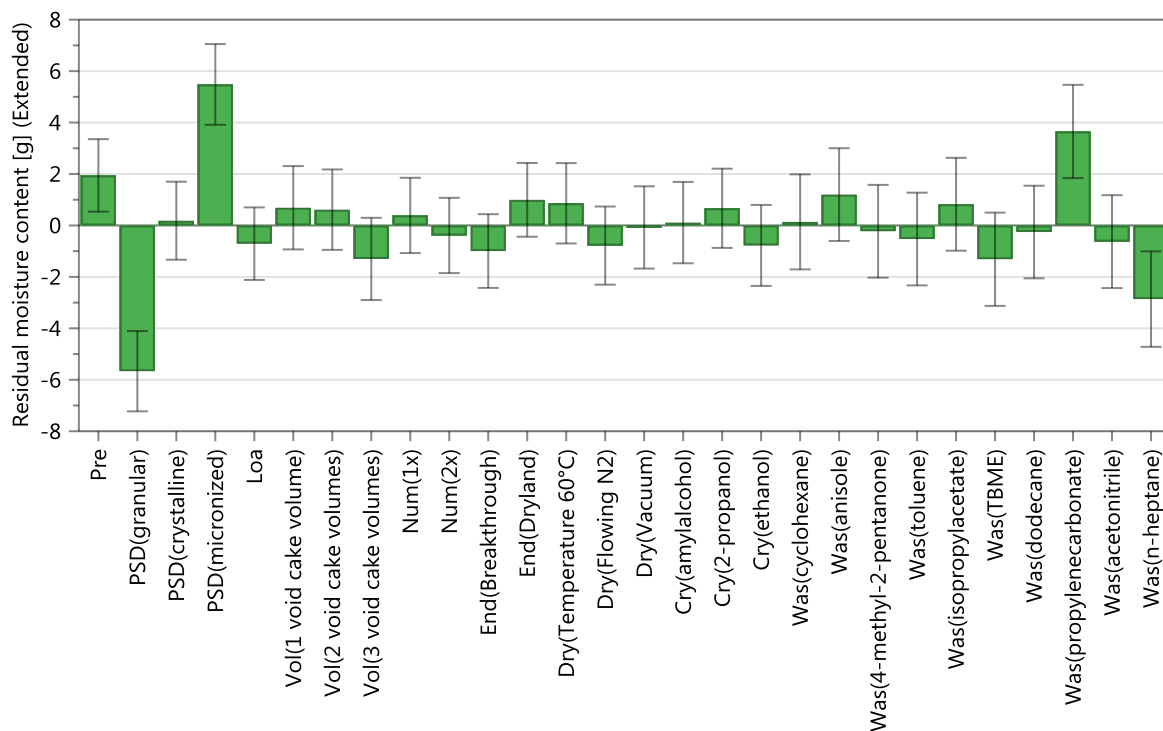


Figure 76 Parameters affecting residual solvent content.

Table 37 Literature values of boiling point, enthalpy of vaporization, viscosity, density and surface tension of the solvent used as wash and crystallization solvents.⁶⁷⁻⁶⁹

Solvent	Boiling point (°C)	Enthalpy of vaporization (kJ/mol)	Viscosity (cP) (Temperature °C)	Density (g/ml) (Temperature °C)	Surface tension (mN/m) (Temperature °C)
n-heptane	98.4	31.77	0.397 (25)	0.68 (20)	19.7 (20)
Isopropyl acetate	88.5	37.2	0.52 (25)	0.87 (20)	22.3 (20)
Toluene	111	38.01	1.16 (25)	0.86 (20)	27.73 (25)
Anisole	155	46.84	1.52 (15)	0.99 (18)	35 (20)
n-dodecane	216.3	44.09	1.5 (25)	0.75 (20)	25.35 (20)

TBME	55.2	27.94	0.35 (20)	0.76 (25)	18.5 (20)
4-methylpentan-2-one	116.1	40.61	0.59 (20)	0.8 (20)	24 (20)
Acetonitrile	81.6	33.2	0.36 (20)	0.79 (15)	29.4 (20)
Propylene carbonate	241.7	55.2	2.5	1.2 (20)	40.9 (25)
Cyclohexane	80.7	33.06	0.98 (20)	0.78 (20)	24.98 (20)
Ethanol	78.4	38.58	1.26 (20)	0.79 (20)	21.99 (20)
Isopropanol	82.2	39.85	2.1 (25)	0.78 (25)	21.4 (20)
isoamyl alcohol	132	55.2	3.74 (25)	0.81 (15)	24.77 (15)

In addition to the centre point replicates required in the DoE to assess reproducibility, a small number of additional duplicate experiments were run to evaluate the variance of residual moisture content due to operator consistently. The data in Table 38 show a good level of reproducibility.

Table 38 Residual moisture content consistency between experiments replicas determined at the end of filtration and deliquoring but prior to drying.

Experiment number	Experiment parameters	Residual solvent content (%)
14 (2 replicas)	Micronised, 10% V/V solid load, isopropanol, 900mbar, 2 void cake volumes *2 times with isopropyl acetate, dryland	43.51 ± 1.25
16 (2 replicas)	Powder, 30% V/V solid load, isopropanol, 500mbar, 3 void cake volumes*1 time with acetonitrile, dryland	26.08 ± 1.32

26 (2 replicas)	Powder, 10% V/V solid load, ethanol, 500mbar, 3 void cake volumes *1 time with n-heptane, dryland	22.38 ± 0.17
31, 32, 33 (DoE centre points)	Micronised, 20% V/V solid load, ethanol, 700mbar, 3 void cake volumes *2 time with n-heptane, dryland	25.84 ± 0.47

From Figure 76, also the drying method influence the residual moisture content. Lekhal et al.¹¹ report that wet particles tend to agglomerate during static drying under reduced pressure. The lack of agitation and consequent absence of disruption of aggregates allows strong interparticle bridges to be formed as consequence of saturated solvent evaporation and solid bridges formation at the points of contact between particles. In case of the use of the drying apparatus, where a flow of gas passes through the cake, agglomeration tendency was marginally reduced. From Figure 77-Figure 78 also the drying time is seen to be affected from the drying methodology. As previously explained vacuum oven drying for solvents presenting both relative low boiling points and heat of vaporization, required approximately few hours to dry. However, for static drying with higher gas flow rate, time to dry was reduced of few tens of minutes for low boiling and heat of vaporization solvents for room temperature nitrogen. Further reduction of drying time occurred when the gas was heated up due to the reduction of the constant rate drying period where the free moisture trapped between particles is removed that caused the increase of drying rate.⁴⁷ High drying temperature also decreases viscosity of the residual solvent implying weaker adhesion forces between the liquid and solid material.

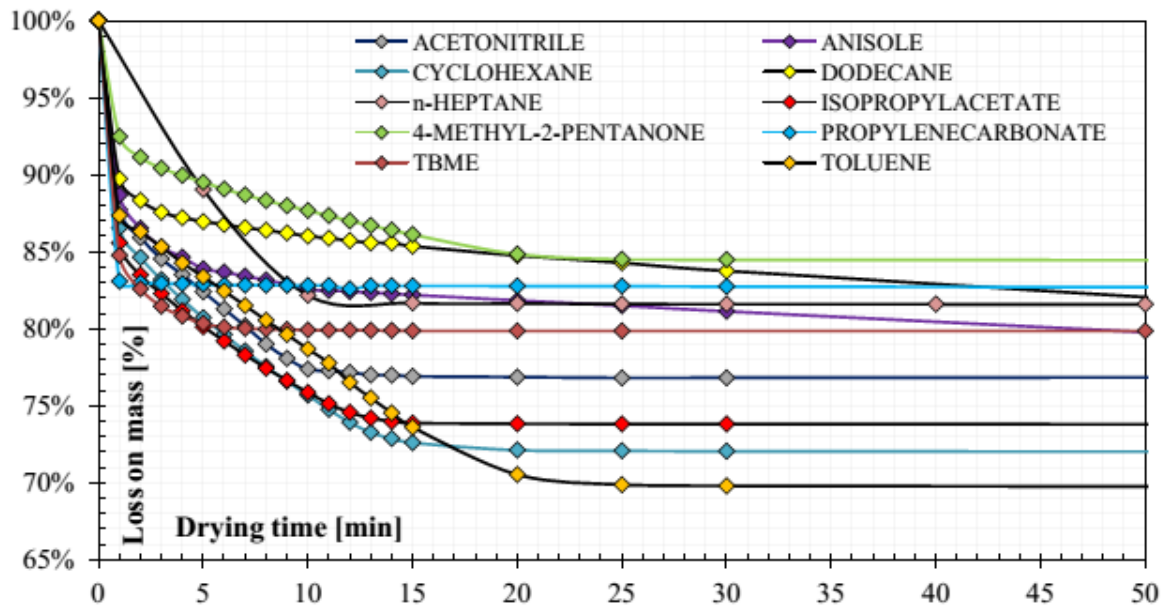


Figure 77 Drying profile of wet cake samples where drying was achieved by flowing nitrogen at ambient temperature through the filter cake with a flow rate of 0.3l/min.

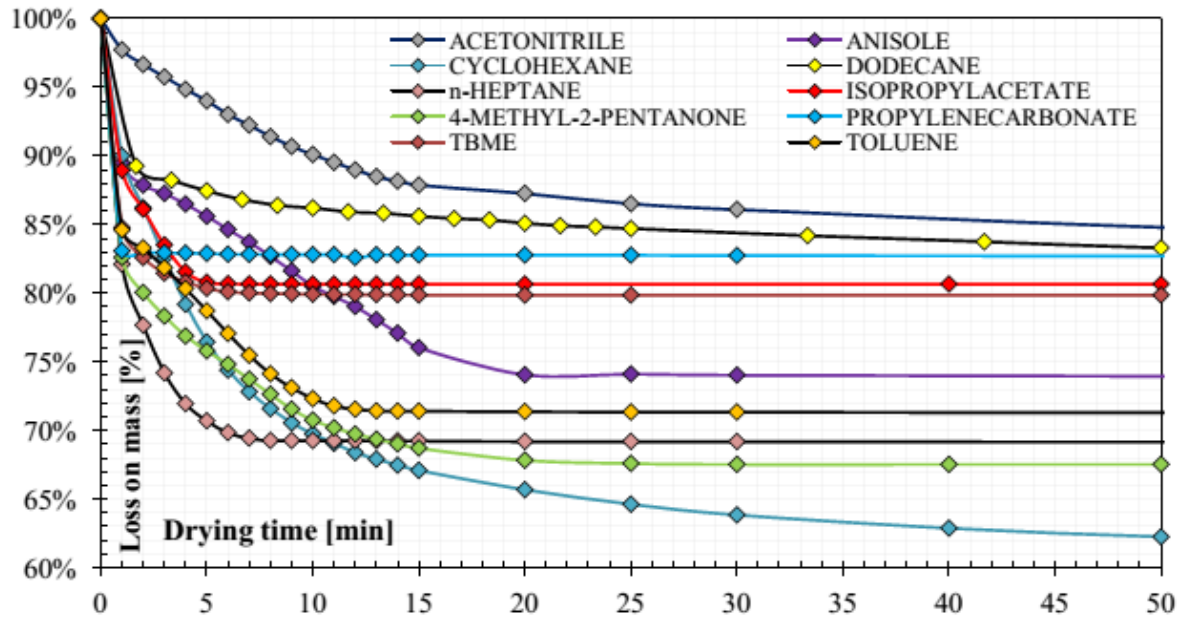


Figure 78 Drying profile of wet cake samples where drying was achieved by flowing nitrogen at 60°C through the filter cake with a flow rate of 0.3l/min.

As seen in Figure 77, volatile solvents with low boiling points such as; TBME, cyclohexane, n-heptane and ethanol, evaporated within 15 minutes; solvents with medium boiling points, such as toluene and 4-methylpentan-2-one, required approximately 25 minutes and high boiling point solvents, such as anisole and n-dodecane, only reached steady-state after many hours. Propylene carbonate has an extremely low evaporation rate, under vacuum drying conditions the sample dried over 75 days. Using hot flowing nitrogen, static drying generally resulted in the drying time being shortened by approximately by half (Figure 78). Cyclohexane and acetonitrile are two exceptions. The data for cyclohexane plotted in Figure 78 relates to a micronised paracetamol slurry with isoamyl alcohol as crystallization solvent, washed once with just 1 wash volume; it is likely that the inefficiency of crystallization solvent displacement resulted in extended drying time due to the high residual quantity of isoamyl alcohol which has boiling point approximately of 50°C higher and higher heat of vaporization by two thirds than cyclohexane.

Another key solvent property that can affect the quality of dried material is the paracetamol solubility. As reported in Table 32 acetonitrile shows the highest paracetamol solubility in the entire set of the wash solvents. This tendency of acetonitrile to dissolve more paracetamol than the other wash solvents serves to promote the formation of solid bridges, to some extent this effect may have been enhanced when hot nitrogen was used as drying agent (paracetamol solubility in acetonitrile at 25°C is 0.0294g paracetamol/g of solvent, the corresponding values at 40°C is 0.0313g/g and at 55°C is 0.0707g/g).

The quantity of wash solvent used to wash the cake and displace mother liquor exhibits its greatest effect by influencing the residual mother liquor (crystallization solvent) content and hence influencing the drying time the remaining crystallization solvent can promote interparticle bridge formation during drying. The formation of lumps and granules causes further obstacles to solvent evaporation when the solvent is trapped between "cemented" particles, prolonging the already slow falling-rate drying step driven by capillary forces.^{35, 39}

A further factor affecting the starting point of drying is identified in Figure 76: the procedure selected to halt the filtration can influence the final moisture content. Analyzing the 4D Contour plots (Figure 79-Figure 82) shows that halting filtration at breakthrough leads to a greater decrease in the final solvent quantity trapped in the cake on the completion of deliquoring. Two extremes are observed when:

- The slurry solid loading was high and the driving force was low: this represents the best case because although the cake was thicker, the lower driving force results in the wash being more efficient in displacing the crystallization solvent, leaving the cake richer in the more volatile solvent which was more easily removable during the drying step
- When the slurry solid load and driving force were both high, the quantity of solvent left behind in the cake reached a maximum: using a high driving force during washing negatively affected the final solvent content; the reduced contact time between the mother liquors and the wash solvent reduced the capability of wash solvent to displace the mother liquor due to lack of diffusion time.

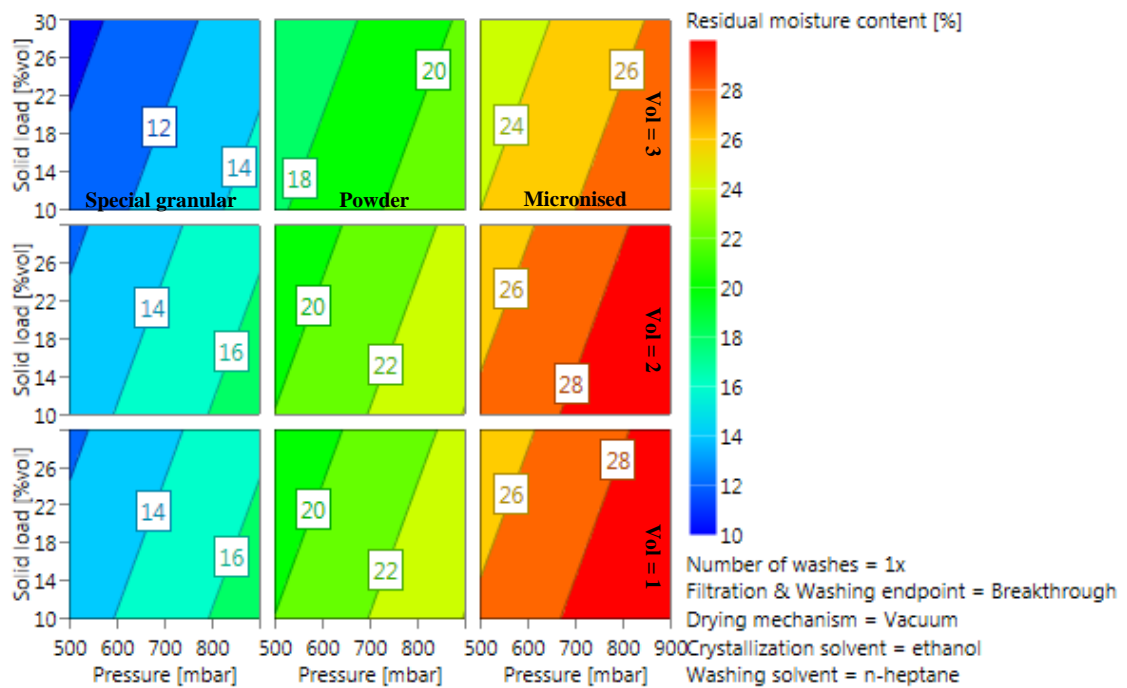


Figure 79 4D response contour plot of residual solvent content in case of filtration halted at breakthrough showing dependence on solids loading of the slurry, pressure driving force and paracetamol grade for an input suspension in ethanol washed once with n-heptane and then dried using the static drying methodology.

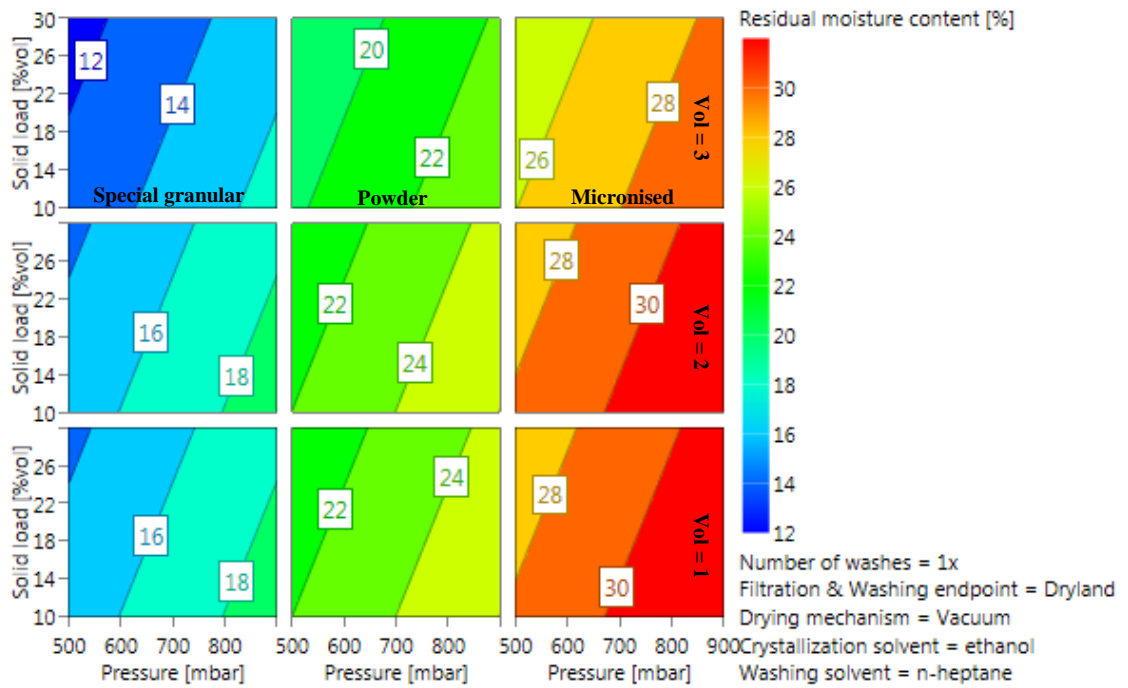


Figure 80 4D response contour plot of residual solvent content in case of filtration halted at dryland showing dependence on solids loading of the slurry, pressure driving force and paracetamol grade for an input suspension in ethanol washed once with n-heptane and then dried using the static drying methodology.

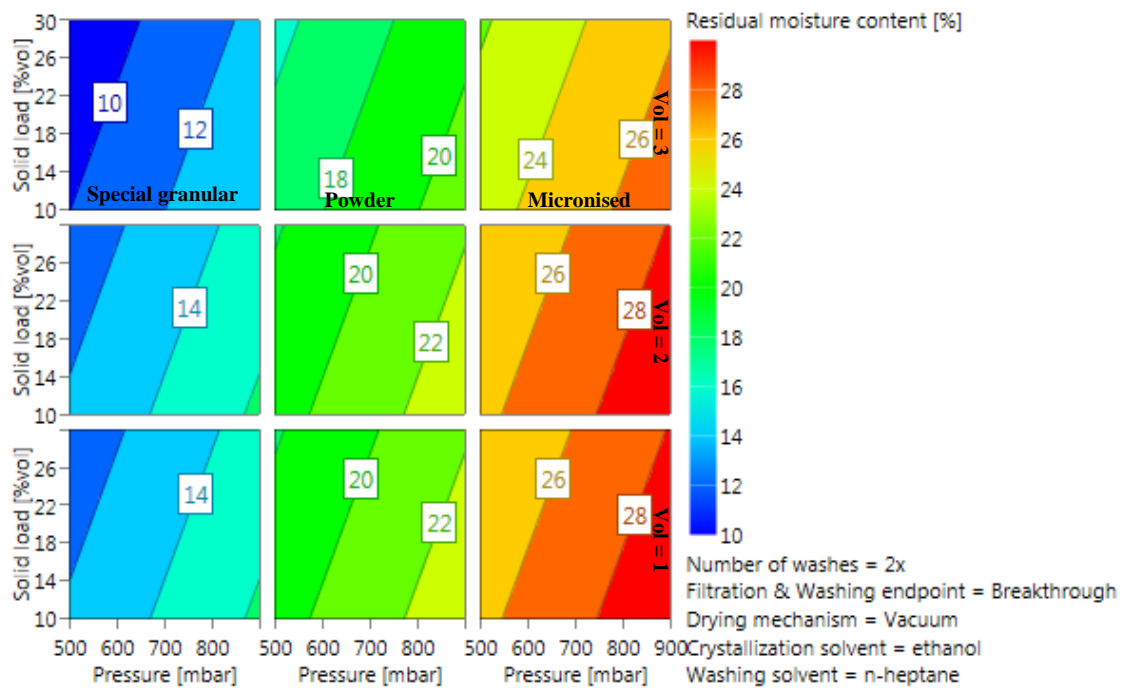


Figure 81 4D response contour plot of residual solvent content in case of filtration halted at breakthrough showing dependence on solids loading of the slurry, pressure driving force and paracetamol grade for an input suspension in ethanol washed twice with n-heptane and then dried using the static drying methodology.

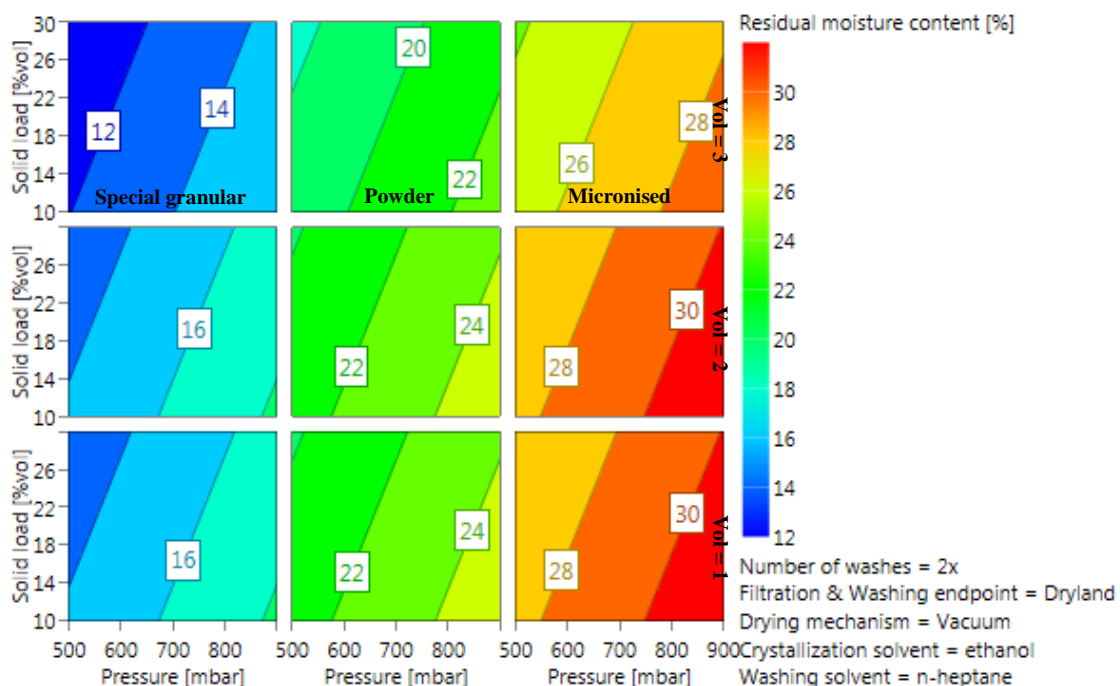


Figure 82 4D response contour plot of residual solvent content in case of filtration halted at dryland showing dependence on solids loading of the slurry, pressure driving force and paracetamol grade for an input suspension in ethanol washed twice with n-heptane and then dried using the static drying methodology.

6.5.4 Agglomeration, mechanical properties and particle size of dried products

Generally, micronised paracetamol tended to form agglomerates during isolation.

Typically, the samples recovered are angular with sharp edges consistent with breakage of a larger particle assemblies (Figure 83). The slightly coarser grade of paracetamol (powder) formed a mixture of fine particles and agglomerates with slightly more friable edges. The granular grade of paracetamol never formed agglomerates, with the exception of samples where propylene carbonate was selected as wash solvent. Solvents that exhibit high boiling points, tend in general to produce more agglomerated particles on isolation.



Figure 83 Appearance of isolated and dried paracetamol (left) micronized (exp 21), (centre) powder (exp 40) and (right) special granular (exp 15) input material (experiments information reported in the appendix).

In the experiments where micronised or powder grades of paracetamol were isolated and the volume of wash solvent used in the DoE was insufficient to displace and fully remove the crystallization solvent, the bulk of the isolated material took the form of a single lump (Figure 84). This observation is similar to the effect of using high boiling point solvents, as discussed previously.



Figure 84 Examples of lump formation (left, exp 53, centre exp 52, right exp 24; experiments information reported in the supplementary information).

The same phenomenon of lump formation during isolation was also observed in the three centre point experiments (parameters reported in Table 39).

Table 39 Variables and set points for the centre point experiments of the DoE.

Variable	Set point
Driving force (mbar)	700
Material	Micronised
Solid load (% V/V)	20
Volume of wash solvent	3 void cake volumes
Number of washes	2
Filtration and washing endpoint	Dryland
Drying mechanism	Vacuum
Crystallization solvent	Ethanol
Wash solvent	n-heptane

However, in the case of the DoE centre point conditions, the dried samples comprised an upper solid block (crust) on the top surface which is the first to be in contact with wash solvent or the drying gas stream and a less agglomerated bulk, this is shown for the centre point replicates (Figure 85).



Figure 85 Isolated and dried filter cake from the three centre point replicate experiments in the DoE.

In this study, three drying approaches were evaluated, in each case the particles were stationary throughout the drying process maximising the potential for particles to be fused

together into agglomerates as solute was deposited when the residual solvent evaporated. In addition, maintaining the particles in a stationary state eliminated the particle breakage typically encountered during agitated drying and the formation of granular material frequently seen when solvent wet particles are agitated:

- 1) Ambient (unheated) vacuum drier. On the initial application of vacuum, there is usually a brief burst of evaporation accompanied by cooling since solvent evaporation is an endothermic process⁷⁴. As the solvent wet product cools, the rate of evaporation declines until the system eventually reaches a thermal equilibrium where the rate of entry of heat energy into the system through conduction from the outside in, is balanced by the rate of heat loss caused by further solvent evaporation. The system continues in this constant rate period until the quantity of solvent available for evaporation is insufficient to sustain this evaporation rate and the drying process enters the falling rate regime.
- 2) Ambient temperature flowing nitrogen drier, here the flow of nitrogen provides a modest contribution to the heat balance leading (the specific heat capacity of nitrogen is small, 1.04kJ/kg/K compared with the latent heat of vaporisation of solvents, for example ethanol 42.3kJ/mol) thus the solvent evaporation rate. As indicated, the particles at the point of entry for the drying gas encounter solvent free gas at ambient temperature. As the gas passes through the filter cake it cools below ambient as solvent evaporates from the particle surfaces, the gas leaving the filter cake is the coolest and most solvent laden. Depending on the cake thickness, the solvent volatility and the gas flow rate, it may be that the gas approaches

saturation at its exit temperature. The particle size distribution plays a major part in defining the filter cake pore network dimensions and tortuosity which is also an important contributor to the resistance to gas flow and hence gas velocity and the opportunity for the gas to contact the wet crystal surfaces.

- 3) Elevated temperature flowing nitrogen drier, the process is very similar to that described in 2 above, the difference being that the solvent molecules on the surfaces of the initial crystals encountering the warm gas are subject to a greater driving force for evaporation and the temperature gradient through the cake is larger.

When a stationary bed of wet particles is dried, the solvent leaves the open surface by evaporation and for a time the lost solvent is replenished by capillary transport from the bulk to the surface. After a time, the rate of fresh solvent delivery declines as the reservoir of residual solvent diminishes and a drying front is established. The solvent content in the cake decreases along the axis of the cake⁴⁷ and in cases 2 & 3 the main limitation on the drying rate is the gas flow. Based on this model which presumes that solvent is carried to the evaporative surface by capillary forces it is reasonable to speculate that the formation of the solid crust of paracetamol starts from the upper surface and slowly progresses through the bulk where the transport of unbound moisture is occurring through particle-particle capillaries. In case of thin cake (in this study thin cakes are the cakes formed with slurry containing 10% of volume of solid content), if the material in the upper cake part stays in contact with the solvent for a long period the material after drying has rather hard shell or crust and relatively soft core. Whereas, for much thicker cakes, the capillary forces

cannot effectively transport the solvent throughout the entire cake volume to the surface. In this case, after a constant rate drying, the process is driven by solvent diffusion through the cake (slower drying rate), causing an even distribution of cake moisture and formation of a single solid block. For the case of the three centre points experiments, where the solubility of the system in wash solvent is negligible, as the material in the upper part stays in contact with the solvent for longer period the material, after drying has rather hard crust and relatively soft core.

As discussed above, the main parameters that affect the extent of agglomeration of the final dried cake are; the PSD of the particles forming the cake, the characteristics of the crystallization and wash solvents, wash solvent volume and drying protocol. The susceptibility of particles to form agglomerates can be correlated with; the solvents propensity to evaporate, API solubility, solvent viscosity and system wettability. If the wettability of the crystallization solvent is high, then the wash solvent needs to present similar wettability to be capable of removing the mother liquor and therefore to reduce the tendency for agglomerates formation.²⁶

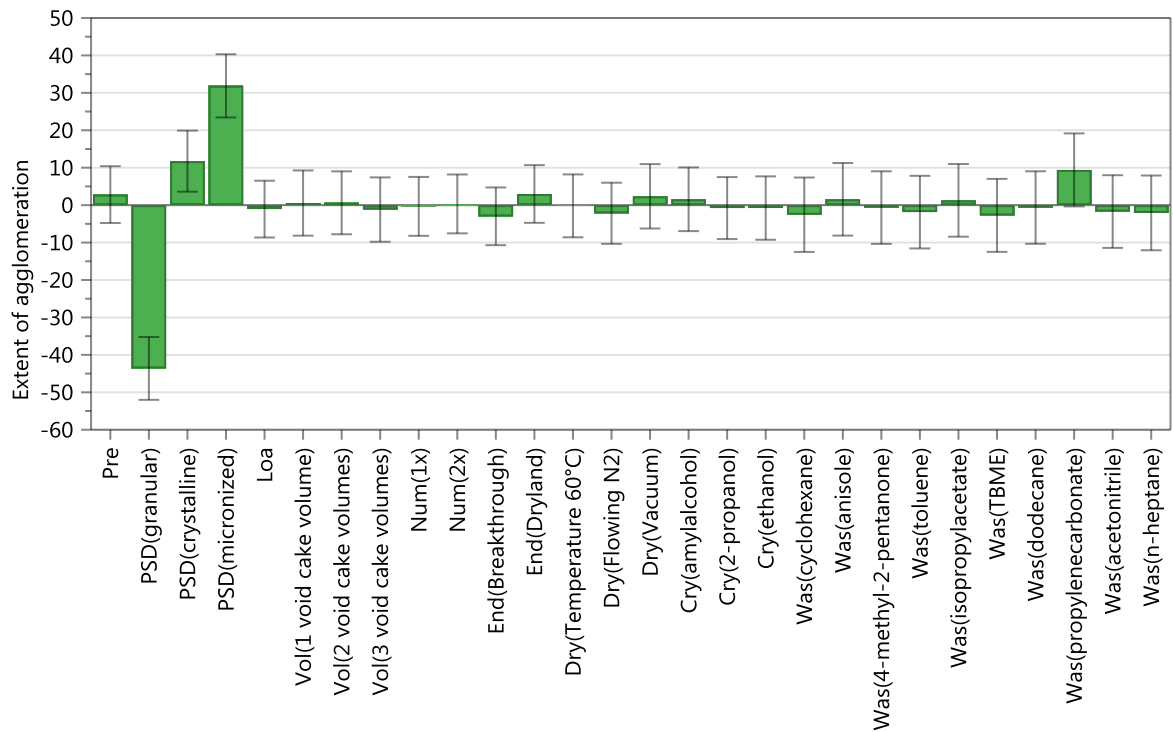


Figure 86 Parameters affecting the extent of agglomeration grouped by; filtration conditions, material particle size, washing and drying procedure and wash solvent identity

The agglomerate brittleness index (ABI) was selected as a descriptor to evaluate agglomerate mechanical properties.³⁵ The dried samples are not necessarily homogeneous in character but varies between the surface and the bulk, this variability is especially noticeable with the mechanical properties of agglomerates collected from the surface or from the bulk of the cake.

Table 40 describes the relationship between isolation conditions, the extent of agglomeration and the strength of the agglomerates formed. The three DoE centre point experiments shown in bold print in the table provide evidence of the consistency of the measurement of ABI (0.076 ± 0.01) and the extent of agglomeration ($93.8\% \pm 1.3\%$). The data in Table 40 indicate that the strength of agglomerates depends principally on the PSD

of the suspended particles being isolated. Micronised material usually formed hard agglomerates with a low ABI index, whereas the typical crystalline powder particles formed softer agglomerates with a higher ABI index. The link between size of the input particles and both the extent of agglomeration and the PSD of the agglomerated particles with size smaller than 1 mm interparticle may be linked with the surface area per unit mass available to form solid interparticle bridges during drying.¹⁵ There is insufficient evidence to make a link between the drying methodology and these two responses; further investigation is required. Another key factor discussed previously is the role of API solubility in crystallization and wash solvent which determines the quantity of material that could be deposited to form inter particle crystal bridges. Solvent volatility also is likely to play an important role in determining how quickly the solvent evaporates and the corresponding opportunity for crystallization to take place on the surfaces of the existing bulk crystals vs at points of contact between crystals.

Table 40 ABI index and extent of agglomeration values of some of the experiments of the DoE.

Material	Crystallization solvent	Wash solvent	Wash solvent volume and number of washes	ABI index	Extent of agglomeration (%)
Micronised (29)	isoamyl alcohol	TBME	2*1	0.006	99.9
Micronised (32)	isoamyl alcohol	Anisole	3*2	0.144	93.69
Micronised (20)	isoamyl alcohol	TBME	2*1	0.008	98.59

Micronised (21)	Isopropanol	Isopropyl acetate	2*2	0.104	95.91
Micronised (9)	Ethanol	n-heptane	3*2	0.075	92.32
Micronised (19)	Ethanol	n-heptane	3*2	0.066	94.81
Micronised (37)	Ethanol	n-heptane	3*2	0.086	94.19
Powder (10)	Ethanol	Anisole	1*1	0.307	74.78
Powder (31)	Isopropanol	Cyclohexane	2*2	0.014	56.02
Powder (26)	Ethanol	n-heptane	3*1	2.621	27.63
Powder (12)	Ethanol	Dodecane	2*2	1.147	75.21
Powder (22)	Isopropanol	Acetonitrile	3*1	0.955	80.41
Granular (30)	Isopropanol	4-methyl-2 pentanone	2*1	N/A	0
Granular (17)	isoamyl alcohol	n-heptane	2*2	N/A	0
Granular (13)	Isopropanol	Toluene	1*2	N/A	0

Figure 87 shows which isolation parameters can modify the size of single particles during filtration, washing and drying steps. Each profile was characterized by cumulative distribution, distribution density and several discrete values – x10, x50, x90, Sauter mean diameter SMD, the volume mean diameter VMD and compared with raw material values. Experiments forming large agglomerates fitting within the dimensions of the filter tube usually did not produce enough particulate material for further PSD analysis. Granular material isolated under comparable conditions remained as free flowing powder exhibiting almost uniform PSD in all cases, indicating a threshold in granule formation. Conversely,

large increases of PSD were observed for micronised samples. The PSD of the dried samples were comparable to the input material. Analyzing Figure 88 and Figure 90, it also appears that; slurry solid load, crystallization solvent viscosity and the filtration and washing stopping points influence the final particle size expressed as the SMD. The same reasons used to explain the level of agglomeration can be easily transferred also for the SMD of single particles. Comparing Figure 89 and Figure 91, no major effect is observed modifying the drying equipment mechanism and its operation while API PDS increases with the solubility of API in wash solvent. (Figure 88 and Figure 91).

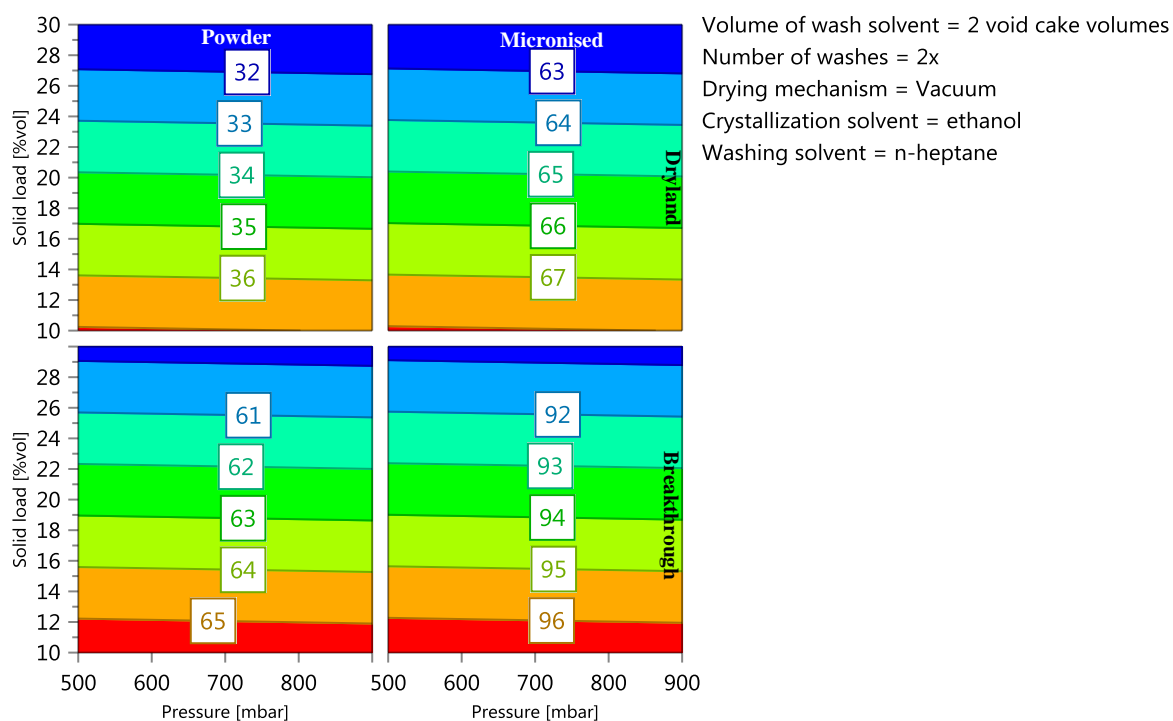


Figure 87 Investigating the effect of crystallization solvent. A 4D response contour plot of Sauter mean diameter (SMD) of the isolated product particles passing through the 1mm screen. In the case of filtration halted at dryland or breakthrough in the range of solid load of the slurry, driving force, paracetamol grade for an ethanol slurry washed 2 times with n-heptane and static drying methodology. SMD of raw powder and micronised paracetamol are respectively 46.35 and 18.66 μ m.

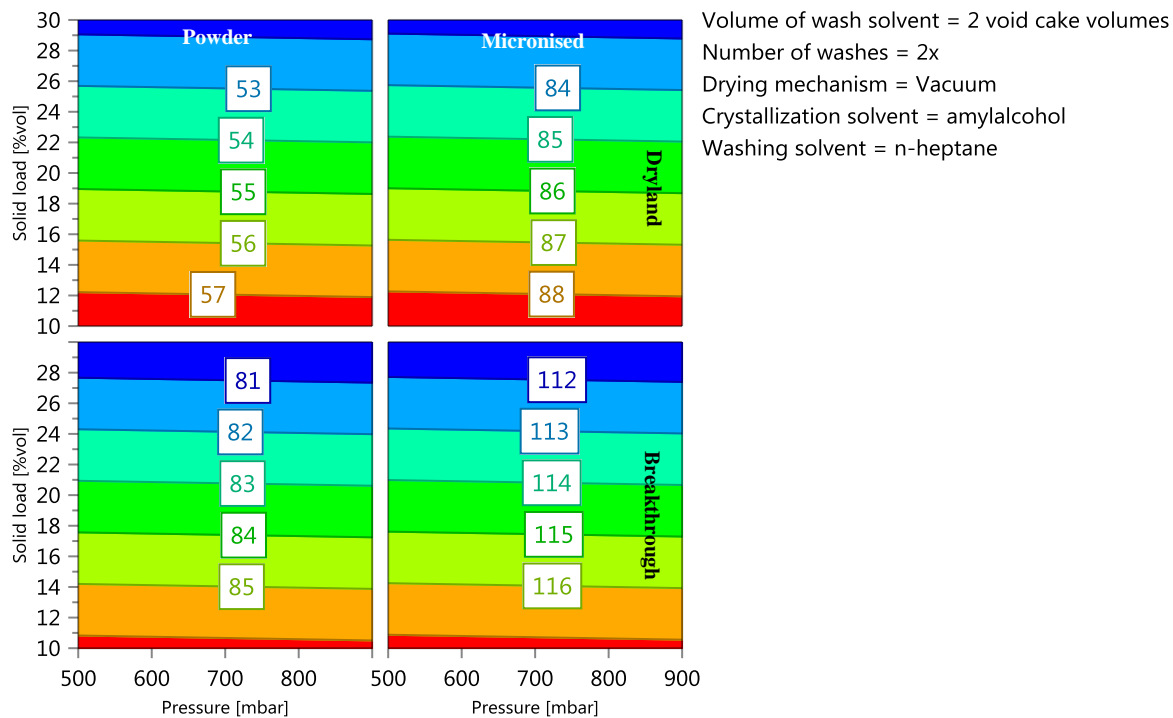


Figure 88 Investigating the effect of crystallization solvent. A 4D response Contour plot of Sauter mean diameter of particles smaller than 1mm in case of filtration halting at dryland or breakthrough in the range of solid load of the slurry, driving force, paracetamol grade for an isoamyl alcohol slurry washed 2 times with n-heptane and static drying methodology. SMD of raw powder and micronised paracetamol are respectively 46.35 and 18.66 μ m.

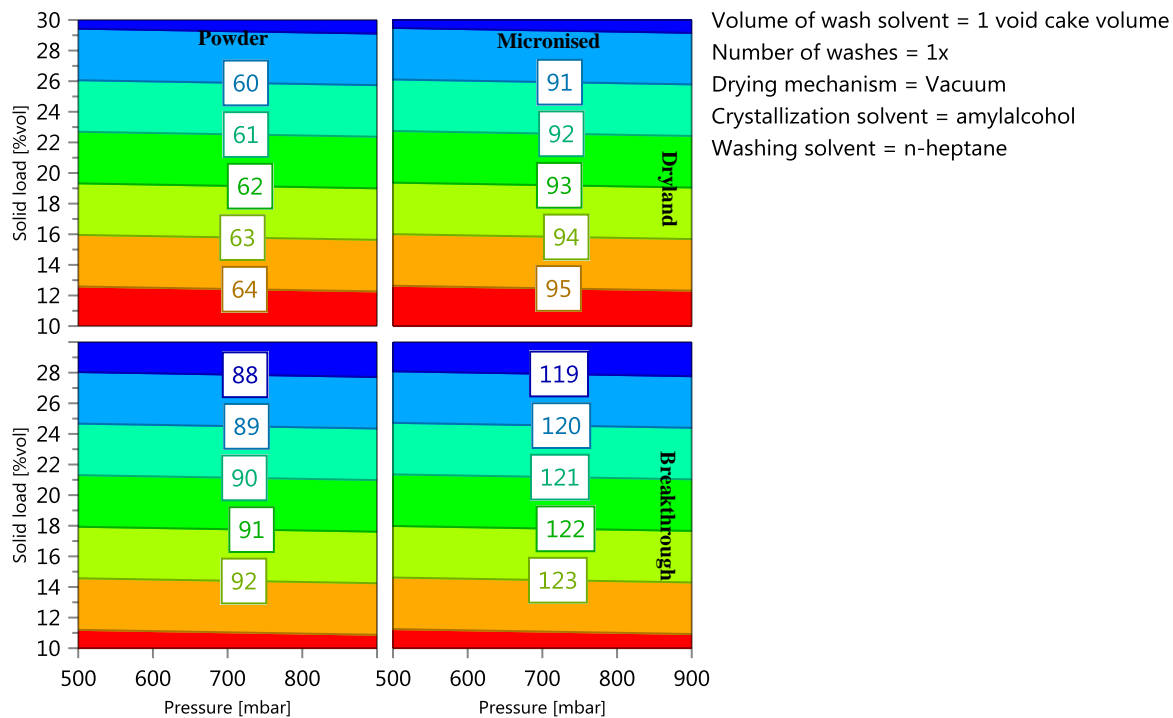


Figure 89 Investigating the effect of wash solvent volume (and number of washes). A 4D response Contour plot of Sauter mean diameter of particles smaller than 1mm in case of filtration halted at dryland or breakthrough in the range of solid load of the slurry, driving force, paracetamol grade for a isoamyl alcohol slurry washed 1 time with n- heptane and static drying methodology. SMD of raw powder and micronised paracetamol are respectively 46.35 and 18.66μm.

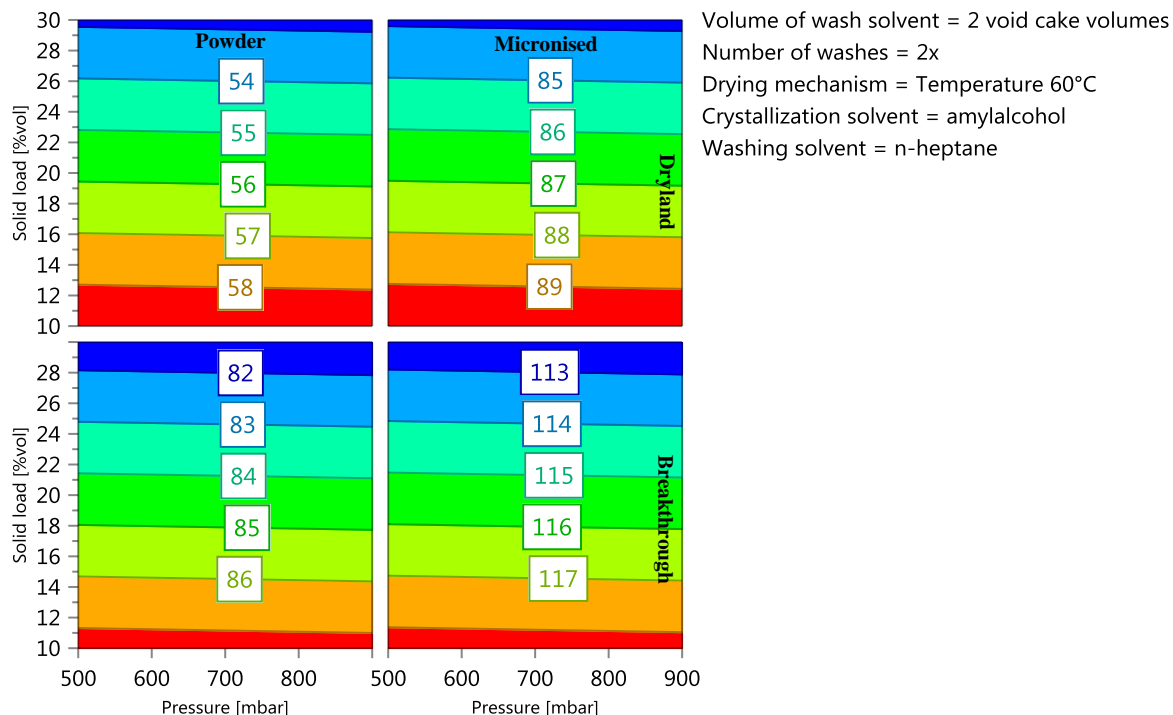


Figure 90 Investigating the effect of drying conditions. A 4D response Contour plot of Sauter mean diameter of particles smaller than 1mm in case of filtration halting at dryland or breakthrough in the range of solid load of the slurry, driving force, paracetamol grade for an isoamyl alcohol slurry washed 2 times with n- heptane and 60°C flowing nitrogen drying methodology. SMD of raw powder and micronised paracetamol are respectively 46.35 and 18.66 μ m.

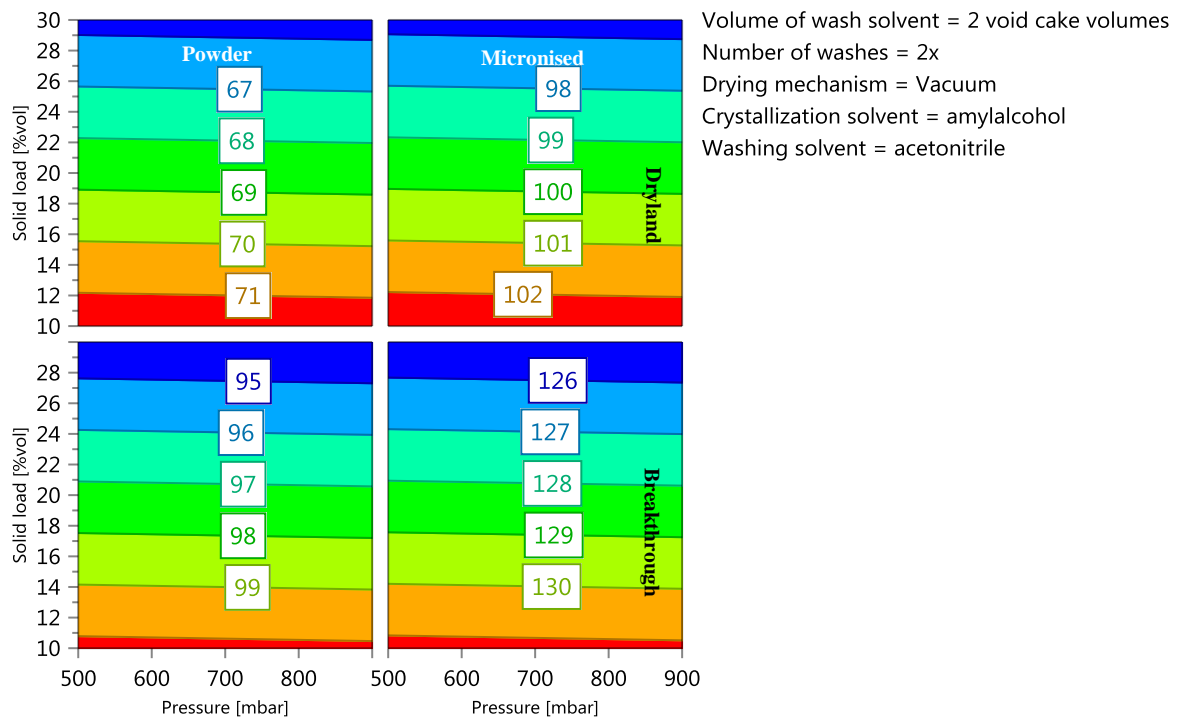


Figure 91 Investigating the effect of solubility in the wash solvent on isolated particle properties. A 4D response Contour plot of Sauter mean diameter of particles smaller than 1mm in case of filtration halting at dryland or breakthrough in the range of solid load of the slurry, driving force, and paracetamol grade for an isoamyl alcohol slurry washed 2 times with acetonitrile with static drying methodology. SMD of raw powder and micronised paracetamol are respectively 46.35 and 18.66 μ m.

From Table 41 the evaluation of robustness of particles with size less than 1mm to shear stress applied using different feeding pressure with the QICPIC are reported. A general trend of particle reduction is visible for micronised and powder materials, showing that particles smaller than 1mm agglomerated during drying. The agglomeration tendency is substantially larger for micronised particles than for powder material (x50 of dried material/x50 of raw material for micronised and powder are 11.96 for 0.5bar and 8.66 for 4bar in case of micronised and 1.09 for 0.5bar and 0.97 for 4bar for powder material). The extent of agglomeration of special granular material remains unchanged.

Table 41 x10, x50, x90, SMD and VMD values of few samples determined at 0.5bar and 4bar to determine particles stability under different feeding pressure of the QICPIC.

Experiment	Experiment parameters	X ₁₀ (0.5bar, 4bar)	X ₅₀ (0.5bar, 4bar)	X ₉₀ (0.5bar, 4bar)	SMD (0.5bar, 4bar)	VMD (0.5bar, 4bar)
Micro nised	Raw material	9.58, 9.47	24.55, 23.85	51.11, 47.17	18.66, 18.19	34.73, 28.06
Powd er	Raw material	23.85, 22.86	64.03, 62.57	179.14, 171.76	46.35, 44.74	86.01, 82.61
Speci al granul ar	Raw material	273.91, 193.9	363.58, 342.91	462.26, 449.22	229.3, 243.16	360.03, 329.45
9	Micronised, 20% V/V solid load, ethanol, 700mbar, 3 void cake volumes*2 times with n-heptane, dryland	14.02, 13.03	36.92, 32.57	611.12, 408.29	30.55, 26.91	163.06, 108.4
10	Powder, 30% V/V solid load, ethanol, 900mbar, 1 void cake volume*1 time with anisole, breakthrough	29.56, 28.24	71.36, 70.04	195.84, 194.16	55.97, 53.76	95.45, 91.28
11	Special granular, 10% V/V solid load, ethanol, 500mbar, 1 void cake volume*2 times with cyclohexane, breakthrough	275.33, 194.6	358.18, 348.48	449.83, 453.07	321.14, 261.69	354.43, 334.5

6.5.5 Model optimization and wash solvent screening

From the data gathered from the initial screening DoE (first DoE, Table 28) to evaluate the effect of different filtration, washing and drying conditions on the final product the conditions that can maximize process performance and product quality, where extracted. The filtration and washing driving force wash was fixed at 500mbar to reduce filtration time. In the Table 42 experimental parameters selected to minimize agglomeration, to get soft agglomerates and to reduce PSD variation of single crystals are reported.

Table 42 Ideal isolation parameters to minimize increase of agglomerates and PSD of single particles and formation of soft agglomerates.

Isolation parameter	Set point
Driving force (mbar)	500
Solid load (%)	30
Material	Powder
Crystallization solvent	Ethanol
Filtration and washing endpoint	Dryland
Volume of wash solvent	3 void cake volumes
Number of washing	2
Wash solvent	Cyclohexane
Drying mechanism	Room temperature flowing nitrogen (dynamic drying)

Based on the optimum parameters, a validation DoE was designed to understand the impact of wash solvent.

By using 4 void volumes divided between two separate washing steps, it was demonstrated that almost complete removal of the mother liquor (Table 43) could be achieved. The highest quantity of residual crystallization solvent are encountered in the experiments were acetonitrile and 4-methyl-2-pentanone were used. This is due to the high solubility of paracetamol in those two solvents that cause entrapment of mother liquor between particles agglomerated during the drying. Also sample washed with n-dodecane shows high crystallization content after drying; this is due to its high boiling point that cause agglomeration.

Table 43 Residual wash and crystallization solvent remained in cake after drying and drying time related to the nature of wash solvent.

Wash solvent used (2void cake volumes * 2 times)	Ratio of residual wash and crystallization solvent after drying (%)		
	Residual wash solvent (%)	Residual crystallization solvent (%)	Drying time (min)
n-heptane,	99.91	0.09	25
Isopropyl acetate	99.91	0.09	30
Toluene	99.97	0.03	120
Anisole	99.99	0.01	1200
Dodecane	99.8	0.2	3500
TBME	99.89	0.11	10
Cyclohexane	99.96	0.04	30
4-methylpentan-2-one	99.76	0.24	80
Acetonitrile	99.38	0.62	2640

The propensity to agglomerate and the mechanical property of the agglomerates are evaluated in Table 44 and Table 43. The sample that showed highest agglomeration was isolated from isopropyl acetate due to its propensity to dissolve paracetamol, while the lowest agglomeration is seen in samples washed with n-dodecane (showing the impact of very low API solubility). The hardest agglomerates are formed with acetonitrile (high API solubility), while the softest agglomerates are generated by washing with n-heptane. From this observation, if the objective is to combine a low propensity for agglomeration and to make soft agglomerates, the best processing option is to use cyclohexane, as seen in Figure 92.

Table 44 Mechanical properties of agglomerates produced from second DoE.

Wash solvent	Extent of agglomeration (%)	ABI index
n-heptane,	91.42	0.223
Isopropyl acetate	99.48	0.113
Toluene	95.52	0.146
Anisole	95.33	0.19
Dodecane	94.59	0.111
TBME	92.57	0.127
Cyclohexane	87.57	0.218
4-methylpentan-2-one	95.47	0.197
Acetonitrile	98.29	0.066

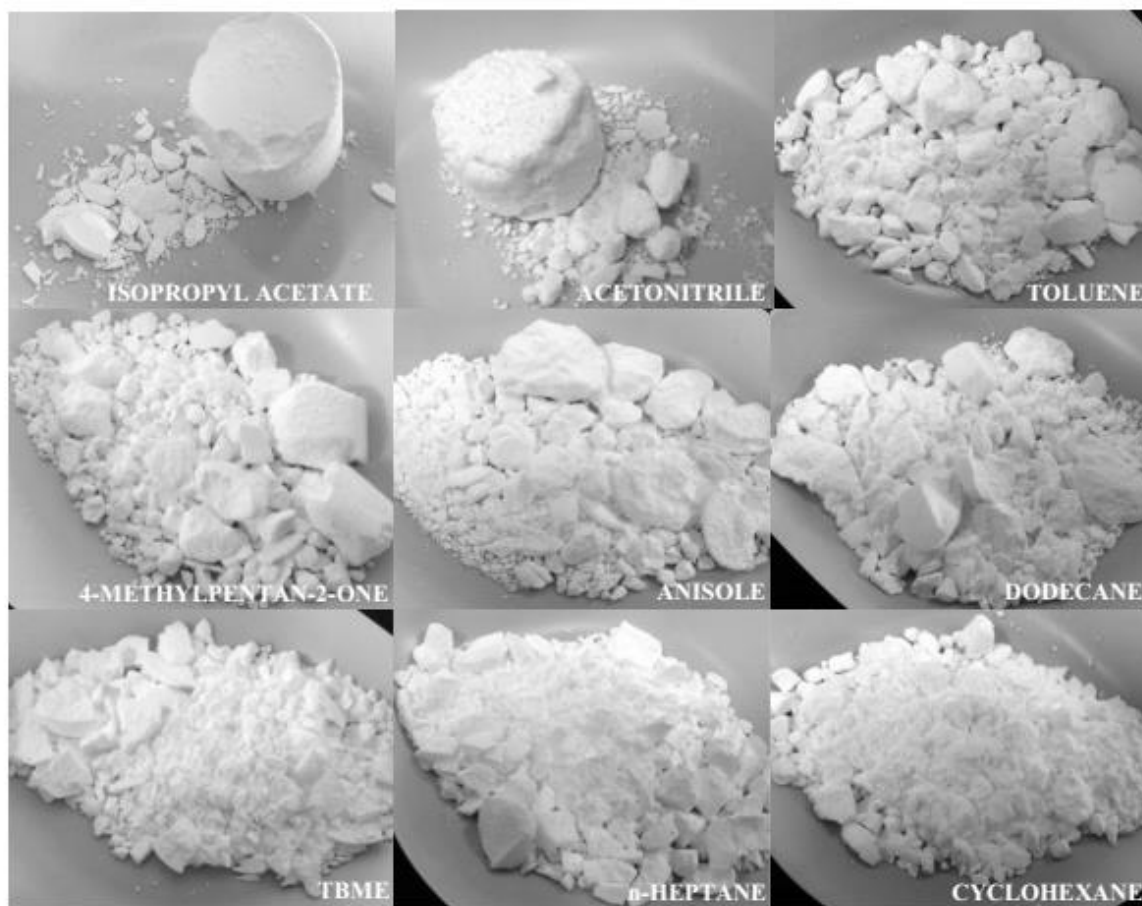


Figure 92 Visual appearance of samples generated during the validation DoE after drying. The best solvent selection to reduce agglomeration and obtain soft agglomerates is cyclohexane.

The particle size was determined using approximately 1g of dried material, the particle size analysis confirmed the best wash solvents for producing the least agglomerated product are cyclohexane and n-heptane which is consistent with previous observations (Figure 93).

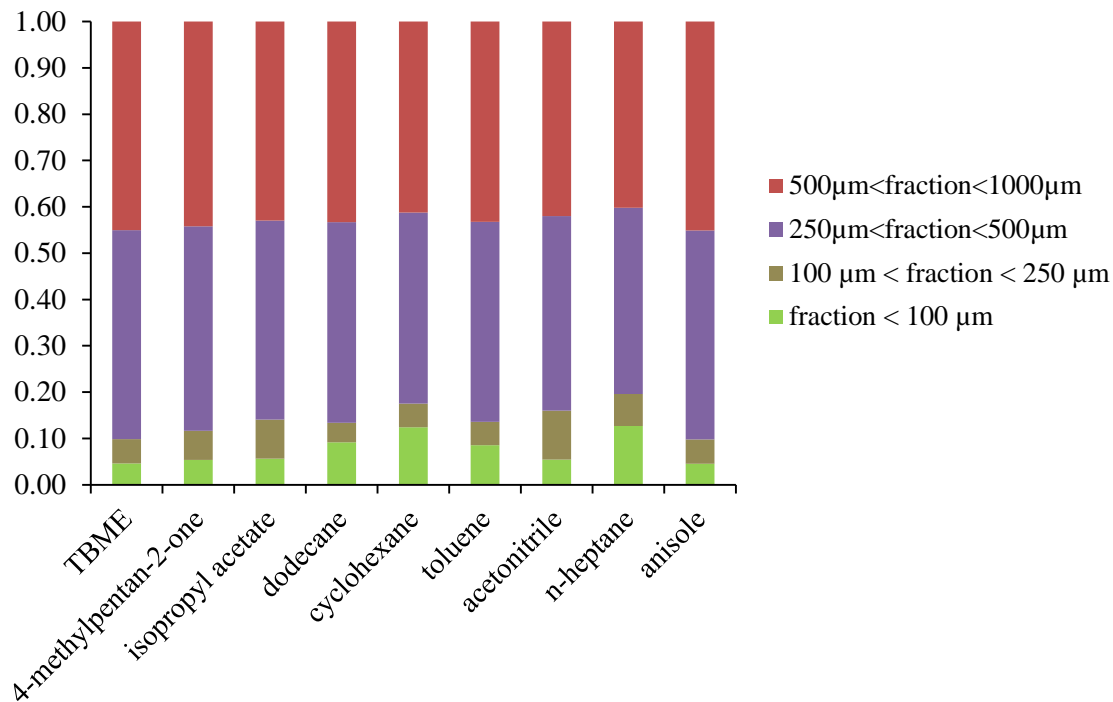


Figure 93 PSD profile of sample of the material isolated in the validation DoE.

6.6 Analytical workflow procedure for isolation strategy development for continuous isolation

The results reported in this chapter were obtained as part of a program to develop a workflow to minimise the number of experiments needed to develop an isolation strategy which maximizes purity, minimizes particle size variation at the end of the isolation process, minimize the solvent use during the washing step and to isolate the compound continuously using the AWL CFD25. In Figure 94 all the steps followed for the developed a continuous isolation strategy are reported.

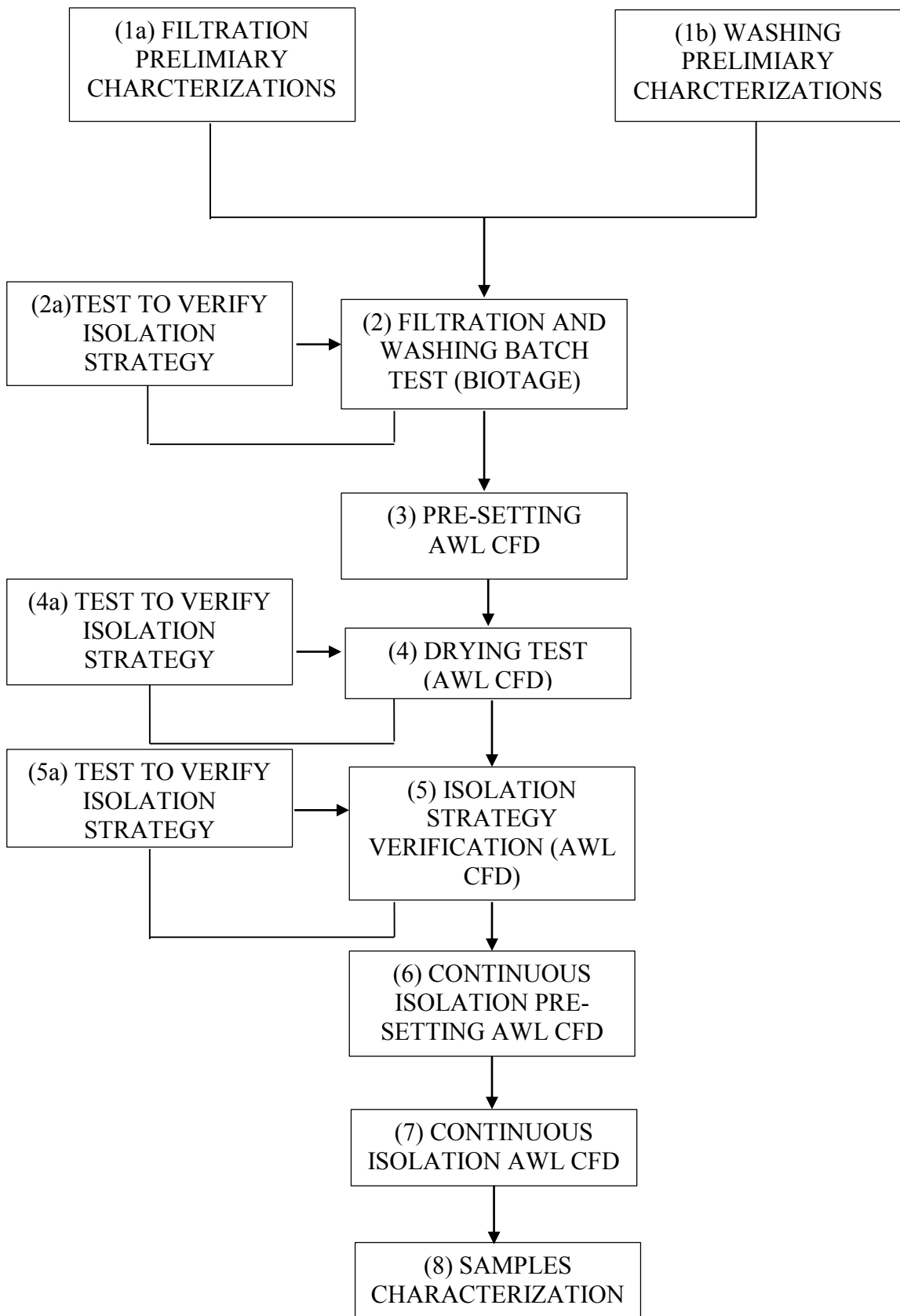


Figure 94 Workflow for the development of an isolation strategy.

Steps 1a and 1b are crucial to determine the properties of the slurry to isolate, this involves raw material characterization to understand filtration (1a) and selection of the washing (1b) strategy to use.

In step 1a a series of analytical test were used to determine solubility of the API and related impurities in the crystallization solvent selected, crystallization yield, or in case of simulated slurry prepared by resuspending previously isolated crystals, the solid load in suspension. Particle size, size distribution and shape are important parameters to determine prior to isolation to understand the behavior of slurry during filtration and washing when subject to a pressure driving force, to estimate the filtration time and cake resistance and permeability and to evaluate whether the isolation strategy modifies the final particle dimensions. In general, the smaller the particles and broader the size distribution the longer the filtration time. This phenomenon is further accentuated in case of higher aspect ratio (plate-needle like crystals). Also the evaluation of the particles size and shape prior to filtration is required to understand whether the filter media mesh size is small enough to prevent the passage of small particles during filtration or to investigate if a clean in place step is required during continuous isolation runs to prevent filter blockage due to fines particle size shape and quantity.^{18, 78, 79} Mother liquor viscosity and density needs to be measured prior to filtration experiments to calculate cake resistance. The viscosity of the pure crystallization solvent tends to overestimate the calculated values of cake and media resistance due to the increase of viscosity in case of a saturated solution. To identify washing parameters for the washing strategy some additional preliminary slurry characterization is required:

- The evaluation of the solubility of API and related impurities in the selected wash solvents under consideration. Purification by washing is working in case the solubility of impurity in the selected solvents is higher than the solubility of API. To avoid reduction of filtration yield, the API solubility in wash solvent should be low/very low to ensure limited API dissolution; however, in case impurities are adsorbed on the crystal surface, the dissolution of crystal surface is suggested to remove the trapped impurities (as seen in chapter 5). The estimation of the bulk and true density of the solid API used to create the cake (suspended material), this is used to calculate the void volume of the cake and therefore the required volume of wash solvent to remove the mother liquor where the impurities are dissolved
- The evaluation of viscosity, density and miscibility of the pure wash solvents with respect to the mother liquor to identify the mechanism of washing occurring during the isolation stage
- The evaluation of antisolvent effect occurring during washing leading to material be precipitated; it is important to evaluate the composition of the initial mixture , as described in the results and discussion paragraph of chapter 7, to avoid precipitation of fines/impurities during the first stage of washing
- The evaluation of the purity achieved during crystallization by HPLC to understand the identity and concentration of residual impurities in the mother liquor after the first step of purification. By knowing the identity and concentration of the impurities present in the slurry a selection of suitable wash solvents to remove the impurities and minimize the dissolution of the API can be made

- Preparation of calibration curves for the HPLC for each component present in the crystallized slurry is required to get a quantitative HPLC analysis.

Knowing all of these slurry properties, a set of experiments based on multivariable approach (DoE) can be undertaken to investigate the effect of filtration driving force, washing steps, wash solvent volume to use, filtration stopping mode (break through or dry land) on the filtered solid material (stage 2 of the workflow). Two different isolation units have been used to evaluate the best filtration parameters to use: the modified Biotage unit and the AWL CFD25 run in the optimization mode (with no cake drying applied). As at the second step of the isolation strategy evaluation, the Biotage unit is recommended because it have very accurate control of the pressure driving force. Responses to analyze after the filtration DoE experiments are:

- The evaluation of cake compressibility as a function of driving force is required to understand the validity of the Darcy's approach to calculate filtration parameters
- Cake resistance, filtration and washing time need to be measured to understand the feasibility of the process: in case of longer filtration time different crystallization solvents, different media pore size and different driving force can be used
- Change in cake height after filtration and washing, provides an indication of whether there were large losses of material for example due to dissolution of the cake during the washing step

- Cake void volume is used to determine the minimum volume of wash solvent required to displace the mother liquor trapped in the cake after filtration
- If appropriate the composition of a mixture of wash solvents for the first wash step used to displace the mother liquor without promoting fine particle precipitation/impurities precipitation (the antisolvent effect)
- The number of washing steps required to achieve the maximum impurity removal, whilst minimizing solvent consumption.
- The filtrate composition after filtration and washing steps to understand the contribution of each step on the final cake purity; also the final cake purity needs to be determined by HPLC to get an impurities essay (stage 2a) and close a mass balance.

From the DoE experiments, the best filtration and wash parameters are selected. These settings are then used to verify with the AWL CFD25 unit in optimization mode the unit setup parameters to be used to get comparable isolated product with the best manual practice using the Biotage unit during step 4 and 4a or if the CFD25 show limitations due to the slurry processability.

During this stage a set of extra experiments (DoE approach) are conducted with the CFD25 in optimization mode to determine best drying conditions to minimize residual solvent content and minimize particle agglomeration. To enhance convective drying, the evaluation of the best combination drying time, drying gas temperature and flow rate is done. Responses checked during this DoE are the residual moisture content after drying (also evaluated as loss on drying), the extent of agglomeration and the strength of the

agglomerates formed during drying (ABI index). In the case of formation of large lumps or hard agglomerates, a series of corrective procedures can be applied:

- Increase drying time, reduce the drying temperature whilst increasing the gas flow rate to minimize particle-particle bridging
- Include a deliquoring step prior drying that reduces the residual moisture content to a level where the agglomeration propensity is reduced, this threshold point is defined as critical moisture content
- Change wash solvent with another that exhibits lower API solubility, density, viscosity and lower boiling point and heat of vaporization: all of these solvent properties can favour bridge formation during drying. The effect of these parameters on the final dried product properties is evaluated in the results and discussions section of this chapter.

When the isolation strategy is developed in batch mode, verification of the strategy proposed in continuous mode may be performed using the AWL CFD25 in production mode (stage 7). During this stage a series of samples are collected during the continuous run to evaluate the consistency of dried material produced over time. For each sample a series of data are collected to evaluate the process stability (stage 8):

- Filtration and washing time is checked to detect filter blockage (to determine whether a clean in place step of the filtration and washing ports is required)
- Residual moisture content, cake purity, extent of agglomeration and strength of agglomerates to determine isolated material consistency
- Process throughput (material isolated in an hour of process)

- Process failures and their causes e.g. instrument issues or characteristics of the selected slurry.

In case of repeated failure of continuous isolation, a few possibilities can be considered:

- Modify the isolation strategy: to evaluate how changing parameters in the AWL CFD25 set up testing in optimization mode is suggested.
- Modify the crystallization procedure to produce a material which can be isolated, e.g. avoid fragile or weakly agglomerated particles
- Isolate the slurry with the AWL CFD25 in optimization mode
- Isolate the slurry with another isolation unit, for example using the Nutsche agitation filter dryer unit.

6.7 Conclusions

The aim of this work was to identify which filtration, washing and drying parameters affect the size of single particles, the formation of agglomerates and the mechanical properties of agglomerates formed during the isolation process. Three different DoEs were designed to evaluate the effect of:

- Filtration and drying procedure on the quality of final product
- Evaluation of sedimentation on filtration parameters
- Wash solvent identity on the dried product properties (PSD, extent of agglomeration and strength of agglomerates).

A model compound, paracetamol, was used in the study the effect of particle size, this was explored as a categorical variable using micronised, powder and granular grades of

paracetamol. Three different crystallization solvents, appropriate for crystallization and isolation of paracetamol (ethanol, isopropanol and isoamyl alcohol) and ten different wash solvent were used to evaluate the effect of solvent properties (viscosity, density, solubility and evaporation capability). A series of filtration, washing and drying variables were evaluated in the DoE screening: solid load in slurry, filtration and washing driving force, filtration and washing endpoint, volume and number of wash steps used and drying mechanism. Cake and media resistance, residual moisture content, and characteristics of the dried material; extent of agglomeration, ABI index and PSD of single particles were selected as responses in the initial screening DoE.

Two different sedimentation approaches were investigated: pre-settling cake prior to filtration and the more complicated filter and reload the filtrate on top of the cake to re-filter it again. This DoE was used to evaluate how cake and media resistance are influenced by cake sedimentation prior to filtration.

The validation DoE used to understand the effect of wash solvent on the dried material was designed, based on the optimal parameters determined from the first DoE, but using a different paracetamol grade and different number of washing cycles to investigate the effect of wash solvent on the dried product.

Filtration and cake washing were studied using vacuum filtration on a modified Biotage unit. Three different drying approaches were used: static drying in a vacuum oven operated at room temperature and two approaches using flowing nitrogen (room temperature nitrogen flow and heated temperature nitrogen flow through the cake).

Analysing cake resistance and media resistance the factors affecting those two filtration responses are PSD, the nature of crystallization solvent, driving force and solid loading. Filtering small particles with a broad PSD causes reduction of filtrate flow rate, linked to the increase of cake resistance and filtration time. High mother liquor viscosity also causes increase of cake resistance and filtration time and reduction of filtrate flow rate.

Sedimentation prior filtration influences the cake and media resistance. The increase in media resistance after sedimentation can be considered as the sum of resistance of the cake sedimented prior filtration and the media resistance of the filter medium.

To analyze the effect of drying on the final product, the extent of agglomeration and PSD of the single particles were selected as responses to evaluate the effect of residual moisture content, drying time and using different drying approaches. The major parameters affecting the percentage of residual moisture content are:

- The grade of the particles forming the cake: the lower the particle size, the higher the quantity of residual solvent retained
- The nature of the wash solvent, due to its boiling point, enthalpy of vaporization and solubility that can promote or impede particle bridge formation during drying
- The number of washes: if insufficient wash solvent is used ineffective washing occurs causing the entrapment of mother liquor between particles that can then promote particle cementation during drying

- The crystallization solvent identity and quantity remaining at the start of drying influence agglomeration, high API solubility and large solvent quantity and high solvent viscosity favour agglomeration
- The drying methodology: when particles remain stationary during drying under vacuum this promotes agglomeration, while drying with a flowing gas marginally reduced agglomerate formation.

Analysing the agglomeration propensity and mechanical properties of the agglomerates formed, sieving provided accurate results only in case of micronised agglomerates, fewer agglomerates were formed using the powder grade of paracetamol and they were softer than those formed with micronised input, showing that the PSD of the raw material is a major parameter that affects the nature of agglomeration. No agglomeration was observed for special granular particle samples, with the exception of samples washed with propylene carbonate, where all conditions produced extremely hard and highly agglomerated products. From the analysis of the parameters affecting agglomeration and agglomerate mechanical properties, the PSD of the particles forming the cake, and crystallization and wash solvent nature (evaporation propensity, API solubility, viscosity and wettability washing step), wash solvent volume and drying mechanism were responsible.

Experimental design was performed to identify the best combination of process conditions to suppress agglomeration. This was followed by a solvent screening study (propylene carbonate was eliminated) where the effect of wash solvent would play a dominant role. Proton NMR spectroscopy was used to monitor cake washing efficiency identifying

washing conditions where agglomeration would not be driven by residual mother liquor acting as a binding agent. In general, solvents presenting high API solubility and/or high boiling point favour the increase of agglomeration propensity with formation of hard agglomerates. From the validation DoE; low boiling aliphatic hydrocarbons (cyclohexane and n-heptane) were shown to be the best wash solvents for paracetamol, they reduce the tendency for agglomerate formation, yielding soft and easy to break agglomerates. These findings were further confirmed from PSD analysis of non-agglomerated fraction.

This work has delivered useful guidance and analytical approaches to design API isolation strategy to minimize agglomeration and to measure agglomerate mechanical properties.

6.8 Abbreviations

EPSRC, Engineering and Physical Sciences Research Council, API, Active Pharmaceutical Ingredient, PSD, particle size distribution, ¹H-NMR proton nuclear magnetic resonance, CQAs, critical quality attributes, ICH, International Conference on Harmonization, DoE, design of experiments, PCM, paracetamol, SMD, Sauter mean diameter, VMD, volume mean diameter, IPA, isopropanol, GC, gas chromatography, TBME, tert-butyl-methyl-ether, ACN acetonitrile, PTFE, polytetrafluoroethylene, LOD%, loss on dry (%), ABI, agglomerate brittleness index, HPLC, high performance liquid chromatography.

References

1. Davey, R., J., Garside, J., From Molecules to Crystallizers, Oxford University Press, 2000.
2. U. S. Department of Health and Human Services, Food and Drug Administration, Center for Drug Evaluation and Research (CDER), Center for Biologics Evaluation and Research (CBER). Q3D Elemental Impurities, Guidance for Industry. ICH, 2015.
3. Murugesan S., Sharma P., K., Tabora J., E. Design of Filtration and Drying Operations in Chemical Engineering in the Pharmaceutical Industry: R&D to Manufacturing. Wiley New York, 2010.
4. Beckmann, W. 14, Downstream Processes in Crystallization: Basic Concepts and Industrial Applications. 1st ed. Weinheim, Germany: Wiley-VCH, 2013.
5. Tien, C. Principle of Filtration. Elsevier, 2012.
6. Kynch, G., J., 1952. A theory of sedimentation. Trans. Faraday Soc, 166.
7. Kuo, M., T., 1960. Filter cake washing performance. AIChE J., 566.
8. am Ende, D., J. Chemical Engineering in the Pharmaceutical Industry: R&D to Manufacturing. 1st ed. Hoboken, New Jersey: Wiley, 2010.
9. Tsotsas, E., Metzger, T., Gnielinski, V., Schlünder, E.-U. Ullmann's Encyclopaedia of Industrial Chemistry, 1, Drying of Solid Materials. Drying of Solid Materials, 2002.
10. Lekhal, A., Girard, K., P., Brown, M., A., Kiang, S., Khinast, J., G., Glasser, B., J., 2004. The effect of agitated drying on the morphology of l-threonine (needle-like) crystals. Int. J. Pharm., 263.
11. Lekhal, A., Girard, K., P., Brown, M., A., Kiang, S., Glasser, B., J., Khinast, J., G., 2003. Impact of agitated drying on crystal morphology: KCl–water system. Powder Technol., 119.
12. MacLeod, C., S., Muller, F., L., 2012. On the Fracture of Pharmaceutical Needle-Shaped Crystals during Pressure Filtration: Case Studies and Mechanistic Understanding. OPR&D, 425.
13. Kougoulos, E., Chadwick, C., E., Ticehurst, M., D., 2011. Impact of agitated drying on the powder properties of an active pharmaceutical ingredient. Powder Technol., 308.
14. Tamrakar, A., Gunadi, A., Piccione, P., M., Ramachandran, R., 2016. Dynamic agglomeration profiling during the drying phase in an agitated filter dryer: Parametric investigation and regime map studies. Powder Technol., 109.
15. Wakeman R., 2007. The influence of particle properties on filtration. Sep. Purif. Technol., 234.
16. Endo, Y., Alonso, M., 2001. Physical Meaning of Specific Cake Resistance and Effect of Cake Properties in Compressible Cake Filtration. Filtr. Sep., 42.
17. Dullien F., A., L. Porous media fluid transport and pore structure, 2nd ed. Academic press inc.; 1992.

18. Wakeman, R., Tarleton, S. 4, Filtration Cake Formation in Solid Liquid Separation: Principles of Industrial Filtration. 1st ed. Amsterdam, Netherlands: Elsevier Science, 2005.
19. Perlmutter, B. A., et al. A Treatise of Filter Cake Washing Mechanisms In Pressure and Vacuum Filtration Systems. BHS Filtration [cited 2016-11-18]. Available at http://www.bhs-filtration.com/A_Treatise_of_Filter_Cake_Washing_Mechanisms.pdf
20. Muskat, M. The Flow of Fluids Through Porous Media. J. Appl. Phys., 1937
21. Scheidegger, A., E. The physics of flow through porous media. University of Toronto Press, 1974.
22. Bear, J. Dynamic of Fluids in Porous Media. American Elsevier Publishing Company, 1972.
23. de Wiest, R., J., M. Flow through Porous Media. Academic Press, New York, 1969
24. Calvo, A., Paterson, I., Chertcoff, R., Rosen, M., Hulin, J., P. In proceedings "Fundamentals of Fluid Transport in Porous Media". May 14-18, Arles, France., 1990.
25. Dullien, F., A., L., 1988. Two-phase flow in porous media. Chem. Eng. Technol.
26. Burisch, M., Peuker, U., A., 2016. Influence of Wetting on Washing and Filtration Properties. Chem. Eng. Technol., 543.
27. Owens, W., W., Archer, D., L., 1971. The effect of rock wettability on oil-water relative permeability relationships. J. Pet. Technol., 873.
28. McCaffery, F., G., Bennion, D., W., 1974. The effect of wettability on two-phase relative permeability. J. Chem. Pet. Technol., 33.
29. Yadav, G., D., Dullien, F., A., L., Chatzis, I., Macdonald, I., F., 1987. Microscopic Distribution of Wetting and Nonwetting Phases in Sandstone During Immiscible Displacements. Soc. Pet. Eng. J.
30. Ruth, B., F., Montillon, G., H., Montonna, R., E., 1933. Studies in Filtration - I. Critical Analysis of Filtration Theory. Ind. Eng. Chem., 76.
31. Yukseler, H., Tosun, I., Yetis, U., 2007. A new approach in assessing slurry filterability. J. Membr. Sci., 72.
32. Spark, T. Solid-Liquid Filtration: A User's Guide to Minimizing Cost and Environmental Impact, Maximizing Quality & Productivity. 1st ed. Elsevier; 2012.
33. Chatzis, I., Dullien, F., A., L., 1983. Dynamic immiscible displacement mechanisms in pore doublets: theory versus experiments. J. Colloid Interface Sci., 199.
34. Jozwiakowski, M., J., Nguyen, N-A., T., Sisco, J., M., Spancake, C., W., 1996. Solubility behavior of lamivudine crystal forms in recrystallization solvents. J. Pharm. Sci., 193.
35. Birch, M., Marziano, I., 2013. Understanding and Avoidance of Agglomeration During Drying Processes: A Case Study. OPR&D, 1359.
36. Ruslim, F., Hoffner, B., Nirschl, H., Stahl, W., 2009. Evaluation of pathways for washing soluble solids. Chem. Eng. Res. Des., 1075.
37. Lamberto, D., J., Cohen, B., Marencic, J., Miranda, C., Petrova, R., Sierra, L., 2011. Laboratory methods for assessing API sensitivity to mechanical stress during agitated drying. Chem. Eng. Sci., 3868.

38. Papageorgiou, C., D., Langston, M., Hicks, F., am Ende, D., Martin, E., Rothstein, S., Salan, J., Muir, R., 2016. Development of Screening Methodology for the Assessment of the Agglomeration Potential of APIs. OPR&D.
39. Zhang, S., Lamberto, D., J., 2014. Development of New Laboratory Tools for Assessment of Granulation Behavior During Bulk Active Pharmaceutical Ingredient Drying. *J. Pharm. Sci.*, 152.
40. Lim, L. H., Hapgood, K. P., Haig, B., 2016. Understanding and preventing agglomeration in a filter drying process. *Powder Technol.*, 146.
41. Michaud, A., Peczalski, R., Andrieu J., 2008. Modelling of vacuum contact drying of crystalline powder packed beds. *Chem. Eng. Process.*, 722.
42. Sahni, E., K., Chaudhuri, B., 2012. Contact drying: A review of experimental and mechanistic modelling approaches. *Int. J. Pharm.*, 334.
43. Terdeng, L.-M., Wohlgemuth, K., 2017. Effect of drying method on agglomeration degree of crystalline products. *Chem. Eng. Sci.*, 88.
44. Intelvi, M. PhD thesis: Contact drying of particulate pharmaceuticals: modelling and simulation. 2010.
45. Wakeman, R. J., Tarleton, E. S. Filtration: equipment selection, modelling and process simulation. 1st ed. Oxford, United Kingdom: Elsevier Science Ltd, 1999.
46. Remy, B. PhD thesis: Granular flow, segregation and agglomeration in blade mixer. October 2010.
47. Conder, E., W., Cosbie, A., S., Gaertner, J., Hicks, W., Huggins, S., MacLeod, C., S., Remy, B., Yang, B.-S., Engstrom, J., D., Lamberto, D., J., Papageorgiou, C., D., 2017. The Pharmaceutical Drying Unit Operation: An Industry Perspective on Advancing the Science and Development Approach for Scale-Up and Technology Transfer. OPR&D, 420.
48. Remy, B., Kightlinger, W., Saurer, E., M., Domagalski, N., 2015. Scale-Up of Agitated Drying: Effect of Shear Stress and Hydrostatic Pressure on Active Pharmaceutical Ingredient Powder Properties. *AIChE J.*, 407.
49. Thompson, C.; Davies, M. C.; Roberts, C. J.; Tendler, S. J. B.; Wilkinson, M. J., 2004. The effects of additives on the growth and morphology of paracetamol (acetaminophen) crystals. *Int. J. Pharm.*, 137.
50. Hendriksen, B., A., Grant, D., J. W., Meenan, P., Green, D. A., 1998. Crystallisation of paracetamol (acetaminophen) in the presence of structurally related substances. *J. Cryst. Growth*, 629.
51. Prasad, K., V., R., Ristic, R., I., Sheen, D., B., Sherwood, J., N., 2001. Crystallization of paracetamol from solution in the presence and absence of impurity. *Int. J. Pharm.*, 215.
52. Ottoboni, S., Chrubasik, M., Burce, L., M., Nguyen, T., T., H., Robertson, M., Johnston, B., Oswald, I., D., H., Florence, A., Price, C., 2018. Impact of Paracetamol Impurities on Face Specific Properties: Investigating the Surface of Single Crystals Using TOF-SIMS. *Cryst. Growth Des.*, 2750.
53. Sudha, C., Srinivasan, K., 2014. Understanding the effect of solvent polarity on the habit modification of monoclinic paracetamol in terms of molecular recognition at the solvent crystal/interface. *Cryst. Res. Technol.*, 865.
54. MODDE software [cited 2018-05-22] <https://umetrics.com/product/modde>

55. Triefenbach, F. Bachelor Thesis: Design of Experiments: The D-Optimal Approach and Its Implementation As a Computer Algorithm. Umeå University, Sweden, 2008.
56. Eriksson, L., Johansson, E. Multivariate Design and modelling in QSAR. *Chemom. Intell. Lab. Syst.* 1996, 1 – 19.
57. Bourcier, D., Féraud, J., P., Colson, D., Mandrick, K., Ode, D., Brackx, E., Puel, F., 2016. Influence of particle size and shape properties on cake resistance and compressibility during pressure filtration. *Chem. Eng. Sci.*, 176.
58. QICPIC. AMS Laboratory Techniques [cited 2017-04-18] <http://amslt.co.za/2016/03/08/qicpic-2/>
59. Siebold, A., Walliser, A., Nardin, M., Opploger, M., Schultz, J., 1997. Capillary Rise for Thermodynamic Characterization of Solid Particle Surface. *J. Colloid Interface Sci.*, 60.
60. Detherm database [cited 2016-11-18] <http://dechema.de/en/detherm.html>
61. Biotage® VacMaster™ 10 & 20 Sample Processing Station Operation Manual, 2017. Biotage. <http://www.biotage.com/product-page/biotage-vacmaster-10-and-20> [cited 2017-03-25]
62. Svarovsky L. Solid-Liquid Separation, Fourth Edition, Butterworth-Heinemann; 2000.
63. Sørensen, P., B., Christensen, J., R., Bruus, J., H., 1995. Effect of Small-Scale Solids Migration in the filter Cake during Filtration of Waste-Water Solid Suspensions. *Wat. Environ.*, 25.
64. Willis, M., S., Tosun, I., 1980. A rigorous cake filtration theory. *Chem. Eng. Sci.*, 2427.
65. Fathi-Najafi, M., Theliander, H., 1995. Determination of local filtration properties at constant pressure. *Sep. Technol., Progress in Separations and Waste Reduction*, 165.
66. Tiller, F., M., Hsyung, N., B., Cong, D., Z., 1995. Role of porosity in filtration: XII. Filtration with sedimentation. *AIChE J.*, 1153.
67. Koenders, M., A., Wakeman, R., J., 1996. The initial stage of compact formation from suspensions by filtration. *Chem. Eng. Sci.*, 3897.
68. Crosier, H., E., Brownell, L., E., 1952. Washing in Porous Media. *Ind. Eng. Chem.*, 631.
69. Tuson, I., Willis, M., S., Batigun, A., 1988. Parameter Estimation in Cake Washing. *Chem. Eng. Commun.*, 151.
70. Hermia, J., Rushton, A. *Mathematical Models and Design Methods in Solid-Liquid Separation. Filter Cake Washing.* Springer, Netherland, 1985.
71. Wypych, A., Wypych, G. *Databook of solvents.* ChemTec Publishing, 2014
72. PubChem website [cited 2018-05-15] <https://pubchem.ncbi.nlm.nih.gov/compound/>
73. Accudynet website [cited 2018-05-15] https://www.accudynetest.com/visc_table.html
74. Kontcho, K., P., Cook, W., Kougoulos, E., 2011. Impact of Laboratory Vacuum Contact Drying on Material Drying Rates and Physical Properties. *OPR&D*, 360.

75. Celsius-process website [cited 2018-08-20] <http://www.celsius-process.com/pdf/isopropanol.pdf>
76. DDBST GmbH website [cited 2018/08/20] http://www.ddbst.com/en/EED/PCP/VIS_C11.php
77. CAMEO Chemicals website [cited 2018-08-20] <https://cameochemicals.noaa.gov/chemical/3659>
78. Wakeman, R., J., Sabri, M., N., Tarleton, E., S., 1991. Factors affecting the formation and properties of wet compacts. Powder Technol., A Special Volume Devoted to the Second Symposium on Advances in Particulate Technology, 283.
79. Wakeman, R., 2007. The influence of particle properties on filtration. Sep. Purif. Technol., 234.

7 Prototyping of a continuous isolation unit: development and tests

The first part of the work reported in this chapter is published as, Development of a novel continuous filtration unit for pharmaceutical process development and manufacturing. Sara Ottoboni, Chris Price, Christopher Steven, Elizabeth Meehan, Alastair Barton, Paul Firth, Andy Mitchell, Furqan Tahir, Journal of Pharmaceutical Science (Special Topic Issue) (DOI: <https://doi.org/10.1016/j.xphs.2018.07.005>).

The full text was accepted as conference proceeding as, Investigating the isolation performance of a novel continuous filtration unit for pharmaceutical process development and manufacturing: A case study using paracetamol and related impurities. Sara Ottoboni, Muhid Shahid, Christopher Steven, Elizabeth Meehan, Alastair Barton, Paul Firth, Richard Sutherland, Andy Mitchell, Furqan Tahir, Chris Price; FiltCon 2018, 24th – 25th April, 2018, Prior Lake, MN, USA.

7.1 Introduction

The overall aim of my research is to design, develop and test the performance of a novel filtration, washing and drying unit (the AWL CFD). The unit is designed to isolate in manual, semi-automated or continuous modes any active pharmaceutical ingredient (API) produced at lab/small scale.

The strengths of this lab/small scale isolation prototype are:

- **Efficiency:** the CFD is able to reach productivity of up to 300g slurry per hour; the productivity of the system is limited by the slowest isolation step which depends on the character of the slurry to filter
- **Flexibility:** the process of separation can be fully manual, semi-automated or fully continuous; fully manual and semi-automated operability are recommended in case of isolation strategy development for new slurry, while fully continuous is recommended for small-scale production
- **Fully equipped:** the CFD is able to run a full isolation process (filtration, washing and drying); the drying step can be run to complete/partial dryness in relation to slurry/wash solvent composition
- **Compact design:** the CFD was designed to be placed inside a fumehood to mitigate the operator exposure to chemicals
- **Versatility:** three different modes of operation are accommodated with full control of slurry and wash solvent dosing, residence time and drying time can be used: manual, optimization and production mode

- End uses: the prototype can be used for research and for small-scale API production.

Currently there is a gap in the available continuous pharmaceutical isolation units, which combine dead end filtration, washing and drying capabilities and can be readily coupled with a continuous upstream process to isolate small quantity of slurry. To address this gap Alconbury Weston in collaboration with Remedies project developed a new isolation prototype¹ called CFD (continuous filter dryer). New product development process (NPDD)¹ is the procedure used to develop the new CFD unit. The process is described in Figure 95.

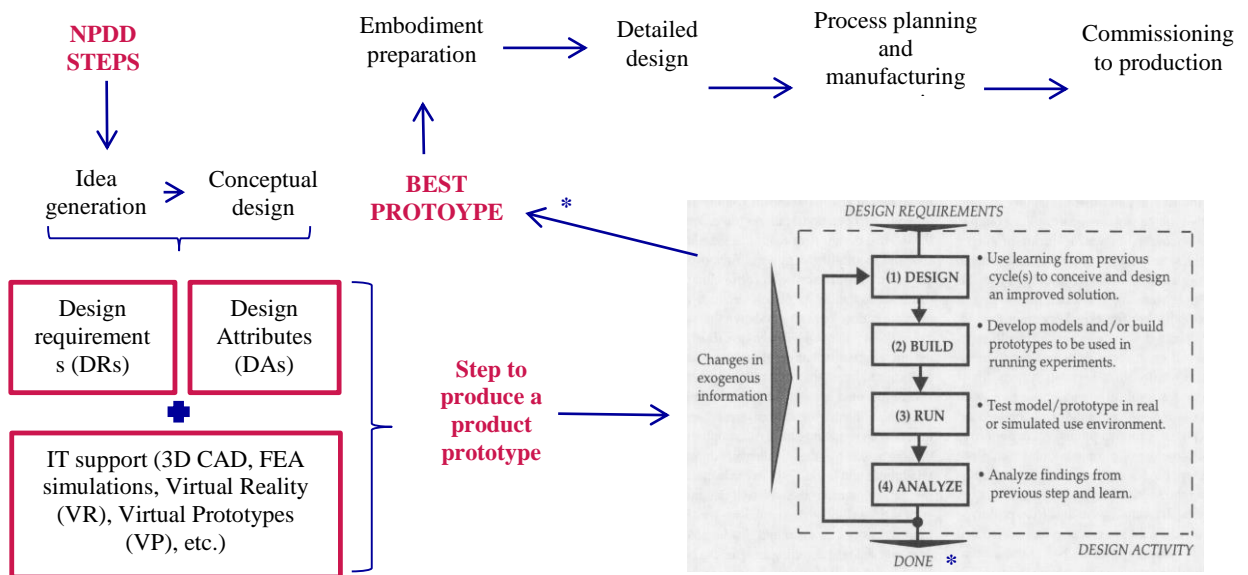


Figure 95 New product development process stages to develop a new prototype.¹

¹ As defined by Polydoros et al. (2011)¹ prototype is defined as an artefact incorporating characteristics of the new product under development that enables designers to test various aspects of their ideas before committing themselves to the expense and risks of producing commercial quantities (hard tooling).

As reported by Ingole et al. (2009)², the key stage to transform an idea to a prototype is the definition of design requirements and design attributes. As design, attributes Polydoros et al. (2011)¹ define all the engineering and non-engineering parameter used to design the final product^j. For each attribute a series of requirements are defined to generate a prototype able to perform in the desired way. During this initial NPDD step, suitable prototyping strategies to reduce time and cost of the product development are selected. In general, two prototypes strategies can be selected; virtual or physical prototyping.¹ Firstly, the list of required attributes is generated. A prototyping strategy (design stage) is elected, the next stage in the NPDD process is to build a physical/virtual apparatus used to conduct test (stage three). The results gathered from the testing stage are then analysed to determine strengths and issues identified in the design stage. During the design stage optimal but also non-optimal design solutions can be generated; the testing stage is therefore used to generate information to identify opportunities for improving the product design and development. The fourth stage of the NPDD process is an iterative design improvement approach where the detection of design errors, the analysis and elimination of those errors are repeated until the prototype functioning is aligned with the attributes defined during the initial design stage (best prototype).³ After this stage the design is finalised and the prototype is ready for manufacturing.

^j A list of 17 attributes is defined by Polydoros et al. (2011)¹; aesthetics, capability, durability, ergonomics, interchangeability, maintainability, manufacturability, marketability, performance, reliability, remanufacturability, safety, shedulability, serviceability, simplicity, testability, transportability. The order of importance of this attribute is defined during the idea generation and conceptual design in presence of a team of engineers/non-engineers people that consider engineering attributes, managerial issues and other general issues (ex. Environmental considerations).

The CFD prototyping procedure was following the 4-stage procedure reported in Figure 96.

A series of prototype modification were made over the course of three years of product development between Alconbury Weston and the partner involved in Remedies App B to get a versatile filtration, washing and drying dead end filtration unit capable of isolating API's slurries in manual, semi-automated and continuous modes.

The design stage was conducted in collaboration between Astra Zeneca (Dr. Elizabeth Meehan and Dr. Claire Macleod), Strathclyde University (Dr. Chris Price and Sara Ottoboni), Alconbury Weston (Paul Firth, Dr. Christopher Steven, Dr. Simon Coleman, Richard Sutherland and Alastair Barton) with minor input from the other partners in Remedies App B.

The commissioning of the initial version of the prototype (CFD20) was undertaken in 2016 at the Astra Zeneca laboratories. The role of Sara Ottoboni, Chris Price and the Astra Zeneca team (Dr. Elizabeth Meehan, Dr. Claire Macleod and Sadie Finn) was to test the first prototype unit to identify design flaws and to suggest improvements.



Figure 96 AWL CFD20 prototype.

During the first set of test a series of design problematics were evaluated during the testing process:

- Some components used in the carousel lacked solvent compatibility: to maintain the seal of the carousel head when the pressure is applied during filtration and washing a series of O-rings where used on top of each port. The requirements for this component were flexibility, good mechanical properties to maintain sealing after multiple carousel head opening-closing cycles, as well as good solvent resistance. The first O-rings selected were made from EPDM (ethylene-propylene-diene monomer elastomer), a material that presents good resistance to hot water and steam, detergents, many polar solvents and many diluted acids and chemicals.

However, during the first set of tests those O-rings showed chemical incompatibility with the solvents used during the filtration and washing process causing the loss of seal. After a series of investigations, new O-rings were selected for their wider chemical compatibility properties (FEP O-rings). Similar issues were encountered for the wash pumps selected to convoy the wash solvents from the wash feed vessels to the carousel head

- The software used to control the carousel operability required further development: the initial software was coupled with another software tool used for data recording (Pharma MV from Perceptive Engineering). A series of software modification were made to couple the two software together.

After a series of component replacements and unit modifications, the unit was delivered to the CMAC laboratory where the University of Strathclyde team (Sara Ottoboni, Dr. Christopher Steven and Dr. Chris Price) in collaboration with Alconbury Weston team (Alastair Barton, Paul Firth and Richard Sutherland) further tested the CFD20.

During 2017 a series of critical implementations were made, where the unit was significantly modified to create the CFD25:

- To stop filtration and washing at dryland point a camera system was used. Further details of this innovation are reported in this chapter. Testing the unit with a series of API's presenting peculiar filterability issues the development of another innovation was made. To isolate fast/slow settling slurries two different filtration modes were developed. Settling mode is used to filter fast settling slurry. This

method is explained in this chapter. The non-settling mode however, is used to filter slow settling slurries

- To prevent cake surface disturbance during wash solvent dispensing a series of atomizers were inserted on top of the washing ports. The atomizers selected spray the wash solvent on the port walls and dispensing the wash solvent on top of the cake surface without damaging its surface
- Three operational modes were developed to isolate API's slurry in fully manual mode, semi-automated (optimization) and continuous (production) mode; the three modes are described later in this chapter
- The unit was developed as a process development tool to allow the investigation of the best isolation strategy for API's. In order to collect the filtrate removed during each stage of the isolation separately, a series of filtrate receivers were connected beneath the carousel ports. This allowed offline characterization of the filtrates to determine the extent of purity achieved during each isolation step
- The implementation of an ejection system to reliably remove the dry/partially dry cake in port 10. The ejector is a piston which mechanically ejects the cake removing the material completely from port 10
- The implementation of a heating system to pre-heat the air or nitrogen that flows through the cake during the drying process to increase drying efficiency.

A series of tests were performed by the Strathclyde University team to evaluate the unit's operability:

- Test the two prototype systems with pure solvent to check for leaks, calibrate and verify the calibration of pumps, verify the liquid transfer through the different components, evaluate sealing efficiency, etc.; these preliminary investigations are not reported in this chapter
- Test the two prototype systems with non-toxic compounds, such as potassium l-tartrate and / or sodium bicarbonate to evaluate the efficiency of camera to track the filtration and washing process and to stop the filtration and washing steps at dryland, verify the slurry transfer through the different components etc.; these investigations are not reported in this chapter
- Compare the CFD20 unit's performance against a modified Biotage VacMaster unit, designed to implement manual best practice at lab scale. To verify the efficiency of the prototype to purify the cake a dye was used.
- Test the CFD25 with an API model compound in presence of related impurities to design and determine the time required to design the isolation strategy for the API selected.

In this work, investigation about the reliability in using the CFD25 unit with compounds/slurry having different chemi-physical properties from paracetamol has been carried out.

In 2016/2017, the unit was tested with the following compounds:

- potassium l-tartrate that presents sharp PSD and smaller particle size compared to the micronized paracetamol (SMD equals to 57 μm and x_{50} of 41 μm)
- sodium bicarbonate that show intermediate particles size respect powder and special granular (SMD equals to 149 μm and x_{50} of 159 μm).

By using paracetamol and these two other compounds, the CFD20 was improved to produce the CFD25.

In 2017, two proprietary Astra Zeneca compounds were selected to test the unit with real manufacturing challenges: AZ200, presenting big size and peculiar cake shrinking effect during deliquoring and drying, and AZ400, presenting filterability issues due to its very slow sedimentation. In case of non-settling particles, the camera is not able to visualize the liquid and cake level to halt filtration to dryland. In collaboration with AWL, a new isolation mode named non-settling mode was developed to address this problem. In this mode the operator runs a set of preliminary test by using the non-settling calibration method available in the CFD25. Using this calibration two cake volume measurements carried using two different slurry volume can be obtained at the driving force selected for the optimization/production mode experiments. After the calibration the experiments can be run in non-settling mode and the unit is able to automatically recognize the cake volume to stop filtration and washing to dryland.

The unit was also used in combination with two continuous crystallization units (MSMPR and Rattlesnake) to crystallize, purify and isolate a Thomas Swann proprietary compound. During this experiment the operation boundary of the CFD25 were observed. Slurry transfer issues from the feed tank to the carousel head were encountered in case of slurry

concentration higher than 40-50% w/w. Furthermore, issues related with low concentrated slurries were observed. In case of slurries with solid load lower than 10%w/w, the minimum cake volume required from the camera to recognize the presence of solid bed in the filtration chamber was not met. The system for this specific case requires multiple doses to approach the minimum cake volume necessary to run the isolation (minimum 12mL that correspond to the minimum height where the cake can be seen from the camera).

The CFD25 was also used during another CMAC microfactory campaign in 2017, where synthesis and crystallization processes were connected to the CFD25 unit to synthesize, crystallize and isolate paracetamol form I. The selected approach to synthesize the paracetamol relayed on the reaction of 4-aminophenol with acetic anhydride in isopropanol to produce paracetamol and acetic acid and acetaminophen acetate as by-product.

In 2018, the unit was physically coupled with a continuous crystallization system implemented with periodic slurry discharge. In this system, a cooling antisolvent crystallization combined with spherical agglomeration of lovastatin was used to build a fumehood size lovastatin crystallization-spherical agglomeration and isolation microfactory. The issues affecting the processability of the slurry with the CFD25 were:

- Low solid load, approximately 1% w/w
- Instability of particles during the process: spherical agglomerated particles were too fragile with consequent breakage during the isolation process

- Slurry degradation during stockage.

To address the inconsistency of slurry, in collaboration with AWL, a simplified isolation mode was developed. The mode, called “lovastatin”, consists in a filtration and multiple washing stages where the camera is disabled and filtration is controlled and stopped to breakthrough by a pre-set time. The number of doses and the cake height are estimated by the operator and pre-set before the experiment, as well as the drying time and drying gas temperature. This new method allowed to run the CFD25 in continuous mode for 4-6h producing semi-dried spherical lovastatin with minimal particles size variation respect to the input material. Moreover, it was possible to isolate slurry with solid load lower than 10%w/w.

7.2 Background

The pharmaceutical industry is in the process of embracing continuous manufacturing of active pharmaceutical ingredients (APIs) in order to reduce production cost, improve manufacturing flexibility, reduce infrastructure cost to improve consistency of API quality critical attributes and to reduce manufacturing lead time (from typically 6 months to 10 days⁴) and to improve sustainability by reducing waste generation. This is taking place in part, as a response to initiatives promoted by the United States Food and Drug Administration (FDA), which in 2003 began to encourage the industry to develop new innovative processing methods to improve product consistency.⁵⁻⁷ A number of innovations have been reported to transition synthesis, crystallization and secondary processes from batch to continuous operations. However, both API, and intermediate isolations are still almost exclusively performed batch wise. There have been very few

attempts to develop equipment to address the gap of continuous pharmaceutical isolation.⁸⁻
¹⁸ Few examples of small-scale continuous isolation equipment have been commercialized. The Steadfast rotary drum filter is a cross-flow isolation unit principally designed for clarification of suspensions from bioprocessing where the desired product is in the solution phase and the solid phase is a waste stream (Figure 97).

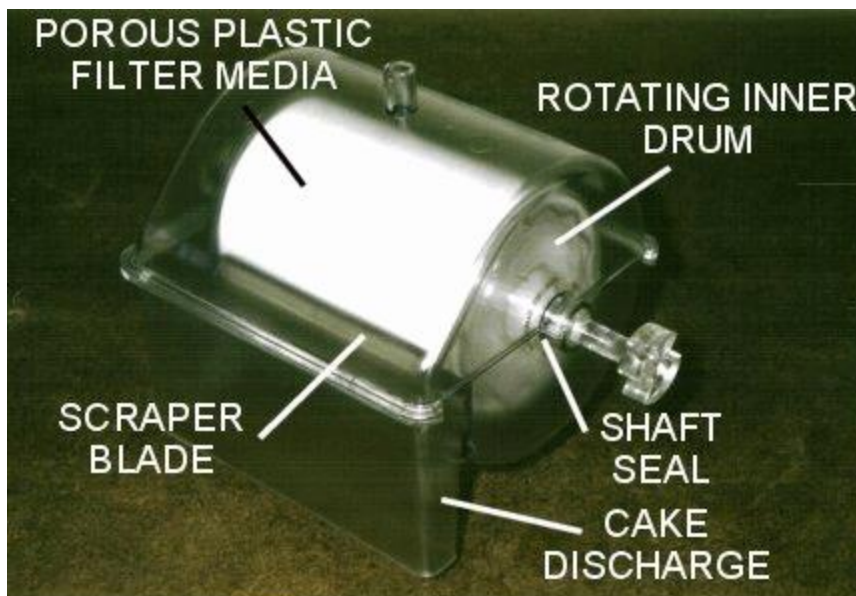


Figure 97 Filtration component of the Steadfast rotary drum filter.¹⁹

The capacity is around 3 litres per minute of slurry.¹⁰⁻¹¹ In 2010, researchers at MIT developed a small-scale continuous Linear Motion Pharmaceutical Filtration Module, which ran for 250 hours and was capable of processing 1 L of mother liquor per hour, corresponding to 100g of API per hour.¹² In 2011 researchers at Pfizer proposed a new filter and dryer prototype, which they termed the D&M continuous filter and dryer (Figure 98).

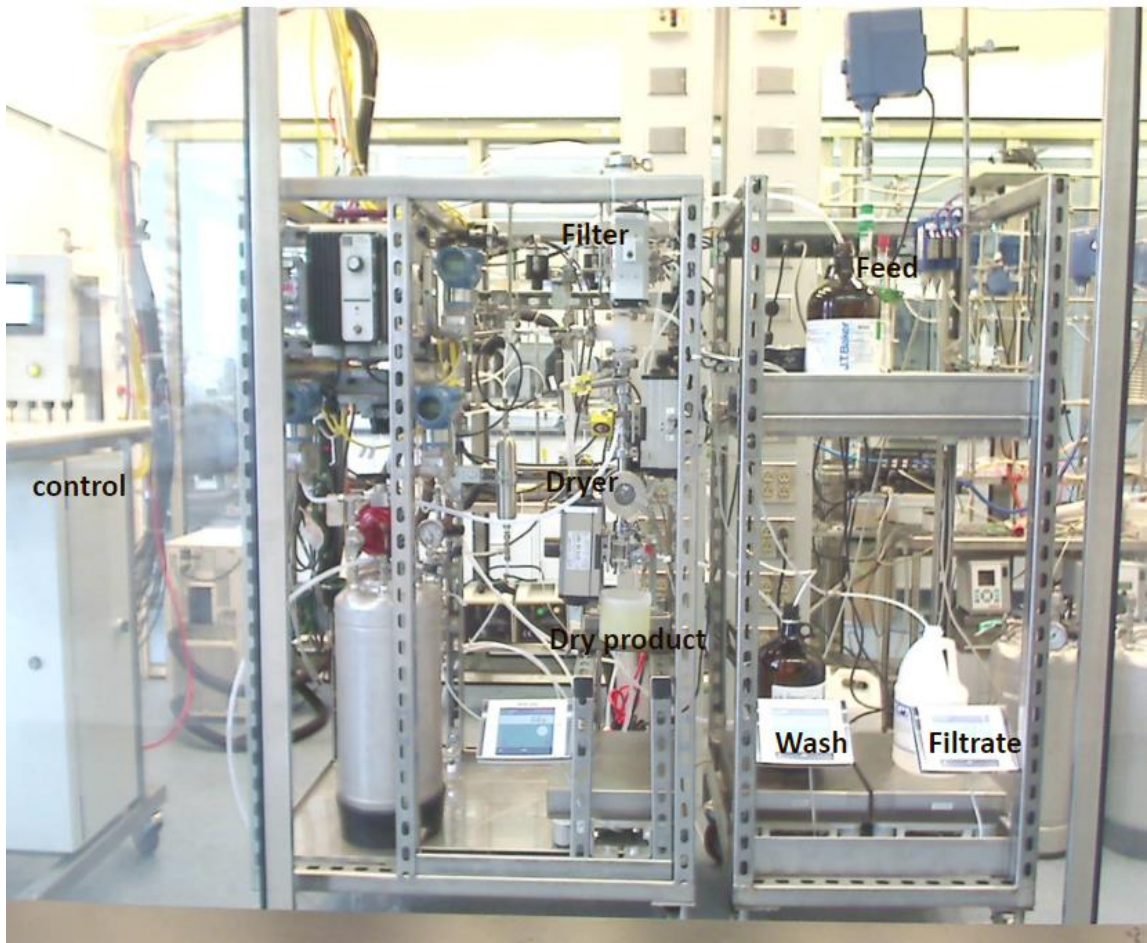


Figure 98 D&M filter dryer unit.⁸

It filters small aliquots of slurry (15-30 mL per aliquot), using a 3-way valve. The Pfizer prototype was able to process approximately 1g of filter cake per minute or 1.4 kg/day.¹³ Moving to large-scale continuous isolation units; in 2015 BHS marketed a Continuous Indexing Vacuum Belt filter (Figure 99).

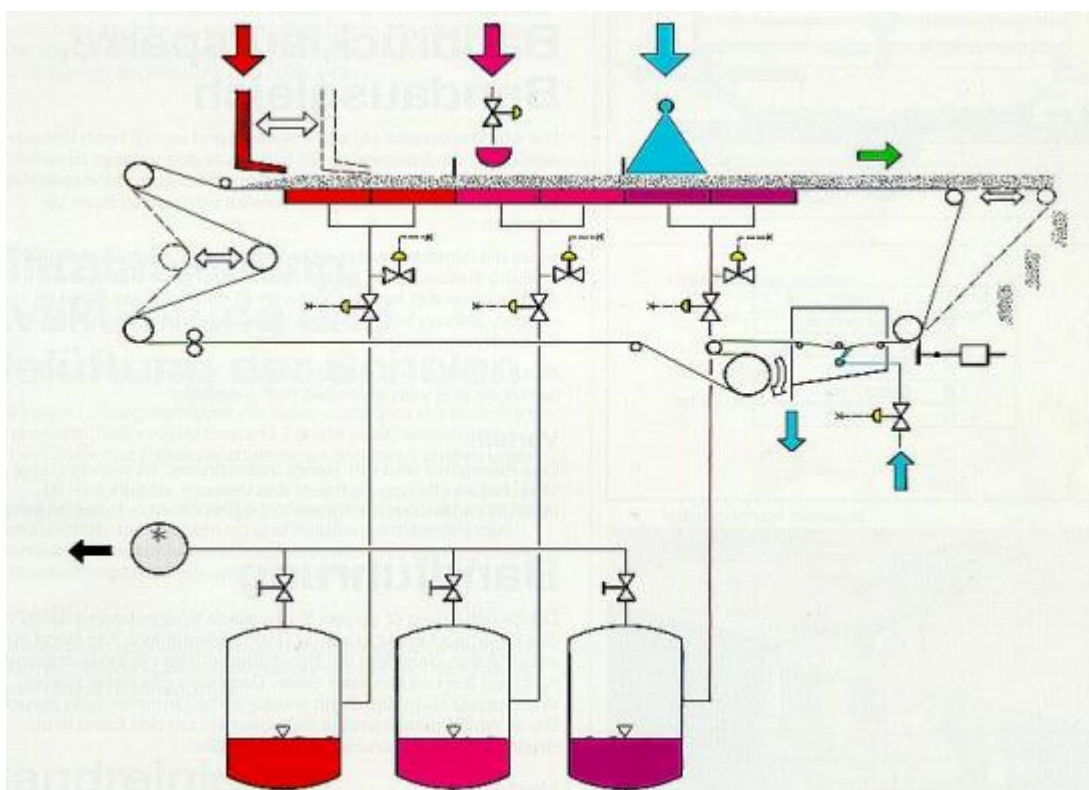


Figure 99 Schematic representation of the BHS belt filter.²⁰

This comprised a vacuum filter with either co- or counter-current washing also with vacuum, it also has convection, pressing and steam drying capabilities, and is reported to filter cake of 5 to 150 mm in thickness and process up to 85 kg/hr of solid crystalline material with cake moisture target of 45%.¹⁴

None of the commercial or prototype continuous isolation units combine dead end filtration^(k) with washing and drying capabilities.

^(k) Dead end filtration is the most common method of filtration where the slurry, with known composition is placed in a chamber, with filter medium at the base, a pressure difference is established across the medium to drive the liquid phase through the medium. Consequently, a cake of solid particles is formed on the top of the medium as the filtrate passes through and its thickness increases with time until eventually the filter cake is harvested. Cross flow filtration is the other method of filtration. Cross flow filtration is a technique for increasing the solids loading of a slurry by taking off a particle free stream. Typical cross flow filters

The REMEDIES project²¹ aims to address this gap in collaboration with Alconbury Weston Ltd by developing a dead end isolation unit, which can operate from lab scale to small-scale manufacture. The unit performs filtration, washing and drying in a fully automated, semi-continuous manner.

Common practice in filter cake washing is to use at least three cake volumes of wash solvent to remove mother liquor and the associated impurities of synthesis. This typically amounts to 5 to 7 mL of solvent per gram of API produced.²² One of the aims of this work is to improve washing efficiency and consequently to minimize solvent use to improve environmental sustainability in API isolation, to improve product purity and reduce manufacturing costs. The main target of continuous isolation is to reduce processing time and cost⁷¹⁰ whilst minimizing negative impacts on API particle physical properties in order to deliver API that is optimal for final processing into drug products, for example eliminating the need for a particle breakage step after isolation.

Product purity and particle size distribution (PSD) are the key critical quality attributes to address during isolation. A major focus of pharmaceutical crystallization research is to generate a suspension of crystals of the required size and purity. However, the challenge of maintaining these particle properties unchanged during the downstream isolation is less

comprise an inner filter encapsulated in an outer cylinder. The thickening process starts when slurry is conveyed into the outer cylinder the rate of flow from the source vessel is sufficient that there is always an overflow back to the source vessel and the flow keeps the particles suspended. A pressure difference is established between the core of the filter and the outer annular region, this causes filtrate to flow through the medium to be collected as clarified filtrate leading to an increase in the solids loading of the circulating slurry.

well researched. In fact, API isolation by filtration, washing and drying poses significant challenges; there is risk of breaking or granulating the crystals, modifying the size distribution; it is also possible to precipitate dissolved product or impurities during washing where the wash solvent acts as an antisolvent. Without effective washing, impurities which are in solution in any filtrate, which is retained in the filter cake, are incorporated in the product during drying, reducing purity. Any dissolved solute is also deposited and tends to promote granulation, changing the product particle size distribution.²³ A washing step is usually employed to minimize these problems.²⁴ Different process and physico-chemical parameters can affect the final product attributes such as; the feed suspension viscosity and density, particle size distribution suspended particle loading,²⁵⁻³⁰ the chemical character of impurities,³¹ the interactions between solvents during washing and drying.³²⁻³⁴ The point at which filtration is halted (dryland or breakthrough), the pressure driving force for both filtration and washing, etc. All of these processes and material attributes can affect the product particle attributes (PSD, aspect ratio, morphology and purity), filtration rate, efficiency of washing and propensity for filter blockage.³⁵⁻³⁹ Equipment design affects filtration performance. The size and geometry of the filtration chamber and the slurry feed system should favor the formation of a uniform cake whilst minimizing wall effects.³⁵ The filter medium should retain product particles without being prone to clogging and the negative effect of filter cake heel (residual solids left on the filter medium from previous filtrations should be minimized).⁴¹ Drying is influenced by a number of particle and process properties, such as; particle size distribution and shape, drying gas flow rate through the cake, residual solvent content and composition, heat applied and the design of the dryer. Many

researchers have investigated possible causes of agglomeration during drying. Common hypotheses suggest that, if the solute has a high solubility in the wash solvent formation of solid bridges during solvent evaporation is the dominant cause of granule formation. Molecular interaction between the solvent and specific function groups exposed on crystal surfaces can promote preferential solvent retention on specific (wetable) faces. During drying material dissolved in this solvent film recrystallizes forming particle-particle bridges “sintering” the crystals together. Dryer geometry, impeller design and mixing rate can significantly affect mixing patterns and change the size of the dried product. Agitators and orbiting elements may induce attrition and breakage through particle collisions resulting in alterations in particle size and shape.⁴¹ Agitation during drying can also be responsible of lump formation, this is especially significant if agitation is applied at a critical liquid to solid ratio known as the sticky point. The sticky point is in fact a small region of composition where there is sufficient solvent to form liquid bridges at contact points between particles but not sufficient to lubricate particle movement. Agitation in this condition can result in the formation of large “dough balls” and for this reason best practice is to avoid continuous or intensive agitation until the sticky point is passed.⁴¹ The use of vacuum to reduce the solvent boiling point or pressure to drive nitrogen through the cake to accelerate drying can also affect the final PSD and morphology.⁴²⁻⁴³

In order to evaluate the effectiveness of the AWL CFD 20 in isolating API without modifying key particle attributes a series of experiments were performed to compare the unit’s performance against a modified Biotage VacMaster unit, designed to implement manual best practice at lab scale.

Three success criteria were used to compare the CFD20 prototype's performance with manual best practice exemplified in the modified Biotage VacMaster unit.

- a) Achieve comparable or better purity than can be achieved using Biotage unit: To evaluate how efficiently the prototype removes impurities a dye, patent blue V was used
- b) Maintain the PSD of the input particles: Paracetamol was selected as model compound to test the unit, two different API grades, micronized and granular particles were used to evaluate the effect of PSD on filtration and washing and the effect of these processes on the resulting particles
- c) Translate the simplicity of process operation and flexibility of the Biotage unit to an automated continuous isolation unit (for example offer the capability to halt filtration at dryland or at breakthrough).

These comparisons of filtration and washing performance drove further improvements, which have been embodied in the subsequent CFD unit (AWL CFD25).

In order to assess the capabilities of the CFD25 to isolate materials that are more challenging a suspension of crystals in a mother liquor containing structurally related API impurities was prepared. A d-optimal design of experiments was used to investigate this multi-variate problem containing both qualitative and quantitative factors in order to minimize the number of experiments required to characterize the system. Slurry properties evaluated include solid concentration in the initial slurry, input particle size distribution and crystallization solvents properties. Two paracetamol grades were used, micronized and typical crystalline which replaced the granular material (details are reported in results

and discussions section). The decision of using micronized and powder (typical crystalline) derives from the results presented in chapter 6. To investigate washing strategy and wash performance in removing paracetamol related impurities such as acetanilide and metacetamol, the effect of different crystallization and wash solvents and wash solvent quantity were considered. The interaction between solvents during washing and drying were investigated using a series of crystallization and wash solvents. Slurries were made using three commonly used crystallization solvents which were suitable for paracetamol crystallization,⁴⁴⁻⁴⁵ ethanol, isopropanol and isoamyl alcohol. These crystallization solvents were selected to investigate the role of solvent viscosity, solubility and washing mechanism on the final dried product. For wash solvents, n-heptane and isopropyl acetate were selected based on their miscibility with the mother liquors to facilitate both diffusion and dilution washing mechanisms; in addition, paracetamol is rather soluble in isopropyl acetate compared to its solubility in heptane. In addition, n-dodecane was selected as immiscible wash solvent to evaluate physical displacement washing without miscibility. Those solvents were selected from the list of wash solvents presented in chapter 6: n-heptane and n-dodecane were selected because of their capability to reduce agglomeration and form few soft agglomerates. The wash strategy was design to minimize impurity and API precipitation during washing. A strategy to evaluate “antisolvent effects” during washing was developed.

Cake resistance, media resistance, filtration flow rate and washing volume relative to cake volume were determined using the CFD’s camera vision system, which was also used to halt filtration at dryland and to facilitate data recording. Cake and filtrate were analyzed

to quantify the purity achieved by HPLC. Isolated product was analyzed to characterize mechanical properties including the agglomerate brittleness index - ABI index,³² the extent of agglomeration⁴⁶ and PSD. Proton nuclear magnetic resonance (¹H-NMR) was used to determine cake washing and drying efficiency. The analytical procedure followed to analyse the isolated material and filtrate is presented in section 6.6 of chapter 6.

7.3 Materials and methods

7.3.1 Materials

Paracetamol was selected as a representative test compound with characteristics typical of APIs. It is commercially available, as are many of its impurities of synthesis. Three size distribution (granular, typical crystalline and micronized) were selected to challenge different aspects of filtration, washing and drying. The granular material (Mallinckrodt Inc., batch 161713J561) represents a challenge for uniform particle suspension and transfer into the filter and exhibits very rapid settling and filtration. The micronized material (Mallinckrodt, Inc., batch 042213E407) settles and filters slowly, has a large wetted surface area to wash and is more challenging to dry than the granular material. The intermediate grade was used to mimic a typical crystalline material (Mallinckrodt Inc., batch 637514D001).

Wash performance and cake purity were evaluated in the first part of the work by using a solvent soluble dye, Patent Blue V sodium salt (Sigma Aldrich, LOT: BCBP1872V). The dye aids visualization of the filtration and washing process as well as being readily quantified spectroscopically. Patent Blue V was selected to avoid spectral overlap with the main paracetamol absorption peak at 243nm. For the second part of the work two structurally related compounds of paracetamol were used, acetanilide and metacetamol,

both are by-products of paracetamol synthesis⁴⁷ and if present at the end of the synthesis, they could affect the crystallization process.⁴⁸⁻⁵⁰ HPLC was used to determine purity of the isolated product. The eluents contained water (Water, ultrapure, HPLC Grade, Alfa Aesar) and methanol (Methanol, ultrapure, HPLC Grade, 99.8+%, Alfa Aesar) the methanol was also used as diluent for some samples. Dimethyl sulphoxide-d (extent of deuteration 99.8% for NMR spectroscopy, VWR) was used as NMR solvent.

During the initial experiments in which the AWL CFD20 was compared with the Biotage unit Ethanol (Absolute, $\geq 99.8\%$, Sigma Aldrich) was used to create the feed suspension. Millipure water from CMAC labs (Milli-Q; water temperature=23.2°C, TOC=2ppb) was selected as wash solvent due to paracetamol's relatively low aqueous solubility and because Patent Blue V dye is very soluble in in water, as reported by Newton et al.⁵¹ To investigate efficiency of AWL CFD25 to isolate a "process real slurry" a series of three crystallization solvents were used: ethanol (purity $\geq 99.8\%$ (GC), from Sigma Aldrich), isopropanol (IPA) (purity $\geq 99.5\%$ (GC), from Sigma Aldrich) and isoamyl alcohol, (purity $\geq 99.5\%$ (GC), from Sigma Aldrich). As wash solvent, n-heptane (purity 99% from Alfa Aesar), isopropyl acetate (purity 99+ % from Alfa Aesar) and n-dodecane (purity 99%, from Alfa Aesar) were selected. The selected solvents are highly flammable. A series of risks are reported in solvents SDS, such as toxicity by ingestion, inhalation, skin and eyes irritation. Isopropanol, isoamyl alcohol, n-heptane and isopropyl acetate also show target organ toxicity. n-heptane is toxic for the aquatic life.

7.3.2 Raw material characterisation

The particle size distribution of micronized, typical crystalline and granular paracetamol was determined by image analysis (QICPIC particle size analysis, Sympatec, QICPIC Rodos/L; trigger conditions: feed pressure 1bar, VIBRI feeder, feed rate 25%, gap width 1.5mm). The solubility of paracetamol crystallization and wash solvents taken from the literature,⁵² when available, compared with predictions made using *COSMOTerm* (COSMOlogic GmbH & Co. KG) and confirmed experimentally by gravimetric approach using an incubator (Incubator S160D, Stuart, Cole-Parmer) on a multi-position stirrer plate.

To quantify impurity content in filter cake and filtrate, calibration curves for pure paracetamol, acetanilide, metacetamol and orthocetamol (an impurity present in the raw paracetamol) HPLC method was used.

To investigate the potential for “anti-solvent effects” to occur during washing a screening procedure to identify appropriate crystallization-wash solvent mixture compositions was conducted. For all the combinations of crystallization and wash solvents screening was conducted by contacting paracetamol saturated primary solvent with each wash solvent analyzing different ratio of the solvent pairings: 50-50, 40-60, 30-70, 20-80, 10-90 and 100% pure wash solvent. For the combination of isopropanol and n-dodecane 60% crystallization solvent and 40% of wash solvent was also tested. Compositions, which resulted in product being precipitated, were rejected.

7.3.3 Slurry preparation: comparison AWL CFD20 with Biotage unit

An appropriate concentration of Patent Blue V dye was selected based on its absorbance maximum determined using UV-vis spectrometry (Variant Cary 5000, Mettler Toledo).

Paracetamol particle suspensions were prepared by dissolving Patent Blue V dye in ethanol at a concentration of 28.6mg/L. Paracetamol was then added in two portions; the first to form a saturated ethanolic solution at 20°C, the second portion was then added without risk of dissolution in order to form a suspension with a known particle size distribution which would ultimately form the filter cake. The combined paracetamol mass per 50 mL aliquot of ethanol was 19.34g. Wash solvent was produced by preparing a solution of paracetamol in water, which was saturated at 10°C to form a slightly undersaturated wash solution at 20°C. Mother liquor density and viscosity were measured and compared with pure ethanol values (GV500 viscometer, Hydramotion).⁵³

7.3.4 Slurry preparation: Test AWL CFD25 with structurally related paracetamol compounds

Suspensions containing dissolved acetanilide and metacetamol the representative impurities of synthesis were prepared as a concentration of 2% by mass of each impurity. The required mass of each impurity was weighted and dissolved fully in the crystallization solvent prior to adding any paracetamol. The amount of paracetamol required to saturate the solvent solution was then added and dissolved. This two-stage addition of paracetamol was crucial to avoid partial dissolution of the cake forming particles affecting the filter cake properties. The last step in suspension preparation was to add the paracetamol required to form the cake, this paracetamol represents the solid load, calculated in % by mass.

To avoid “antisolvent effect” leading to dissolved API being precipitated during the first wash step the first stage wash was prepared using a mixture of pure crystallization and wash solvents. The composition was selected based on the wash solvent screening methodology outlined in the raw materials characterization section. The second washing step was conducted using pure wash solvent. In each instance, the wash solvent quantity was based on the cake volume and the criteria set up in the experimental design.

7.3.5 Biotage manual filtration system overview

A modified Biotage VacMaster and a V850 vacuum controller (BÜCHI) was used to filter and wash the paracetamol suspensions using manual best practice.

The final wash was followed by cake deliquoring after which each of the collected filtrates was weighed, their volumes recorded and samples were taken to quantify the Patent Blue V dye spectroscopically.

7.3.6 CFD20 and 25 continuous filtration, washing and drying system overview

The procedure of isolation followed during the experiments with the CFD20 and 25 are reported in the method chapter, isolation units section (chapter 4).

7.3.7 Experimental design: comparison AWL CFD20 with Biotage unit

Five sets of experiments were performed to investigate the effect of purity and particle breakage. Success criteria to be met were:

- Purity (API should be chemically stable with negligible residual solvent);
- Particle size (no breakage, granulation, dissolution or fines precipitation).

The wash solvent volume used during the experiments was 5 and 10mL, respectively equal to just less and almost double the cake volume. The effect of different filtration stopping conditions were investigated by stopping filtration to dryland and allowing it to continue to breakthrough to determine the effect of filtration strategy on washing and final cake purity^{1,54} Equivalent experiments were performed with Biotage and AWL CFD20. In the case of Biotage, data collection was performed manually, recording the quantity of filtrate collected against time. The CFD20 was controlled locally through a touchscreen HMI and PharmaMV software to collect process data in line and ejected isolated cake and filtrates were manually weighted (to verify consistency of the load cell data) and sampled.

For Biotage experiments, 50 mL slurry aliquots were prepared for each experiment to ensure a constant slurry solid loading. CFD20 filtration experiments were conducted automatically in optimization mode, while washing and drying were run in manual mode. A large aliquot of slurry was prepared to run experiments 2 and 4. Experiment 1 and 3 were performed to quantify the effect of halting filtration at breakthrough (Table 45).

Table 45 Experimental conditions.

Experiment code	Material
2 and 4	Micronised (M)

¹ The significance of the two filtration stopping conditions; dryland or breakthrough; arise from the tendency for cracks to form in filter cakes as a result of deliquoring. Halting the filtration at dry land ensures that the cake is fully saturated and makes cracking unlikely but retains impure mother liquor in all the inter-particulate pores Alternatively breakthrough occurs when the cake is deliquored sufficiently for air or nitrogen from above the cake to form bubbles on the low pressure side of the medium supporting the cake. In this case more of the impure mother liquor is removed but the cake is very likely to have cracks running all the way through the cake from top to bottom making subsequent washing much less effective.

1 and 3	Special granular (SG)
D	5mL wash solvent
E	10mL wash solvent
Parameter	Value
Dose	50mL
ΔP during filtration	800mbar
ΔP during wash 1	800mbar
ΔP during wash 2	800mbar
Hold time before washing	60s
Deliquor mode	Dryland (exp 2) Breakthrough (exp 3 and 4)
Wash mode	Dryland (exp 2) Breakthrough (exp 3 and 4)

7.3.8 Experimental design: test AWL CFD25 with structurally related paracetamol compounds

A design of experiment (DoE) approach was used to analyze this multifactorial problem minimizing the number of experiments to run and to maximize the number of results achievable. MODDE was selected as software for the DoE data analysis. Table 46 provides the description of the list of quantitative and qualitative factors used to generate the responses below listed. The selected factors and responses were selected to investigate the effect of solid load, raw material PSD, crystallization and wash solvent, wash solvent volume and drying time on final dried product; purity, PSD and solvent content.

Table 46 Design of experiment factors and responses selected to investigate a multivariable problem.

	Factors			
	Abbreviation	Units	Type	Settings
API solid load	API	w/w (%)	quantitative	15 to 25
PSD (grade)	PSD	-	qualitative	Micronised, powder
Isolation pressure	FP	mbar	quantitative	200 to 800
Crystallization solvent	Crys	-	qualitative	Ethanol, isopropanol, isoamyl alcohol
Wash solvent	Wash	-	qualitative	n-heptane, n-dodecane, isopropyl acetate
Volume of wash solvent^m	WV	volume ratio relative to cake volume	quantitative	2 to 4 ⁿ
Drying time	Dry	s	quantitative	180 to 600
Responses				
Cake volume after first filtration			mL	
First filtration flow rate			mL/s	
Cake resistance			m/kg	
Medium resistance			1/m	
X50			µm	

^m Wash solvent volume is automatically calculated by the camera vision software. Knowing the tapped density of paracetamol and cake volume after the filtration, the volume of wash solvent added corresponds to 1, 2 or 3 void volumes in the cake. Tapped density of micronized paracetamol corresponds to 0.46g/ml, while typically crystalline (named also powder) corresponds to 0.44g/ml.

ⁿ As suggested in chapter 6.

Mean diameter (xsv)	μm
LOD	%
Percentage wash solvent in MC	%
Percentage crystallization solvent in MC	%
Extent of agglomeration	%
ABI index	Ratio
First filtrate metacetamol concentration	$\mu\text{g/ml}$
First filtrate orthocetamol concentration	$\mu\text{g/ml}$
First filtrate acetanilide concentration	$\mu\text{g/ml}$
Second filtrate metacetamol concentration	$\mu\text{g/ml}$
Second filtrate orthocetamol concentration	$\mu\text{g/ml}$
Second filtrate acetanilide concentration	$\mu\text{g/ml}$
Third filtrate metacetamol concentration	$\mu\text{g/ml}$
Third filtrate orthocetamol concentration	$\mu\text{g/ml}$
Third filtrate acetanilide concentration	$\mu\text{g/ml}$
Cake orthocetamol concentration	$\mu\text{g/ml}$

7.3.9 Off-line filtrate and cake characterization techniques

Offline sample characterization follows a precise sequence to prevent destruction of material required for the further characterization, the sequence is:

- Cake resistance and media resistance³⁵⁻³⁷ and filtration flow rate. For Biotage experiments collected filtrate volume against time, cake height and mass of cake and filtrates were gathered manually. For the CFD20 data was collected using the HMI and Pharma MV software (Perceptive Engineering Limited), while for the

CFD25 data were collected using the on-board vision system software. Cake and filtrate masses were weighed at the end of each experiment (for CFD20 load cells provided mass of filtrate collected)

- To determine how effectively residual solvent has been removed a few mg of “wet” filter cake were collected at the end of the allocated drying time to determine by NMR the total residual solvent and to quantify individual solvent residues (percentage of crystallization and wash solvent)
- Cakes were dried to stable mass in vacuum oven (Gallenkamp) at 50°C and 20mbar as reduced pressure to determine solvent content (LOD %)
- The acetanilide and metacetamol content in filtrates and cake were determined using HPLC
- In experiments where Patent V Blue dye had been used as an impurity both cake and filtrate purity were analysed by UV-vis spectrometry. A zero/baseline correction was applied and 2mm path length cuvettes were used
- The extent and strength of agglomerates formed in both the Biotage and CFD20 equipment comparison methods are reported in the methods chapter, mechanical characterization analysis section
- The PSD of dried cake was measured using the same method used for the raw paracetamol characterization.

7.4 Results and discussions

7.4.1 Comparison AWL CFD20 with Biotage unit

7.4.1.1 *Operability comparison*

Key challenges encountered during manual isolation are:

- Suspending material uniformly to avoid decantation or incomplete recovery of solid material from the glassware (Figure 100).
- Transferring a representative sub-sample to a filtration chamber such that the solids loading of successive sub-samples where the first batch dosed from the bulk slurry contains significantly less product than the second and third doses of slurry processed (Figure 100)



Figure 100 (a) Uneven solids distribution after filtering successive batches of the same slurry (b) Particles and liquid left in a measuring cylinder after dispensing slurry and followed by repeated back transfers.

The CFD20 overcomes these challenges by automating the suspension sampling and using a vacuum transfer to a dosing vessel to load material into the filter. The slurry feed tank has an agitator geometry and baffles which favor uniform particle suspension. In order to dose the slurry and transfer it into the carousel a syringe connected to the slurry tank and the dosing vessel allow a defined and consistent slurry dosage. Free draining of the slurry charge vessel into port 1 results in an even distribution of solids within the glass filter tube. Material holdup is limited by the geometry of the slurry charge vessel. Consistent solid loadings were obtained as the slurry was constantly suspended throughout

dispensing. The variation in the solids content was typically 1.1% of the total solids content (Figure 101).



Figure 101 (a) the stirred slurry vessel, (b) the filtration unit with dosing vessel above and (c) the slurry dosing vessel.

- Halting filtration at an appropriate point: with manual equipment a precise observation combined with quick and consistent responses from the operator is required. With the CFD20, a vision system was used to determine the relative heights of the liquid phase and accumulated solid (cake). This data was processed in real time using the premise that when dryland is reached both the liquid and solid will report the same height (Figure 102).

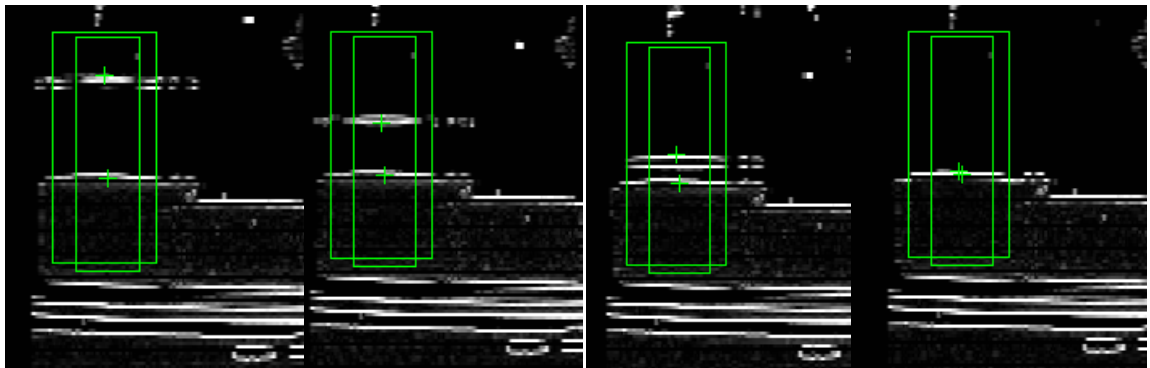


Figure 102 Series of processed camera images as filtration progresses. The green crosses indicate the levels of the liquid and solid that the camera has determined.

- Wash solvent transfer onto top of the cake without disturbing the cake surface: In manual best practise the wash solvent is slowly dispensed, running it down the sides of the filter tube using a disposable pipette to minimise cake disturbance. The CFD20 uses an atomizer spray nozzle to dispense droplets of around 100µm in diameter. The atomisation also allows the wash solvent to be dispensed across the whole surface of the cake and the filter tube walls, assisting in washing the whole cake volume efficiently.

7.4.1.2 *Filtration rate, cake and media resistance, loss on drying, purity and PSD*

The process of dead end filtration is described in the equation first formalized by Darcy, which in its most compact and widely used form (see Equation 93).^{37, 38}

Comparing the filtration performance of the approaches, the parameters derived from Darcy's law; specific cake resistance, media resistance and permeability all showed good agreement. Granular material where the large PSD favored rapid sedimentation producing a constant flow rate implied a negative or null slope of the t/V versus V plot. Special granular material (experiment 3) filters rapidly and the particles did not increase the resistance to filtrate flow above that of the filter medium because of the large pores in the cake.⁵⁵⁻⁵⁷

Table 47 Cake and filter medium resistance values calculated using Darcy's equation to analyse the data collected in experiments 2 and 4, conducted using the Biotage and CFD20 systems.

Unit	Experiment	Cake resistance (α , m/kg)	Media resistance (R_m , m ⁻¹)
Biotage	2d(micronized 2 x 5mL wash)	2.22E+09	2.06E+09
Biotage	2e(micronized 2 x 10mL wash)	2.19E+09	1.04E+08
CFD20	4d(micronized 2 x 5mL wash)	9.24E+09	-5.92E+09
CFD20	4e(micronized 2 x 10mL wash)	5.25E+09	-2.94E+09

Comparison of Biotage experiments 2d and 2e with CFD 4d and 4e experiments (Table 47) show the same order of cake resistance and permeability, although experiments 4d and 4e present slightly higher values. However, a big difference is observed in the media resistance. The filter media resistance in the Biotage unit is lower than that in the AWL experiments this is consistent with the different materials and construction of the different media.

Wash performance was evaluated by the removal of patent blue V from two very different filter cakes prepared from micronised and granular paracetamol. Using the extinction coefficient of the patent blue dye, the concentration in the mother liquors and each sample of spent wash solvent was calculated from the absorbance at 638nm. Combining this with the quantity of liquid recovered at each stage enabled the construction of Figure 103 and Figure 104, which show the effectiveness of successive washing steps. Overall, the

performance of the units was similar, although the Biotage unit was capable of removing slightly more of the surrogate impurity from the filter cake.

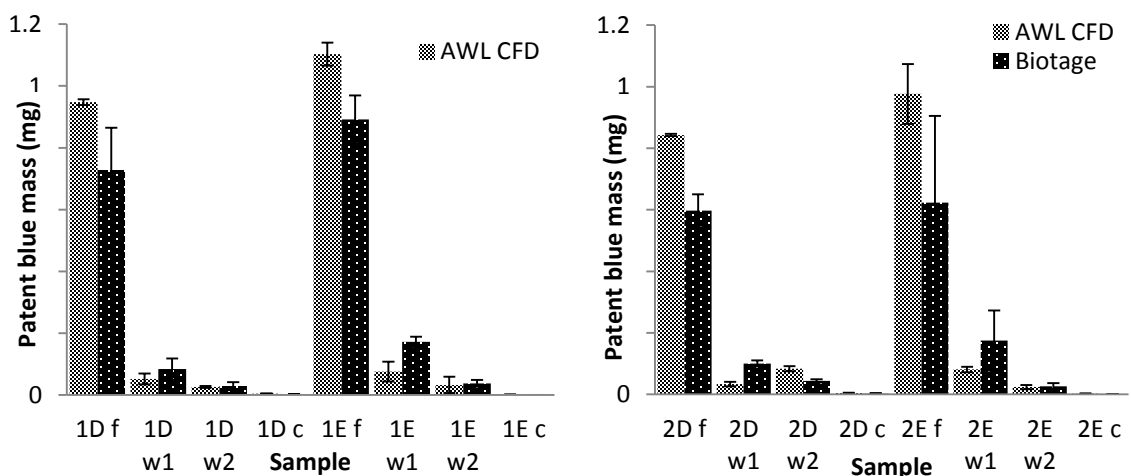


Figure 103 (a) Patent blue mass removal at each stage in the filtration and washing of special granular paracetamol (D = 2 x 5mL wash, E = 2 x 10 mL wash) f = filtrate, w1 = wash 1, w2 = wash 2, c = cake) (b) Patent blue mass removal at each stage in the filtration and washing of micronised paracetamol.

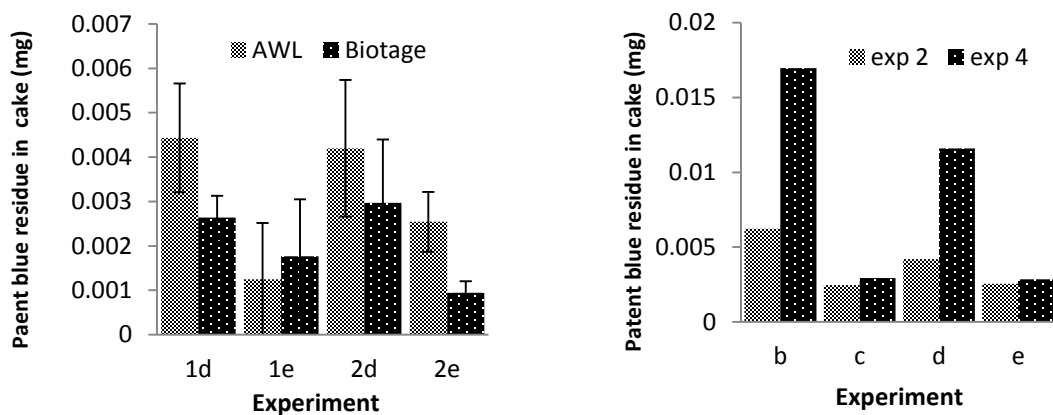


Figure 104 (a) Residual patent blue mass in filter cakes comparing the AWL CFD and Biotage. (1 = granular 2 = micronised, d = 2 x 5mL e = 2 x 10 mL) (b) Residual patent blue mass in filter cakes comparing filtration to dry-land (exp 2) and breakthrough (exp 4) for micronised paracetamol, b = 1 x 5mL, c = 1 x 10 mL, d = 2 x 5mL e = 2 x 10 mL).

The mass of dye in the filtrate is significantly higher than any other stage, as expected for filtration of a soluble impurity. 10mL washes (1E) are much more effective than 5ml

washes (1D).⁵⁴ Very little patent blue dye was left in either sample after drying. With the larger wash volume, less patent blue remained to be removed by the second wash, hence this removed less material.

Particle damage or agglomeration was assessed by sieving the isolated product (Figure 105); both platforms caused considerable changes in particle size after filtering and washing which is consistent with industrial experience. Micronized particles showed a substantial increase in size caused by agglomeration. Careful washing of the micronized powder caused some reduction in the extent of formation of very large agglomerates but the filtered washed and dried material did not recover the same particle size distribution as the feed material.

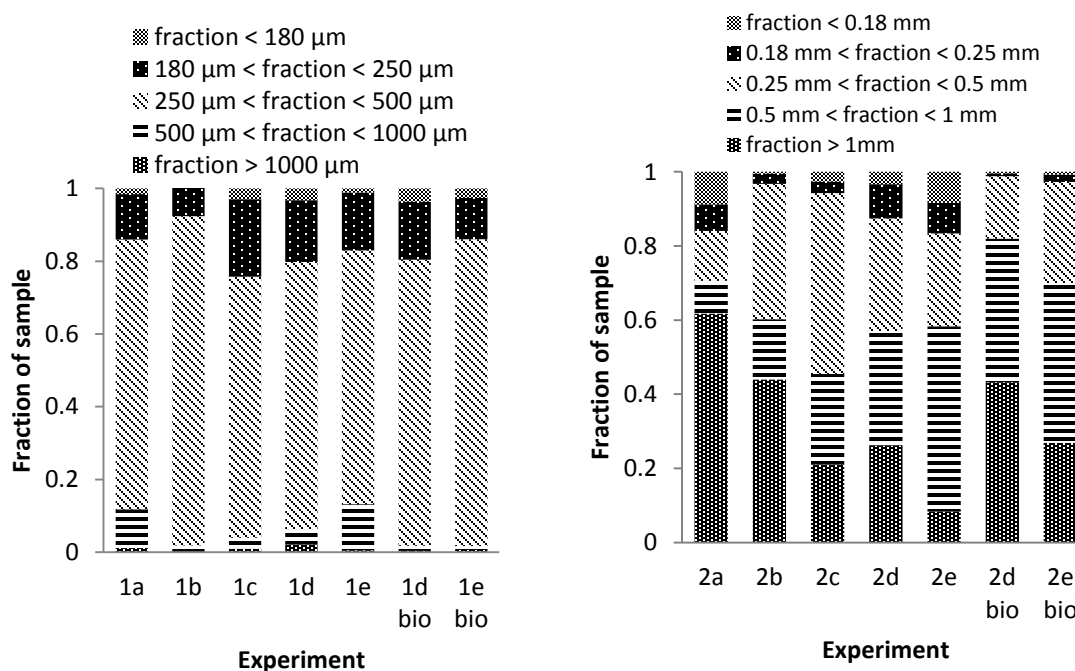


Figure 105(a granular paracetamol) AWL CFD20 (first five columns) and Biotage (last two columns) fractions collected from sieving analysis. (b micronized paracetamol) AWL CFD20 (first five columns) and Biotage (last two columns).

7.4.2 Test AWL CFD25 with structurally related paracetamol compounds

7.4.2.1 Antisolvent effect screening

In Table 48 the combination in volume ratio of crystallization and wash solvent that minimize API dissolution and avoid precipitation of finer and/or impurities during the first washing step.

Table 48 “Antisolvent screening” to determine suitable wash solvent mixture for washing 1 to prevent nucleation of particles from mother liquor and reduce paracetamol dissolution. In bold the ratio of crystallization solvent, while not in bold the ratio of wash solvent used.

	Heptane	n-dodecane	Isopropyl acetate
Ethanol	50-50% (v/v)	30-70% (v/v)	30-70% (v/v)
Isopropanol	50-50% (v/v)	60-40% (v/v)	10-90% (v/v)
Isoamyl alcohol	20-80% (v/v)	20-80% (v/v)	0-100% (v/v)

7.4.2.2 Effects on filtration

Three different summary fittings were analysed to determine parameters affecting; cake volume, filtrate flow rate during filtration in port 1 and cake resistance. Variation of cake volume (Figure 106) after filtration experiment in port 1 is mainly affected by

the density of solvent: in the case of isoamyl alcohol the final cake volume is higher with respect to the other crystallization solvents (ethanol, 0.789g/mL, isopropanol, 0.786g/mL and isoamyl alcohol, 0.81g/mL).

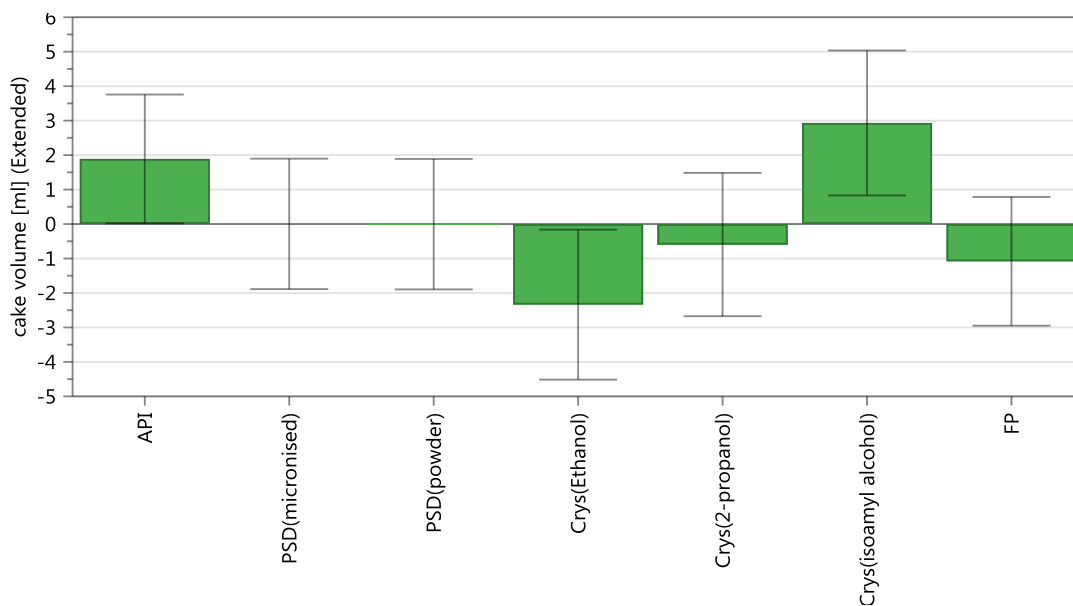


Figure 106 DoE variables that affect cake volume during filtration.

Filtrate flow rate (Figure 107) is another key parameter used to evaluate the processability of the slurry.²⁸ A major parameter that affects the filtrate flow rate is the viscosity of the mother liquor, as described from the equation of the volumetric flow rate:²⁵ faster flow rates are observed for less viscous solvents; (ethanol, 1.61cP, isopropanol, 2.88cP, isoamyl alcohol, 4.81cP). In addition, the grade of paracetamol from which the filter cake is formed affects the filtrate flow rate:²⁵ during filtration, finer particles tend to migrate towards the filter medium reducing the void volume and increasing the tortuosity of the cake adjacent to the filter medium. This phenomenon impacts cake resistance, resulting in a gradient of alpha along the axis of the cake,⁵⁷⁻⁵⁸ this also slows washing and deliquoring potentially causing higher residual solvent content in the deliquored cake. Increasing solid content in slurry and reducing driving force also reduce filtrate flow rate, causing longer filtration process.

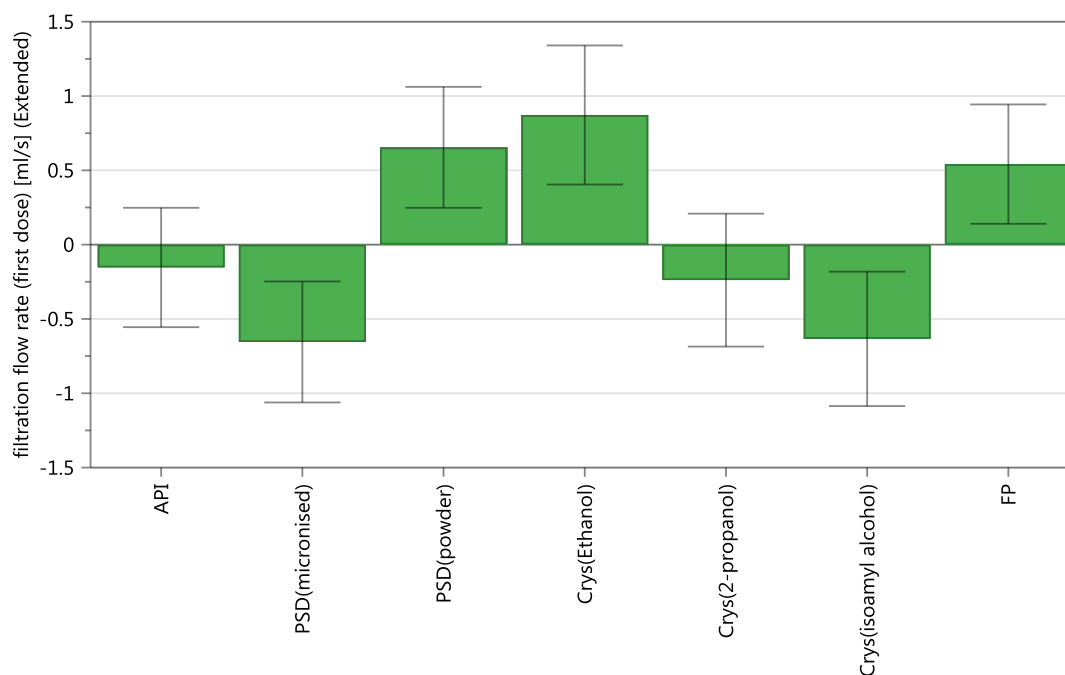


Figure 107 DoE variables that affect filtrate flow rate during filtration.

The selection of crystallization solvent potentially impacts crystal purity not just through the effectiveness of the crystallization but also of the washing step through its capability to solubilize impurities. However, a disadvantage choosing a solvent in which API related impurities are soluble implies that the API is likely to be quite soluble with a corresponding reduction of crystallization yield.²³ Of the three crystallization solvents evaluated in this study isoamyl alcohol appears to be the most promising candidate as crystallization solvent based on the quantity of API remaining in solution at 20°C (ethanol, 0.184g/g of solvent, isopropanol, 0.109g/g, isoamyl alcohol, 0.047g/g at 20°C) implying a high yield. However, analyzing the impurity concentration in the mother liquors, the capability of this solvent to remove impurities is lower than the other two solvents due to lower API and impurity solubility and higher viscosity. The increased viscosity makes it more difficult to remove the solvent from small capillaries in the cake, reducing the

efficiency in displacing mother liquor during washing.²³ As suggested in previous research, the viscosity of mother liquor and wash solvent should be similar to promote good displacement washing.⁵⁶ Those results are in agreements with the key finding reported in chapter 6.

7.4.2.3 *Effects on washing*

To investigate how the variables selected in the DoE affect washing, the effect of; wash driving force, wash solvent properties, quantity and the interaction between mother liquor and wash solvent were investigated with regard to the individual impurity concentrations in both filtrates and cake. Further links with the % of wash solvent relative to the overall residual solvent quantity after drying, the ABI index and the extent of agglomeration.

The residual moisture content composition, evaluated as relative percentage of residual mother liquor (Figure 108) and wash solvent (Figure 109) after drying, varies in relation to the boiling point of the wash solvent. n-dodecane has a high boiling point and when it is employed as a wash solvent it becomes the dominant factor, this effect is reversed when the more volatile solvents heptane and especially isopropyl acetate are used the other factors; solid loading and to the total volume of wash solvent used during washing shown the anticipated trends. In this regard, Figure 108 and Figure 109 are reciprocals of each other.

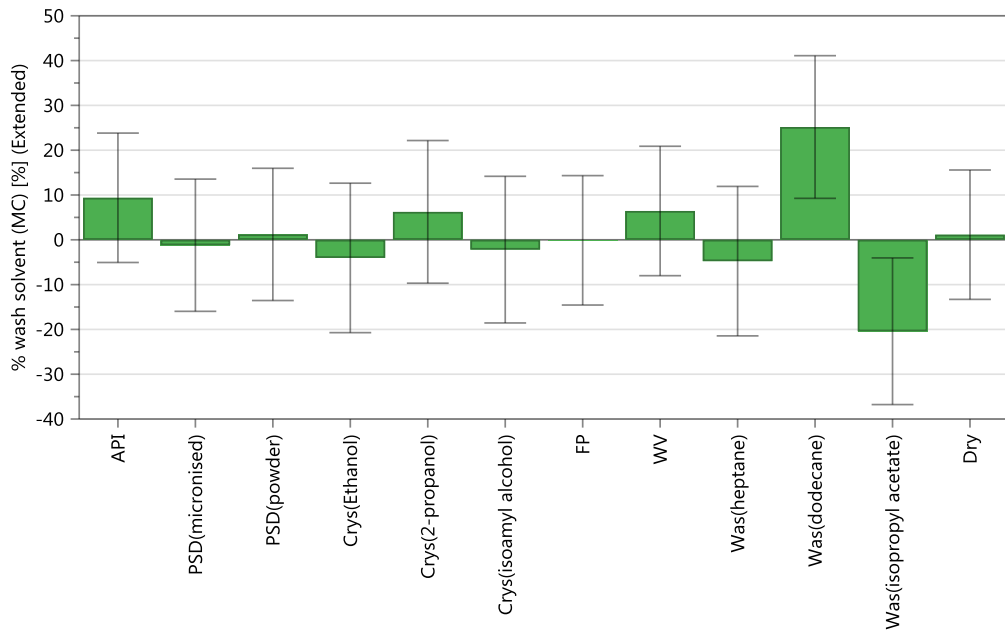


Figure 108 Fitting summary of variable affecting the relative percentage of wash solvent in the dried cake moisture content.

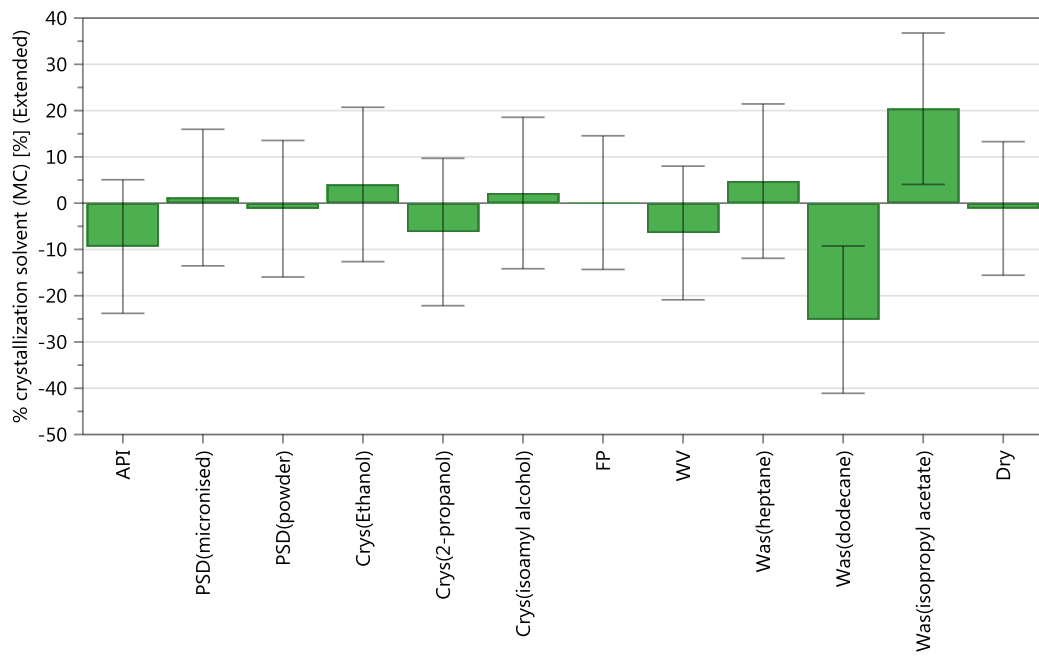


Figure 109 Fitting summary of variable affecting the relative percentage of crystallization solvent in the dried cake moisture content.

The effect of the selected parameters on the orthocetamol concentration in second filtrate (wash 1) is shown in Figure 110, the combination of crystallization solvent ethanol and wash n-heptane enhance the purity of cake. Conversely the combination of isoamyl alcohol as crystallization solvent and isopropyl acetate as wash solvent yield the poorest washing outcome due to the big difference in solvent viscosity and the one order of magnitude higher API solubility in isopropyl acetate (0.0076g/g at 25°C) respect the others wash solvents (n-heptane, 0.0001g/g and n-dodecane 0.0007g/g at 25°C). API solid load and particle size grade also affect impurity removal: typical crystalline paracetamol has larger crystals which form larger inter-particle channel where solvent can flow easily and displace any mother liquor present.²⁵ The cake height also affects wash performance, which can be seen in Figure 110.

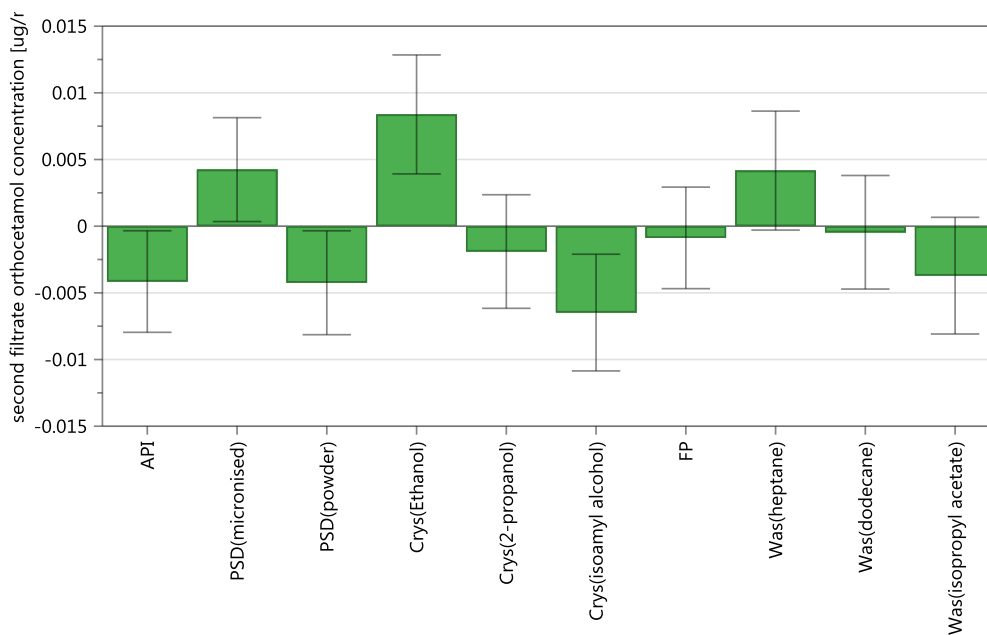


Figure 110 Second filtrate orthocetamol concentration fittings with DoE variables.

Figure 111 shows how the selected factors affect the concentration of orthocetamol impurity in filtrate removed from the filter cake during wash 2. This plot needs to be considered in the opposite way compared to Figure 110. Here the presence of higher concentration of the impurity in the third filtrate relates to poor washing evidenced in the positive trend is mainly influenced by; the grade of paracetamol, the solubility and viscosity of crystallization solvent and the wash solvent, the driving force used and the quantity of wash solvent used. The higher the tortuosity of the cake, as seen in micronized paracetamol, the higher the propensity to trap impure mother liquor in cake during filtration and wash 1 and lower the capability of wash 2 to remove the impure mother liquor completely.^{20,49} The ideal case as seen in Figure 111 is the washing of a small typical crystalline paracetamol cake with ethanol – n-heptane mixture in wash 1 and with pure n-heptane in wash 2 using a total of four void volumes of wash solvent (1 in wash 1 and 3 in wash 2), using a low driving force to maximize the contact time to enhance dilution and diffusion washing mechanism.

The effect of n-dodecane should be similar than n-heptane, due to their similar viscosity (n-heptane, 0.4cP, n-dodecane, 1.36cP, isopropyl acetate, 0.8cP from Detherm database⁵⁹). A further investigation on the effect of n-dodecane during washing needs to be considered, even if fitting validity and reproducibility show high values. In Figure 113 isopropanol is considered the best case of mother liquor to have trapped in the cake porosity as dirty mother liquor; in case of washing the cake just with pure wash solvent isopropanol is preferable because the API loss by dissolution in mother liquor is less than ethanol, due to the relative lower solubility.

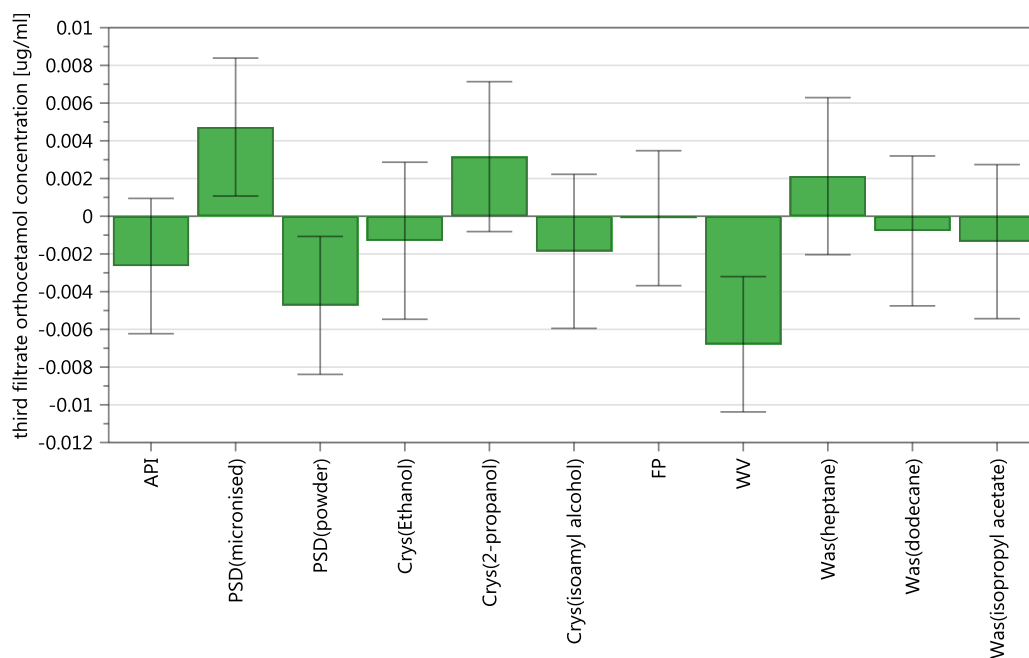


Figure 111 The dependence of the concentration of the impurity orthocetamol in the different wash solvents on the DoE variables.

7.4.2.4 Effects on drying

Drying was accomplished by flowing ambient air through the wet cake under reduced pressure in port 5, without agitation. Lekhal et al.⁴³ report that wet particles tend to agglomerate during static drying under reduced pressure. The lack of agitation and consequent absence of disruption of aggregates allows strong inter-particle bridges to form as solute saturated solvent evaporates from the points of contact between particles. The supply of material from inter-particle bridges is determined by the quantity of residual solvent evaporated and the amount of solute dissolved in it.

The effects of the variables investigated in the DoE on; PSD, extent of agglomeration (particles bigger than 1 mm), agglomerate strength of the final dried material and the LOD after drying are summarized in the subsequent plots.

Figure 112 focuses on the final solvent content in dried sample (LOD). The factors which influence this in order of decreasing importance are: the paracetamol grade (the lower the particle size the higher the quantity of residual solvent retained), the wash solvent identity mediated principally through the wash solvent viscosity (more viscous solvents are more readily retained) the boiling point and enthalpy of vaporization of the wash solvent affect the ease of removal during drying. n-heptane and isopropyl acetate are more easily removed than n-dodecane (n-heptane, 98.42°C, 36.6J/mol, isopropyl acetate, 89°C, 37J/mol, n-dodecane, 216.2°C, 62.1J/mol); in terms of importance the next factor is the crystallization solvent identity mediated through the viscosity and volatility of the crystallization solvent, (the least viscous and most volatile crystallization solvent ethanol is retained least); the next factor is the drying time, longer drying produces a drier product, the driving force during washing is similarly important. Increasing the wash solvent volume used to displace the crystallization solvent also serves to reduce the ultimate LOD, the least important factor is the filtration pressure. Combining all these factors the most favorable conditions occur when the API particle size is large, ethanol is the crystallization solvent and washing is with four cake void volumes of n-heptane using a low driving pressure to promote displacement, diffusional and dilution washing and this is followed by an extended drying period.

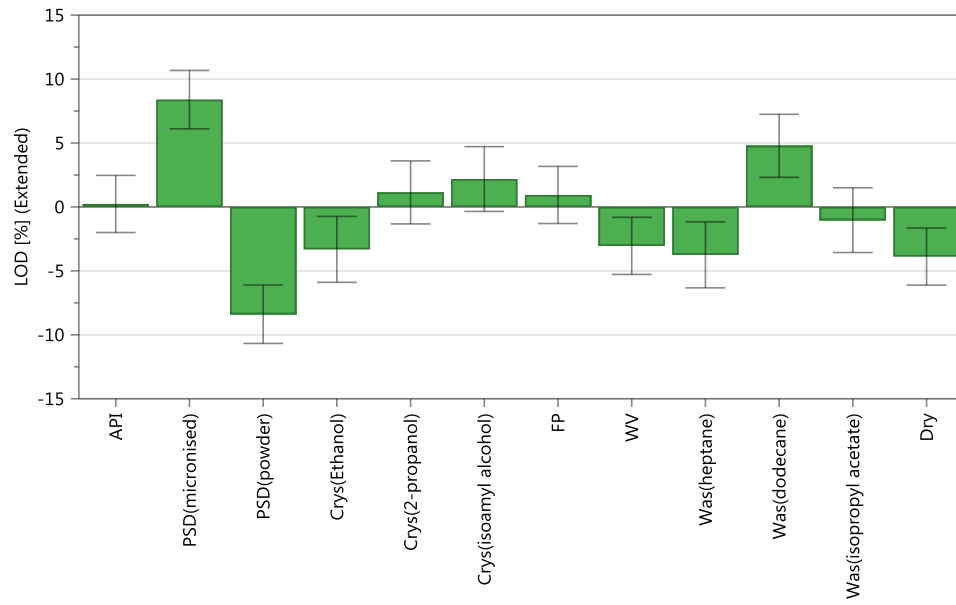


Figure 112 DoE variables that affect LOD of the dried samples.

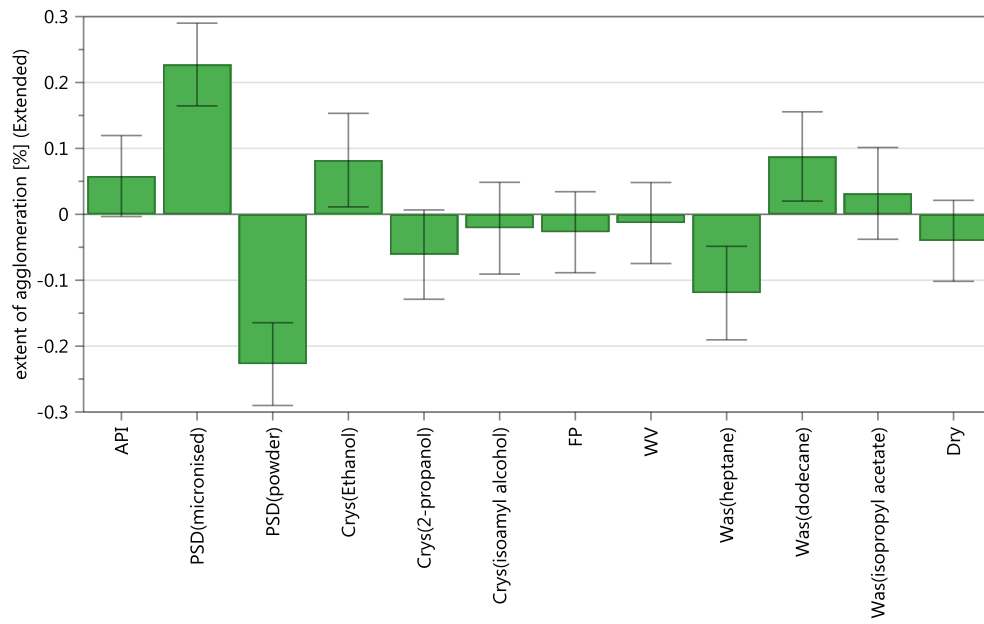


Figure 113 DoE variables that affect extent of agglomeration of the dried samples.

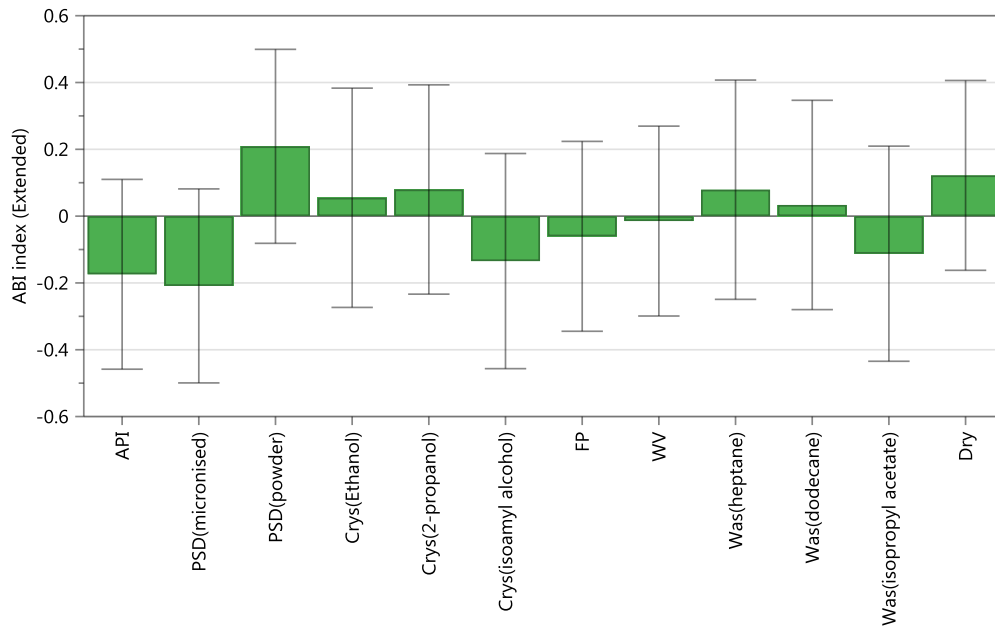


Figure 114 DoE variables that affect ABI index of the dried samples.

Higher the solid load causes higher the agglomeration propensity and stronger agglomerates, as seen in chapter 6. However, the regression coefficient plots of the extent of agglomeration and ABI index show dubious correlation. The big error bar respect to the the estimated correlation value can be correlated to the qualitative analytical approach used to estimate these two values. This effect is due to mechanism of drying used.⁴⁴ During this step, named also constant rate drying,⁶⁰ material starts drying from the surface and proceeding to the bulk (drying front) and moisture content in the cake decreases linearly and it is limited just by the gas flow. During this step the formation of a solid block of product starts from the upper surface and slowly progresses through the bulk where the transport of unbonded moisture is occurring through particle-particle capillaries. In the case of a thin cake, if the material in the upper part of the cake stays in contact with the solvent for longer period, the material after drying has rather hard shell or crust and relatively soft

core. On the contrary, for thicker cakes, capillary forces cannot effectively transport the moisture to through the whole cake volume to the surface. In this case, after a constant rate drying, the process is driven by moisture diffusion through the cake (slower drying rate), causing an even distribution of cake moisture and formation of a single solid block.

Particle size and particle shape play a role in deliquoring results: as reported by Wakeman,²⁵ increasing particle size shortens deliquoring time due to the increase of gas flow rate through the cake. On contrary, during drying fine solids provide larger surface area than bulky particles, producing faster drying. Effective moisture removal during constant rate period is affected by surface area, while internal particle morphology (or porosity) limits the falling rate period. Moreover, PSD affects enthalpy transfer mechanism: as a particle dries, the outer layers shield further heat propagation and form a diffusion barrier. In case of large bulky porous particles, removing all the liquid from the core requires prolonged drying time. Otherwise, finer particles rapidly dry; therefore, the larger ones would dominate the whole process. Wide particle size distributions increase the risk of agglomerate formation and cake hardening due to finer particles located in small voids of the cake that can act as bridges formation agents.⁶¹ On the other hand, finer particles tend to form hard agglomerates.

One approach to reduce agglomeration is therefore to tailor the wash solvent composition to minimize concentration of the highly soluble component during the drying operation. Papageorgiou et al.(2016)⁴⁶ investigated how solvent selection is crucial to reduce/increase particles agglomeration analysing the effect of solvent selection and critical moisture content.⁶² Well-designed solvent selection can have a much larger impact

on particle clustering than particle size. From Figure 113 ethanol emerges as the worst crystallization solvent to be used for drying purpose: the high solubility of paracetamol in residual ethanol trapped in cake after washing step brings a high propensity to form particle-particle bridges. Isoamyl alcohol could be considered a good candidate, but as said in the previous paragraph, due to the different viscosity with respect to the wash solvents this solvent is difficult to remove during washing causing bridge formation with high mechanical resistance (low ABI index). Therefore, isopropanol is preferred as crystallization solvent. The extent of agglomeration can also be reduced by increasing the wash solvent quantity used: increasing the wash solvent volume of the pure wash solvent (wash 2) from 1 to 3 brings a drastic reduction in crystallization solvent/mother liquor trapped in the cake during the drying process. The best wash solvent to use for reducing agglomeration propensity is n-heptane for the very low API solubility (see appendix) and the lower boiling point and enthalpy of vaporization. Even though n-dodecane shows similar solubility with respect to n-heptane, this solvent has the highest boiling temperature, so during drying low drying rate also causes agglomeration. Isopropyl acetate is the worst wash solvent, due to its high API solubility, which allows the formation of extensive agglomeration with low ABI index (hard agglomerates). Finally, agglomeration and strength of aggregates can be reduced by increasing the drying time.

Particle size distribution of particles smaller than 1 mm were analyzed to determine if agglomeration mechanisms were also observed in single particles. In general, particle size increase is observed in all the samples. As seen for the extent of agglomeration, PSD of single particles is affected by the solvent selection, paracetamol grade, wash volume used,

driving force (increase the wash solvent contact time and removal of impurities and mother liquor) drying time.

7.5 Conclusions

The pharmaceutical industry requires the development of a continuous system capable of filtering, washing and drying crystallised APIs. Such a system has been prototyped in collaboration with Alconbury Weston Ltd to produce a continuous filtration and drying unit called the CFD20. This work has identified key performance measures and developed some testing methodologies to evaluate device performance. The CFD20, as a prototype continuous filtration, washing and drying unit, was tested against the obvious success criteria of; achieving comparable cake purity at the end of isolation with respect to the Biotage unit, delivering an unaltered product PSD consistent with the material produced by crystallization and achieving the flexibility and simple operability of the Biotage system but with enhanced control and automated data collection. Key challenges of suspending material uniformly, transferring a representative sub sample to a filtration chamber, halting filtration at an appropriate point and recovering the filtered material were identified. These challenges were evaluated using a manual system representative of current best practice in pharmaceutical process development and compared to the solutions embodied in the CFD20. In each area, the CFD20 performed comparably well, if not better, than manual best practice. Comparing the filtration performance of the approaches, the parameters derived from Darcy's law showed good agreement. Automated data collection supports improved understanding of filtration process development.

Wash performance was evaluated by the removal of patent blue V from two very different filter cakes prepared from micronised and granular paracetamol. Overall, the performance of the units was similar, although the Biotage unit was capable of removing slightly more of the surrogate impurity from the filter cake.

Particle damage or agglomeration was assessed by sieving the isolated product; both platforms caused considerable changes in particle size after filtering and washing which is consistent with industrial experience. Micronized particles showed a substantial increase in size caused by agglomeration. Careful washing of the micronized powder caused some reduction in the extent of formation of very large agglomerates but the filtered washed and dried material did not recover the same particle size distribution as the feed material. This work has shown the potential for an automated solution to address challenges encountered in manual filtration, washing and drying processes and indicates how automation can facilitate continuous isolation. The CFD20 performed comparably well with the Biotage system, and required much less manual intervention and material handling.

After further development of the unit, the new version of the CFD unit (CFD25) was tested using a more challenging slurry where the presence of related compounds of paracetamol was used: acetanilide, metacetamol and orthocetamol (already present in the raw material). The success criteria used to test the CFD25 with paracetamol related impurities were to select the best isolation strategy to:

- Minimize impurity content in the final cake

- Minimize the final LOD in the dried cake
- Try to maintain PSD of the input single particles
- Minimize agglomeration during drying; if this goal is difficult to achieve to understand how to design the isolation strategy to obtain easy to break agglomerates.

To systematically investigate the impact of API solid load, input PSD particles, crystallization solvent nature, isolation driving force, wash solvent nature, wash solvent volume used and drying time, a Design of Experiment (DoE) was performed. A series of responses were set to investigate the role of this multi variable problematic on the succeed criteria above listed.

In conclusion, the CFD25 is a valid lab scale isolation unit capable of filtering and washing a real API in presence of related compounds by using dead end filtration and washing under constant vacuum and then drying it in condition of static drying with flow of ambient temperature gas flowed through the cake by reduce pressure built beneath the filter media. By using the CFD25 in optimization mode, it was possible in two weeks to run a full set of DoE experiments to determine the best isolation strategy for the API analysed. Future investigation to determine the throughput of the unit in continuous mode, further development to improve drying efficiency by convective drying, and evaluation of the isolation capability with even more challenging APIs will be undertaken.

7.6 Abbreviations

AWL CFD20, Continuous filter dryer prototype unit, version 1, AWL, Alconbury Weston Ltd, REMEDIES, RE-configuring MEDICines End-to-end Supply, AWL CFD25,

continuous filter dryer prototype unit, version 2, API, active pharmaceutical ingredient, FDA, Food and Drug Administration, PSD, particle size distribution, HPLC, High-performance liquid chromatography, ABI, agglomerate brittleness index, ¹H-NMR, Proton nuclear magnetic resonance, HMI, Human Machine Interface, DMSO-d, Dimethyl sulfoxide-d, TOC, total organic carbon, DoE, design of experiment.

References

1. Polydoros, S., Sfantsikopoulos, M., Provatidis, C., 2011. Rational Embracing of Modern Prototyping Capable Design Technologies in the Tools Pool of Product Design Team. *Int. J. Resear. Netw.*, 1.
2. Ingole, D., S., 2009. Rapid prototyping-A technology transfer approach for development of rapid tooling. *Rapid Prototyp. J.* 280.
3. Thomke, S., H., 1998. Managing Experimentation in the Design of New Products. *Manag. Sci.*, 743.
4. Wong K W S. Design of a small-scale continuous linear motion pharmaceutical filtration module. <https://dspace.mit.edu/handle/1721.1/60210#files-area> [cited 2017-09-30].
5. Mollan, J., M., J., Mayur, L., 2004. Continuous processing in pharmaceutical manufacturing. *Pharmaceutical Manufacturing Magazine*, 1.
6. Kossik, J. Think Small: Pharmaceutical Facility Could Boost Capacity and Slash Costs by Trading in Certain Batch Operations for Continuous Versions. *Pharmamag.com*, article ID/DDAS-SEX 52B/<http://www.pharmamanufacturing.com> [cited 2017-09-30]
7. US Food and Drug Administration, Center for Drug Evaluation and Research: Guidance for Industry PAT A Framework for Innovative Pharmaceutical Manufacturing and Quality Assurance. August 2003 <http://www.fda.gov/cder/guidance/5815dft.htm> [cited 2017-09-30]
8. Am Ende, D., J., Pfisterer, D., Girard, K., P., Blackwood, D., Plocharczyk, E., 2011. Development of a Continuous Filter-Drier for Lab to Kilo-Lab Scale. *AIChE*, 16.
9. Garrick, J. Process Design Strategy: The Advantages of Continuous Filtration for Pharmaceutical Manufacturing. *informEx* 2015 Feb 3-5.
10. Kossik, J., 2003. Small Scale Continuous Cake Filtration using the Disposable Rotary Drum Filter. *Filt. Sep.*, 26.
11. Kossik, J., 2001. Operation of a Disposable Rotary Drum Filter. *AIChE*, 4.
12. Söhnel, O., 1981. Analysis of the precipitation reactor-separation equipment system. Continuous reactor and the rotary vacuum filter operating at the selected negative pressure drop. *Collect. Czech. Chem. Commun.*, 2364.
13. Flynn, E., D. Continuous rotary drum filter. 1940, Google Patents.
14. Burtsev, N.A., Continuous drum vacuum filter. 1971, Google Patents.
15. Flynn, E.D., Design for a continuous rotary drum filter. 1940, Google Patents.
16. Kosonen, V.J., Continuous drum filter with improved agitator structure. 1978, Google Patents.
17. Hillier, G.O., Continuous rotary disk and drum filter. 1937, Google Patents.
18. Iwatani, A., Continuous rotary drum vacuum filter. 1971, Google Patents.
19. Steadfast website <http://www.steadfastequipment.com/> [cited 2018-09-24]
20. BHS website <http://bhs-filtration.com/> [cited 2018-09-24]

21. REMEDIES (RE-configuring MEDICines End-to-end Supply) Advanced Manufacturing Supply Chain Initiative. Workstream App. "B" – Primary to Secondary. <http://remediesproject.com/research-2/project-structure/app-b/> [cited 2016-09-02].
22. Murugesan, S., Sharma, P. K., Tabora, J., E. Design of Filtration and Drying Operations p315-346 in Chemical Engineering in the Pharmaceutical Industry: R&D to Manufacturing. Wiley NewYork; 2010.
23. Ruslim, F., Hoffner, B., Nirschl, H., Stahl, W., 2009. Evaluation of pathways for washing soluble solids. Chem. Eng. Res. Des., 1075.
24. Kuo, M., T., Barrett, E., C., 1970. Continuous filter cake washing performance. AIChE, 633–8.
25. Wakeman, R., 2007. The influence of particle properties on filtration. Sep. Purif. Technol., 234.
26. Wakeman, R., J., Sabri, M., N., Tarleton, E., S., 1991. Factors affecting the formation and properties of wet compacts. Powder Technol., 283.
27. Bourcier, D., Féraud, J., P., Colson, D., Mandrick, K., Ode, D., Brackx, E., Puel, F., 2016. Influence of particle size and shape properties on cake resistance and compressibility during pressure filtration. Chem. Eng. Sci., 176.
28. Ripperger, S., Gösele, W., Alt, C., Loewe, T., 2013. Filtration, 1. Fundamentals. Ullmann's Encyclopedia of Industrial Chemistry, Major Reference Works.
29. Beckmann, W. Crystallization Basic Concepts and Industrial Applications, WILEY-VCH Verlag GmbH & Co. KGaA; 2013.
30. Wakeman, R., Tarleton, S. Solid Liquid Separation: Principles of Industrial Filtration. 1st edition, Amsterdam, Netherlands: Elsevier Science, 2005. 4, Filtration - Cake Formation, 96.
31. Business Insights: Global [WWW Document], n.d. URL <http://bi.galegroup.com/global/article/GALE%7CA290735580/049a9a3f271d08a0b7cf1523fb30cb02?u=ustrath> [cited 2018-03-17].
32. Birch, M., Marziano, I., 2013. Understanding and Avoidance of Agglomeration During Drying Processes: A Case Study. OPR&D, 1359.
33. Perlmutter, B. A., et al. A Treatise of Filter Cake Washing Mechanisms In Pressure and Vacuum Filtration Systems. BHS Filtration. http://www.bhs-filtration.com/A_Treatise_of_Filter_Cake_Washing_Mechanisms.pdf [cited 2016-11-18]
34. Tamrakar, A., Gunadi, A., Piccione, P. M., Ramachandran, R., 2016. Dynamic agglomeration profiling during the drying phase in an agitated filter dryer: Parametric investigation and regime map studies. Powder Technol., 109.
35. Tien, C., 2002. Cake filtration research—a personal view. Powder Technol., 1.
36. Tien, C., Bai, R., Ramarao, B., V., 1997. Analysis of cake growth in cake filtration: Effect of fine particle retention. AIChE, 33.
37. Tien, C., Bai, R., 2003. An assessment of the conventional cake filtration theory. Chem. Eng. Sci., 1323.
38. Bürger, R., Concha, F., H., Karlsen, K., 2001. Phenomenological model of filtration processes: 1. Cake formation and expression. Chem. Eng. Sci., 4537.
39. Stamatakis, K., Tien, C., 1991. Cake formation and growth in cake filtration.

- Chem. Eng. Sci., 1917.
40. Tiller, F., M., Haynes, S., Lu, W.-M., 1972. The role of porosity in filtration VII effect of side-wall friction in compression-permeability cells. *AIChE*, 13.
 41. Wakeman, R., J., Tarleton, E., S., *Filtration: equipment selection, modelling and process simulation*. 1st edition, Oxford, United Kingdom: Elsevier Science Ltd, 1999.
 42. Macleod, C., S., Muller, F., L., 2012. On the Fracture of Pharmaceutical NeedleShaped Crystals during Pressure Filtration: Case Studies and Mechanistic Understanding. *OPR&D*, 425.
 43. Lekhal, A., Girard, K., P., Brown, M., A., Kiang, S., Glasser, B., J., Khinast, J., G., 2003. The effect of agitated drying on the morphology of l-threonine (needle-like) crystals. *Powder Technol.*, 119.
 44. Kontcho, K., P., Cook, W., Kougoulos, E., 2011. Impact of Laboratory Vacuum Contact Drying on Material Drying Rates and Physical Properties. *OPR&D*, 360.
 45. Sudha, C., Srinivasan, K., 2014. Understanding the effect of solvent polarity on the habit modification of monoclinic paracetamol in terms of molecular recognition at the solvent crystal/interface. *Cryst. Res. Technol.*, 865.
 46. Papageorgiou, C., D., Langston, M., Hicks, F., AM Ende, D., Martin, E., Rothstein, S., Salan, J., Muir, R., 2016. Development of Screening Methodology for the Assessment of the Agglomeration Potential of APIs. *OPR&D*, 1500.
 47. Ellis, F. *Paracetamol: A Curriculum Resource*; Royal Society of Chemistry, 2002.
 48. Hendriksen, B., A., Grant, D., J., W., Meenan, P., Green, D., A., 1998. Crystallisation of paracetamol (acetaminophen) in the presence of structurally related substances. *J. Cryst. Growth*, 629.
 49. Hendriksen, B., A., Grant, D., J., W., 1995. The effect of structurally related substances on the nucleation kinetics of paracetamol (acetaminophen). *J. Cryst. Growth*, 156.
 50. Kuvadia, Z., B., Doherty, M., F., 2013. Effect of Structurally Similar Additives on Crystal Habit of Organic Molecular Crystals at Low Supersaturation. *Cryst. Growth Des.*, 1412.
 51. Newton, D., W., Breen, P., J., Brown, D., E., Mackie, J., F., Kluza, R., B., 1981. Physicochemical Characteristics of Patent Blue Violet Dye. *J. Pharm. Sci.*, 122.
 52. Granberg, R., A., Rasmuson, Å., C., 1999. Solubility of Paracetamol in Pure Solvents. *J Chem Eng Data.*, 1391.
 53. McConville FX. *The pilot plant real book: a unique handbook for the chemical process industry*, 1st edition, FXM Engineering and Design, 2002.
 54. Ruslim, F., Nirschl, H., Stahl, W., Carvin, P., 2007. Optimization of the wash liquor flow rate to improve washing of pre-deliquored filter cake. *Chem. Eng. Sci.*, 3951.
 55. Buscall, R., 1987. White LR. The consolidation of concentrated suspensions. Part 1.—The theory of sedimentation. *J Chem Soc, Faraday Trans 1*, 873.
 56. Dullien, F., A., L. *Porous media fluid transport and pore structure*, 2nd edition, Academic press inc.; 1992.
 57. Willis, M., S., Tosun, I., 1980. A rigorous cake filtration theory. *Chem. Eng. Sci.*, 2427.

58. Fathi-Najafi, M., Theliander, H., 1995. Determination of local filtration properties at constant pressure. *Sep. Technol., Progress in Separations and Waste Reduction*, 165.
59. Dechema website <http://dechema.de/en/detherm.html>, [cited 2016-11-18].
60. Conder, E., W., Cosbie, A., S., Gaertner, J., Hicks, W., Huggins, S., MacLeod, C., S., Remy, B., Yang, B-S., Engstrom, J., D., Lamberto, D., J., Papageorgium, C., F., 2017. The Pharmaceuticla Drying Unit Operation: And Industry Perspective on Advancing the Science and Development Approach for Scale-Up and Technology Transfer. *OPR&D*, 420.
61. Am Ende, D., Birch, M., Brenek, S. J., Maloney, M. T., 2013. Development and Application of Laboratory Tools To Predict Particle Properties upon Scale-Up in Agitated Filter-Dryers. *OPR&D*, 1345.
62. Lim, L., H., Hapgood, K., P., Haig, B., 2016. Understanding and preventing agglomeration in a filter drying process. *Powder Technol.*, 146.

8 Conclusions and future works

In the pharmaceutical industry drug substance must maintain chemi-physical properties throughout the entire manufacturing process. Purity, particle size and solid-state form need to be controlled to guarantee that the marketed drug product is safe and stable over time.

The purity of drug intermediates, and especially active pharmaceutical ingredients (API's) is monitored during the entire manufacturing process, from synthesis (during the work-up stage) through purification and isolation, formulation and on to packing. The key step that enhances compound purity is the purification process (down-stream process of work-up). Purification is divided in crystallization and isolation. Crystallization is used to control crystal bulk purity, the crystal size, shape, habit, morphology and polymorph. During crystallization, a 3D molecular structure is formed and the impurities produced during the previous manufacturing steps are rejected from the crystal structure forming a relatively pure crystal that mainly contains the molecules of the desired compound and that segregates the impurities in the crystallization solvent phase (the mother liquor). As result, a gradient of purity is observed from the bulk to the crystal surface. To remove the liquid phase containing dissolved impurities, and to clean the crystal surfaces, another purification step is required, isolation.

During isolation, the liquid and solid phase of the slurry are separated (filtration stage). The cake formed is then washed with a single pure solvent or mixture of solvents that removes the residual impurities from the cake. Finally, a drying stage is used to remove the residual wash solvent to produce pure dry isolated particles.

Decisions taken during the isolation stage can be responsible modification of particle characteristics. It is crucial to design the isolation process to maintain the required properties of the crystals produced during crystallization.

Substantial research effort during the last decade has been made to study crystallization to understand process and material properties, which affect the final crystallized material. Proportionately less effort was been dedicated to understanding the physic-chemical and process parameters affecting the attributes of the final isolated material. To understand how to design an isolation strategy capable of maintaining the crystal properties of the material and delivering the required material purity, a full understanding of the physic-chemical interactions between; API, impurities, crystallization and wash solvent at micro/meso and macroscopic point of view is required.

This work focuses on understanding these physic-chemical and process characteristics which affect the properties of the final isolated product to reduce process development time, the consumption of of API and solvents in R&D and for the final manufacturing process and to avoid the use of post-processing steps to adjust the crystal properties unintentionally modified during the isolation process.

Paracetamol was selected as the test compound because this project has many questions related to equipment capability and the chemical and physical material interactions during isolation, that the use of a well-researched compound is necessary to facilitate both experimental work and data interpretation. Impurities selected in this work are structurally related paracetamol impurities, reagents and reaction by-products.

A serie of crystallization and wash solvents were used in this work. Four solvents were selected as crystallization solvents for paracetamol: ethanol, isopropanol, isoamyl alcohol and water. A series of wash solvents were chosen based on exhibiting low or very low paracetamol solubility and different miscibility behaviours with the selected crystallization solvents.

In chapter 5 alternative analytical techniques were investigated to study their effectiveness in determining the quantity and spatial distribution of impurities on crystal surfaces and to identify any associated morphological and surface texture changes. Three different approaches, epitaxy, droplet evaporation and cooling crystallization were used to create paracetamol crystals with molecules of 4-nitrophenol present on the crystal surface in order to evaluate the sensitivity of the selected techniques to detect residual impurities.

TOF-SIMS and Raman Microscopy in mapping mode were selected as alternative analytical techniques in combination with the classical techniques used to evaluate crystal form, morphology and surface structure to better understand if impurities show preferential anchoring behavior on the paracetamol single crystal facets or if it is depositing homogeneously on the entire single crystal surface.

TOF-SIMS allows the presence of 4-nitrophenol to be verified by the distribution of the secondary-ion fragments when the impurity concentration is very low (which was achieved by cooling crystallization).

Raman Microscopy mapping reveals the impurity location when the main peak intensity ratio is more intense than the baseline.

From the results gathered from the investigation performed with 4-nitrophenol as a model impurity, a series of other related paracetamol impurities were used to analyze surface and sub-surface impurity interactions with single crystals of paracetamol crystallized by cooling crystallization. A cooling crystallization approach was used to grow single crystals in ethanol in presence of 4% mol/mol paracetamol related impurities. Two crystals of each combination were grown to analyse if related impurities of paracetamol show preferential face anchoring behavior. Overall, this work helps to design isolation strategy or to make process decision respect to the purification method chosen by the operator. Depending on the location of the impurities, three different cases can be encountered:

- The impurity is mainly located in mother liquor. This phenomenon can be seen from TOF-SIMS because the intensity count of the characteristic ion fragments of the impurity are null. Pure crystals can be obtain for example when the solubility of impurity and crystals are different and the API molecules blocks the impurity to enter in the crystal lattice. The purification strategy to follow in this case is to design the washing process in order to get a wash solvent miscible with the crystallization solvent maximizing the mother liquor removal.
- The impurity is located in the mother liquor and mainly on the crystal surface/sub-surface layers. This example can be seen in chapter 9 with the 4-acetamido benzoic acid-paracetamol single crystals, where the intensity count of the characteristic ion fragment (Figure 133, Figure 134, Figure 135 and Figure 136) shows a drastic reduction of the impurity in the first layers of the crystal. In

this case, a wash solvent miscible with the crystallization solvent that allow the removal of the mother liquor is recommended. Moreover, the wash solvent should also show partial API solubility to dissolve the first layers of the crystals and remove the impurities trapped in the surface crystal lattice.

- The impurity is located in all the crystal lattice and in the mother liquor. If the impurity is non toxic and does not change drastically API properties, it is possible to simply isolate the crystals using a wash solvent miscible with the crystallization solvent in order to wash out the mother liquor. In case of toxic impurity or impurity that modify API particles properties, it is recommended to re-crystallize the compound in a crystallization solvent/s that reject from the crystal lattice the impurity. In case the impurity show lower solubility respect to the API in all the possible wash solvent candidates and the impurity is toxic the only option to purify the system is to consider another synthesis route to exclude the formation of that specific impurity.

In all the aforementioned cases, TOF-SIMS is a useful analytical approach to track the position of impurity on the crystal surface/bulk only if the impurity presents distinctive ion fragment respect the API compound. The possibility to modify ion fragmentation of the API/impurity and the use of calibration methods reported in literature can possibly be used to perform quantitative analysis. However, this methodology cannot guarantee full success to quantify impurities on crystal surface (see chapter 5).

In chapter 6, the chemical and physical properties of slurries and wash solvents and the isolation process parameters used were studied to evaluate the impact of these factors on

the final isolated single particles. The aim of this work was to understand how to design an isolation strategy that maintains the same characteristics of particles produced during the crystallization process. During this work the effect of filtration, washing and drying was analysed to evaluate which stages are responsible for particle agglomeration, and how isolation parameters affect the mechanical properties of any agglomerates, which formed.

A series of filtration, washing and drying variables were evaluated in DoEs: solid load in the slurry, filtration and washing driving force, filtration and washing endpoint, filtration in presence of sedimented cake, volume and number of washes, wash solvent identity and drying mechanism. Cake and media resistance, residual moisture content, and characteristics of the dried material; extent of agglomeration, ABI index and PSD of single particles were selected as responses in the initial screening DoE. Filtration and cake washing were studied using vacuum filtration on a modified Biotage unit. Three different drying approaches were used: static drying in a vacuum oven operated at room temperature and two approaches using flowing nitrogen (room temperature nitrogen flow and heated temperature nitrogen flow through the cake).

During this work an analytical workflow was developed. This workflow is a useful tool that allows stepwise use of analytical techniques to collect the key information required for the isolation strategy design. The proposed workflow has been verified using it to analyze isolated cake and filtrate to select the isolation strategy to minimize agglomeration and maximize purity (in chapter 7).

This work has delivered useful guidance and analytical approaches to design an API isolation strategy to minimize agglomeration and to measure agglomerate mechanical properties. However, to model the agglomeration phenomenon and correlate agglomerates mechanical properties with the chemi-physical properties of slurry and with the process parameters selected during isolation an improvement of the analytical techniques is further required to quantify mechanical properties of agglomerates.

The results and information obtained in chapter 6 and 7 were used to design a new lab/small scale isolation prototype (chapter 7). The lack of commercial continuous isolation platform able to process in a flexible way small quantities of API's to reduce API required for isolation step development in R&D and to reduce the amount of material consumed to define the isolation strategy of an NCE under-development in the pharmaceutical industry. Such a system has been prototyped in collaboration with Alconbury Weston Ltd to produce a continuous filtration and drying unit called the CFD20 during the Remedies project (App B). The CFD20, continuous filtration, washing and drying unit, was tested against the success criteria of; achieving comparable cake purity at the end of isolation with respect to the Biotage unit, delivering an unaltered product PSD consistent with the material produced by crystallization and achieving the flexibility and simple operability of the Biotage system but with enhanced control and automated data collection. The data gathered from this test were used to further develop the unit and to design the new version of the CFD unit (CFD25). The CFD25 was tested using a more challenging slurry where the presence of related compounds of paracetamol was used: acetanilide, metacetamol and orthocetamol (already present in the raw

material). The success criteria selected to evaluate the unit efficiency were the capability to minimize the impurity content in the final cake, minimizing also the final LOD after drying, maintain same particle size and size distribution of the input particles and minimize agglomeration during the washing and drying stages. In cases where it was impossible to prevent agglomeration, it was important to understand how to design the isolation strategy to obtain agglomerates, which break easily.

In conclusion, the CFD25 can be used as an isolation unit in R&D to filter and wash a real API in presence of related compounds by using dead end filtration and washing under constant vacuum and then dry it under condition of static drying with ambient temperature or heated gas flowing through the cake by reduced pressure applied beneath the filter media. This unit is able also to minimize material consumption and research time during the development of a new product isolation strategy.

8.1 Further work

8.1.1 Use of other crystallization solvents to evaluate variation in impurity interaction with paracetamol single crystal facets

The single crystals used to investigate alternative analytical techniques to determine character and spatial distribution of impurities were crystallized using ethanol as crystallization solvent. Further investigation using other crystallization solvents would be useful to determine whether impurity anchoring behaviour can be modified by a competitive interaction between impurity and solvent molecules. The use of simulation tools like CCDS Mercury would facilitate this by exploring possible interactions between the functional groups exposed on different paracetamol facets with different solvent and impurity molecules.

8.1.2 Fundamental understanding of solid bridge formation during drying in presence of residual mother liquor and /or wash solvent

A poorly understood phenomenon highlighted during this work is the formation of solid bridges between crystals during drying responsible for agglomeration. From the evidence shown in chapter 6 and chapter 7, the nature of crystallization and wash solvent, the efficiency of washing to remove residual mother liquor from the cake, the tortuosity of the cake and the drying approach used may all affect the extent of agglomeration and the mechanical properties of the final agglomerates. To extend our understanding of the mechanism of agglomeration a further investigation can be suggested to examine the effect of:

- Residual impurities (their transport and deposition)
- Character of crystallization and wash solvents correlating these factors with the size and extent of the bridges formed.

8.1.3 Investigation of alternative drying procedures to minimize particles agglomeration

In chapter 6 three convective drying approaches were used to investigate the effect of drying on the final isolated product without particle motion. To extend knowledge about drying approaches for API's which do not alter the properties of the particles, other drying approaches should be investigated.

In the literature a series of alternative approaches have been used in different industrial applications to dry powder beds, such as dynamic convective approaches, dynamic intermittent drying (used for fragile particles), fluidized bed drying (mainly used in food industry), freeze drying, etc. A comparative study of different drying techniques using a series of different API's presenting different properties to develop a strategy to select

suitable drying approaches in relation to API's properties to avoid particles agglomeration, breakage or phase change.

8.1.4 Test the CFD25 with a series of different APIs and evaluate the unit in continuous (production) mode for an extended period.

Future investigation is needed to determine the throughput of the unit in continuous mode, and to evaluate its robustness. Further development could also be undertaken to improve drying efficiency using convective drying, and to evaluate the isolation capability with more challenging APIs. Future investigation should also evaluate the flexibility of the unit to process “problematic slurries” with a variety of different undesirable characteristics.

9 Appendix

9.1 Materials and methods

Compound	Hazards identification	Risk identification
Paracetamol	H302, H315, H319, H335	R22, R36/37/38
4-acetamido benzoic acid	none	none
4-aminophenol	H302, H332, H341, H400, H410	R68, R20/22, R50/53
4-chloro-acetanilide	none	none
4-hydroxy-acetophenone	H319, H412	none
4-methyl-hydroxy-benzoate	H412	none
4-nitrophenol	H301, H332, H312, H373	none
Acetaminophen acetate	H319	none
Acetanilide	H302	none
Metacetamol	H315, H319, H335	R36/37/38
Orthocetamol	none	none
Patent Blue V sodium salt	none	none
3-methyl-1-butanol	H226, H332, H315, H319, H335	none
Acetonitrile	H225, H302, H332, H312, H319	none
Anisole	H226	none
Cyclohexane	H225, H315, H336, H304, H400, H410	none
n-decane	H226, H304	none
n-dodecane	H304	R65

Ethanol	H225, H319	none
Ethyl acetate	H225, H319, H336	none
n-heptane	H225, H304, H315, H336, H410	none
n-hexane	H225, H315, H361, H336, H373, H304, H410	none
Isopropyl acetate	H225, H319, H336	EUH066
Methyl-isobutyl-ketone	H225, H332, H319, H335	EUH066
n-nonane	H226, H304, H400	none
n-octane	H225, H304, H315, H336, H410	none
Isopropanol	H225, H319, H336	none
Propylene carbonate	H319	R36
Tert butyl methyl ether	H225, H315	none
Toluene	H225, H315, H361d, H336, H373, H304	none
Water	none	none
Dimethyl sulphoxide-d	none	none
Methanol	H225, H331, H311, H301, H370	R11, R23/24/25, R39/23/24/25

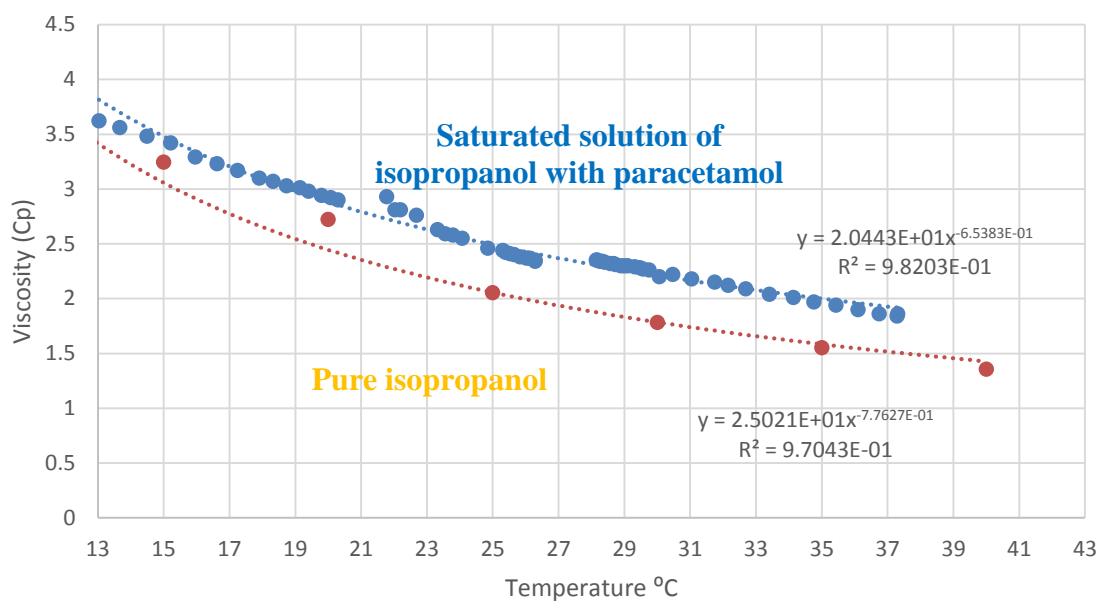


Figure 115 Isopropanol - paracetamol saturated solution viscosity at different temperatures.^{71,1}

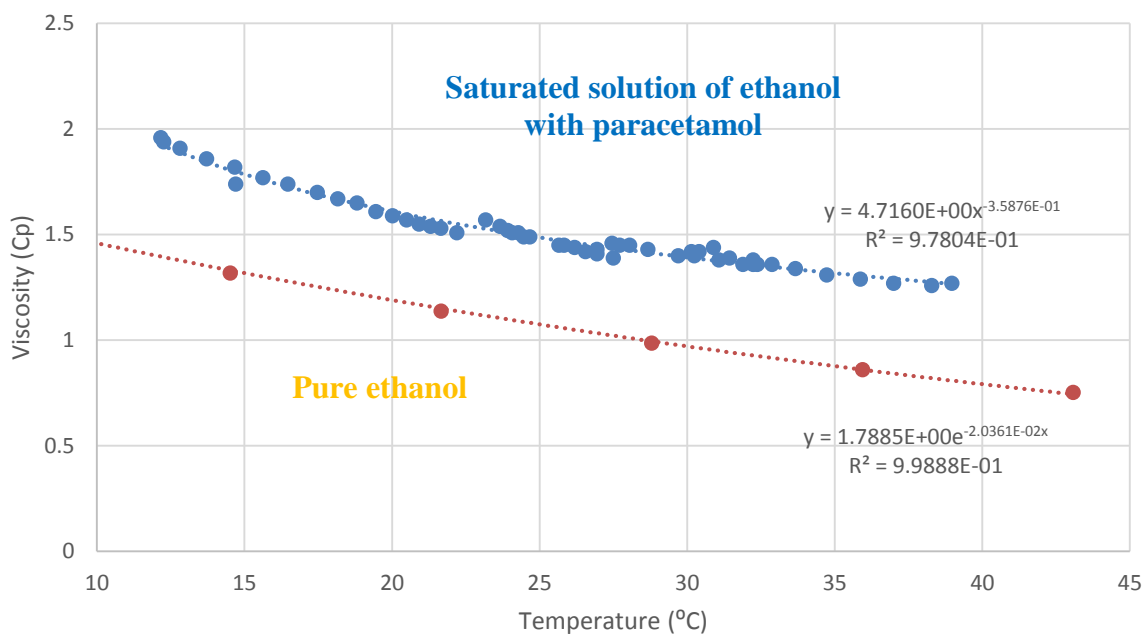


Figure 116 Ethanol - paracetamol saturated solution viscosity at different temperatures.^{72, II}

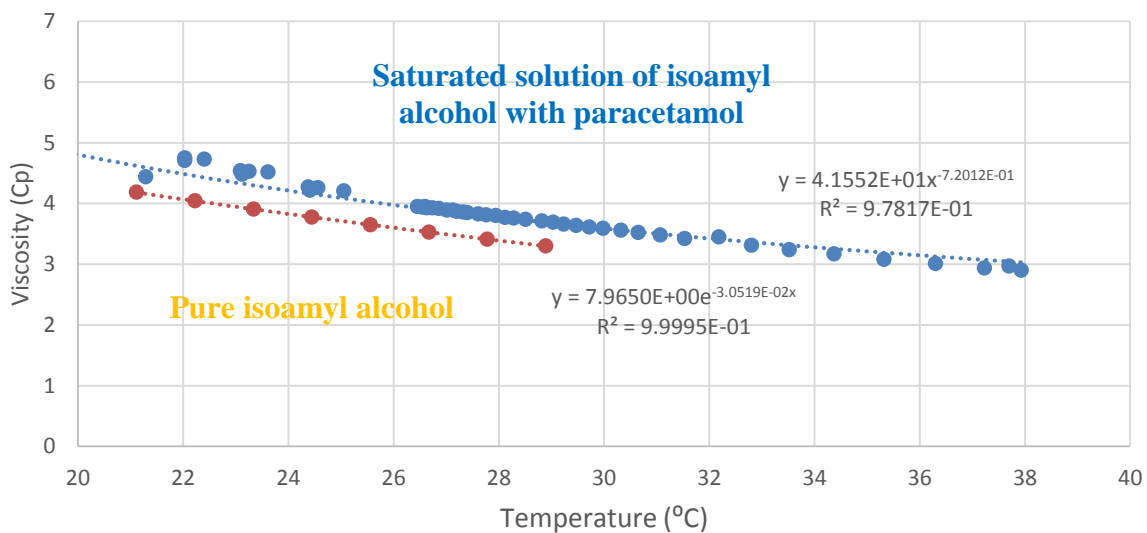


Figure 117 Isoamyl Alcohol - paracetamol saturated solution viscosity at different temperatures.^{73, III}

9.2 Isolation parameters

9.3 Solubility by equilibration

Table 49 Solubility by equilibration of paracetamol in ethanol and hexane and 4-nitrophenol in ethanol and hexane.

Solute-solvent (temperature, °C)	Solubility and standard deviation (g/g)
Paracetamol-ethanol (8.3 °C)	147.8309 ± 0.0005
Paracetamol-ethanol (13.7 °C)	159.9914 ± 0.0006
Paracetamol-ethanol (20 °C)	184.1409 ± 0.0031
Paracetamol-ethanol (25 °C)	205.6479 ± 0.0045
Paracetamol-ethanol (30 °C)	224.6287 ± 0.0039
4-nitrophenol-ethanol (25 °C)	2265.6393 ± 0.1213
4-nitrophenol-ethanol (40 °C)	2763 ± 0.0173
4-nitrophenol-ethanol (55 °C)	2802.4372 ± 0.0519
Paracetamol-hexane (25 °C)	2.9074 ± 0.0033
Paracetamol-hexane (40 °C)	1.9100 ± 0.0014
Paracetamol-hexane (55 °C)	7.3725 ± 0.0047
4-nitrophenol-hexane (25 °C)	3.34914 ± 0.0032
4-nitrophenol-hexane (40 °C)	6.2864 ± 0.0057
4-nitrophenol-hexane (55 °C)	8.2176 ± 0.0053

9.4 The impact of paracetamol impurities on crystal face properties: investigating the surface of single crystals using TOF-SIMS.

9.4.1 4-aminophenol mass spectra

4-aminophenol (molecular weight: 109.13g/mol)

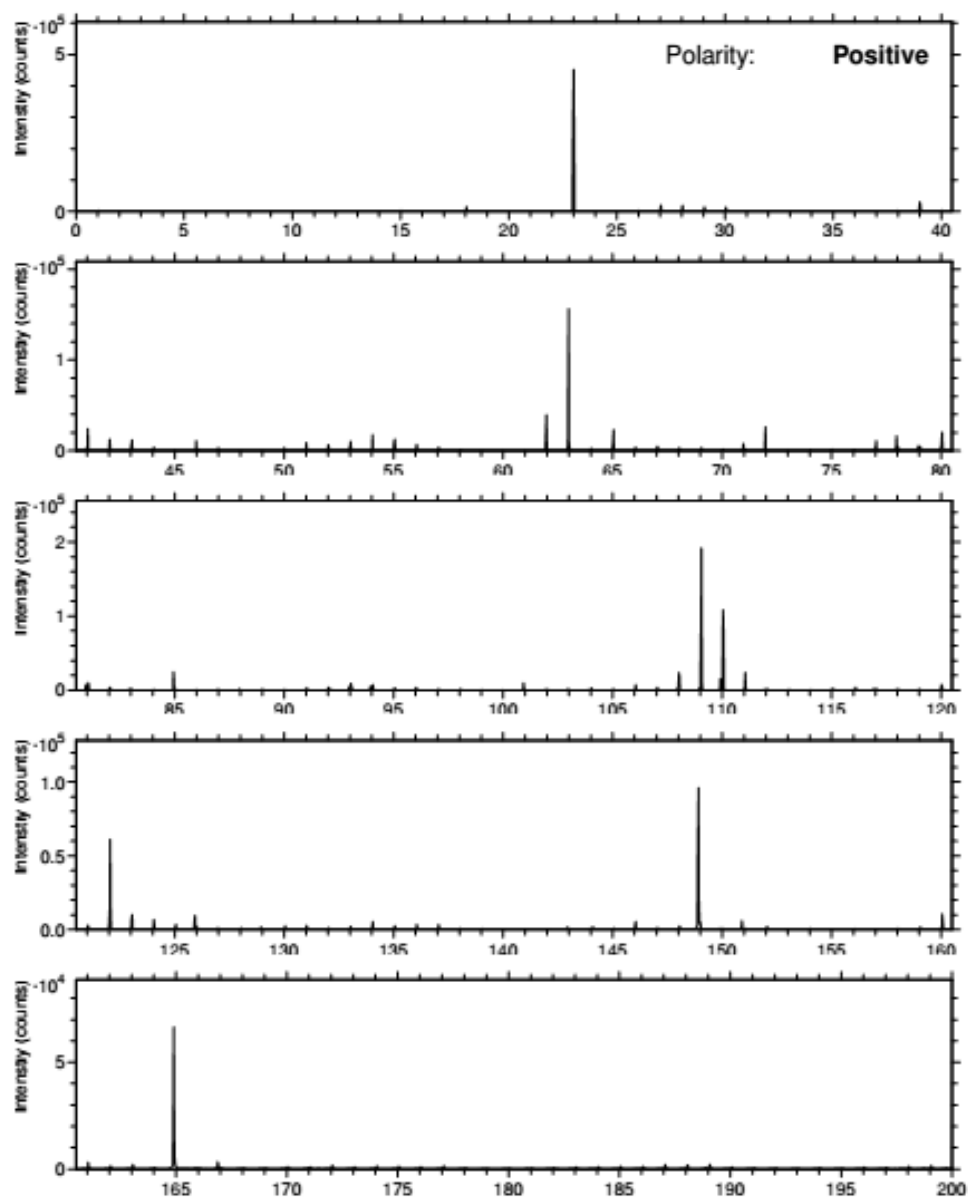


Figure 118 Positive mass spectra of pure 4-aminophenol with TOF-SIMS in spectroscopy mode.

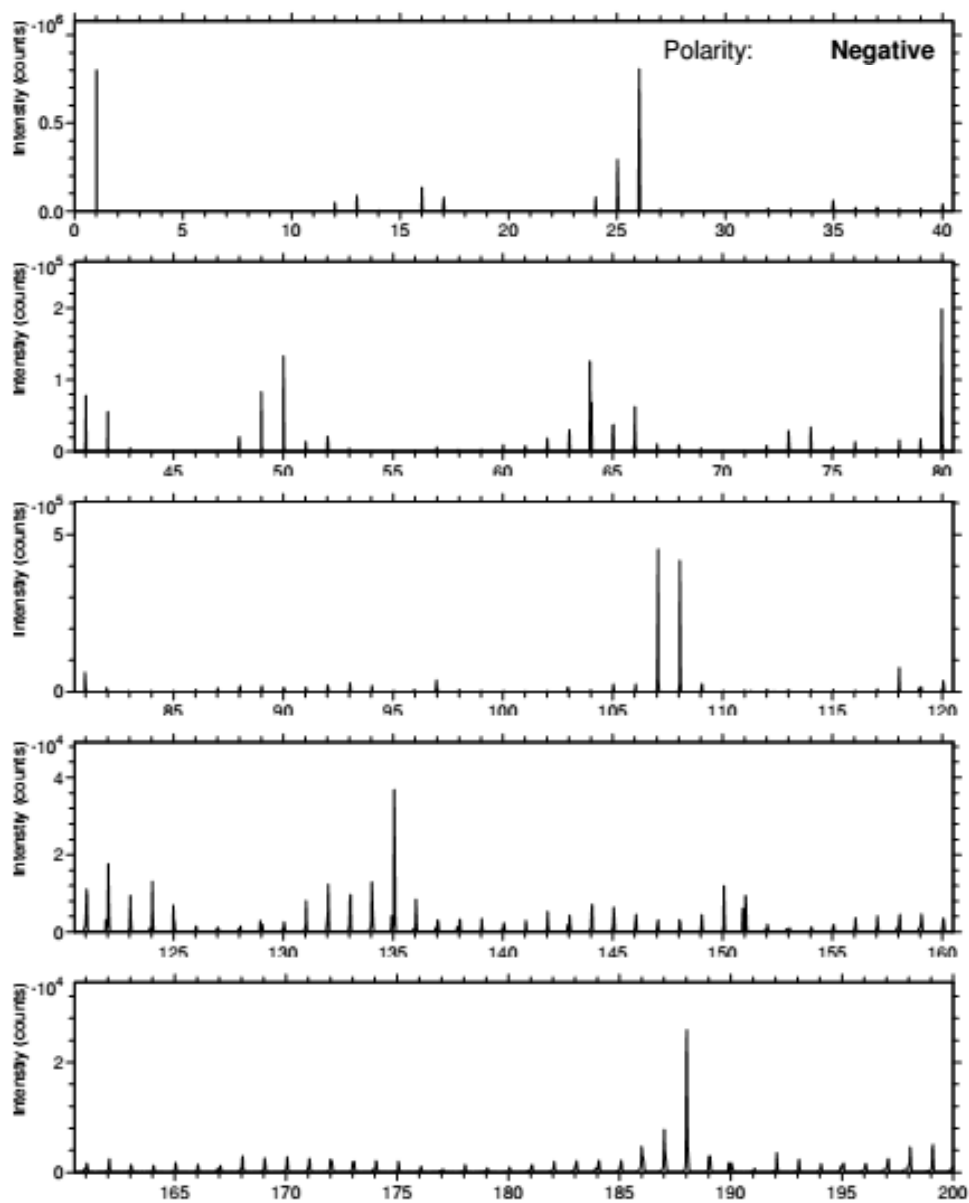


Figure 119 Negative mass spectra of pure 4-aminophenol with TOF-SIMS in spectroscopy mode.

9.4.2 Single crystals crystallized in presence of other paracetamol related impurities

The aim of the second part of the TOF-SIMS work was to evaluate the capability of TOF-SIMS to detect different paracetamol related impurities on single crystals made by cooling

crystallization. For each crystal the two biggest facets were analyzed to evaluate differences in impurity absorption and to evaluate whether the difference of protruding functional groups on each facet of paracetamol can influence impurity absorption (do impurities have preferential facets for absorption due to differences in the surface functionality of different faces). The TOF-SIMS investigation was conducted on the surface of the crystal faces (surface imaging) but it also allows investigation of a series of layers below the surface to evaluate whether the impurities were located in sub-surface position (3D depth profile).

Some of the crystals produced were not used for the TOF-SIMS investigation:

- Orthocetamol and metacetamol are isomers of paracetamol; those impurities are impossible to detect by TOF-SIMS because they present the same ion fragmentation pattern as paracetamol, even though the hydroxyl group is in different position of the aromatic ring
- Analysing the relative solubilities of paracetamol and 4'-chloroacetanilide in ethanol, the two molecules exhibit distinctly different solubilities in ethanol, first paracetamol crystallizes and then 4'-chloroacetanilide. The crystallized material yielded two distinct sets of crystals: pure paracetamol and pure 4'-chloracetanilide as seen in Figure 120 (not verified by X-ray diffractometry).

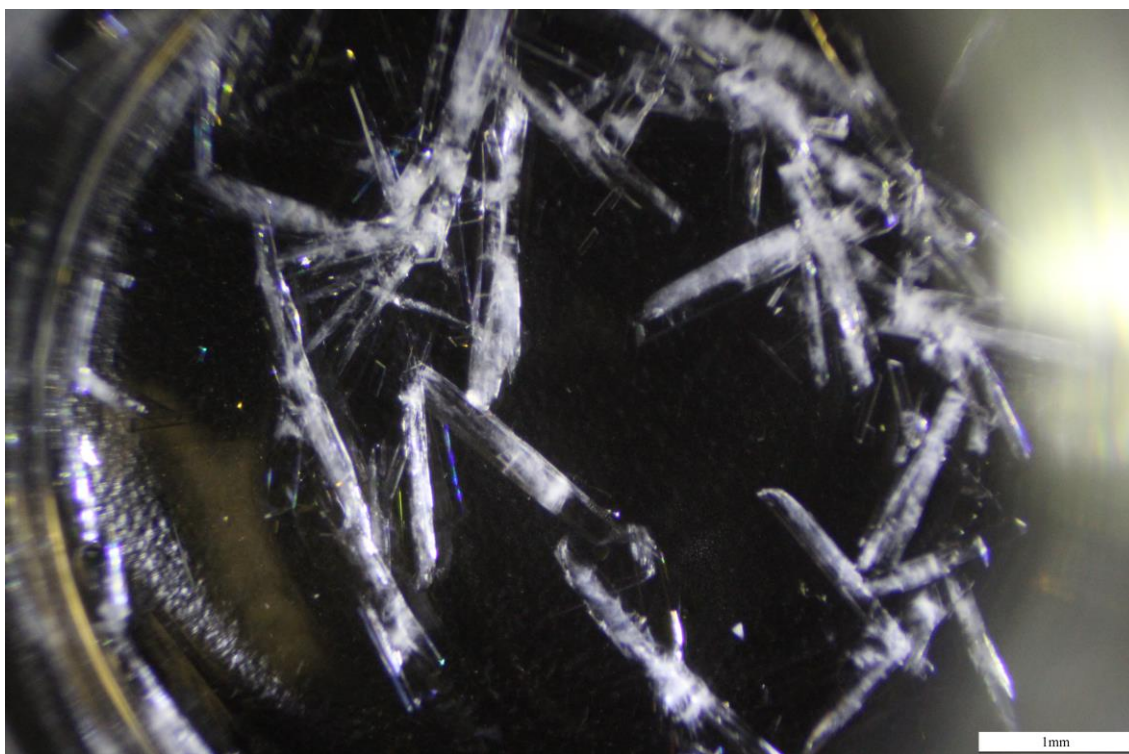


Figure 120 Stereomicroscopy of crystal produced with cooling crystallization of paracetamol with 4% mol of 4'-chloroacetanilide, $S=1.5$ in ethanol, 1x. 4'-chloro acetanilide crystallized separately to paracetamol forming needle-shape (pure 4'-chloro acetanilide crystals) and hexagonal-like shape of pure paracetamol crystals.

- The same result as seen for 4'-chloracetanilide and paracetamol was obtained for crystals of paracetamol with 4% mol of acetaminophen acetate in ethanol. In this particular case, solubility of acetaminophen acetate is much higher than paracetamol the concentrations used resulted in the initial crystallization of pure acetaminophen acetate crystals followed then by pure paracetamol crystals (Figure 121). This result needs to be verified by X-ray diffractometry.

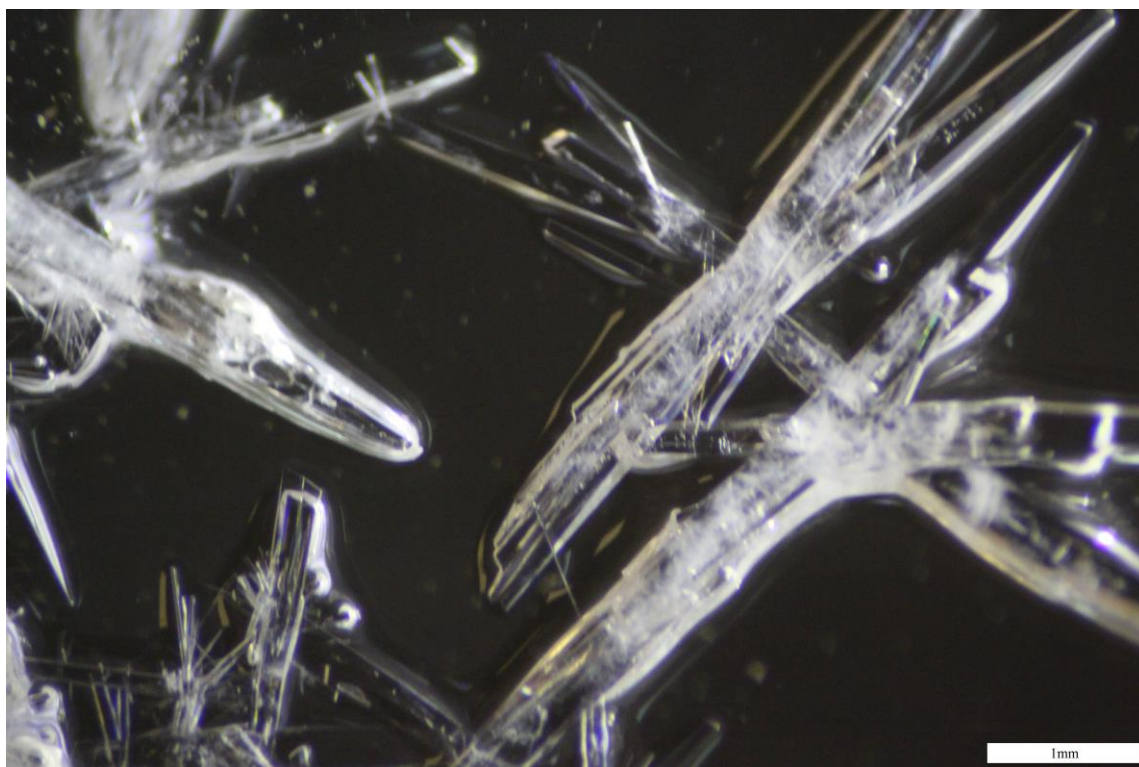


Figure 121 Stereomicroscopy of crystal produced with cooling crystallization of paracetamol with 4% mol of acetaminophen acetate, $S=1.5$ in ethanol, 1.5x. Acetaminophen acetate crystallized separately to paracetamol forming needle-shape (pure acetaminophen acetate crystals) and hexagonal-like shape of pure paracetamol crystals.

A series of stereomicroscopy images were collected to show the facets analysed with TOF-SIMS of each single crystal.

- Single crystal formed by cooling crystallization of paracetamol with 4%mol of acetamido benzoic acid in ethanol (P4% AMBA-EtOH): in this case the interaction solvent-impurity caused the growth of a rod shaped crystal with sharp edges and non-parallel lateral facets. As reported in literature, also solvent may interact with crystal growth promoting crystal morphology changes. Two different effects were proposed to occur due to the incorporation of solvent in the crystalline structure; the transition from smooth to rough surfaces, and the concomitant faster surface

growth and preferential adsorption at specific faces. The latter inhibits growth due to the interaction and blockage of surface crystal functional groups with the adsorbed solvent molecule. From the stereomicroscopy images, as seen in Figure 122) it appears that the lateral small faces grow faster than the bigger faces producing this elongated shape of the crystal. Indeed, the lateral faces show a rough surface in comparison to the other facets.

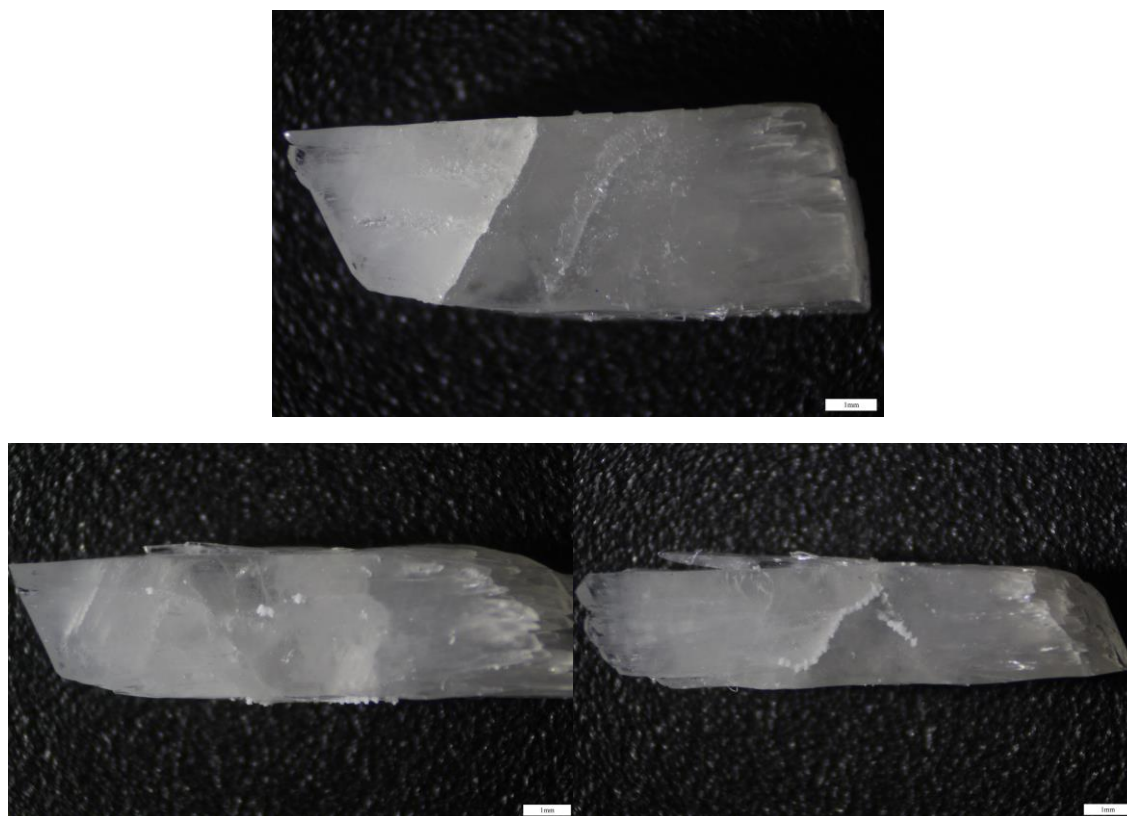


Figure 122 Top: single crystal of paracetamol with 4% mol of acetamido benzoic acid, $S=1.5$ in ethanol, stereomicroscope 1x; Bottom left and right: two details of the surface of the single crystal of paracetamol with 4%mol of acetamido benzoic acid, $S=1.5$ in ethanol, stereomicroscope 1x. Different faces.

- Single crystals formed by cooling crystallization of paracetamol with 4% mol of 4-aminophenol in ethanol (P4%AP-EtOH): the presence of 4-aminophenol causes a variation of crystal morphology. Comparing the pure paracetamol crystal (Table 26 and Figure 123) and the paracetamol crystal with 4% by mol of 4-aminophenol, some crystal faces were blocked resulting in a rhombic-like morphology. Another variation is the coloration of the crystal caused by the presence of 4-aminophenol. As supplied 4-aminophenol crystals show a brown coloration.

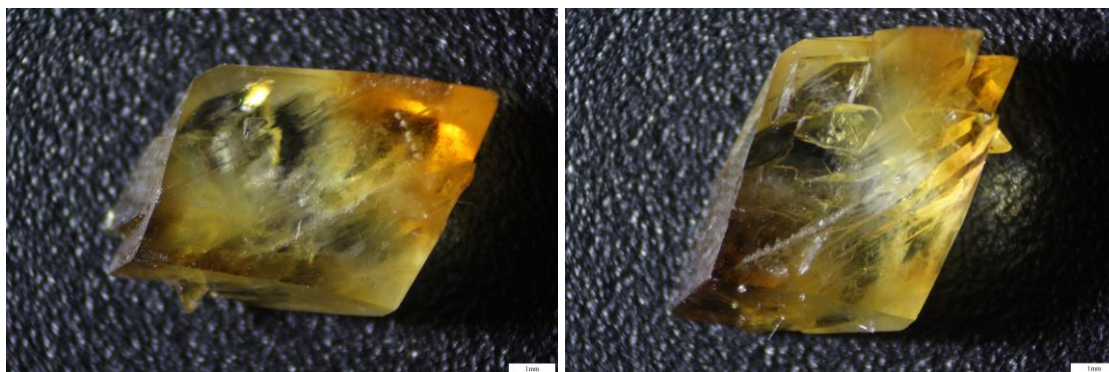


Figure 123 Stereomicroscopy of single crystal of paracetamol with 4% mol of 4 aminophenol, S=1.5 in ethanol, 1x. Different faces.

- Single crystals formed by cooling crystallization of paracetamol with 4% mol of 4-hydroxy acetophenone in ethanol (P4%HA-EtOH): from the stereomicroscopy images (Figure 124) it is difficult to establish if morphology variations occurred in presence of the paracetamol related impurity at this concentration. Future SC-XRD investigation can better define possible morphology changes.

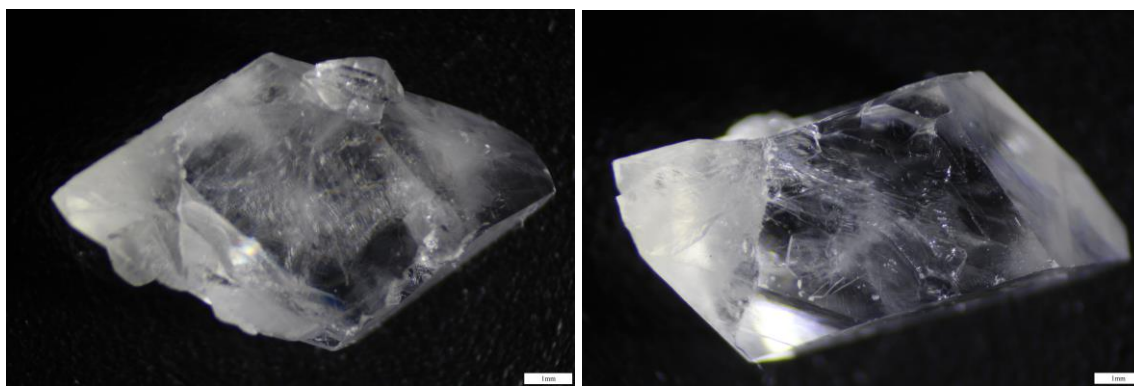


Figure 124 Stereomicroscopy of single crystal of paracetamol with 4% mol of 4 hydroxyl acetophenone, $S=1.5$ in ethanol, 1.3x. Different faces.

- Single crystals formed by cooling crystallization of paracetamol with 4% mol of acetanilide in ethanol (P4%A-EtOH): show similar effects to P4%AMBA-EtOH crystals observed. Formation of rod-like crystals with rough lateral surfaces were observed due to the concomitant interaction of impurity and solvent during the crystal growth (Figure 125).

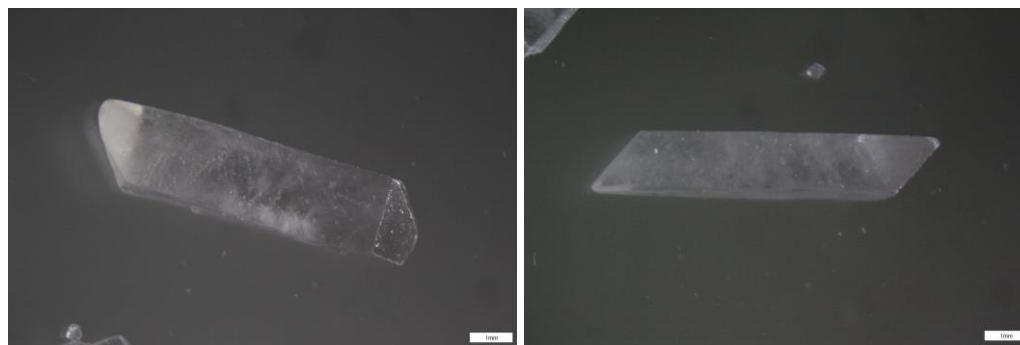


Figure 125 Stereomicroscopy of single crystal of paracetamol with 4% mol of acetanilide, $S=1.5$ in ethanol, 1x. Different faces.

- Single crystals formed by cooling crystallization of paracetamol with 4% mol of 4-methyl hydroxyl benzoate in ethanol (P4%MHB-EtOH): the presence of the 4-

methyl hydroxyl benzoate caused growth of a series of new small facets around the entire crystal forming a more rounded hexagonal-like morphology (Figure 126).

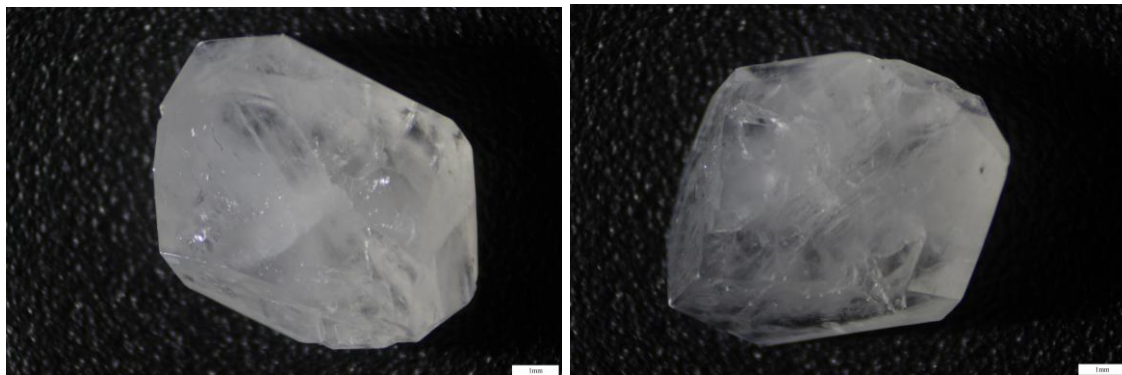


Figure 126 Stereomicroscopy of single crystal of paracetamol with 4% mol of 4 methyl hydroxyl benzoate, $S=1.5$ in ethanol, 1x. Different faces.

To better understand the interactions of solvent and impurities during the crystal growth, a more detailed evaluation of the kinetics of crystallization in presence of these two impurities needs to be performed. However, as previously suggested, this lies outside the scope of this investigation, which is why the crystal growth experiments are not reported.

Examining whether it is possible to detect these related impurities on the surface and in the sub-surface layers of those single crystals with TOF-SIMS, two sets of TOF-SIMS analysis were done:

- Analysis of the surface with a delayed extraction method to determine spatial distribution of the impurities on the two largest crystal facets

- 3D depth profile measurement to map the composition of the crystal facets layer by layer.

AFM and optical microscopy in DIC mode were used to visualize the craters produced during the 3D depth profile TOF-SIMS measurement and to determine the depth of the total erosion. AFM is not able to determine the topography variation in case of big surface height variations (Figure 128 and Figure 129). However, using the optical microscope an average crater profoundness of 8-10um was estimated. The method used for the estimation of the crater depth was to measure the variation of depth of focus used to focus an external and an internal area of the crater. This was done by adjusting the illumination to get a narrow depth of field and then measuring the difference in height using the calibration of the stage movement. An example of crater images evaluated with optical microscopy is shown in Figure 127.

Optical microscopy and AFM are both able to show texture modification due to the sputtering, where the secondary ion beam caused damages to the surface due to prolonged exposure.

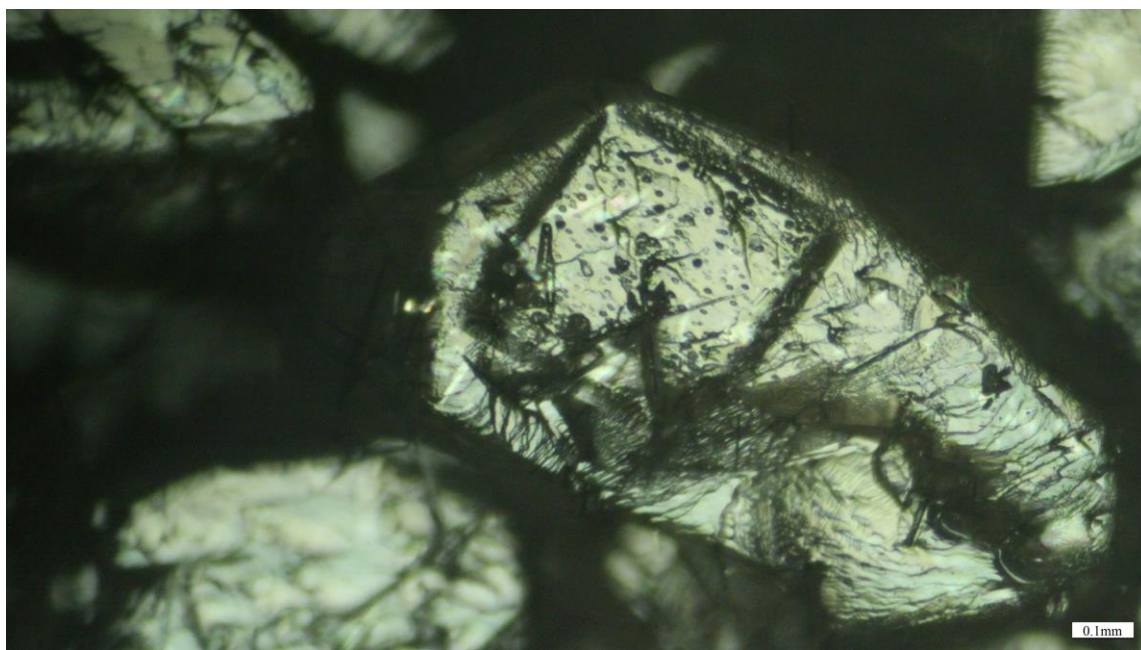


Figure 127 Example of craters formed by the 3D depth TOF-SIMS analysis evaluated with optical microscopy in DIC modes (5x).

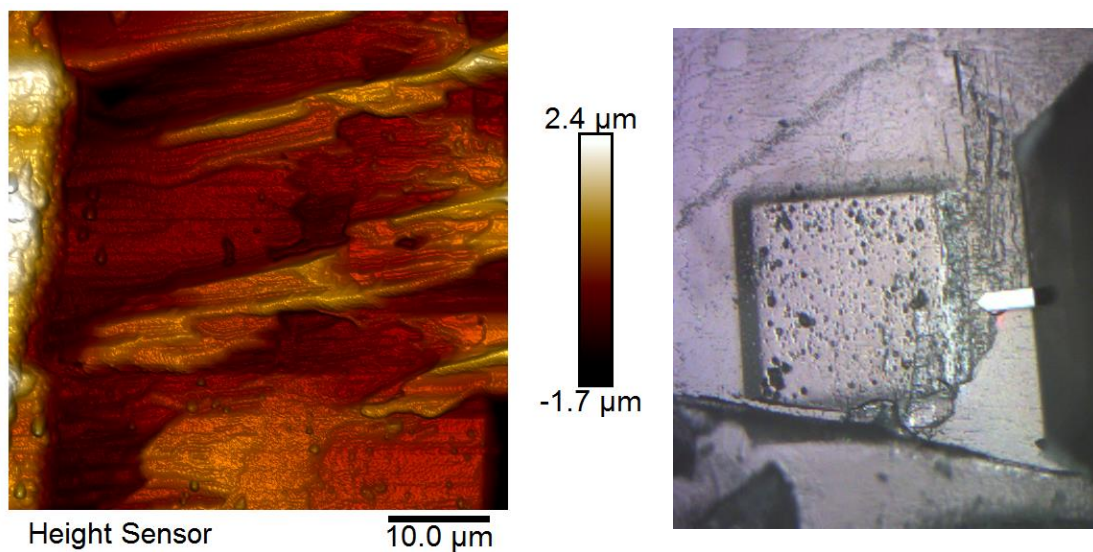


Figure 128 Example of AFM topographic map (left) of the cooling crystallization crystal produced with paracetamol with 4% mol of 4-acetamido benzoic acid on the right side of the TOF-SIMS crater. On the right the image of the area where the analysis was done (no scale-bar is reported by the instrument).

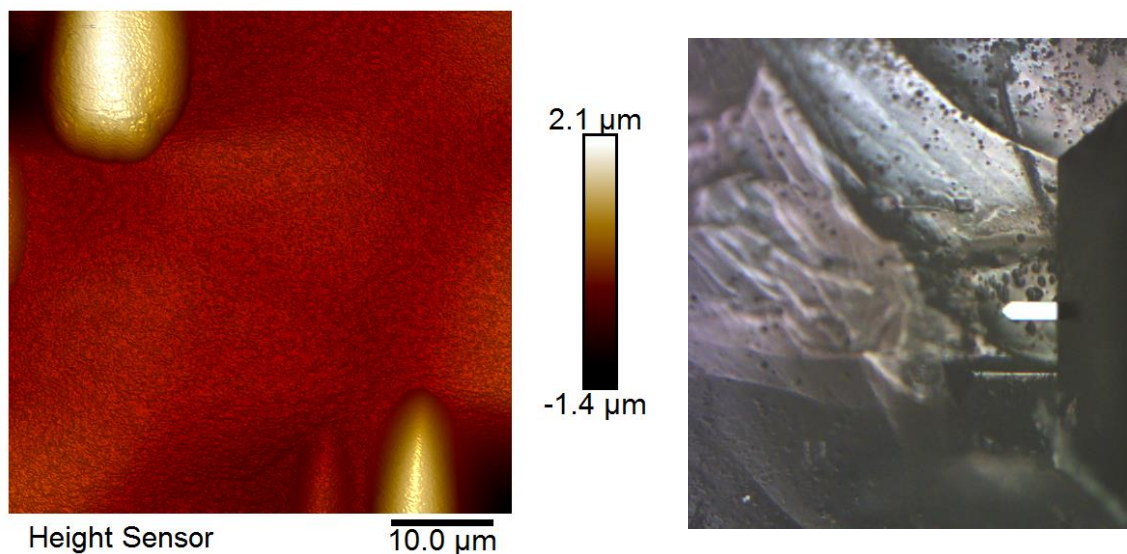


Figure 129 Example of AFM topographic map (left) of the cooling crystallization crystal produced with paracetamol with 4% mol of 4-acetamido benzoic acid of an internal area of the TOF-SIMS crater. On the right the image of the area where the analysis was done (no scale-bar is reported by the instrument).

Analyzing the mass spectra of each impurity, only 4-acetamido benzoic shows specific impurity peaks that do not overlap with the paracetamol mass spectra peaks. The overlapping is due to the capability of TOF-SIMS to create single and double ionized fragment species.

Spectra of the pure impurity compounds were obtained by analysis of the specific compounds in powder form. These were obtained directly from available supplier sources.

Molecular weight of 4-acetamido benzoic acid corresponds to 179.17g/mol.

The reported positive and negative mass spectra of ion fragments of pure 4-acetamido benzoic acid are shown in Figure 130 and Figure 131.

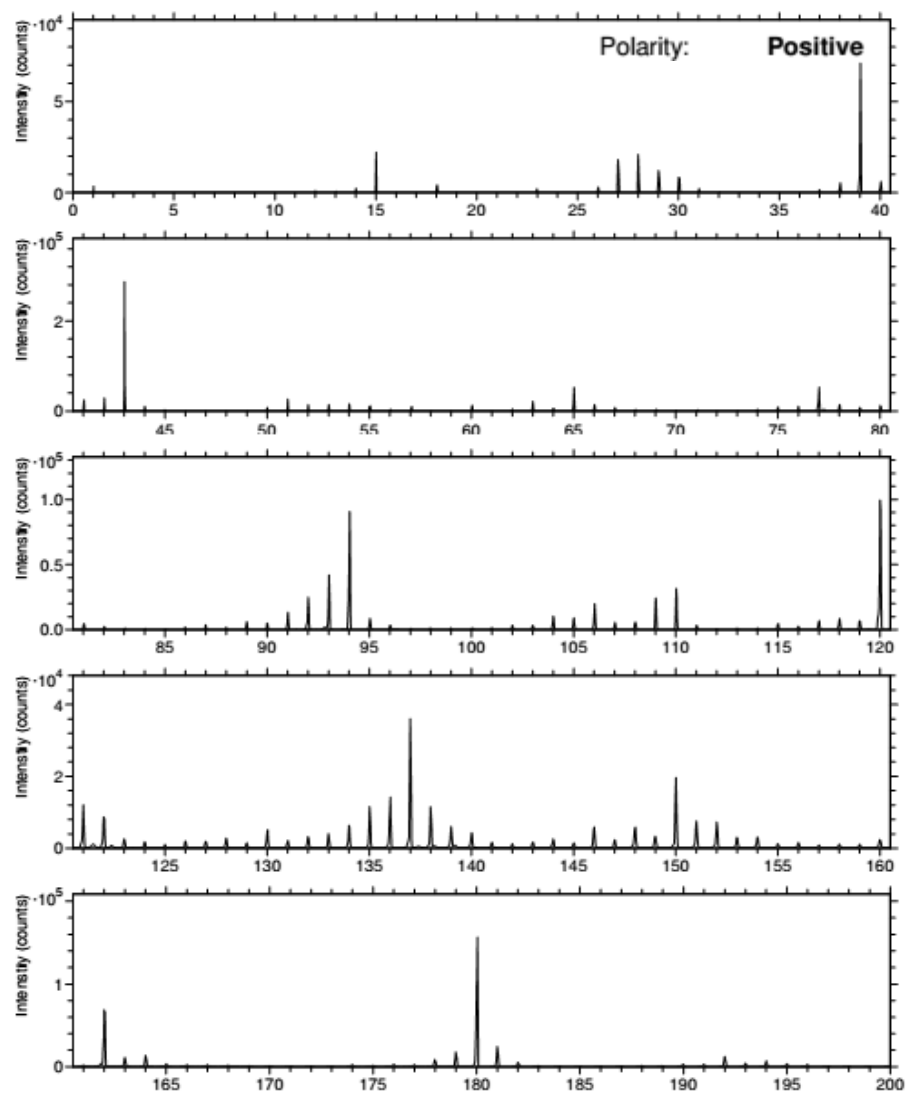


Figure 130 Positive mass spectra of pure 4-acetamido benzoic acid with TOF-SIMS in spectroscopy mode.

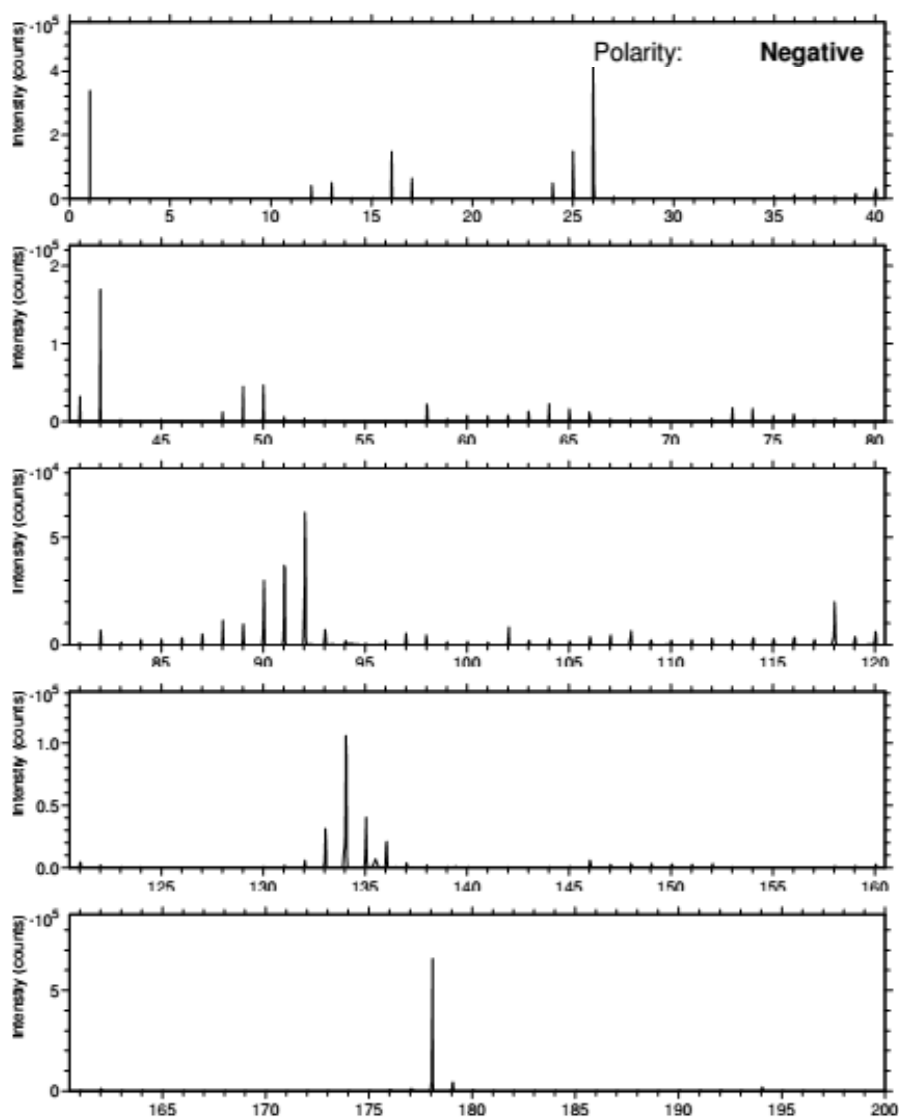


Figure 131 Negative mass spectra of pure 4-acetamido benzoic acid with TOF-SIMS in spectroscopy mode.

Analyzing the surface imaging maps of crystal face 1, 4-acetamido benzoic acid is clearly visible as a non-homogeneously distributed layer on the crystal surface (Figure 132).

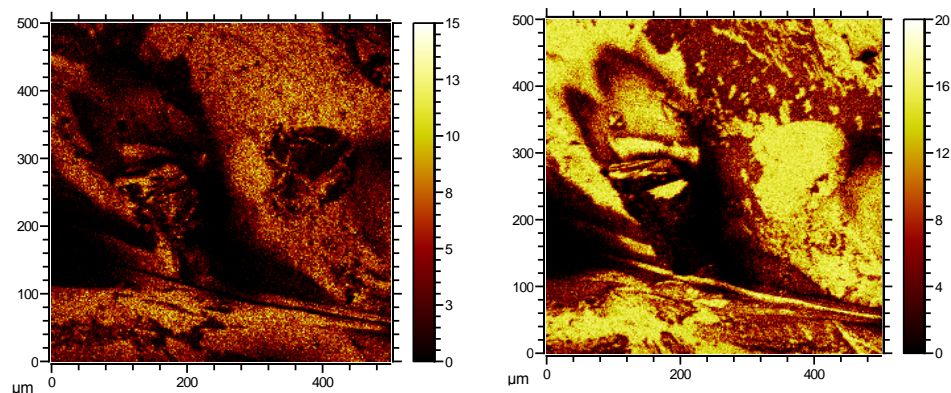


Figure 132 TOF-SIMS surface imaging of the sample secondary ion molecular images at 151m/z (maximum count = 15), left, corresponding to paracetamol, 178m/z (maximum count = 20) right, corresponding to 4-acetamido benzoic acid. Measurements taken on the bottom of the crystal face 1.

From the intensity count plot obtained during the 3D depth profile analysis (Figure 133) it is apparent that paracetamol is uniformly distributed in the bulk of the crystal, while 4-acetamido benzoic acid is mainly deposited on the crystal surface. Indeed, the impurity ion fragment intensity at 178m/z drops one order of magnitude (from 10^5 to 10^4) in the first 100s of sputtering.

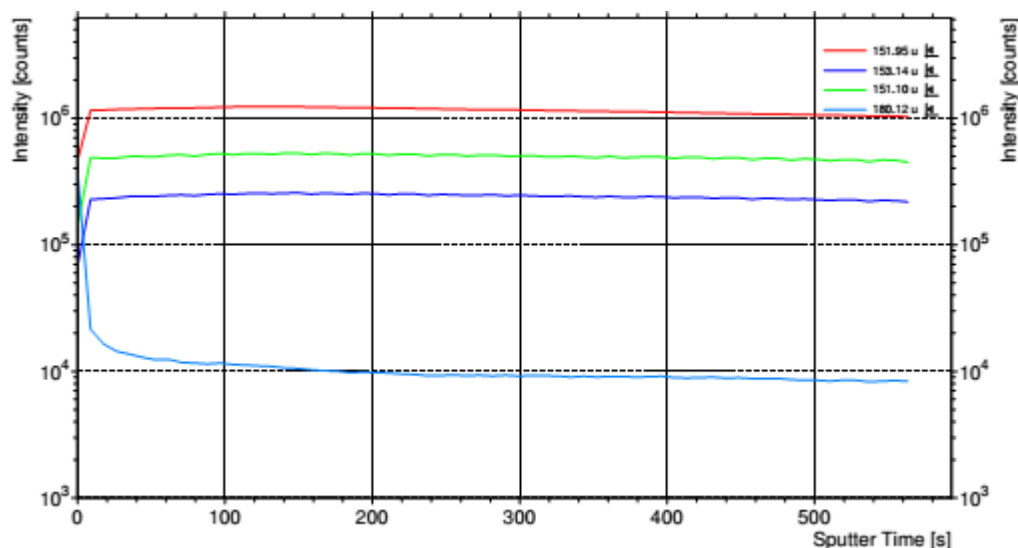
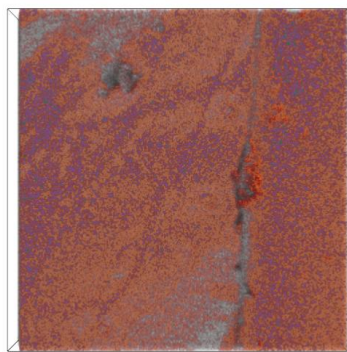
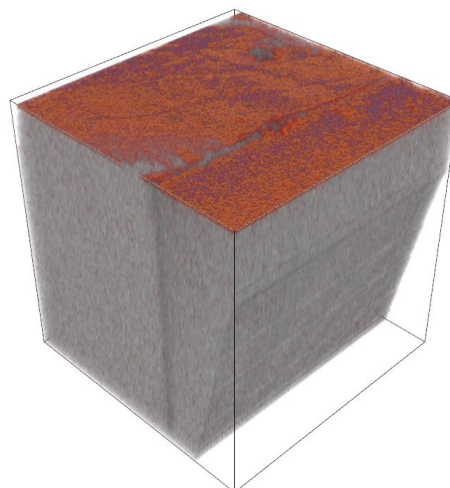


Figure 133 Intensity count of paracetamol ion fragment red, green and light blue, corresponding to 150 and 151 and 153 m/z) and 4-acetamido benzoic acid ion fragment (light blue, 178 m/z). Crystal face 1. 3D depth profile shows constant paracetamol content along the sputtered depth, while 4 acetamido benzoic acid curve is increasing during the first 200s of sputtering and then it stabilizes.

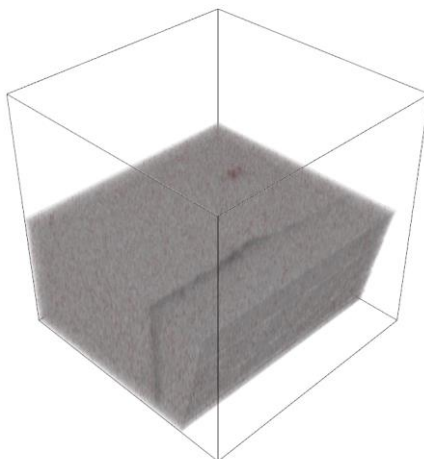
The distribution of the impurity during the sputtering of sample layers is observed in the 3D render overlay image (Figure 134): at approximately half the sputtering time the impurity intensity counts reduced by two orders of magnitude suggesting a significantly higher concentration of the impurity on the surface.



3D Render Overlay of: 180.12 u, 151.95 u



3D Render Overlay of: 180.12 u, 151.95 u



3D Render Overlay of: 180.12 u, 151.95 u

Figure 134 3D render overlay of paracetamol ion fragment (151m/z, grey) and 4-acetamido benzoic acid (178m/z, red). Different section of the 3D depth render of the crystal face 1.

The same deposition mechanism of 4-acetamido benzoic acid is also observed on the other larger crystal face (face 2, Figure 135 and Figure 136).

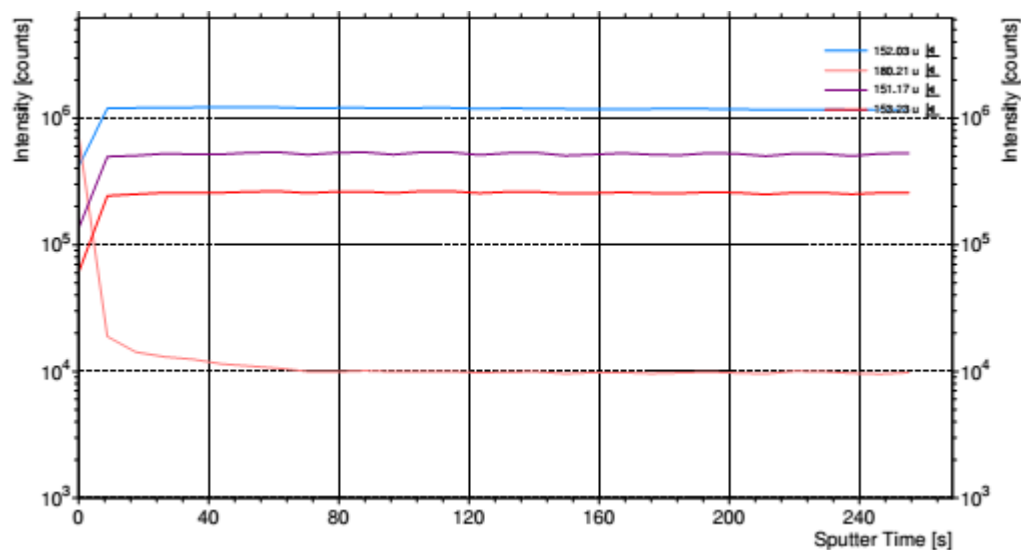
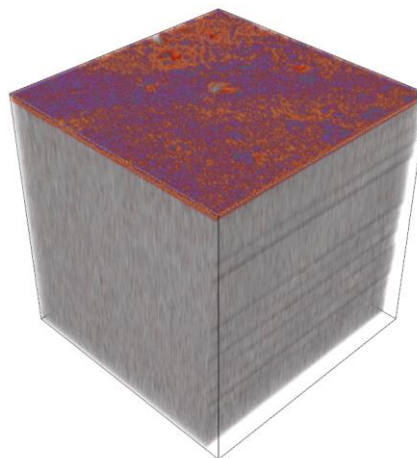
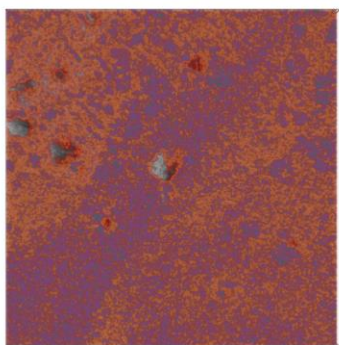
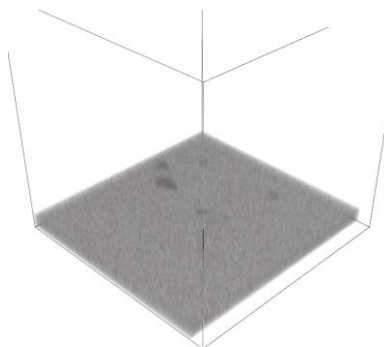


Figure 135 intensity count of paracetamol ion fragment (blue, red and violet, corresponding to 152, 153 and 151m/z) and 4-acetamido benzoic acid ion fragment (pink, 178m/z). Crystal face 2. 3D depth profile shows constant paracetamol content along the sputtered depth, while 4 acetamido benzoic acid curve is increasing during the first 200s of sputtering and then it stabilizes.



3D Render Overlay of: 152.03 u, 180.21 u

3D Render Overlay of: 152.03 u, 180.21 u



3D Render Overlay of: 152.03 u, 180.21 u

Figure 136 3D render overlay of paracetamol ion fragment (151m/z, grey) and 4-acetamido benzoic acid (178m/z, red). Different section of the 3D depth render of the crystal face 2.

9.4.3 Mass spectra of other paracetamol related impurities

9.4.3.1 4-hydroxy acetophenone (molecular weight: 136.15g/mol)

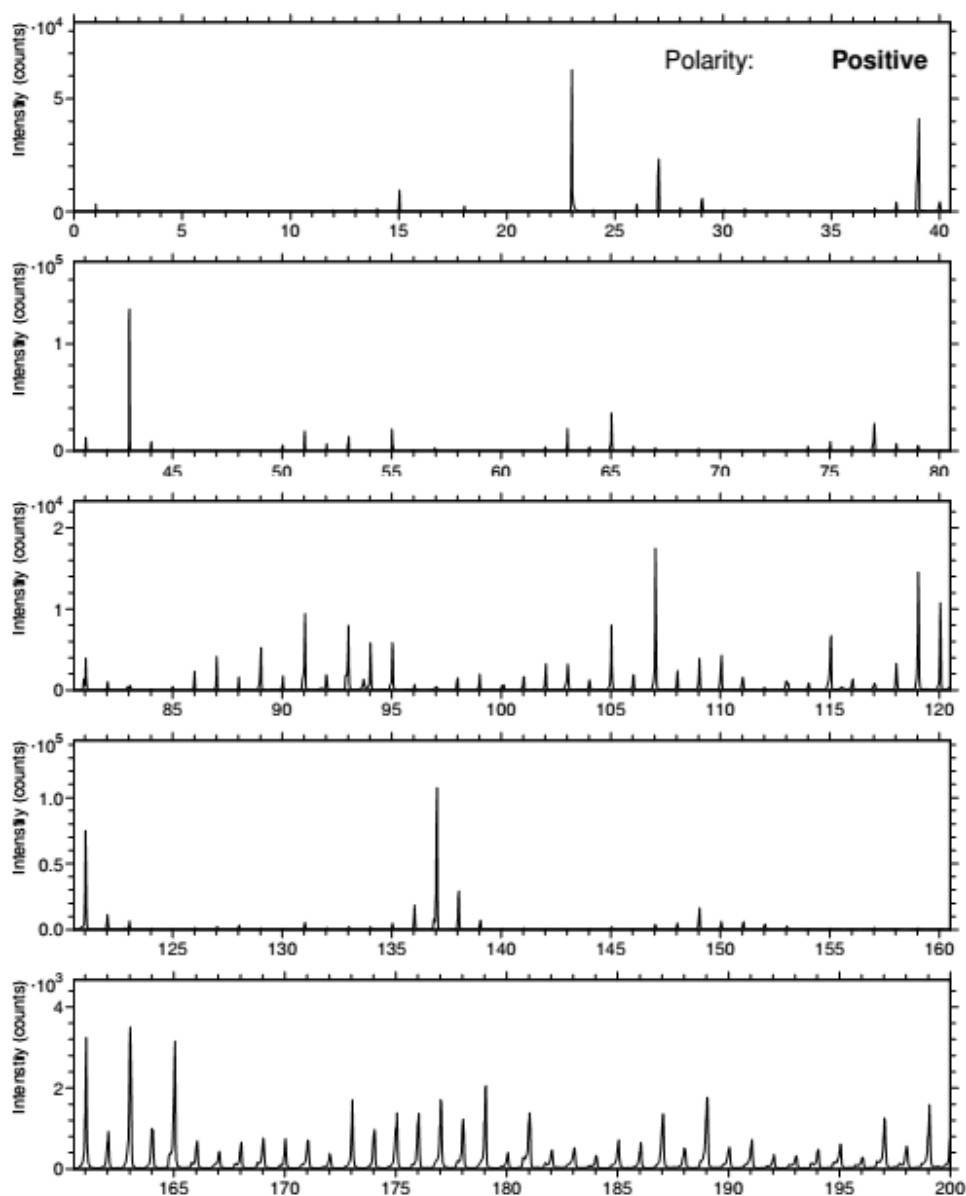


Figure 137 Positive mass spectra of pure 4-hydroxy acetophenone with TOF-SIMS in spectroscopy mode.

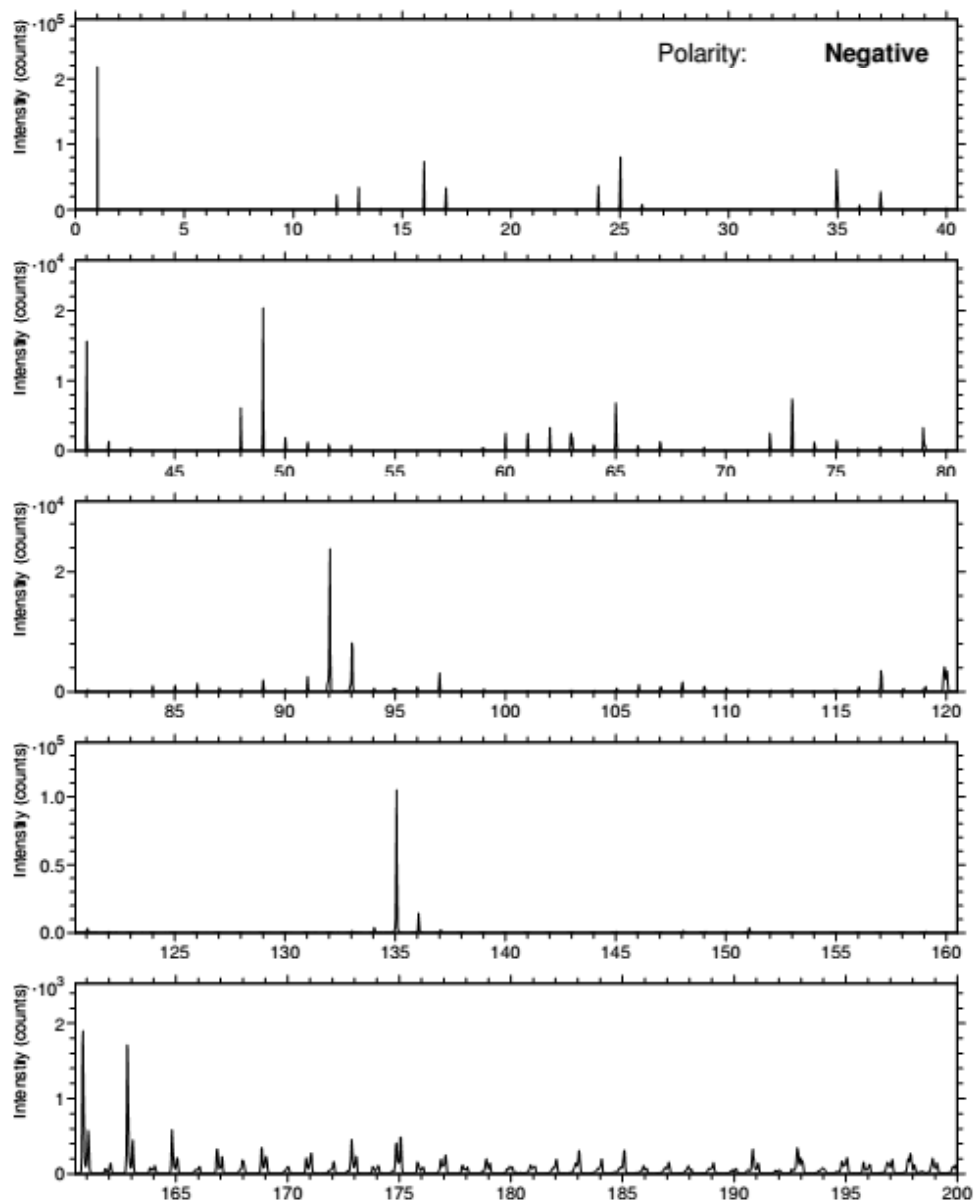


Figure 138 Negative mass spectra of pure 4-hydroxy acetophenone with TOF-SIMS in spectroscopy mode.

9.4.3.2 4'-chloroacetanilide (molecular weight: 169.61g/mol)

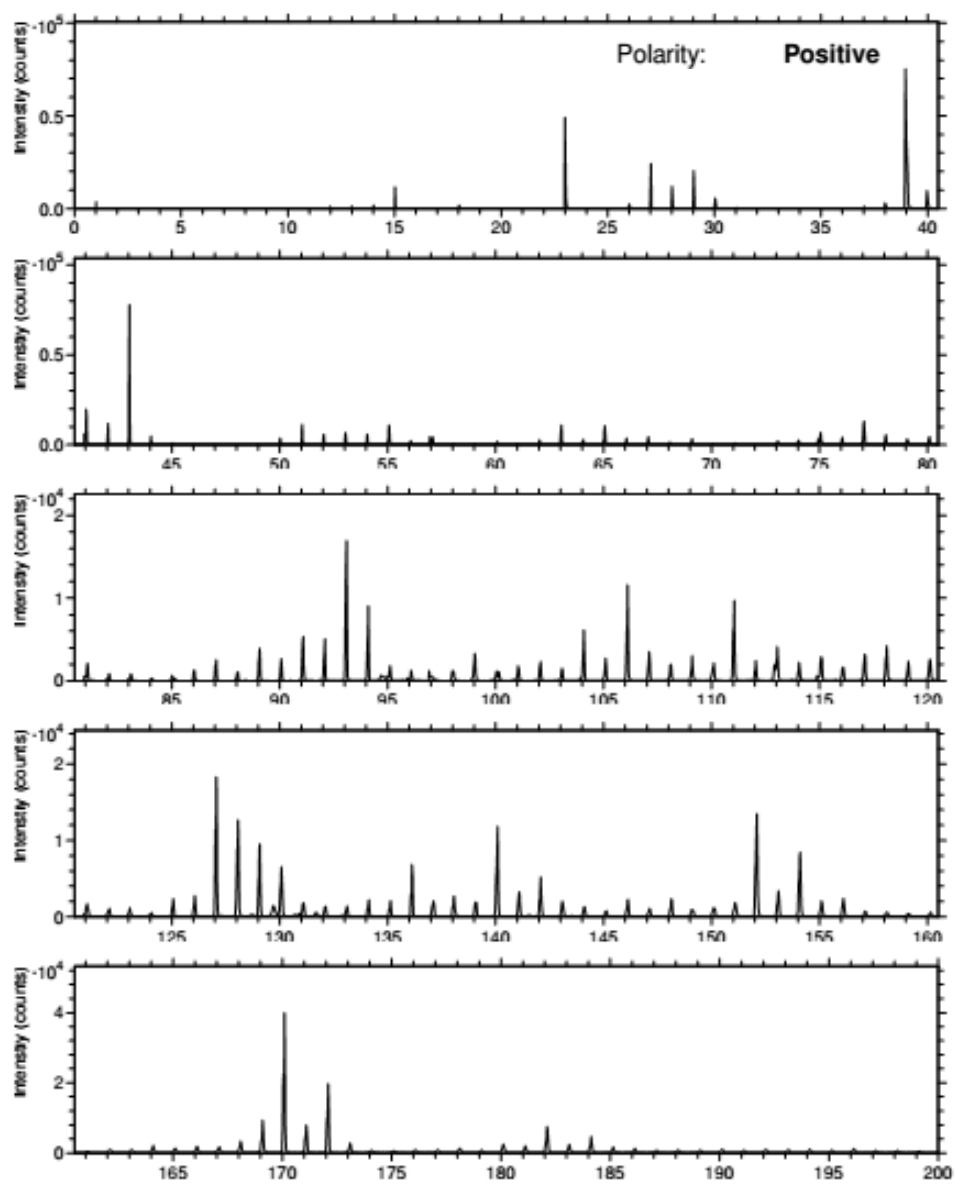


Figure 139 Positive mass spectra of pure 4'-chloro acetanilide with TOF-SIMS in spectroscopy mode.

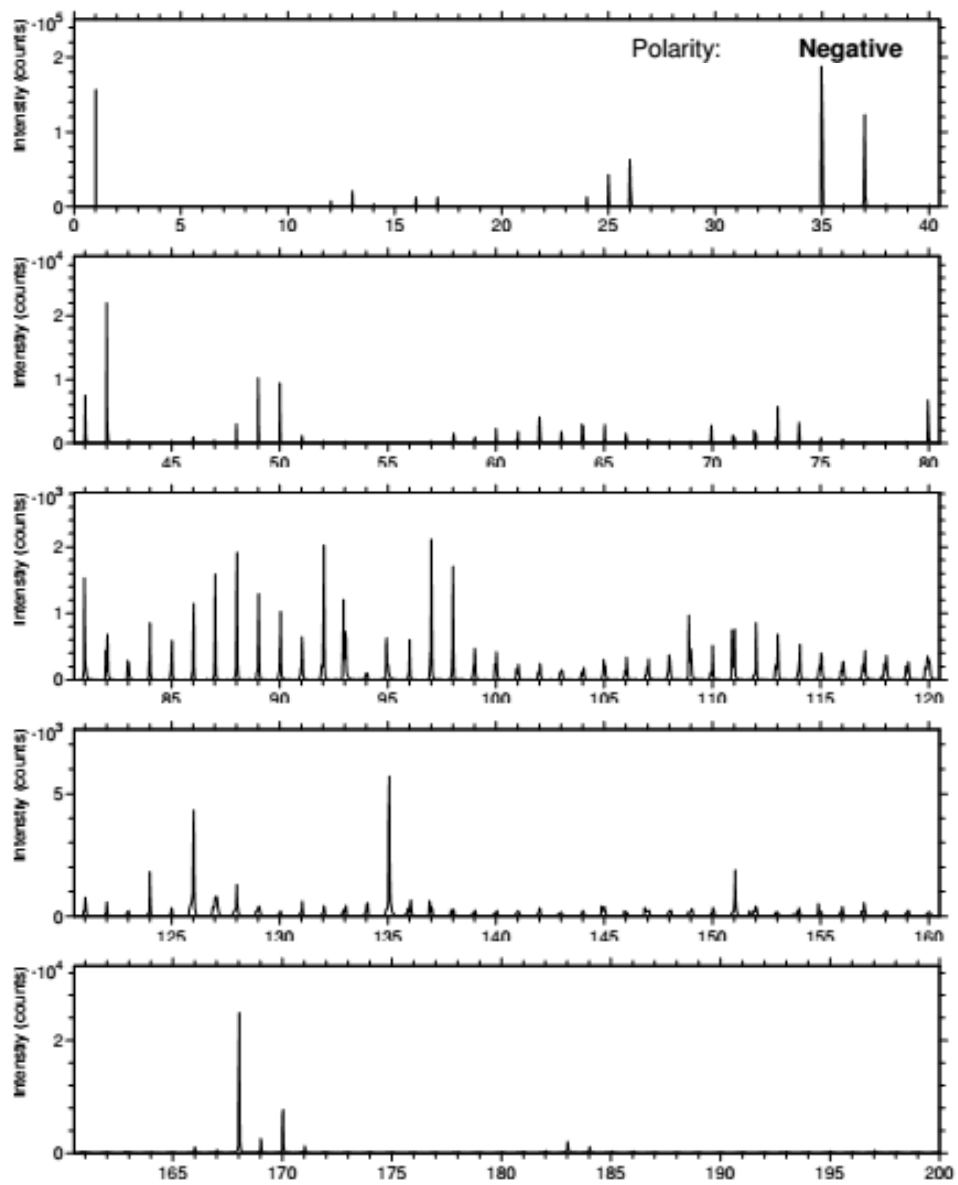


Figure 140 Negative mass spectra of pure 4'-chloro acetanilide with TOF-SIMS in spectroscopy mode.

9.4.3.3 Acetanilide (molecular weight: 135.17g/mol)

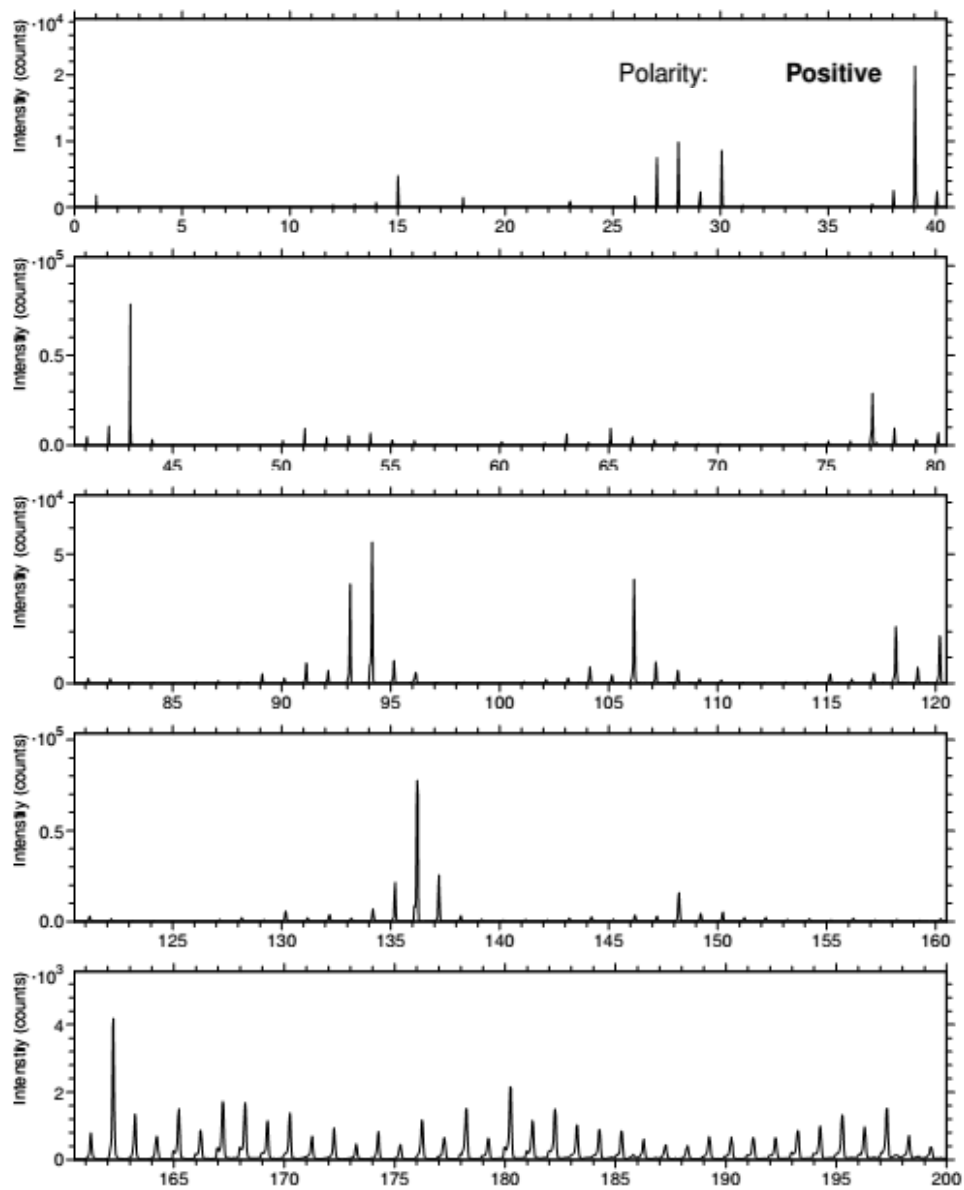


Figure 141 Positive mass spectra of pure acetanilide with TOF-SIMS in spectroscopy mode.

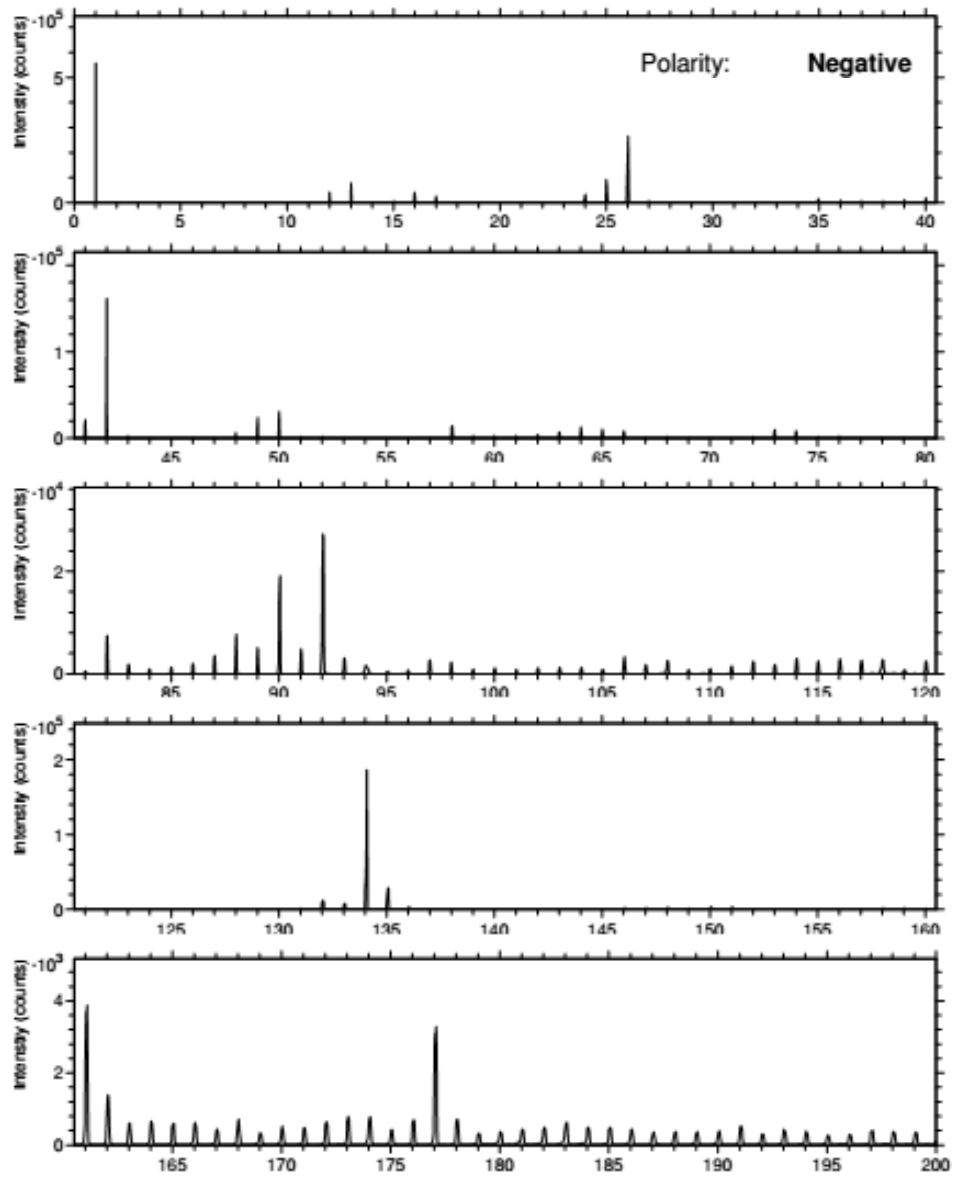


Figure 142 Negative mass spectra of pure acetanilide with TOF-SIMS in spectroscopy mode.

9.4.3.4 *4-methyl hydroxyl benzoate* (molecular weight: 152.14g/mol)

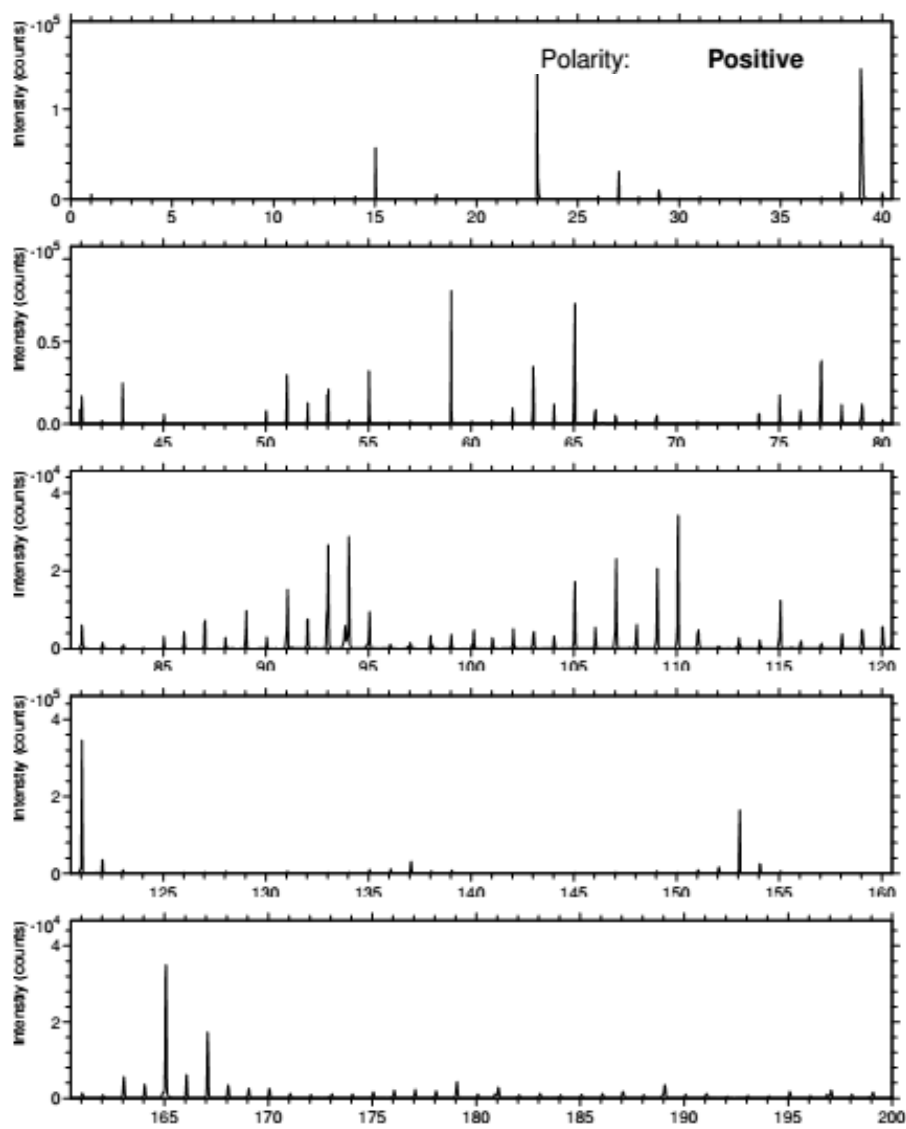


Figure 143 Positive mass spectra of pure 4-methyl hydroxyl benzoate with TOF-SIMS in spectroscopy mode.

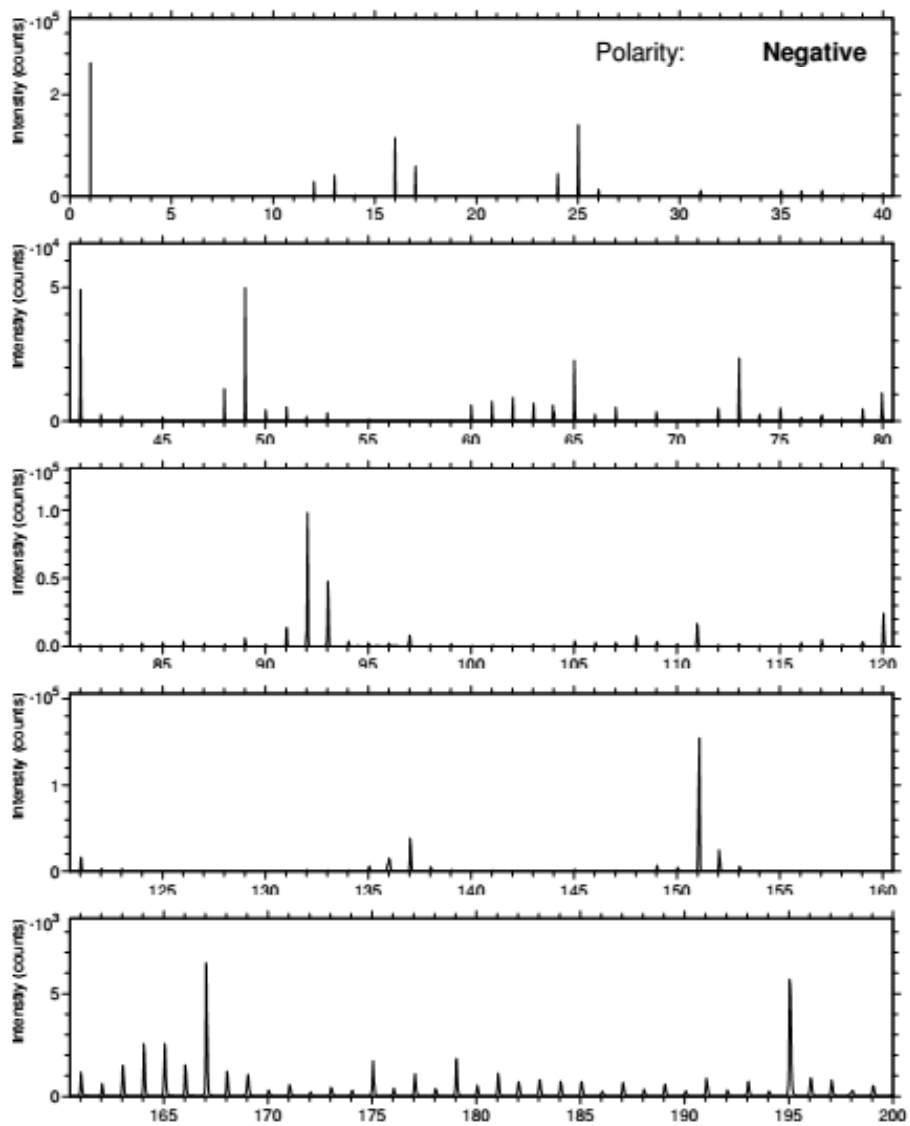


Figure 144 Negative mass spectra of pure 4-methyl hydroxyl benzoate with TOF-SIMS in spectroscopy mode.

**9.5 Effect of filtration, washing and drying on the isolated product:
Paracetamol case study.**

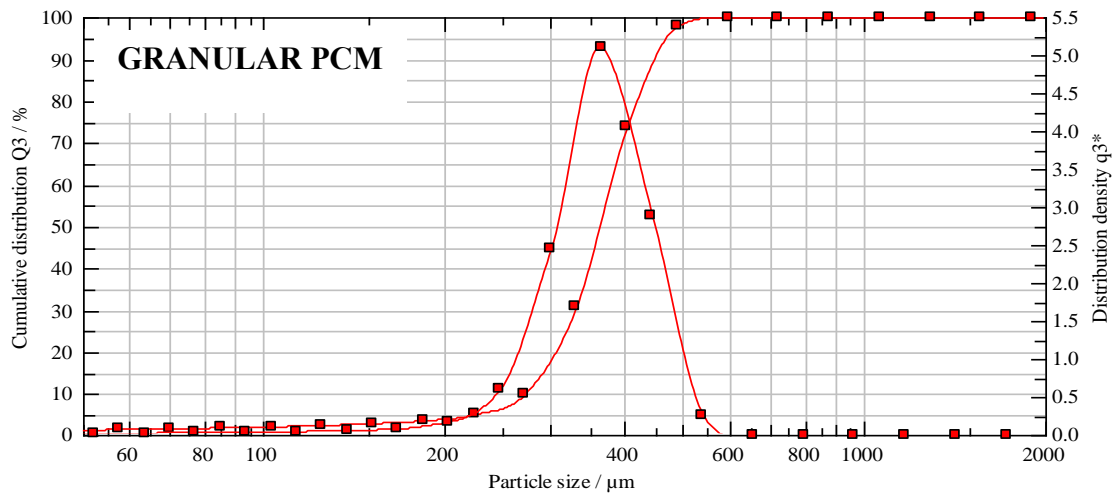


Figure 145 Cumulative distribution and distribution density of raw granular paracetamol.

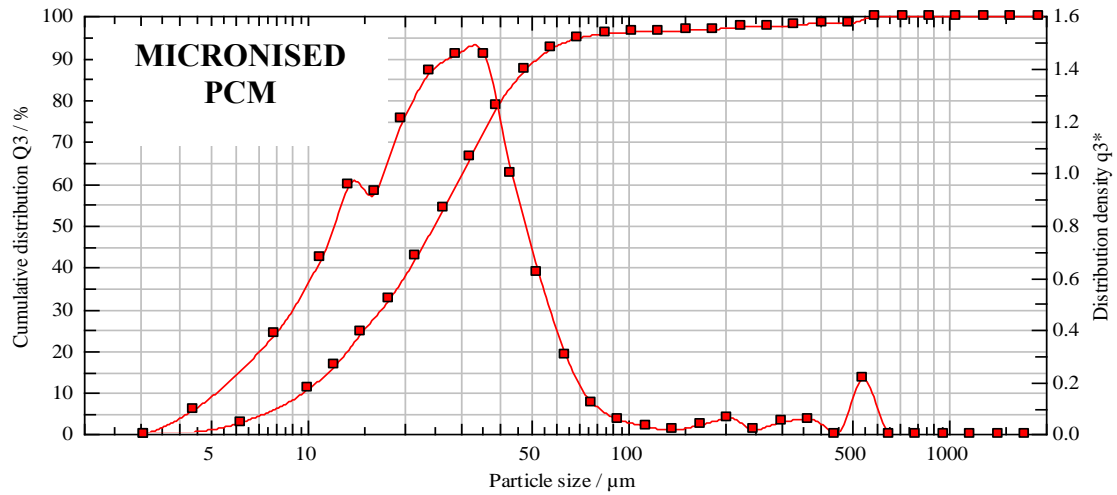


Figure 146 Cumulative distribution and distribution density of raw micronised paracetamol.

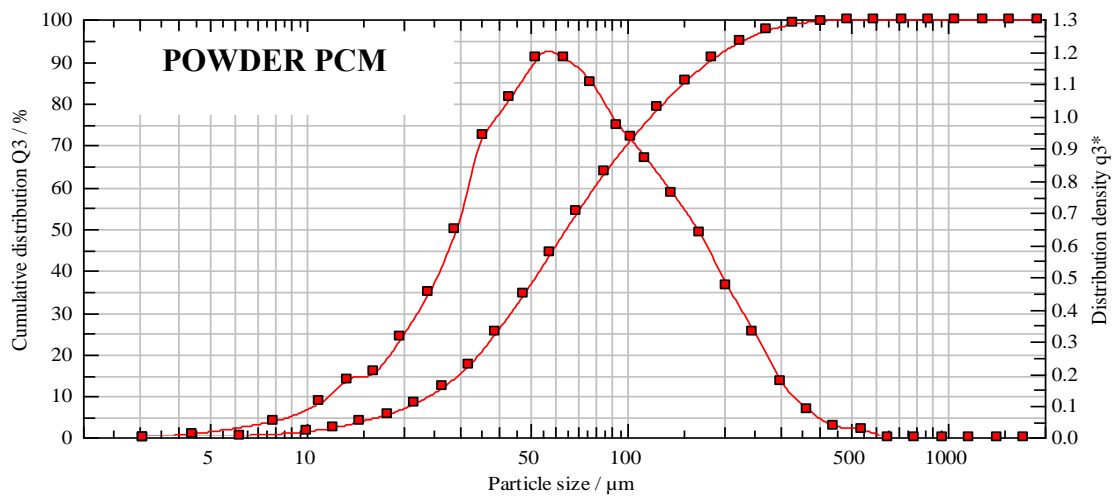


Figure 147 Cumulative distribution and distribution density of raw powder paracetamol.

Exp No	Exp Name	Run Order	Incl/Excl	Pressure	Material	Solid load	Volume of wash solvent	Number of washes	Filtration & Washing endpoint	Drying mechanism	Crystallization solvent	Washing solvent
31	MS_009	1	Incl	700	micronized	20	3 void cake volumes	2x	Dry/land	Vacuum	ethanol	n-heptane
6	MS_010	2	Incl	900	crystalline	30	1 void cake volume	1x	Breakthrough	Vacuum	ethanol	anisole
3	MS_011	3	Incl	500	granular	10	3 void cake volumes	2x	Breakthrough	Vacuum	ethanol	cyclohexane
21	MS_012 & MS_038 & MS_040	4	Incl	900	crystalline	10	2 void cake volumes	2x	Breakthrough	Vacuum	ethanol	dodecane
11	MS_013	5	Incl	500	granular	10	1 void cake volume	2x	Breakthrough	Vacuum	2-propanol	toluene
14	MS_014 & MS_021	6	Incl	900	micronized	10	2 void cake volumes	2x	Dry/land	Vacuum	2-propanol	isopropylacetate
23	MS_015	7	Incl	900	granular	30	3 void cake volumes	1x	Dry/land	Vacuum	2-propanol	propylencarbonate
26	MS_016 & MS_022	8	Incl	500	crystalline	30	3 void cake volumes	1x	Dry/land	Vacuum	2-propanol	acetone
28	MS_017	9	Incl	500	granular	30	2 void cake volumes	2x	Breakthrough	Vacuum	amylalcohol	n-heptane
7	MS_018	10	Incl	900	crystalline	10	3 void cake volumes	1x	Breakthrough	Vacuum	amylalcohol	4-methyl-2-pentanone
32	MS_019	11	Incl	700	micronized	20	3 void cake volumes	1x	Dry/land	Vacuum	ethanol	n-heptane
16	MS_020 & MS_023 & MS_024 & MS_029	12	Incl	500	micronized	30	2 void cake volumes	1x	Dry/land	Vacuum	amylalcohol	TBME
30	MS_026	13	Incl	500	crystalline	10	3 void cake volumes	1x	Dry/land	Flowing N2	ethanol	n-heptane
18	MS_027	14	Incl	900	granular	10	1 void cake volume	1x	Dry/land	Flowing N2	ethanol	TBME
20	MS_028	15	Incl	500	micronized	30	1 void cake volume	1x	Breakthrough	Flowing N2	2-propanol	dodecane
8	MS_030	16	Incl	900	granular	30	2 void cake volumes	1x	Breakthrough	Flowing N2	2-propanol	4-methyl-2-pentanone
2	MS_031	17	Incl	900	crystalline	30	2 void cake volumes	2x	Breakthrough	Flowing N2	2-propanol	cyclohexane
4	MS_032	18	Incl	900	micronized	30	3 void cake volumes	2x	Breakthrough	Flowing N2	amylalcohol	anisole
13	MS_033	19	Incl	500	crystalline	30	1 void cake volume	2x	Dry/land	Flowing N2	amylalcohol	isopropylacetate
25	MS_034	20	Incl	900	granular	10	1 void cake volume	2x	Dry/land	Flowing N2	amylalcohol	acetone
24	MS_035	21	Incl	500	micronized	10	2 void cake volumes	2x	Dry/land	Flowing N2	ethanol	propylencarbonate
10	MS_036	22	Incl	500	micronized	10	3 void cake volumes	1x	Breakthrough	Flowing N2	amylalcohol	toluene
33	MS_037	23	Incl	700	micronized	20	3 void cake volumes	2x	Dry/land	Vacuum	ethanol	n-heptane
12	MS_041	24	Incl	900	crystalline	30	2 void cake volumes	2x	Dry/land	Temperature 60°C	ethanol	toluene
17	MS_042	25	Incl	500	micronized	10	3 void cake volumes	2x	Breakthrough	Temperature 60°C	2-propanol	TBME
9	MS_043	26	Incl	500	micronized	10	1 void cake volume	2x	Breakthrough	Temperature 60°C	2-propanol	n-heptane
15	MS_044	27	Incl	500	micronized	30	1 void cake volume	2x	Dry/land	Temperature 60°C	2-propanol	4-methyl-2-pentanone
1	MS_045	28	Incl	500	granular	30	3 void cake volumes	1x	Breakthrough	Temperature 60°C	ethanol	isopropylacetate
19	MS_046	29	Incl	900	micronized	10	1 void cake volume	1x	Dry/land	Temperature 60°C	amylalcohol	cyclohexane
27	MS_047 & MS_049	30	Incl	900	granular	30	3 void cake volumes	2x	Dry/land	Temperature 60°C	amylalcohol	dodecane
5	MS_050	31	Incl	900	micronized	30	2 void cake volumes	1x	Breakthrough	Temperature 60°C	ethanol	acetone
22	MS_051	32	Incl	500	granular	10	2 void cake volumes	1x	Dry/land	Temperature 60°C	2-propanol	anisole
		33	Incl	500	crystalline	10	1 void cake volume	1x	Breakthrough	Temperature 60°C	amylalcohol	propylencarbonate

Figure 148 Factors selected for the screening DoE (first DoE).

Percentage loss	Residual moisture content	Extent of agglomeration	Specific cake resistance	Filter medium resistance	Sauter mean diameter	Volume mean diameter
92.5	25.4	92.32	1.4e+10	6.72e+09	30.55	163.06
26.67	33.09	74.78	1.96e+09	2.23e+09	55.97	95.45
0	14.5	0	0	0	321.14	354.43
9.01	26.55	89.89	1.99e+09	3.64e+09	69.86	118.45
0	0	0	2.61e+09	-4.51e+09	337.91	365.14
92.75	44.08	96.68	1.46e+10	7.15e+09	48.6	339.61
48.48	28.67	43.5	2.14e+08	4e+09	338.37	376.18
35.8	22.45	80.41	5.37e+09	6.56e+09	59.16	113.29
0	13.46	0	2.38e+08	1.93e+09	321.54	363.02
37.26	28.22	85.87	3.84e+09	3.38e+09	77.53	166.02
92.36	26.19	94.81	1.72e+10	5.97e+09	72.71	577.04
99.5	26.68	99.98	5.93e+10	1.96e+10	136.89	623.59
0.75	18.45	27.63	3.69e+09	6.02e+09	54.31	99.53
0	20.13	0	3.54e+07	2.5e+09	323.31	360.12
87.5	30.83	98.47	3.15e+10	4.33e+09	90.85	552.91
0	16.1	0	7.76e+07	2.32e+09	329.33	367.91
0.95	27.98	56.02	2.85e+09	5.31e+09	50.53	91.99
89.09	34.58	93.69	2.49e+10	4.52e+10	98.65	610.72
4.54	26.32	84.01	7.75e+09	2.26e+09	50.23	91.9
0	23.15	0	7.71e+07	1.2e+09	305.13	344.99
87.32	42.62	99.63	2.64e+10	4.18e+07	22.18	25.81
94.29	30.31	82.26	5.75e+10	1.52e+10	140.87	694.07
93.33	26.1	94.19	1.97e+10	6.81e+09	55.97	500.36
0.73	28.73	66.43	1.41e+09	3.12e+09	57.35	107.05
4.31	23.38	79.72	4.15e+09	2.6e+09	56.88	95.75
89.67	30.81	89.88	1.43e+10	5.7e+09	128.23	526.7
93.27	32.46	95.5	2.26e+10	4.77e+09	26.57	58.37
0	19.57	0	3.93e+08	1.91e+09	318.78	354.97
96.83	38.13	99.25	2.87e+10	8.09e+09	57	170.33
0	22.87	0	7.32e+07	1.43e+09	316.56	352.75
94.55	29.76	91.78	1.91e+10	7.88e+09	121.97	254.13
0	26.07	0	4.84e+09	-1.25e+09	338.83	372.73
100	34.97	99.37	6.21e+09	3.04e+09	0	0

Figure 149 Responses of the screening DoE (first DoE).

Exp No	Exp Name	Run Order	Incl/Excl	Pressure	Filter pore size	PCM grade	solvent	methodology	solid load
1	N1	10	Incl	900	10um	micronised	IPA	settling and reload	10
2	N2	1	Incl	500	10um	powder	IPA	settling and reload	30
3	N3	4	Incl	500	10um	micronised	ethanol	settling and reload	30
4	N4	13	Incl	500	5um	powder	ethanol	settling and reload	30
5	N5	5	Incl	900	20um	powder	ethanol	settling and reload	30
6	N6	9	Incl	500	20um	micronised	isoamyl alcohol	settling and reload	10
7	N7	7	Incl	900	5um	powder	isoamyl alcohol	settling and reload	10
8	N8	14	Incl	900	5um	micronised	IPA	filter and reload	30
9	N9	16	Incl	500	20um	powder	IPA	filter and reload	10
10	N10	2	Incl	500	5um	micronised	ethanol	filter and reload	10
11	N11	8	Incl	900	10um	powder	ethanol	filter and reload	10
12	N12	12	Incl	900	20um	micronised	isoamyl alcohol	filter and reload	30
13	N13	6	Incl	500	10um	powder	isoamyl alcohol	filter and reload	30
14	N14	11	Incl	700	20um	powder	isoamyl alcohol	filter and reload	20
15	N15	3	Incl	700	20um	powder	isoamyl alcohol	filter and reload	20
16	N16	15	Incl	700	20um	powder	isoamyl alcohol	filter and reload	20
17	n17	17	Incl	500	10um	powder	ethanol	settling and reload	30

Figure 150 Factors selected for the pre-settling DoE (second DoE).

cake resistance	media resistance	cake height	filtration time to dryland	cake resistance 2	media resistance 2	filtration time 2	Height 2
5.7e+09	6.75e+09	5	274	1.9e+09	2.25001e+10	412.51	5
6.91e+08	1.92e+09	18	87.17	2.76e+08	1.35e+10	157.23	18
1.56e+10	9.91e+09	19	126.27	5.19e+09	1.8266e+11	277.39	19
2.73e+09	1.46e+11	24.5	188.09	2.73e+09	1.46128e+11	200.51	24.5
1.14e+09	8.06e+09	20.25	86.03	2.27e+08	2.01522e+10	125.53	20.25
4.16e+10	6.11e+09	6	509.36	1.78e+10	2.45e+11	1168.05	6
2.67e+09	1.21e+10	6	383.59	1.33e+09	2.69796e+10	492.27	6
1.02e+10	1.13e+10	25	662.49	1.02e+10	1.12501e+11	1435.26	24
3.46e+09	-4.85e+08	7	20.5	-1.04e+09	2.04e+10	55.01	7
1.48e+10	1.64394e+11	6.75	279.1	3.71e+09	1.8266e+11	321.2	5.75
1.72e+09	4.03e+09	6	59	4.3e+08	1.61217e+10	101.75	6
6.17e+10	8.06e+10	23	2374.14	4.11e+10	8.06087e+11	3540	23
3.72e+09	4.03e+09	21	126.75	9.3e+08	1.22272e+11	385.67	21
5.24e+09	3.71e+08	17	149	3.49e+09	3.73e+10	385.99	17
3.46e+09	2.55e+09	18	121.66	3.46e+09	3.73e+10	407.1	18
3.2e+09	1.19e+09	17	141.52	8e+08	7.46256e+10	496.41	17
1.95e+09	2.41e+09	20	22.47	9.48e+08	3.56e+10	48.03	20

Figure 151 Responses of the pre-settling DoE (second DoE).

Table 50 Experiments parameters of the cake shown in Figure 80 and Figure 81 of the main manuscript.

Experiment number	Experiment parameters
21	Micronised, 10% V/V solid load, isopropanol 900mbar, 2 void cake volume *2 with isopropyl acetate, dryland
40	Powder, 10% V/V solid load, ethanol, 900mbar, 2 void cake volume *2 with dodecane, breakthrough
15	Special granular, 30% V/V, isopropanol, 900mbar, 3 void cake volume *1 with propylene carbonate, dryland
53	Powder, 30% V/V solid load, isoamyl alcohol, 500mabr, 2 void cake volumes *2 time with n-heptane, breakthrough
52	Powder, 30% V/V solid load, isopropanol, 900mbar, 1 void cake volume *1 with toluene, dryland
24	Micronised, 30% V/V solid load, isoamyl alcohol, 500mabr, 2 void cake volume *1 with TBME, dryland

9.6 Prototyping of a continuous isolation unit: development and tests

Exp No	Exp Name	Run Order	Incl/Excl	API solid load	PSD	Crystallization solvent	Isolation pressure	Volume of wash solvent	Wash solvents	Drying time
1	N1	3	Incl	15	micronised	Ethanol	200	4	heptane	180
2	N2	6	Incl	25	micronised	Ethanol	800	4	heptane	600
3	N3	18	Incl	15	powder	2-propanol	200	2	heptane	180
4	N4	4	Incl	15	powder	2-propanol	800	2	heptane	600
5	N5	12	Incl	25	micronised	isoamyl alcohol	200	2	heptane	180
6	N6	5	Incl	25	powder	isoamyl alcohol	800	4	heptane	600
7	N7	13	Incl	25	powder	Ethanol	800	2	dodecane	180
8	N8	11	Incl	25	powder	Ethanol	200	4	dodecane	180
9	N9	17	Incl	25	micronised	2-propanol	200	2	dodecane	600
10	N10	16	Incl	15	micronised	2-propanol	800	4	dodecane	600
11	N11	20	Incl	15	micronised	isoamyl alcohol	800	2	dodecane	180
12	N12	2	Incl	15	powder	isoamyl alcohol	200	4	dodecane	600
13	N13	1	Incl	15	micronised	Ethanol	200	2	isopropyl acetate	600
14	N14	14	Incl	15	powder	Ethanol	800	2	isopropyl acetate	600
15	N15	15	Incl	25	micronised	2-propanol	800	4	isopropyl acetate	180
16	N16	10	Incl	25	powder	2-propanol	200	4	isopropyl acetate	180
17	N17	9	Incl	15	micronised	isoamyl alcohol	800	4	isopropyl acetate	180
18	N18	7	Incl	25	powder	isoamyl alcohol	200	2	isopropyl acetate	600
19	N19	8	Incl	20	powder	isoamyl alcohol	500	3	isopropyl acetate	390
20	N20	19	Incl	20	powder	isoamyl alcohol	500	3	isopropyl acetate	390
21	N21	21	Incl	20	powder	isoamyl alcohol	500	3	isopropyl acetate	390

Figure 152 Factors of the DOE.

cake volume	filtration flow rate (first dose)	D50 1bar	first filtrate acetanilide concentration	cake resistance	medium resistance	LOD	mean diameter (xsv from QICPIC)	% wash solvent (MC)	% crystallization solvent (MC)
11.69	0.47	41.92	0.2254	6.3e+08	-1.06e+09	6.22	35.11	5.88	94.12
15.05	0.46	34.58	0.2497	1.86e+09	-1.8e+10	2.93	29.98	51.77	48.23
12.03	0.76	79.21	0.1679	5.9e+07	1.55e+09	1.09	61.88	9.84	90.16
12.29	2.06	79.02	0.1504	4.3e+08	2.54e+09	1.09	61.21	60.22	39.78
22.68	0.07	42.9	0.1856	7.01e+09	-1.63e+10	24.37	39.3	86.98	13.02
17.81	0.31	71.11	0.2256	2.66e+09	-1.22e+09	0.4	52.95	52.77	47.23
12.08	4.41	83.41	0.2204	8.98e+08	-1.24e+09	10.91	66.71	97.66	2.34
19.7	0.72	93.79	0.2225	1.45e+08	2.8e+09	11.2	72.14	98.34	1.66
21.55	0.03	94.82	0.2795	6.51e+09	2.07e+10	26.32	48.14	81.52	18.48
12.02	0.41	40.48	0.1067	5.53e+09	-3.75e+09	15.64	34.57	98.81	1.19
18.83	0.03	0	0.1405	4.79e+09	-4.93e+09	40.61	0	54.82	45.18
21.73	0.29	83.02	0.1579	5.63e+08	-3.4e+08	8	61.49	99.54	0.46
11.21	0.76	101.42	0.18	3.5e+08	-6.64e+09	13.81	68.08	23.98	76.02
12.11	4.49	102.35	0.1869	1.75e+08	-3.24e+09	0.6	79.76	11.36	88.64
17.49	0.2	41.24	0.2503	5.51e+09	1.94e+10	24.99	34.88	19.73	80.27
18.13	0.38	71.43	0.2399	6.16e+07	6.27e+09	3.21	55.39	91.54	8.46
15.51	0.09	43.98	0.1538	1.57e+10	3.92e+09	26.61	35.84	41.29	58.71
16.46	0.04	89.95	0.2158	-3.55e+09	3.19e+10	3.63	68.48	0.56	99.44
26.24	0.27	71.28	0.2115	1.14e+09	-4.2e+09	2.26	56.77	31.08	68.92
15.06	0.27	80.8	0.1865	1.69e+09	3.38e+09	2.83	62.54	21.28	78.72
27.56	0.3	79.53	0.2074	1.01e+09	-4.07e+09	0.58	59.26	32.04	67.96

first filtrate metacetamol concentration	first filtrate orthoacetamol concentration	second filtrate acetamide concentration	second filtrate metacetamol concentration	second filtrate orthoacetamol concentration	third filtrate acetamide concentration
0.2059	0.1016	0.243	0.2227	0.2228	0.0933
0.1921	0.0669	0.1704	0.1512	0.1704	0.0636
0.1286	0.0611	0.1512	0.1512	0.1146	0.058
0.1146	0.0572	0.1555	0.1555	0.1186	0.0478
0.142	0.0639	0.1544	0.1544	0.118	0.0441
0.1716	0.0432	0.2013	0.2013	0.1537	0.036
0.169	0.0575	0.2045	0.2045	0.1558	0.053
0.1707	0.0583	0.2169	0.2169	0.1659	0.0532
0.215	0.0693	0.1622	0.1622	0.1239	0.048
0.1235	0.0663	0.0803	0.0803	0.0925	0.0544
0.1093	0.0374	0.1195	0.1195	0.0928	0.0529
0.1186	0.0448	0.1377	0.1377	0.1034	0.0459
0.1375	0.0653	0.1571	0.1571	0.12	0.0515
0.1426	0.0614	0.1501	0.1501	0.1128	0.0569
0.1923	0.0636	0.1824	0.1824	0.1397	0.0544
0.1852	0.0407	0.1797	0.1797	0.1386	0.038
0.12	0.0544	0.1161	0.1161	0.0901	0.043
0.1651	0.0374	0.1403	0.1403	0.1073	0.0314
0.1641	0.043	0.1484	0.1484	0.115	0.0383
0.1454	0.0407	0.1379	0.1379	0.107	0.0381
0.1608	0.0463	0.1596	0.1596	0.1238	0.0393
					0.0178

cake orthocetamol concentration	extent of agglomeration	ABI index
0.0383	0.9617	0.0516
0.0418	0.9354	0.0196
0.0428	0.3513	0.2426
0.0416	0.1199	2.1533
0.0381	0.9886	0.0032
0.0462	0.3152	0.1234
0.0353	0.8695	0.2073
0.0353	0.8355	0.965
0.0588	0.9689	0.0278
0.0584	0.917	0.0386
0.0427	0.9635	0.0076
0.0232	0.5459	0.9937
0.0386	0.9707	0.991
0.0479	0.5999	0.1378
0.0343	0.9858	0.0057
0.0407	0.4968	0.1972
0.0211	0.9956	0.0031
0.0436	0.865	0.0607
0.0459	0.5194	0.1078
0.0395	0.3521	0.1255
0.0418	0.4807	0.114

Figure 153 Responses of the DoE.

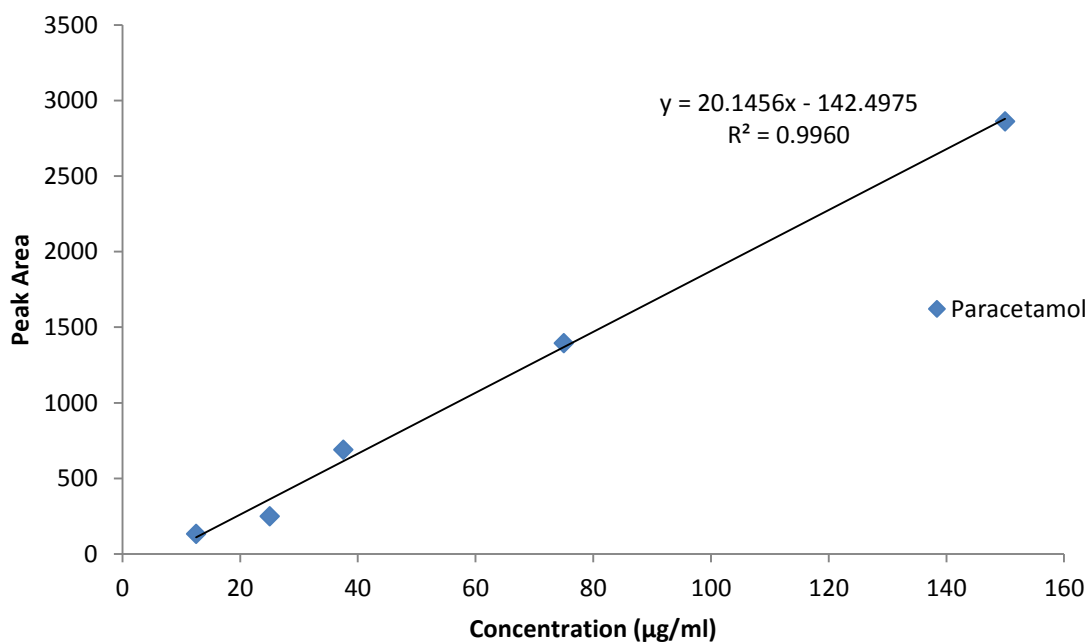


Figure 154 HPLC calibration curve of paracetamol.

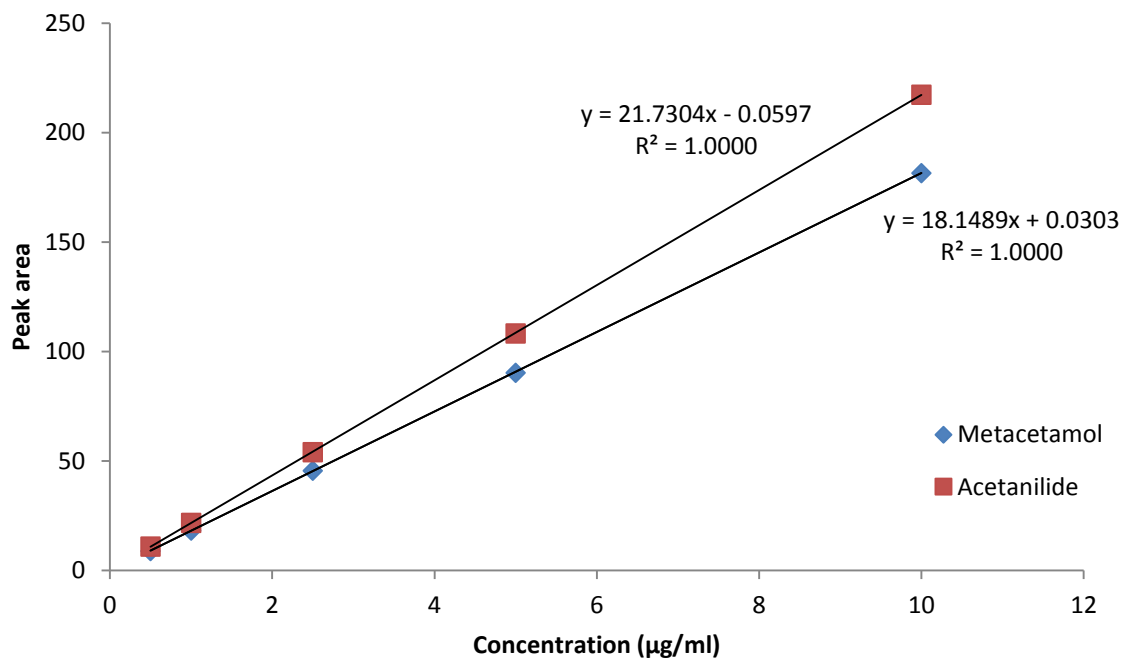


Figure 155 HPLC calibration curve of metacetamol and acetanilide.

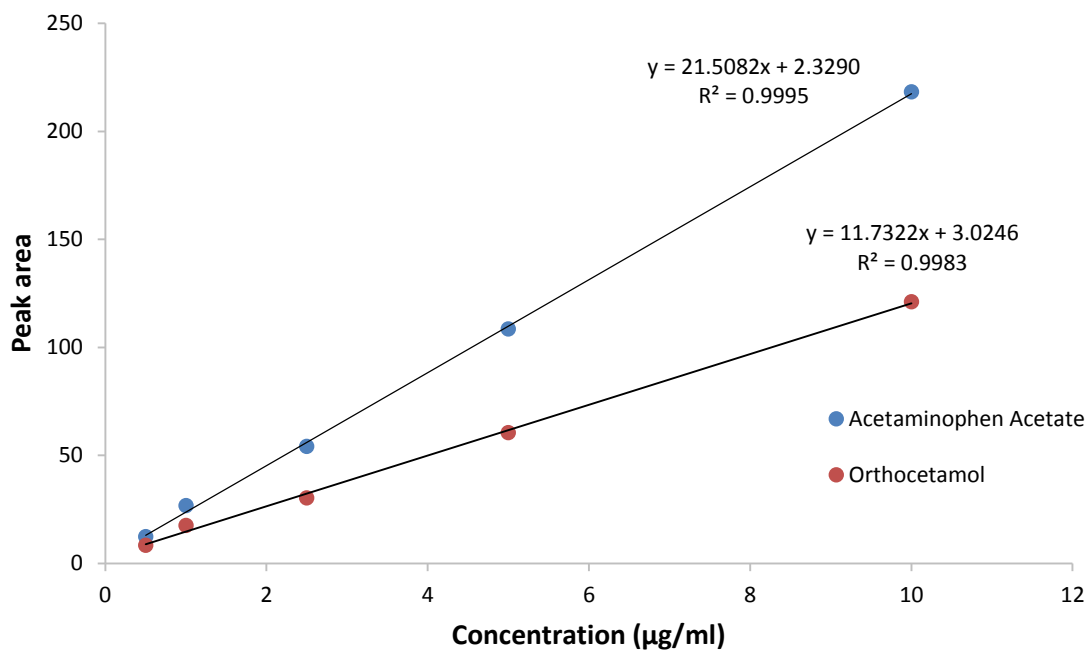


Figure 156 HPLC calibration curve of acetaminophen acetate and orthocetamol.

References

- I) Wypych, A., Wypych, G. Databook of solvents. ChemTec Publishing, 2014
- II) PubChem website [cited 2018-05-15]
<https://pubchem.ncbi.nlm.nih.gov/compound/>
- III) Accudynet website [cited 2018-05-15]
https://www.accudynetest.com/visc_table.html